FLEXURAL BEHAVIOR OF STEEL FIBER REINFORCED PRESTRESSED CONCRETE BEAMS AND DOUBLE PUNCH TEST FOR FIBER REINFORCED CONCRETE

by

NETRA BAHADUR KARKI

Presented to the Faculty of the Graduate School of

The University of Texas at Arlington in Partial Fulfillment

of the Requirements

for the Degree of

DOCTOR OF PHILOSOPHY

THE UNIVERSITY OF TEXAS AT ARLINGTON

December 2011

ACKNOWLEDGEMENTS

First of all I would like to express my sincere appreciation to my research advisor, Dr. Shih-Ho Chao for his continuous support, advice and help during whole period of my PhD course. Dr. Chao was persistent from the project's inception, giving priceless advice on ideas and critiquing. I would also like to thank Dr. Ali Abolmaali for his advice and support at starting of my PhD course. Thank to Dr. Frank Lu, Prof. Joe Lundy and Dr. John Matthys for their valuable suggestions during the dissertation proposal defense. I would also like to thank Vartan Babakhanian and Hanson Pipe and Precast, Grand Prairie, TX, for continuous help on experimental work providing all kind of facilities and materials. I would like to thank to Maccaferri Co. for donating steel fibers. I would also like to thank Texas Department of Transportation (partial funding support). I would like to thank my friends Dr. Jae-Sung Cho, Dr. Xuejian Liu, Sanputt Simasathien, Tarun Pareek, Regina Waweru, Jiansinlapadamrong Chatchai, Brandon Price, Rachel Simer and Dr. Dipti Ranjan Sahoo for their continuous help during the experimental works.

I would also like to thank Department Chair Dr. Yazdani and the support staffs at from the Department of Civil engineering, The University of Texas at Arlington for all kinds of the logistic and financial support.

Finally I would like thanks to my family including my wife, sons, parents and brothers, who always encouraged me for this work, without which it could be possible.

December 15, 2011

ABSTRACT

FLEXURAL BEHAVIOR OF STEEL FIBER REINFORCED PRESTRESSED CONCRETE BEAMS ANDDOUBLE PUNCH TEST FOR FIBER REINFORCED CONCRETE

Netra Bahadur Karki, PhD

University of Texas at Arlington ,2011

Supervising Professor: Shih-Ho Chao

Steel fibers have widely been used in the past to reinforce brittle materials in many nonstructural applications such as pavement, tunneling lining, etc. On the basis of numerous previous studies, ACI 318-11 [2011] has recently accepted steel fiber as a minimum shear reinforcement replacement with minimum 0.75% volume fraction for both reinforced concrete and prestressed concrete members. However, not much previous research has talked about the flexural behavior of fiber reinforced concrete (FRC). As per ACI 318-11 for tension-controlled sections, the net tensile strains in the outermost layer of steel, ε_t, should be greater than or equal to 0.005 and for the moment redistribution in continuous beam the section should sufficiently ductile ($\varepsilon_t \geq 0.0075$). For this, the sections should have small longitudinal reinforcement ratio which ultimately leads to an inefficient beam section with a large cross-sectional area. In contrast, the use of smaller concrete cross sections can lead to a diminished ductile flexural behavior as well as premature shear failure. In this context, the use of steel fiber reinforced concrete could be

a potential solution since fiber can increase both the concrete shear strength and it's usable compressive strains. However limited previous researches on the flexural behavior on SFRC beams are available and most of them are of small scales and concentrated only basically for shear behavior. To the best of our knowledge, the large-scale prestressed fiber reinforced concrete beam specimens have yet to be studied for flexure behavior. In this project, six large scale prestressed concrete beams with or without steel fiber along with some material test were tested. Our experimental investigations indicated that even with inclusion of small percentage volume of fraction of steel fiber *(V_f =0.75%)* could not only increase the ductility and shear strength of the SFRPC beam but also change the failure pattern by increasing usable strain in concrete and steel. A modification on the limit for c/d_t ratio and ϕ factor for design of flexural member given in current ACI could be proposed which could imply the smaller sections with higher longitudinal reinforcement ratio and less shear reinforcement. could be used.

Any standard material test results have to ensure that FRC has, at least, been batched properly and it can give indications of probable performance when used in structures. In the current material testing method suggested by ACI, the third point bending test (ASTM C1609) has an inherent problem in that the coefficients of variations for post cracking strength and residual strength are generally very high on the order of 20%. The direct tensile test can be a more appropriate material. However, it is currently not recommended as standard method in the U.S. Because of it's difficultly in gripping arrangement which will lead to cracking of the specimen at the grips. Both the test methods also require close loop servo controlled machine. The round panel test method

(ASTM C1550) requires large size specimen and heavy steel supports prevents performing test in small laboratories. Split cylinder test (ASTM C496), do not necessarily reflect the true properties of the material as the specimen is forced to fail in the line of the application of the load and the test method is also not recommended by ACI for SFRC. In order to improve the material assessment procedure, the double Punch Test (DPT) introduced by Chen in 1970 [Chen, 1970] was extensively evaluated to develop a simple, quick and reliable testing method for SFRC. Various tests were carried out in order to evaluate peak and residual strength, stiffness, strain hardening and softening, toughness and other post crack properties. Our test results indicated that the DPT method could be immersed as reliable, easier and economical material test method. It could be used to distinguish the peak strength, residual strength, toughness stiffness and crack resistance, of different SFRC mixtures with less scatter results compared to other material test methods.

TABLE OF CONTENTS

LIST OF ILLUSTRATIONS

Figure Page

LIST OF TABLES

CHAPTER 1

INTRODUCTION

1.1 General

Due to its relative low cost, concrete is widely used as construction material despite the fact that it is neither as strong nor as tough as steel. Plain concrete is brittle in nature and has a low tensile strength and strain capacity upon loading, which leads to limited resistance to tensile stress and cracking. The mechanical properties of concrete can be enhanced through the introduction of reinforcing steel that has high tensile strength and ductility. Steel has been extensively used in the form of rods, wire, and fiber as a reinforcing material in conventional reinforced concrete (RC), prestressed concrete (PC), and steel fiber reinforced concrete (SFRC).

This chapter consists of general introduction to the dissertation, and presents the overall context into which the work is placed. The inspiration for the research is presented. It has two major parts: first, the flexural behavior of steel fiber reinforced prestressed concrete, and second, the development of a simple and reliable material evaluation method for fiber reinforced concrete. The objectives of the dissertation are discussed in this chapter. Organization of the dissertation and methodology are described at the end of this chapter.

1.2 Motivation

1.2.1 Flexural Test of SFRPC beams

Determining the amount of longitudinal flexural reinforcement is one of the most important aspects of the design of a typical reinforced concrete (RC) or prestressed concrete (PC) beam. The shear capacity of a beam is checked after determining the flexural strength and then the required shear reinforcement is added based on the code's requirements. In general, the design process will ensure that the beam will fail due to flexure when overloaded, rather than shear, which is beneficial because shear failure is brittle and less predictable. In order to avoid premature shear failure, sufficient shear reinforcement should be provided. Beam sections are generally designed to be tension-controlled, in which case the amount of longitudinal steel reinforcement in the section is governed by certain limits to ensure that the steel yields before the concrete reaches its crushing strain (i.e., ε_{cu}, which is approximately 0.003 as specified by the current ACI code [2011]). If the excessive steel is used then the concrete strain may reach its ultimate value before the steel yields, causing a brittle, compressive failure to occur with little visible warning (i.e., a compression-controlled behavior), which is not desired. In order to avoid such failures, beams are generally designed to be tension-controlled so that high ductility can be achieved. Higher ductility is particularly important for sections of interior supports in continuous beams, in order to allow for moment redistribution when overloaded.

Various fibers have been used to reinforce brittle materials in the past. The first scientific investigation regarding the use of steel fibers as shear reinforcement was

conducted by Baston et al. (1972). Their study showed that the replacement of shear reinforcement by steel fibers provided an effective mechanism to resist shear failure. Since then, various studies have shown that the ductility of plain concrete can be considerably increased with the addition steel fibers. As a result of numerous previous research studies, ACI 318-11 [2008] has a new provision which allows steel fibers as alternate shear reinforcement, if a minimum amount volume fraction of 0.75% is used. This provision applies for both reinforced concrete and prestressed concrete members. However, prior researches have very limited information regarding the flexural behavior of steel fiber reinforced prestressed concrete (SFRPC).

As per ACI 318-11, for tension-controlled sections, the net tensile strains in the outmost layer of steel, ε_t, should be greater than or equal to 0.005. As an example for typical case with 4 ksi concrete and conventional reinforcement of 60 ksi, this criterion will be satisfied only for members that have a longitudinal steel reinforcement ratio less than approximately 1.8%. This ratio needs to even less than approximately 1.3% from equation $\left[\rho = 0.85\beta_1 \frac{f_c^{'}}{f_y} \frac{0.003}{0.003+\varepsilon_t}\right]$ [Nilson et al., 2007] in order for moment redistribution to have as net tensile strain ε_t, should greater than or equal to 0.0075 as per ACI 2011. The moment redistribution is really important for continuous beams to allow the structure to take further load after plastic hinge formation in any section of the beam due to yielding and allowing inelastic rotation. Hence for a continuous beam should have highly ductility in section to have sufficient rotational capacity and allow for moment redistribution. Such section requires a low reinforcement ratio and this

leads to an inefficient beam section with a large concrete cross-sectional area as compared to that of steel. This is a problem, particularly for longer span prestressed concrete (PC) bridge girders where the self-weight of the beams is the dominant loading. In contrast, the use of smaller concrete cross sections can lead to diminished ductile flexural behavior as well as premature shear failure. To avoid such shear failure larger amount of stirrups have to be provided which makes the construction complex. In this context, the use of steel fiber reinforced concrete could be a potential solution because SFRC increases both the concrete shear strength and its useable compressive strains, thus a smaller/lighter section can be used with increased in ductility.

There is very limited research regarding the flexural behavior of prestressed concrete beams with steel fibers. Moreover, most of the prior investigations were based on small scale specimens. And also most of studies addressed only for shear behavior. Hence, in this research an attempt was made to address the gaps in previously performed research through the testing of large-scale, steel fiber reinforced prestressed concrete (SFRPC) beams. It was expected that the experimental program would provide useful information on the failure mechanisms and behavior of SFRPC beams while resulting in a greater longitudinal reinforcement ratio than that allowed by current code and new limit for the reinforcement design for a flexure member could be proposed. In addition, other properties of SFRC, such as toughness, loads-strain responses, cracking patterns, energy and ductility ratios, and flexural strengths, were also evaluated.

1.2.2 Simple and Reliable Material Test for FRC

Although material properties resulting from any standard material test methods might not precisely represent the actual properties of the fiber reinforced concrete (FRC) used in structural members, those test results can ensure that the FRC has at least been batched properly and can give indications of probable performance when used in structures. On the other hand, an ideal material test method for FRC needs to account for many factors. Mindess et al. [(2003]) suggested that, for a suitable FRC evaluation method, there should be low variability in any measurement of a given property; it should be able to quantify certain criteria with regard to FRC's mechanical performance in terms of strength, crack resistance, toughness, and should also reflect the characteristics depicted by a load versus deflection curve. An ideal material test method should be as independent as possible of the specimen size and geometry. The fundamental significance is that it can be used for both specification and quality control of FRC mixtures.

The current testing method used to determine the material properties of FRC is based on the standard third point bending test, ASTM C1609 (2010). This is the only material method suggested by ACI. This method however has an inherent problem in that the coefficient of variation for residual strength is generally very high, on the order of 20% [Bernard, 2003]. This large scatter in the residual strength can be a significant hindrance when it comes to determining characteristic values. The complex test setup also precludes its use in small laboratories. A more appropriate method is the direct tensile test which can identify the key properties of FRC such as strain-hardening or

strain-softening, elastic modulus, and stress versus strain relationships under tension. These are the constitutive properties of FRC that are useful for modeling and design of FRC structural members [Naaman et al., 2008]. However, currently there is no standard method for this test in the U.S., in part because it is difficult to create a gripping arrangement which will not lead to cracking of the specimen at the grips. Some recent tests utilizing some special double dog-bone shaped specimens were conducted at the University of Texas at Arlington [Chao et al., 2011]. Many of the test results were generally not useful due to the unpredictable location of the major crack and its propagation, which in turn led to high variability in the test results. Both the ASTM C1609 and direct tensile test methods require a closed-loop, servo-controlled machine. Hence, these tests are generally time consuming and expensive, as they may require more specimens to obtain sufficient reliable test data. These methods normally show a considerable scatter in results that make quality control difficult.

The round panel test method (ASTM C1550) requires large specimen sizes and a heavy steel support so there is difficultly of performing the test in small laboratories and also requires close loop servo controlled machine. So this test is also time consuming and expensive. In case of split cylinder test (ASTM C496), the specimen is forced to fail in the line of the application of the load. Therefore, the true properties of the material may not be reflected and the test method is also not recommended by ACI for FRC. So of all these material test methods are not very much reliable particularly the case with tensile properties intended to estimate the strength of structural members. Hence in order to overcome these limitations of current material test methods and to

improve the material assessment procedure, the search of an alternative simple and reliable material test method is necessary. In this regard the double punch test (DPT) which originally introduced by Chen in 1970 has been reintroduced for the evaluation of tensile properties and quality control for FRC. This test method can be carried out in small laboratories with conventional compression test machines in order to determine certain material properties such as stiffness, tensile strength, residual strength, and toughness of FRC materials. In this research, the DPT method has been extensively evaluated to develop a simple, quick, and reliable testing method for FRC.

1.3 Objectives

This research work documented in this dissertation consists of extensive experimental programs, as shown in Figure 1.1 and Figure 1.2. Six large scale, prestressed concrete beams with and without steel fibers were tested along with various other material tests. Similarly, a large number of double punch tests with different mixtures, different volume fractions of fibers and different types of fibers at different ages were carried out in different phases. The two main objectives of this research work are:

(a) To investigate the flexural behavior of large-scale, steel fiber reinforced, prestressed concrete beams.

(b) To develop a simple and reliable material test method (double punch test) for fiber reinforced concrete.

To achieve the first goal, various properties of the six large scale beams, such as ultimate loads, load-deflection curves, failure modes, crack patterns, toughness, ductility, and load-steel strain curves, were evaluated. For the second goal, an extensive study of double punch test (DPT) with various properties of fiber reinforced concrete such as peak strength, residual strength, stiffness, toughness, deflection hardening, and deflection softening, and other post-cracking properties were evaluated. DPT method was also compared with other types of material test methods.

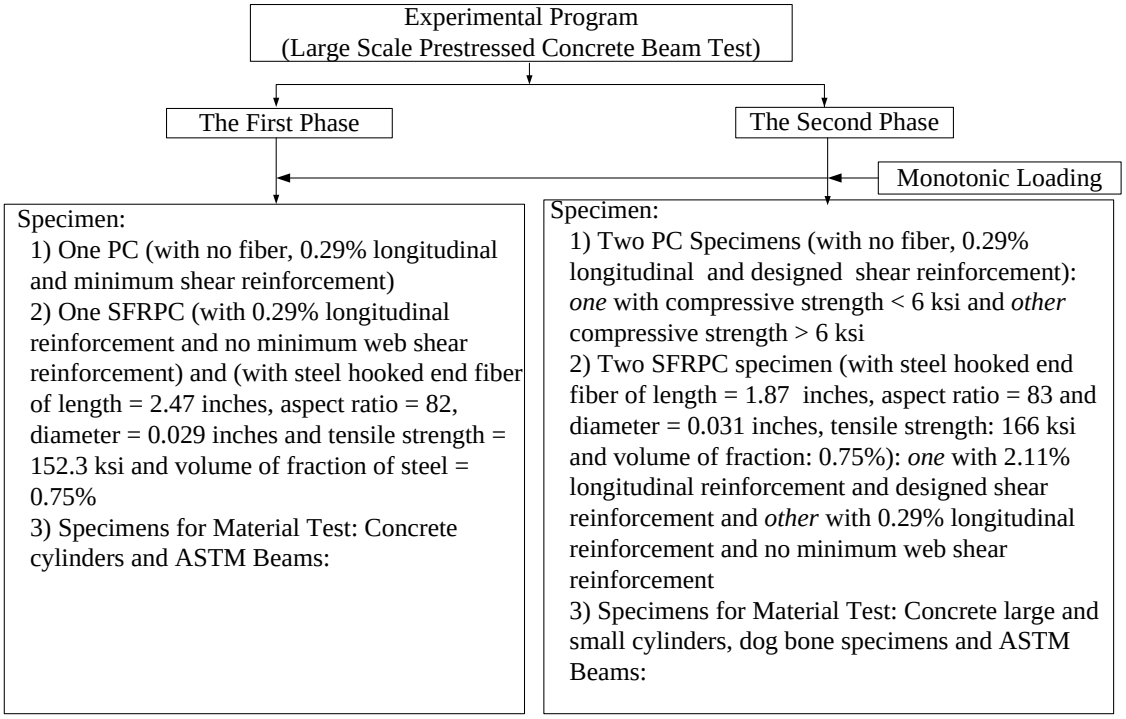

Figure 1.1 Flowchart of Experimental Program: Large Scale Prestressed Concrete Beam Test

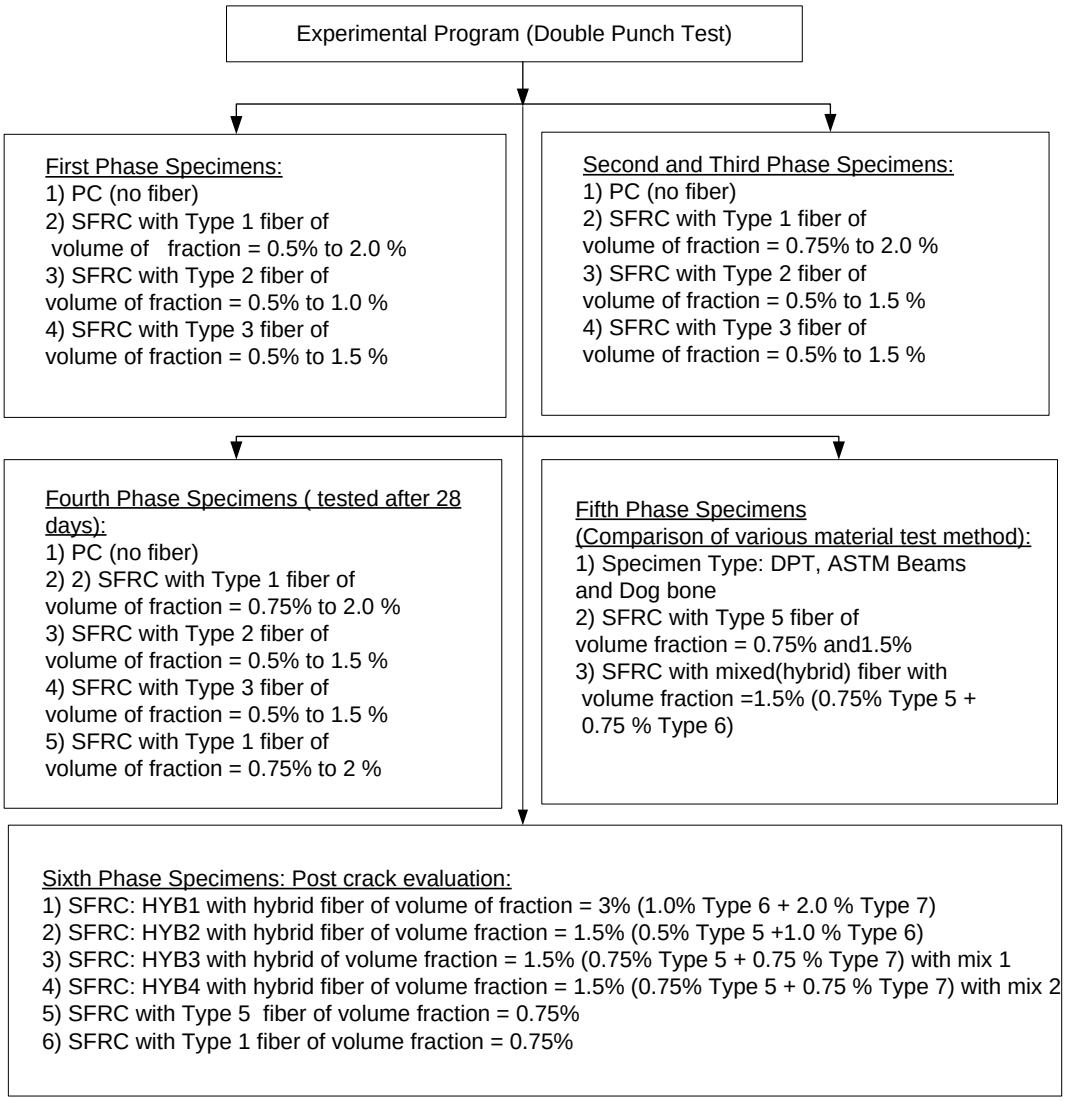

Figure 1.2 Flowchart of Experimental Program: Double Punch Test

1.4 Structures of the Dissertation

In Chapter One, a general introduction of plain concrete, reinforced concrete, and reinforcing material have been discussed. The motivation for current research work is discussed in this chapter. Objectives of this research work and methodology are also discussed in this chapter.

In Chapter Two, a literature review regarding reinforced concrete, prestressed concrete, fiber reinforced concrete, fiber types, and previous works carried out regarding SFRC beams and different material test methods are elaborated on.

In Chapter Three, a detailed experimental investigation with large scale prestressed concrete beams with and without steel fibers is discussed. Different material tests carried out, along with the large scale beams, are also covered in this chapter.

In Chapter Four, a detailed experimental investigation for the evaluation of the double punch test method in order to develop a simple and reliable material test method for FRC is explained. FEM analysis for the DPT model is also included in this chapter.

In Chapter Five, the analysis of the experimental results and a discussion regarding the large scale beam test is covered.

In Chapter Seven, finite element analysis, discussion and comparison of the experimental result and recommendations for design provisions, are discussed.

In last Chapter Eight the summary of the work, conclusion and recommendations for future study are discussed.

1.5 Methodology

To fulfill the objectives listed above, the following methodology has been adopted.

1.5.1 Literature Review

Various references and the study of previous related works have been reviewed in connection with types of fibers, flexural test of SFRC, and material test methods.

1.5.2 Materials Used and Collection

The necessary materials for the specimens such as cement, fly ash, fine aggregate, and steel were donated by a local precast plant (Hanson Pipe and Precast)**.** The steel fibers were provided by different companies.

1.5.3 Preparation of Materials and Molds

Fabrication of molds and the placing of reinforcements and the attachment of steel and concrete strain gauges in the specimens were carried out.

1.5.4 Mobilization of Equipment Machines and Apparatus

In order to carry out various experiments, preparation of experimental setups and their mobilization were made prior to the start of the relevant experiments.

1.5.5 Preparation of Specimens

Detailed experimental schemes were prepared, in which the required number of specimens for experimentation was identified. Based on experimental schemes various specimens were prepared.

1.5.6 Material Tests

Various material tests, such as the third point bending test (ASTM C1609), compressive strength test (cylinder test), direct tensile test (dog bone type specimen), and double punch test (DPT) were carried out along with large scale beam tests.

1.5.7 Testing of Specimens

Large scale beams were tested on steel frame built by University of Texas at Arlington (UTA) in local precast plant (Hanson Pipe and Precast) and other specimens for the material tests, including the DPT tests, were carried out civil engineering lab building (CELB) of UTA as per the proposed experimental scheme. Details of the experimental work have been presented in relevant chapters.

1.5.8 Data Analyzing and Conclusion

The results obtained from various experimental investigations were analyzed and discussed and conclusions were drawn.

CHAPTER 2

LITERATURE REVIEW

2.1 General

Steel fibers have been used in concrete structures for an extended period of time; however, most of the steel fibers used in concrete in the past were limited to non-structural applications, essentially only for crack control. In this chapter, various works on steel fiber reinforced concrete (SFRC), mechanical properties of SFRC composites, failure mechanism of reinforced concrete beams, moment redistribution of continuous beam, behavior of steel fiber reinforced concrete beams, prediction of the ultimate strength of PC and SFRPC beams, and different SFRC material test methods are reviewed.

2.2 Mechanical Properties of SFRC

2.2.1 Toughening Mechanism of Fiber Reinforced Concrete (FRC)

Fiber reinforced cementitious composite (FRCC) is a material made from a hydraulic cement, fine aggregates (such as fly ash and silica fume, or sand) and discrete, discontinuous fibers, thus it does not contain course aggregates. Fiber reinforced concrete (FRC) is made with hydraulic cement, aggregates of various sizes, and discrete, discontinuous fibers. In both cases, fibers play a major role in bridging the gap

across the cracked matrix in the post-cracking zone. In this zone, the fibers in FRCC/FRC can serve two functions [Bentur and Mindness, 2007]:

- They can increase the strength of the composite over that of the matrix by providing a means of transferring stresses and loads across cracks. If an ascending stress–strain curve after first cracking occurs; this behavior is referred to as *strain hardening*.
- More importantly, they can increase the toughness of the composite by providing energy absorption mechanisms due to the de-bonding and pull-out processes of the fibers bridging the cracks. This occurs when the stress–strain curve is descending after the first crack, referred to as *strain softening*.

The sequence of events following the first crack in the composite determines whether these strengthening and toughening effects will take place. As cracking occurs in the brittle matrix, the load is transferred to the fibers. If failure is to be prevented at this stage, the load-bearing capacity of the fibers, $\sigma_{fu}V_f$ in the case of aligned and continuous fibers, should be greater than the load on the composite at the first crack. This relation can be quantified on the basis of the elastic stresses at the cracking strain of the matrix in the composite, ϵ_{mu} [Bentur and Mindness, 2007]:

$$\sigma_{fu}V_f > E_m\epsilon_{mu}V_m + E_f\epsilon_{mu}V_f \qquad (2.1)$$

The right-hand term in Eq. 2.1 represents the first crack strength of the composite. When Eq. 2.1 is satisfied (i.e. when the fiber content, V_f , is sufficiently high), the first crack to occur in the composite will not lead to catastrophic failure, but

will instead result in the redistribution of the load between the matrix and the fibers. That is, the load carried by the matrix in the cracked zone will be imparted on the fibers bridging the crack, and the matrix at the edges of the crack will become stress-free. Post-multiple cracking range is a region where the fibers are being stretched or pulled out of the cracked matrix.

Naaman discussed in the book edited by Shi and Mo [2008] more about the tensile model of FRC composite with randomly oriented and distributed discrete fibers as shown in Figure 2.1(a). The model generally consists of at least two states. The first state is the pre-cracking state which is the elastic portion as shown in part I of Figure 2.1(b). The second state is the post-cracking state.

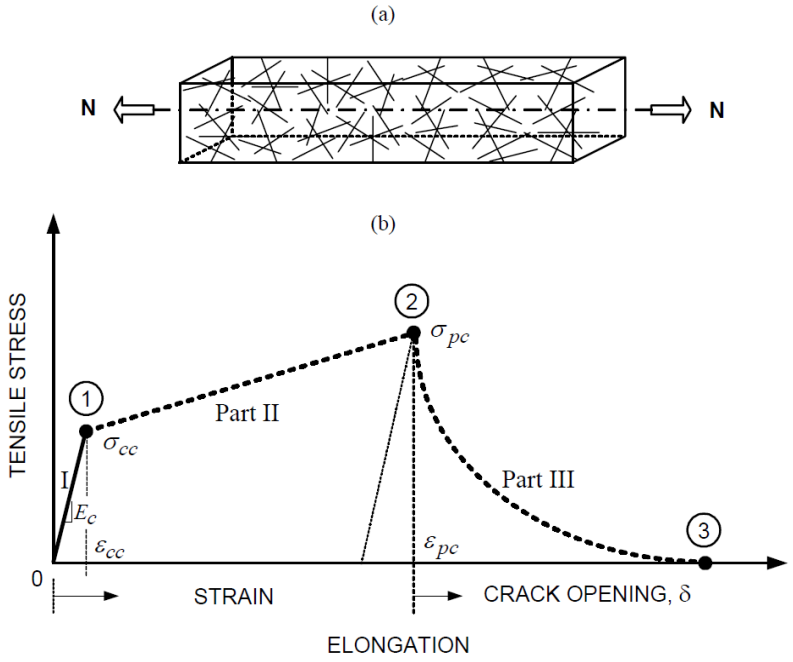

Figure 2.1 (a) Tensile Model with Discrete Fiber (b) Idealized Stress-Elongation Response in Tension of a Strain-Hardening FRC Composite for Modeling [Naaman, 2008]

This state consists of two phases. First phase of second state is the strain hardening with multi cracking phase as shown in Part II of Figure 2.1(b). This phase may not always exist as it depends upon fiber types, fiber content and cementitious composites. Second phase of the post-cracking state involves the fiber pull-out or failure of fibers (Part III of Figure 2.1(b)).

The tensile model consists of three key coordinates of tensile stress–strain response as shown in Figure 2.1 These are: (1) stress and strain at first crack (σ_{cc}, ε_{cc},) and elastic modulus of elasticity of the composite (E_c); (2) stress and strain at maximum post-cracking point (σ_{pc}, ε_{pc}); and (3) general pull-out response after crack localization.

FRC is a composite material which can be characterized by a linear stress-strain curve in tension with three parameters E_m, σ_{mu}, and ε_{mu} as shown in Figure. 2.2(a). The steel fibers are ductile materials with an initial elastic response. They can be well defined with yielding behavior, the yield stress, σ_{fy} and the corresponding strain ε_{fy} as shown in Figure 2.2(b).

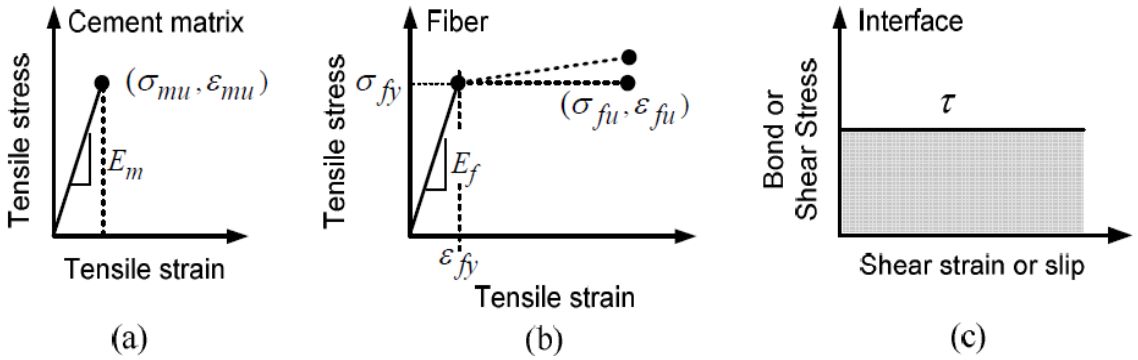

Figure 2.2 (a) Assumed Tensile Stress-Strain Response of the Cement Matrix. (b) Assumed Tensile Stress-Strain Response of the Fiber. (c) Assumed Bond Stress versus Slip Response at Very Small Slips [Naaman, 2008].

At failure the tensile strain of the matrix is smaller than that of the fiber.

$\varepsilon_{mu} < \varepsilon_{fy}$ for ductile fibers (2.2)

This indicates that cracking will occur in the matrix prior to failure of fiber or pull-out of the fibers from the composite. The value of bond strength between fiber and matrix is assumed to represent an average value with reasonable small value of slip of fiber from the matrix (Figure 2.2(c)).

Naaman further discussed that for a FRC composite member with discrete fibers in tension, after cracking upon increased elongation or straining the following three possible cases can happen:

- Failure of all fibers
- Pull-out of all fibers (specially in case of high strength fiber)
- Combined case: some fiber fails and some fiber being pulled out

The tensile stress in FRC composite just before the first cracking is given by:

$$\sigma_{cc} = \sigma_{mu}(1 - V_f) + \alpha\tau\frac{L}{d}V_f \quad (2.3)$$

And strain

$$\varepsilon_{cc} = \frac{\sigma_{cc}}{E_{cc}} \quad (2.4)$$

where $\alpha = \alpha_1\alpha_2\alpha_3$ is the parameter used to account for several factors such as average bond contribution, efficiency factor of the fiber orientation and reduction in bond strength with external applied stress.

L=Length of fiber

$V_f = Volume\ of\ \ fraction\ of\ \ fibers$

$d = diameter\ of\ fiber$

$L/d = \ fiber\ aspect\ ratio$

$\sigma_{mu} = tensile\ stength\ of\ \ matrix$

$\tau = assumed\ average\ or\ equivalent\ bond\ strength\ at\ \ fiber\ matrix\ interface$

For first case when all fibers fail, the ultimate strength of the composite is given by:

$$\sigma_{cu} = \alpha_2 V_f \sigma_{fu} \qquad (2.5)$$

where $\sigma_{fu} = Ultimate\ strenght\ of\ the\ \ fiber$

For second case when all fibers being pulled out the post-cracking strength is given by:

$$\sigma_{pc} = \lambda \tau \frac{L}{d} V_f \qquad (2.6)$$

where, λ is product of several parameters accounting for several factors given by:

$$\lambda = \lambda_1 \lambda_2 \lambda_3 \lambda_5 \qquad (2.7)$$

where $\lambda_1 = \dfrac{Shorter\ embedded\ distance\ of\ \ fiber\ \ from\ a\ \ forming\ crack}{Total\ length\ of\ \ fiber}$

$$\lambda_2 = 4\alpha_2 \lambda_4 \qquad (2.8)$$

$\alpha = Efficiency\ \ factor$

$\lambda_3 = Group\ reduction\ \ coeifficient\ \ for\ bond$

$$\lambda_4 = \frac{Maximum\ pull\ out\ load\ \ for\ \ fiber\ oriented\ at\ angle\ \theta}{maximum\ pull\ out\ load\ of\ same\ \ fiber\ aligned\ in\ direction\ of\ \ pull\ out}$$

$$\lambda_5 = reduction\ coefficinet\ to\ account\ \ for\ \ fiber\ inclination\ more\ than\ 60\ degree$$
$$with\ pull\ out\ load\ dirrection$$

2.2.2 Types of Fibers and Their Properties

There are large varieties of fibers used with hydraulic cement. Asbestos fibers were oldest fiber used with cement. Other common fibers used are steel and glass fibers (conventional fibers), carbon or Kevlar (new fiber), polypropylene or nylon (low modulus fibers and man-made fiber) and cellulose, sisal, jute (natural fiber).

As fibers are made from various materials such as steel, glass, carbon, or synthetic materials, they also have different geometrical characteristics such as length, diameter, longitudinal shape, cross-sectional shape, and surface roughness. Some common fibers and their typical properties are listed in Table 2.1 [Bentur and Mindness, 2007].

In early period of 1950 and 1960, the conventional fibers (steel and glass fibers) used in FRC were straight and smooth. In order to improve mechanical bonding with cementitious matrix the fibers with more complicated geometries have been developed. In later decades, the steel fibers with profiled shapes, twisted, cramped, hooked or deformed at ends, were manufactured in form of bundled filaments or fibrillated films. They were also used in a continuous form such as mats, woven fabrics or textiles.

Among the various types of fibers discussed earlier, steel fibers are most commonly used in the concrete industries. Steel fibers are of different geometries and

shape. They have varied lengths from 0.5 to 2.5 inches. They also have straight or deformed shapes as shown in Figure 2.3. Most of available commercial steel fibers have a tensile strength of 150 to 350 ksi.

Table 2.1 Typical Properties of Various Types of Fibers [Bentur and Mindness, 2007]

Fiber	Diameter (μm)	Specific gravity	Modulus of elasticity (Gpa)	Tensile strength (Gpa)	Elongation at break (%)
Steel	5-500	7.84	200	0.5-2	0.5-3.5
Glass	9-15	2.6	70-80	2-4	2-3.5
Asbestos: Crocidolite	0.02-0.4	3.4	196	3.5	2.0-3.0
Asbestos: Chrysolite	0.02-0.4	2.6	164	3.1	2.0-3.0
Polypropylene	20-400	0.9-0.95	3.5-10	0.45-0.76	15-25
Aramid (Kevlar)	10-12	1.44	63-120	2.3-3.5	2-4.5
Carbon (high strength)	8-9	1.6-1.7	230-380	2.5-4	0.5-1.5
Nylon	23-400	1.14	4.1-5.2	0.75-1.0	16-20.0
Cellulose	-	1.2	10	0.3-0.5	-
Acrylic	18	1.18	14-19.5	0.4-1.0	3
Polyethylene	25-1000	0.92-0.96	5	0.08-0.60	3-100
Wood fiber	-	1.5	71	0.9	-
Sisal	10-50	1.5		0.8	3
Cement matrix (for comparison)		1.5-2.5	10-45	0.003-0.007	0.02

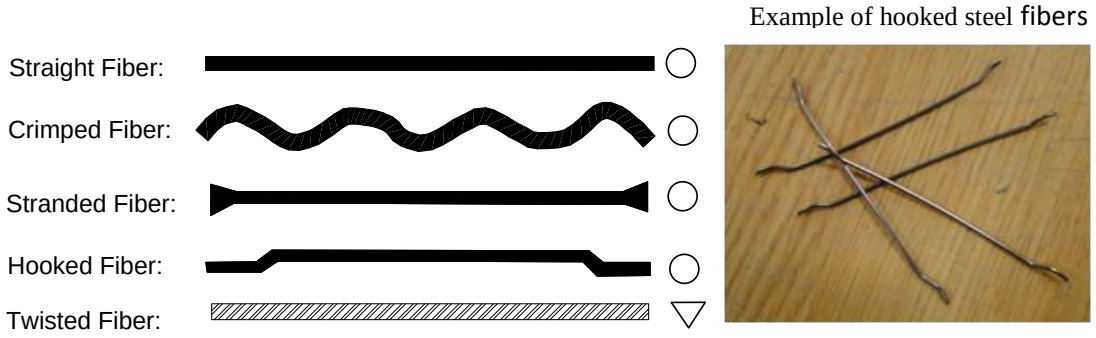

Figure 2.3 Different Types of Steel Fibers

When steel fibers are used in concrete mix, a composite matrix is formed which is known as steel fiber reinforced concrete (SFRC). SFRC has an improved post-cracking behavior compared to that of plain concrete. The performance of SFRC greatly depends on the bond characteristics between the steel fibers and the concrete, the fiber contents, and the distribution of fibers in the concrete matrix.

As discussed earlier, the primary role of steel fibers is to bridge cracks formed in concrete under tension. Fibers can be either fractured or pulled out of the concrete as the cracks open. This phenomenon largely depends upon bond strength of the matrix. Fiber pull-out is more desirable as it makes the SFRC more ductile with absorbing a greater amount of energy.

In order to improve the bond strength of SFRC different types of steel fibers have been developed as discussed earlier. In the early 1960s, only straight steel fibers were in use. As there were no hooked at ends the bond between fiber and concrete was controlled only with friction. Therefore, fibers which have larger surface area to volume ratio can have higher bond strengths. Hence fibers with rectangular sections are more efficient than fibers with circular sections. For the same length, fibers with smaller diameters or higher aspect ratio are more efficient.

2.2.3 Use of Steel Fiber in Concrete

Various literatures have shown that when steel fibers are added to concrete they can improve the various properties of concrete. They can significantly improve concrete's post-cracking tensile resistance and toughness [Hannant, 1978]. SFRC has been used mainly for non-building structural members in the past. It has been used in

construction of industrial floors, bridge deck overlays, airport runways, highway pavements, tunnel linings, spillways, dams, slope stabilizations, and other precast products. For examples they been used in the floor slab for the Chrysler Jefferson North Assembly Plant [Robinson et al., 1991], in the Barr Lake Dam [Mass, 1997], and the Gotthard Base Tunnel [Kronenberg, 2006]. Use of SFRC in building structures has been found very limited. Even though steel fibers have shown some increase in flexural strength and enhance shear strength the main reason behind the limited uses of steel fiber in building structures may be due to lack of design guide lines and provision in building codes.

As discussed above steel fibers have been traditionally applied in non-structure members; like pavement, slope stabilization, lining etc. Some structural application of steel fibers in cast-in-place concrete has begun to increase worldwide. Some more examples of the application of steel fibers outside the U.S. are discussed in the following paragraphs.

Serna et al. [2009] have mentioned the structural application of SFRC in Spain in their paper. They studied two recent applications to promote the use of steel fibers and justified the convenience of SFRC in terms of structural properties evaluation and durability under seawater and its ability to partially or totally replace traditionally reinforcement in this scenario.

Rokongo et al. [2009], has discussed the first design recommendation for high performance fiber reinforced cementitious composites (HPFRCC) with multiple fine cracking and it was published by the Japan Society of Civil Engineers (JSCE).

Similarly, Foster [2009] has discussed the research and application of FRC for use in a structural application in Australia. He summarized the latest experiments and observations obtained from radiographic imaging for the SFRC specimens under loading in the laboratory.

2.2.4 Flexural Properties of SFRC

As per ACI Committee 544 [1988] two strength values should be evaluated from a bending test. These are the first-crack flexural strength and the peak post-cracking flexural strength. These strengths are calculated using the assumption of a linear stress distribution. The first-crack flexural strength is also referred as *modulus of rupture*. This is generally expressed in terms of the square root of the concrete compressive strength. Other important property determined by bending test is the toughness which is defined as the area underneath the load versus deflection curve as discussed later.

Table 2.2 First-cracking Flexural strength of SFRC according to different authors

Authors	Type of Steel Fibers	Volume of Contents	Increase in First crack strength	Other parameters
Shah and Rangan (1871)	Straight fiber	1%	<100%	Rectangular cross sections
Wafa and Ashour (1992)	Not mentioned	1.5%	67%	Aspect ratio: 80
Song and Hwang (2004)	Hooked Steel Fibers	2%	127%	Aspect ratio: 67
Thomas and Ramaswamy (2007)	Hooked steel fibers	0.50 % to 1.5%	Up to 40%	Aspect ratio: 60

Various researchers have found that the first crack flexural strengths have been increased with addition of steel fibers in concrete. Increase in flexural strength of concrete mix depends upon different parameters such as volume of fractions, geometrical properties of fibers. Table 2.2 shows a few selected results for first flexural strength of SFRC obtained by different researchers.

As per Ramakrishnan et al. [1980] hooked steel fibers showed better performance as compared to straight fibers in terms of ultimate flexural strength and flexural toughness. Figure 2.4(a) compares the load versus deflection curves of SFRC with different types of steel fibers. It can be seen that SFRC with hooked steel fibers even with less amount of fibers showed higher first crack and peak strengths. In case of SFRC with hooked fiber the post-cracking strength was found nearly equal to or greater than the first-crack strength. Soroushian and Bayasi [1991] also compared SFRC with hooked fibers and straight fibers and found that SFRC with hooked steel fibers was superior to straight steel fibers as shown in Figure 2.4(b).

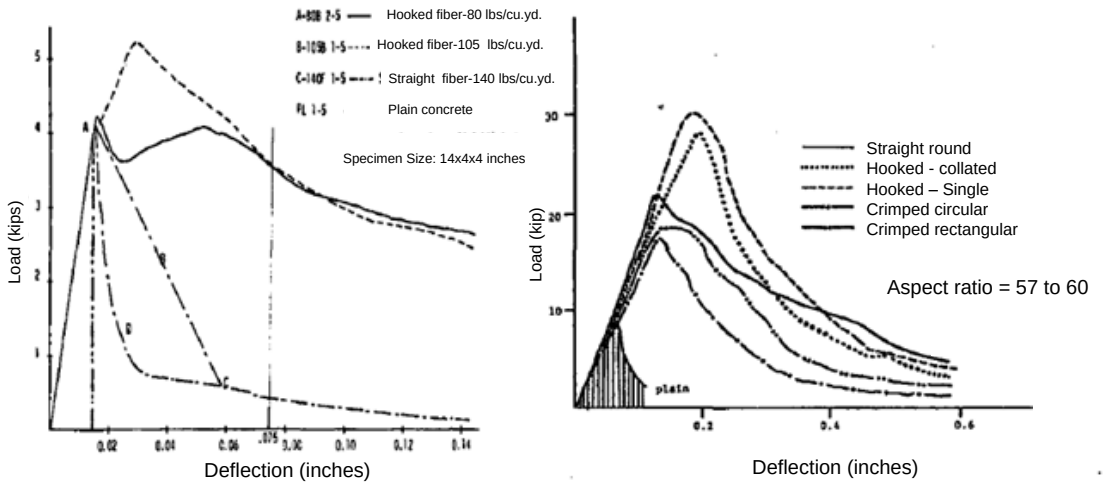

(a) from Ramakrishnan et al., 1980 (b) from Soroushian and Bayasi, 1991

Figure 2.4 Effect of Hooked and Straight Steel Fibers on the Flexural Performance of Concrete

Khaloo and Kim [1996] found that the modulus of rupture was increased with higher values in case of 4.5 ksi concrete as compared to concrete with 7.3 ksi concrete and 12 ksi concrete, even though the type of fibers and fiber volume fractions were same in all case.

2.2.5 Tensile Properties of SFRC

Tensile properties are the constitutive properties of FRC that are useful for modeling and design of FRC structural members. Though the tensile properties are very important parameters for SFRC, due to lack of standard direct tensile tests it is very difficult to assess such properties experimentally. There is no standard test method available in United States to evaluate the direct tensile behavior of SFRC. To achieve similar fiber distribution as in the real structure members, sufficiently large specimen

should be evaluated. In general it is difficult to hold and grip the ends of such large specimens. Therefore, direct tensile test results are usually found scattered. It is also difficult to fix the gauge length for interpreting the strain as the location of crack formation is uncertain. Once the crack form it is widening of the crack. In most of recent direct tensile test results, researchers used the deformation in terms of crack width or extension, particularly for strain-softening materials [Dinh, 2009].

Direct tensile test results for SFRC are very not common and can be hard to determine because of various problems associated with this type of tests. Example tensile stress versus tensile strain curves obtained from direct tensile tests with straight, hooked, and enlarged end steel fibers in a cement-based matrix [ACI Committee 544, 1988] are as shown in Figure 2.5.

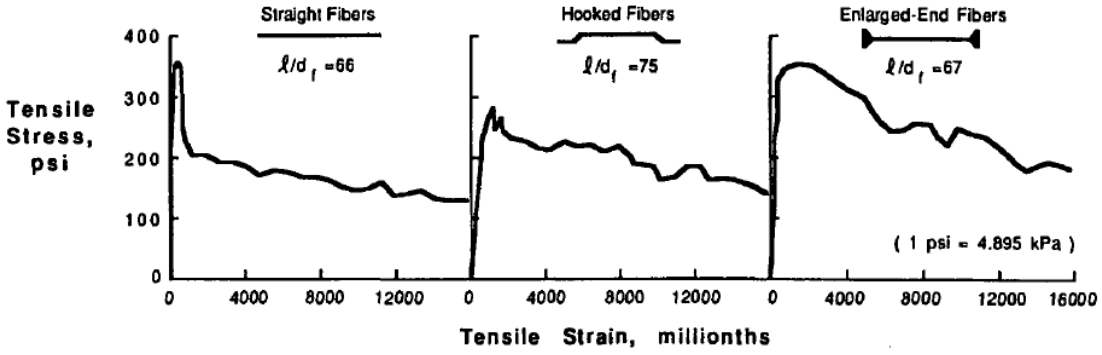

Figure 2.5 Direct Tensile Stress-Strain Curves for SFRC with Different Types of Steel Fibers [ACI Committee 544, 1988]

Lim et al. [1987] tested a dog-bone shaped specimens with a gauge length of 7.87 inches (200 mm) and a width of 2.76 inches (70 mm), to evaluate the performance

of SFRC with straight and hooked steels fibers. Figure 2.6 shows the load-extension relationship for the specimens containing hooked steel fibers with a diameter of 0.02 inches (0.5 mm).

As they did not report the thickness of the specimens, the tensile strength of the specimens could not be determined. From test results it was shown that with the increase in volume fraction of fiber from 0.5% to 1.5% the post-cracking load was also proportionally increased from 1.35 kips (6 kN) to 4.05 kips (18 kN) for same length (see first, second and fourth figure of Figure 2.6). Similarly, the test results also showed that with increase in length from 1.18 inches (30 mm) to 1.97 inches (50 mm) the post-cracking load increased from 2.7 kips (12 kN) to 3.83 kips (17 kN) for same volume of content of 1% (see second and third figure of Figure 2.6).

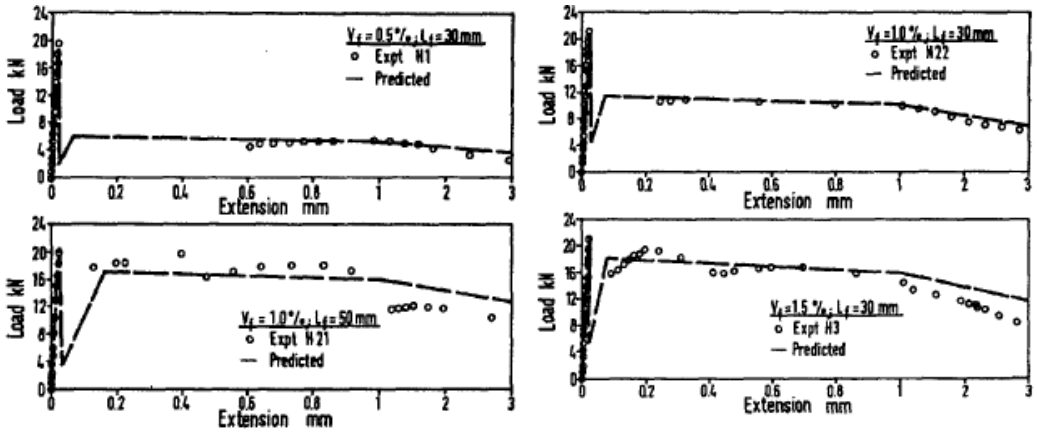

Figure 2.6 Load-Extension Relationships for Different SFRC Mixes
[Lim et al, 1987]

2.2.6 Compressive Properties of SFRC

The various previous studies have shown that use of steel fibers in concrete did not have much improvement on the compressive strength of concrete. The effects of the

steel fiber in compressive strength were found variable. Prior studies showed [Ramakrishnan et al., 1980; Soroushian and Bayasi, 1991; Khaloo and Kim, 1996; and Thomas and Ramaswamy, 2007] that SFRC did not significantly increase the peak compressive strength. Thomas and Ramaswamy [2007] stated that even with 1.5% of fibers the increase in peak strength was under 10%.

On the other hand, Khaloo and Kim [1996] reported that maximum increase in compressive strength was up to 37% for a SFRC with volume fraction of 1.5%. There was only slight increase in the strain at the peak stress. Thomas and Ramaswamy [2007] also reported that the increase in strain at the peak compressive stress was less than 30%. They stated that the key role of steel fibers is only to reduce the rate of strength loss after the peak stress.

Soroushian and Bayasi [1991] carried out some compressive strength tests and found that hooked and crimped steel fibers are more effective in enhancing the compressive strength and post-peak behavior as compared with straight steel fiber (Figure 2.7). They did not notice much difference in the post-peak behavior of concrete with hooked and crimped steel fibers. In case of mortar mixtures, there was also not much increase in compressive strength. Williamson [1974] found no increase at all while Fanella and Naaman [1985] found only slight increase in compressive strength of mortar mixture.

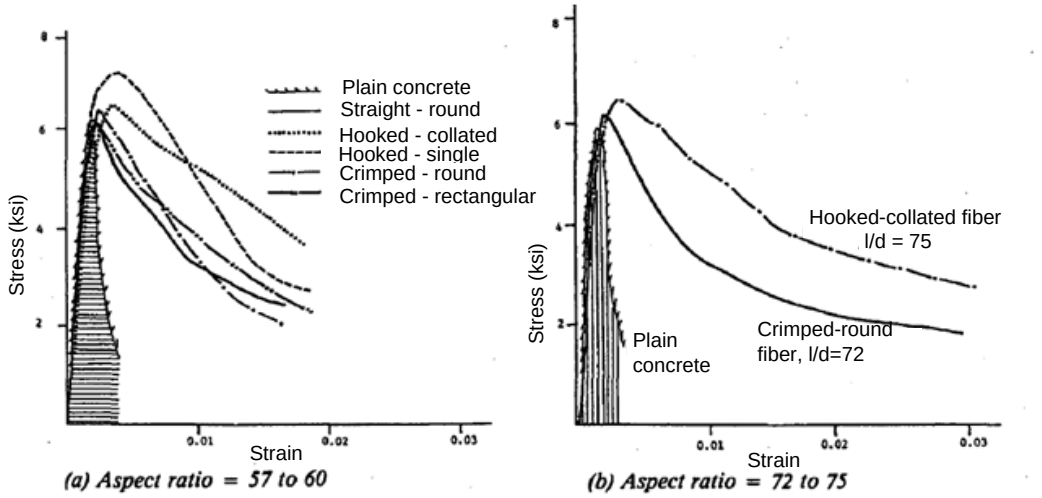

Figure 2.7 Examples of Compressive Stress-Strain Relationships with Different Types of Steel Fibers and Aspect Ratios [Soroushian and Bayasi, 1991]

2.2.7 Flexural Toughness and Ductility Index for SFRC

Toughness is an important characteristic for steel fiber reinforced concrete. Under static loading, flexural toughness may be defined as the area under the load versus deflection curve while in flexure, which is the total energy absorbed to complete separation of the specimen [ACI 544.1R, 1996]. Typical load versus deflection curves for concrete with different types and amounts of fiber are shown in Figure 2.8 [Gao et al, 1997].

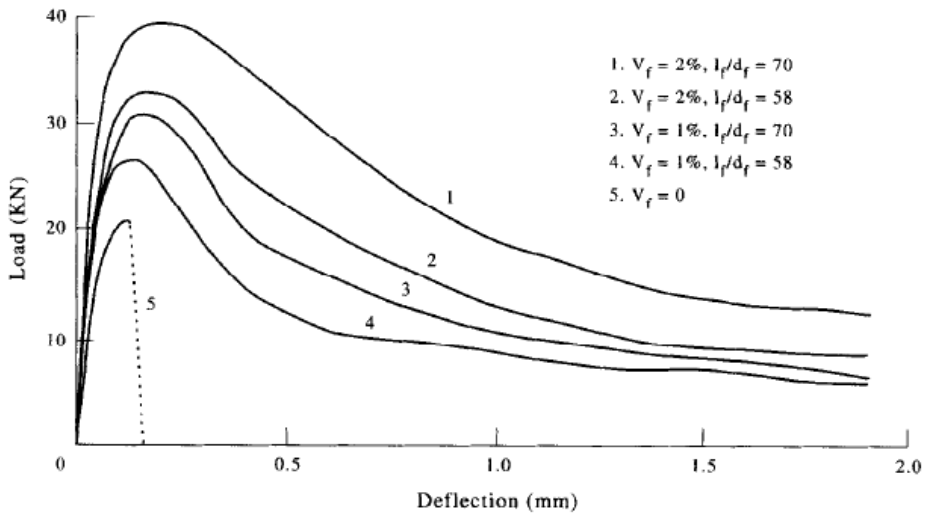

Figure 2.8 Typical Flexural Load-Deflection Curves of SFRC
[Gao et al., 1997]

In general, ductility is mostly qualitative as it is a comparison of the maximum deflection and response after the peak load. Naaman et al. [1992] suggested that a better qualitative ductility measurement can be made in terms of energy absorption (area under curve).

In 2007, Sivakumar and Santhanam developed procedure to determine the flexural toughness index in FRC using the Japanese Concrete Institute's JCI-SF4 ("Method of tests for flexural strength and flexural toughness of fiber reinforced concrete using beam with third-point load"). The toughness index is defined as the sum of the area under the load-deflection curve up to a deflection of 0.12 inches (3 mm) in JCI-SF4. They used hybrid fiber concrete, a combination of metallic and non-metallic fibers. They used up to 0.50% volume of fraction with steel and other hybrid fibers.

As shown in Figure 2.8, as compared to other hybrid fiber reinforced concrete, the flexural toughness of steel–polypropylene hybrid fiber concrete (0.4% steel fiber and 0.1% Polypropylene fiber) was found slightly larger than steel fiber concrete.

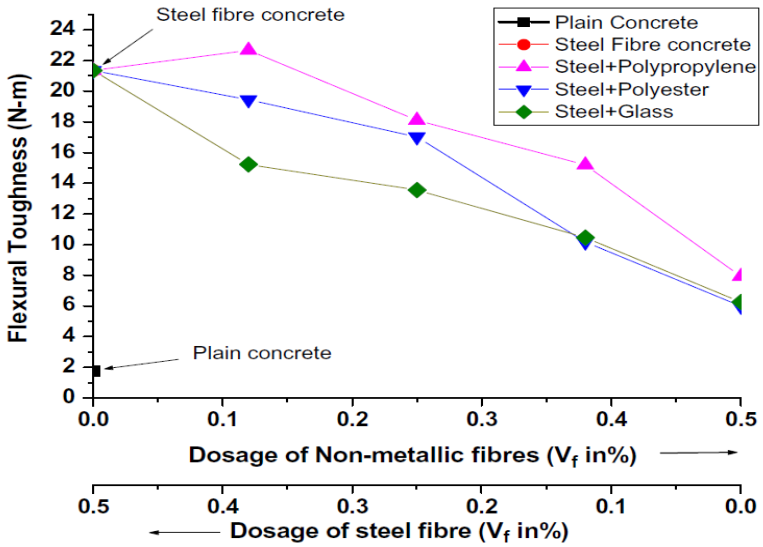

Figure 2.9 Flexural Toughness of Various Hybrid Fiber Concretes
[Sivakumar and Santhanam, 2007]

2.3 Structural Tests of Steel Fiber Reinforced Concrete (SFRC) in Flexure

2.3.1 Failure Modes of Conventionally Reinforced (RC) Beams

When longitudinal reinforcement is added to a beam the flexural strength increases significantly. The beam will exhibit more flexural cracks, as shown in Figure 2.10, due to the ability of the longitudinal reinforcement to bridge cracks and redistribute the stress throughout the concrete. In general, an RC beam fails due to either moment or shear action depending upon sizes of the sections and the amount of

reinforcement of the section. The types of flexural failures depend upon where section is tension-controlled, compression-controlled and d balanced section. Note that although the failures could be grouped into these three types based on the relative stress states in steel and concrete, the ultimate failure is always induced by crushing of concrete no matter which type of failure.

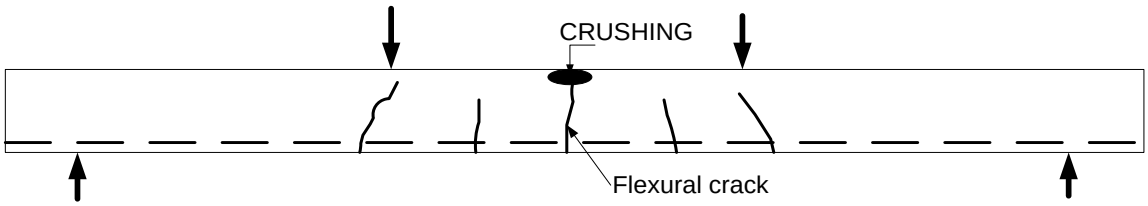

Figure 2.10 Typical Flexural Failures with Multi Cracking and Crushing of RC Beam

2.3.1.1 Tension-Controlled Section

If the steel content in a section of RC beam is small, the steel will reach the yield strength f_y before the concrete reaches its maximum capacity. After the steel yields, the steel force (force in the tension side) remains constant at $A_s f_y$ with further loading (unless the strain hardening is considered). When a section is overloaded, it causes large plastic elongation of the steel across the flexural cracks, resulting in widening of the cracks and a large increase in the strain in the concrete that are in the extreme compression section of the beam. With this increase in strain, the distribution of compressive stress of the concrete along a section becomes distinctly nonlinear. The flexural strength of the section is reached when the strain in the extreme compression fiber of the concrete is reached to approximate 0.003 [ACI 318-11]. With a further

increase in the strain, the strength reduces and the concrete in compression region starts crushing and failure occurs. A typical flexural failure due to positive moment is shown in Figure 2.10. This type of failure is initiated by the yielding of the steel in tension so the section is called as a "tension-controlled section".

2.3.1.2 Compression-Controlled Section

If the steel content of the section is large, the concrete may reach its maximum capacity before the steel in the section yields. The flexural strength of the section is reached when the strain in the extreme compression fibers of the concrete is approximately 0.003. The section then fails suddenly in a brittle fashion if the concrete is not confined, for example a section without stirrups. There may be only little visible warning of failure because the widths of the flexural cracks in the tension zone of the concrete section at failure are small due to low stress in the steel. During this type of failure the steel remains in the elastic range if the stress in the steel (f_s) is less than the yield stress (f_y). This type of section is called as a "compression-controlled section".

2.3.1.3 Balanced Section

In ideal case for a particular steel content of the section, steel reaches yield strength f_y and concrete of the extreme fiber reaches to maximum compression strain of 0.003 simultaneously. In this case, the flexural failure occurs in this manner is named balanced failure.

The ratio steel content ratio for a balanced section is given by the following equation [Wight and MacGregor, 2011];

$$\rho_b = \frac{0.85 f_c^{'} \rho_1}{f_y} \frac{0.003 E_s}{0.003 E_s + f_y} \qquad (2.9)$$

ACI 318-11 uses the net tensile strain ε_t to define the tension-controlled, compression-controlled, and transition section. For tension-controlled sections, the net tensile strains in the outermost layer of steel (ε_t) should be greater than or equal to 0.005 (Figure 2.10).The net tensile strain (ε_t) is the tensile strain in the extreme tension steel at nominal strength exclusive of strain due to prestress, creep, shrinkage and temperature.. If the value of ε_t is less than 0.002, the section is compression-controlled. In between for value of ε_t from 0.002 to 0.005, the section is under transition zone and strength reduction factor (ϕ) is calculated based on equation as shown in Figure 2.11.

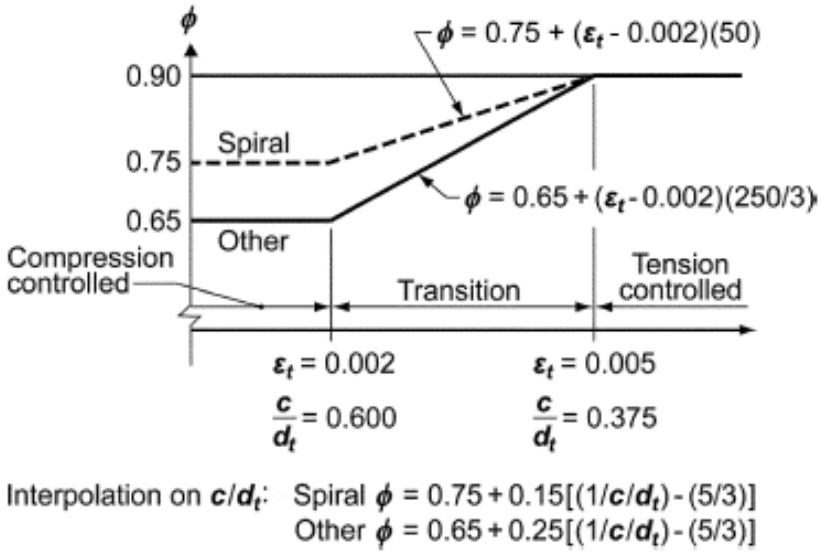

Figure 2.11 Variation of ϕ with Net Tensile Strain in Extreme Tension Steel, ε_t, and $\frac{c}{d_t}$ for Grade 60 Reinforcement and Prestressing Steel [ACI 318-11].

2.3.2 Behavior of a Continuous Beam

When a continuous beam (an indeterminate structure) is loaded the largest moments typically occur near mid-spans and internal supports. In common case the greatest moments are the negative moments at interior supports. As the beam is further loaded possibility of formation of plastic hinges due to the yielding would start at internal supports. For instance let's look at a two-span continuous beam shown in Figure 2.12 and assume the external moments in interior supports due to applied point loads at mid-spans are greater than moments at mid-spans. The first yielding occurs at interior supports and plastic hinges form when moment capacity of the section is exceeded by moment induced by the applied load at that section. When the plastic hinge forms in the interior support, the member has three hinges and member becomes

statically determinate structure, which is equivalent to two simply-supported beams sitting together.

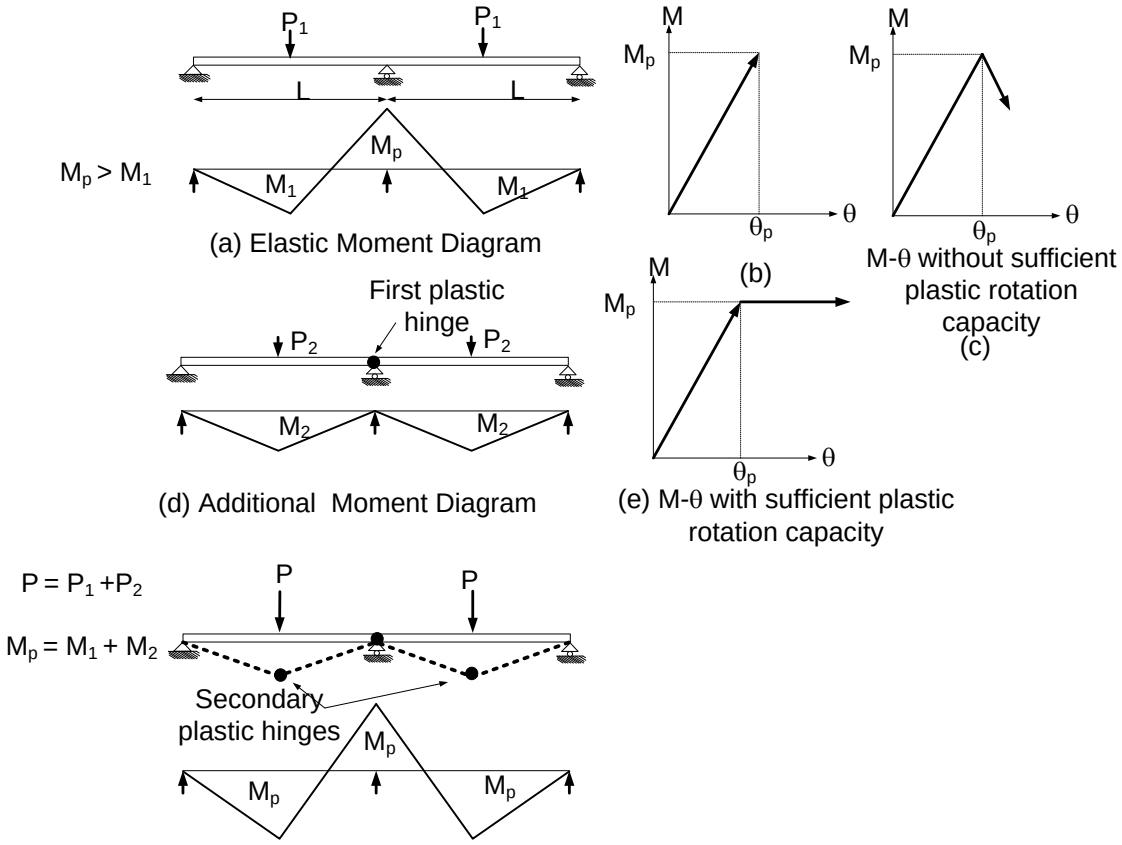

Figure 2.12 Moment Redistribution in Continuous Beams (assuming EPP model for plastic hinges)

If the section has not sufficient rotational capacity, as shown in Figure 2.12(c), structure immediately failed without taking any additional load. If the section has sufficient rotational capacity as shown in Figure 2.12(e), the entire beam can take further load without increasing total moment in first yielded section. So after first yielding occurs the moment is redistributed to other sections (mid-spans) which are still elastic. In this way the mid-spans of the member can take addition load (Figure 2.12

(d)) until those sections yield and other plastic hinges form. As moment at mid-span reaches the plastic moment capacity this section yields and additional plastic hinge forms. Then the yield mechanism forms and failure occurs. In this way the structure is able take total load of P even though some section reaches its moment.

In order to have the moment redistribution to occur an interior support of a continuous beam member should have a high ductility (inelastic rotational capacity).

2.3.3 Rotational Capacity and Moment Redistribution in RC Beams

As per Section 8.4 of ACI 318-11, a negative moment calculated by elastic theory at support of the continuous flexural members shall be permitted to be redistributed (increase or decrease) for any loading arrangement (Figure 2.13). The amount of redistribution may not be more than $1000\varepsilon_t$ percent, with a maximum of 20 percent; ε_t is the net tensile strain in the steel. This redistribution of negative moments shall be made only when ε_t is equal to or greater than 0.0075.

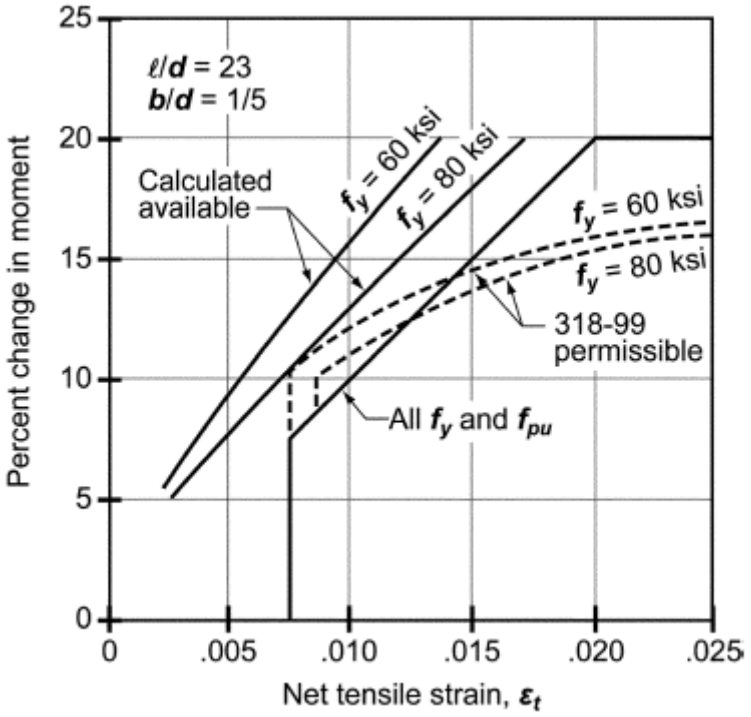

Figure 2.13 Moment Redistribution in Continuous Member Based on Net Tensile Strain ε_t [ACI 318-11]

In order to have the redistribution of moments in reinforced concrete continuous beams, the section should have high ductility, which is generally achieved when ε_t is greater than or equal to 0.0075 as per the ACI 318-11 provision. As a consequence the longitudinal reinforcement ratio is to be limited to certain upper bound amount.

As per studied carried out by Kenneth [2003], the limit of moment redistribution in mid-span can be more liberal even up to 30% for prestressed continuous beams. Since there is secondary moment induced due to prestressing force which decreases the moment at mid-span and increases the moment at interior support.

In order to fulfill the criteria as per ACI code for the moment redistribution and to make the section sufficiently ductile, the tensile longitudinal steel ratio should be limited. For example for the section with $f'_c = 4\ ksi$ concrete and $f_y = 60$ ksi the longitudinal tensile steel ratio of the section is only about 1.3% as per equation $\left[\rho = 0.85\beta_1 \frac{f_c'}{f_y} \frac{0.003}{0.003 + \varepsilon_t}\right]$ [Nilson et al.,2010] . Hence larger sizes of the beam section should be provided if the moment demand is large. This leads to uneconomical use of beam sections due to increase in the self-weight in case of long span PC girders of a bridge.

As discussed earlier when a section has larger longitudinal tensile reinforcement ratio it will be less ductile and the section tends to be compression-controlled and brittle failure can occur. If the ductility of the interior support of a continuous beam section can be improved even with high longitudinal tensile reinforcement ratio in the section, the moment redistribution will be possible if the section have sufficient inelastic rotation. The steel fiber reinforced concrete could permit this situation because previous studies have shown that the steel fibers can increase both the ductility and shear strength of concrete. So it is possible to use smaller section with greater amount of longitudinal steel ratio with reduction on sizes and shear reinforcement. However, only limited and small-scale investigations were carried out in the past to study the flexural behavior of fiber reinforced concrete beams. The prior studies carried out for small-scale fiber reinforced concrete beams, are discussed later.

In order to study moment redistribution and rotational capacity of steel fiber reinforced concrete beams the test of large-scale continuous beams is necessary. However testing of large-scale continuous beams is complex, time-consuming and expensive. In this regard, prior research by Mattock [1964] has indicated that the distribution of moment of simply supported beam can be used to somewhat represent the distribution moment near the interior support of inverted continuous beam as shown in Figure 2.14.

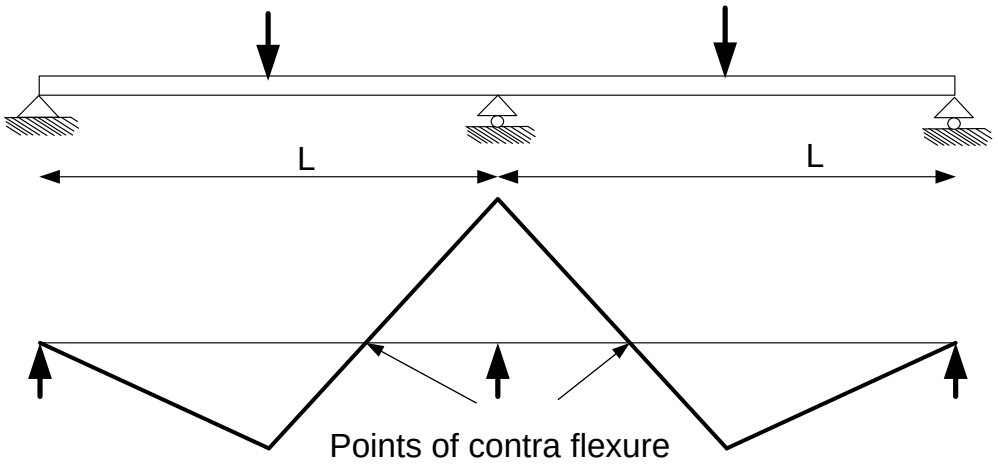

(a) Moment diagram in Continuous Beam

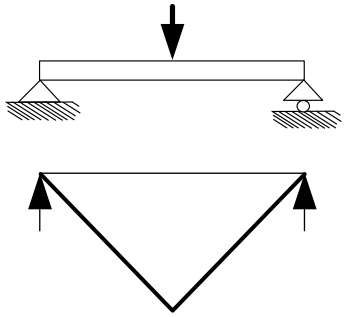

(b) Moment diagram in Simple supported Beam

Figure 2.14 Comparisons of Moment Diagrams in Continuous and Simply Supported Beams

In this regard Mattock [1964] has carried out study with reinforced concrete beams. He had conducted an investigation on the rotational capacity of reinforced concrete beams in the region of the plastic hinge. He investigated thirty seven beams of different geometries, concrete, and steel grades. The beams were tested through a simply supported layout. The loads were applied through a 1 × 3 × 6 inches (depth ×

width × length) steel plate on the top surface of the beam at the mid-span. He used the moment induced by the point load at the mid span of the beams in order to stimulate the distribution of moment at the internal support of the continuous beams. As shown in Figure 2.15, half of the span of a simply supported beam represents that portion of a continuous beam between the interior support and an adjacent point of contra flexure.

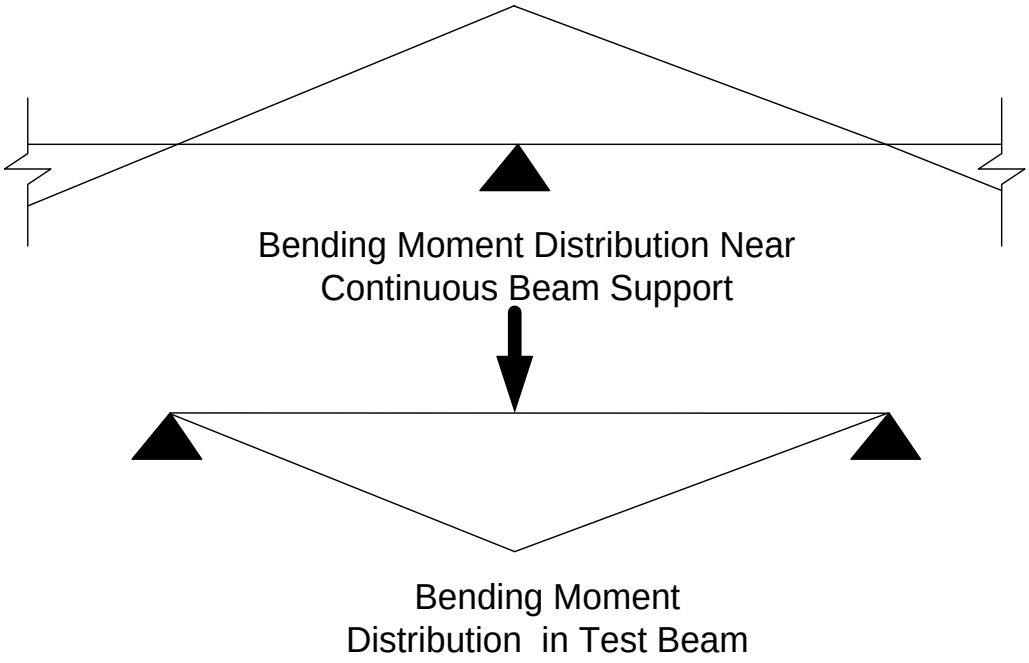

Figure 2.15 Moment Diagrams in Continuous and Simply Supported Beams [Mattock, 1964]

The maximum moment for simply supported beams loaded at the mid span through steel plates can be determined as follows;

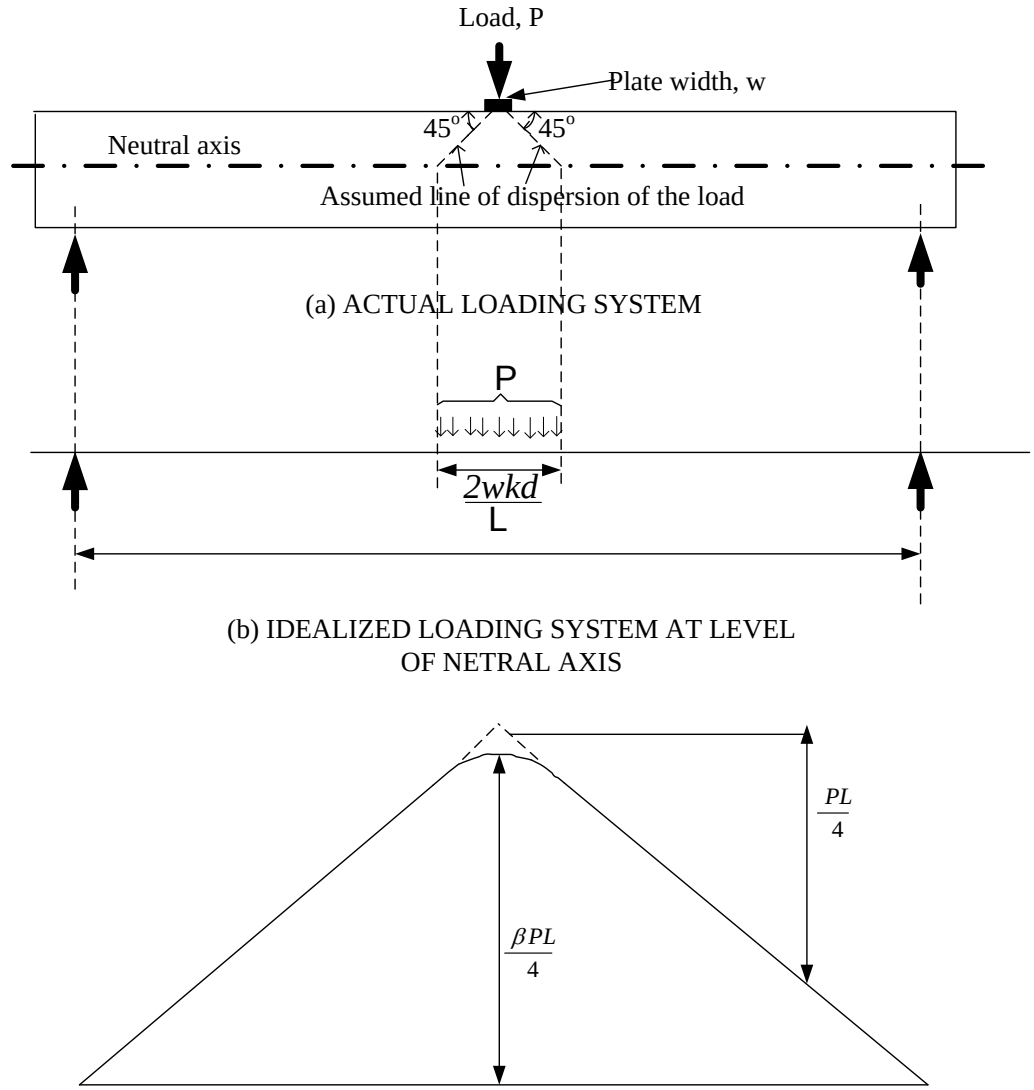

Figure 2.16 Bending Moment Diagram Due to Idealized Loading through a Steel Plate at Mid-Span [Mattock, 1964]

It was assumed that the load P is dispersed at 45 degrees, as shown in Figure 2.16. The maximum moment can be determined by;

$$M = \frac{\beta PL}{4} \tag{2.10}$$

Where,

$$\beta = \left[1 - \left(\frac{w + 2kd}{2L}\right)\right] \quad (2.11)$$

Hence the expected failure load is more than the concentrated load as the β factor is less 1.

2.4 Prior Investigation and Research Works with SFRC Beams

2.4.1 SFRC Beams Tests

As discussed earlier there are very limited numbers of studies on flexural behavior of SFRC beams. Most of these studies are of small-scale and for shear behavior of SFRC. The depths of the beams are only about 10 inches. Some previous studies with test of SFRC beams are reviewed below.

Naaman et al. [1992] carried out some studies with SFRC beams including beam sections with high longitudinal steel ratio and larger volume of content of steel end hooked fibers. The type of SFRC they used was the slurry infiltrated fiber concrete (SIFCON) (with higher volume of content of fiber). The test was carried out in a four-point loading for seven 118 × 10 × 6 inches (length × height × width) rectangular beams and two 118 × 12 × 5 inches (length × height × width) T-beams with fiber volume contents ranging from 3.5% to 8.8%. The percentage of conventional reinforcement ranged from 1.48% to 8.4%. From moment versus deflection curves (Figure 2.17) it can be seen that RC beam with high percentage of longitudinal reinforcement (compression-controlled) failed immediately when it reached to peak load. However, it was shown that there even with very high longitudinal steel ratio

(8.4%) the SFRC beam exhibited some ductility and energy absorption with the use of a SIFCON matrix. The ductility increased with decrease in steel ratio. The use of a SIFCON matrix in led to smaller crack spacing and narrow crack width. The SIFCON matrix changed the crack development for reinforced concrete. The crack formation increased in number up to the yielding of the steel in case of SIFCON matrix with steel fiber.

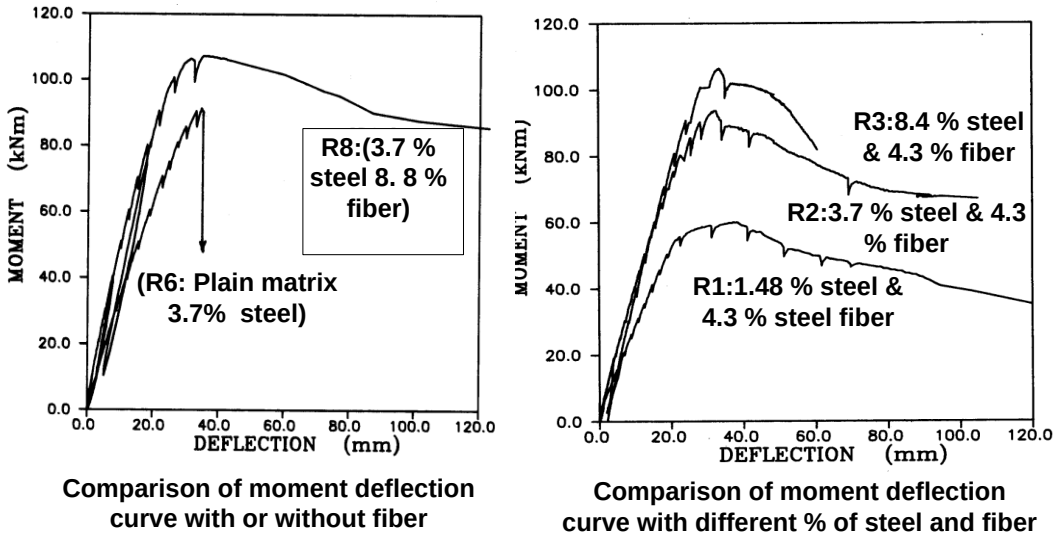

Figure 2.17 Moments versus Deflection Curves for SIFCON Matrix Beams (Naaman et al., 1992)

Naaman and et al. [1992] also discussed about energy absorption. The ductility index can be defined as the ratio of ultimate deflection to deflection at yielding of the tensile reinforcement. The deflection at which the load is stopped may be considered to be the ultimate deflection. Similarly, the energy ratio is defined as the ratio of energy at the end of the test to the energy at the yielding of the first tensile reinforcement.

Ductility can no doubt be defined as the ability to absorb the inelastic energy without losing its loading capacity. Higher inelastic energy means higher ductility.

Similarly, Swamy et al. [1981] conducted small-scale tests of 110 × 8 × 5 inches (length × depth × width) beams with conventional reinforcement as well as crimped steel fibers. They tested several beams with a fiber content ranging from 0.5% to 1% with a single point loading at the mid-span. They had provided fiber in the concrete for the whole depth of the beam or in the effective tension zone surrounding the steel reinforcement bars. It was shown that although the increase in ultimate strength was only marginal, fiber arrested the advancing cracks and increased the post-cracking stiffness at all stages of the loading up to failure. The beams with fiber in the whole depth of the beam generally resisted more deformation than the beam without fiber or the beam with fiber located only in the tension zone. The maximum compressive strains measured in the concrete ranged from 0.005 to 0.006. In most of the beams, the tension bar yielded before failure, and after yielding of the bar the beam exhibited significant inelastic deformations.

Williamson and Knab [1975] carried out some full-scale testing on conventionally reinforced concrete beams with steel fibers. They compared four beams with and without shear reinforcement. They used a 1.5% volume fraction of steel fibers in the SFRC beams. The same longitudinal reinforcements were used for all of the beams. They found that the beam without shear reinforcement had a lower ultimate strength than the other beams (for both plain and SFRC beams). SFRC beams without shear reinforcement failed in shear with a slightly lower ultimate load than the beam

with shear reinforcement, which did not fail in shear. The reason this failure occurred was because there was no yielding of the tensile bars as they provided higher longitudinal ratio (2.6%) and the beams failed in shear prematurely meaning the beams failed in shear prematurely. The energy obtained for all of the beams, except the beam without the shear reinforcement, was almost same.

Kwak et al. [2003] conducted experimental studies on small-scale SFRC beams of sizes 60-90 × 10 × 5 inches (length × height × width) with conventional reinforcement. They tested several SFRC beams with steel fiber fraction of 0%, 0.5% and 0.75%, with three shear spans (a/d ratio) of 2, 3, and 4 and with two concrete compressive strength of 4.5 ksi and 9.5 ksi. From the test results they concluded that both initial shear stress in first cracking and ultimate shear strength was increased with use steel fibers. The shear strength was increased by about 70% for beams with smaller a/d ratio and 22 to 28% for beams with larger a/d ratio. Results also showed that steel fiber also decreased crack spacing, sizes, increased deformation capacity and ductility of SFRC beams.

2.5 Prediction of Ultimate Nominal Strength for SFPRC and PC Beams

2.5.1 Ultimate Strength of Prestressed Concrete (PC) Beam (Without Steel Fiber)

The ultimate load of a prestressed concrete beam without steel fiber (PC) can be calculated based on ACI 318-11. By knowing the cross-sectional dimensions, material properties, and amount of reinforcement, the nominal moment at the ultimate load of

the section can be determined. Widely accepted assumptions mentioned in the various codes, including the ACI code, were considered:

- Plane sections remain plane under loading
- There is a perfect bond between steel and concrete
- The limiting compressive strain of concrete ε_{cu} is equal to 0.003
- Tensile strength of concrete is negligible and not taken in to account.

The total force in the concrete compressive zone can be accurately approximated by this behavior, as shown in Figure 2.18. The typical stress-strain curves for pre-stressing steel and reinforcing steel is shown in Figure 2.19. It was assumed that the stress-strain curve for mild steel reinforcement as elastic and perfectly plastic and yield strength f_y as the ultimate stress of the steel.

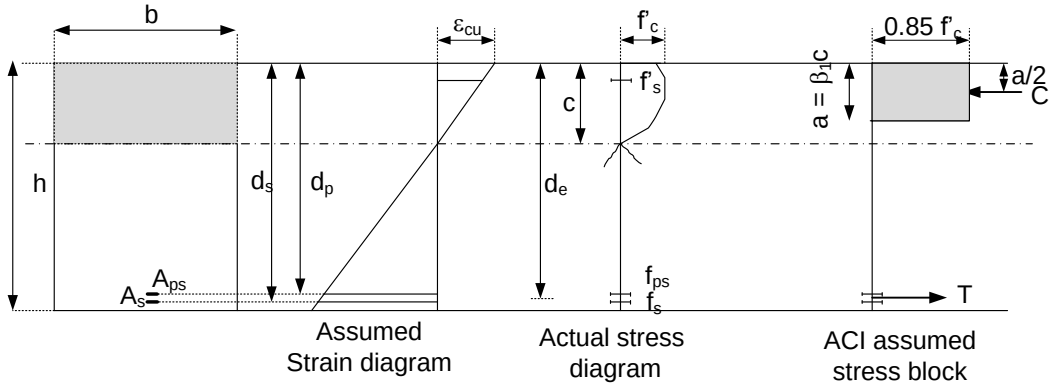

Figure 2.18 Stress and Strain at Ultimate Behavior, as Assumed by the ACI Code [Naaman, 2004]

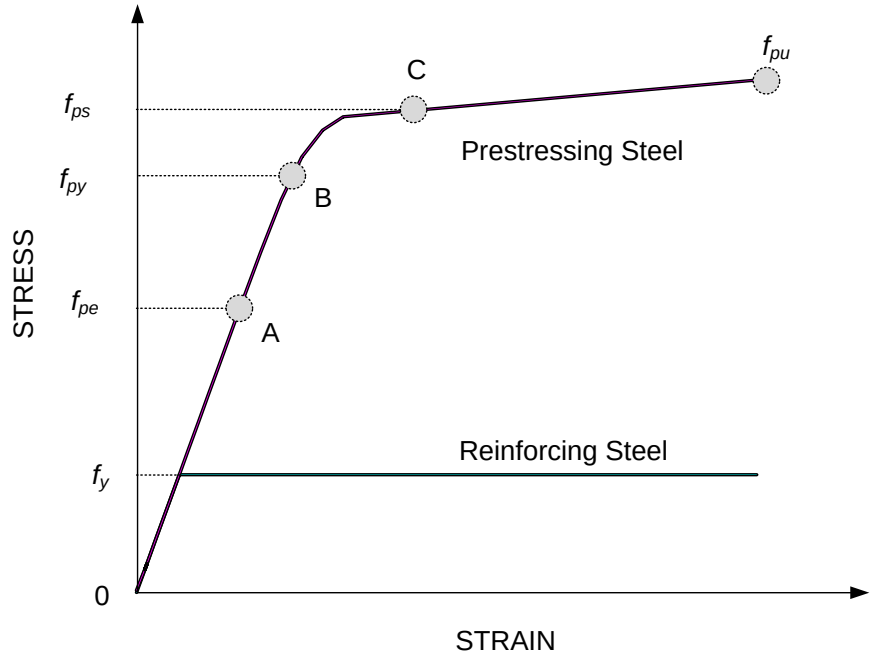

Figure 2.19 Typical Stress –Strain Curves Assumed for Reinforcement [Naaman, 2004]

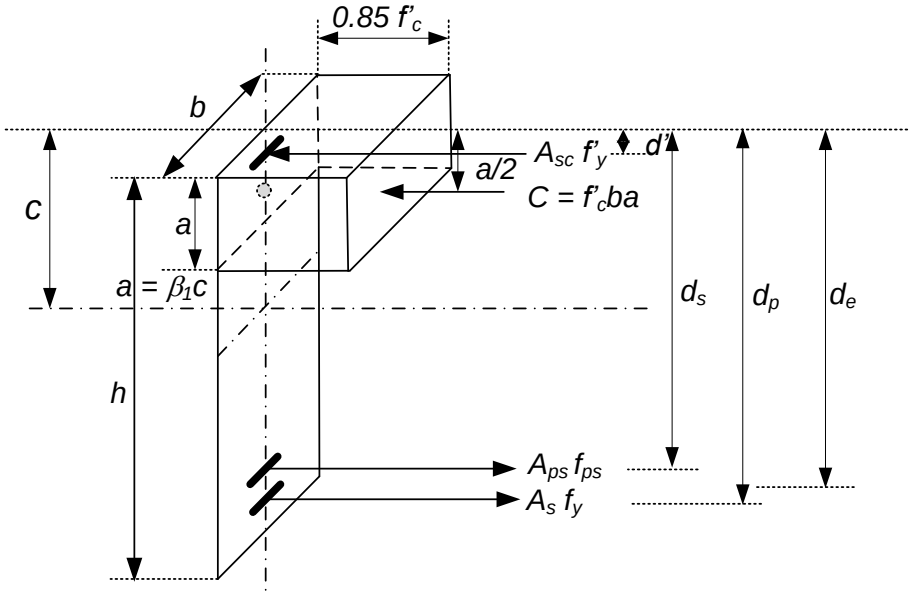

Figure 2.20 Rectangular Section Forces at Ultimate for Partially Prestressed Concrete Beam [Namaan, 2004]

The equilibrium equation of the compressive and tensile forces, as shown in Figure 2.20, can be determined in the following manner;

$$0.85 f'_c b \beta_1 c = 0.85 f'_c a = A_{ps} f_{ps} + A_s f_y - A_{sc} f'_y \qquad (2.13)$$

Where,

A_{ps} = *the area of the pre-stressing reinforcement in the tensile zone*

f_{ps} = *the stress in the pre-stressing steel at the nominal flexural resistance of the section*

A_s = *the area of the non pre-stressed tension reinforcement*

f_y = *the specified yield strength of the non pre-stressed tensile reinforcement*

A_{sc} = *the area of the non pre-stressed compression reinforcement*

f'_y = *the specified yield strength of the non pre-stressed compression reinforcement*

c = *the depth of the neutral axis at the ultimate load*

a = *the depth of the rectangular stress block* = $\beta_1 c$

b = *the width of the section*

Then, a can be calculated as follows;

$$a = \frac{A_{ps} f_{ps} + A_s f_y - A_{sc} f_y}{0.85 f'_c f_{ps} b} \qquad (2.14)$$

The moment resistance of the section is given by the following equation;

$$M_n = A_{ps} f_{ps} \left(d_p - \frac{a}{2} \right) + A_s f_y \left(d_s - \frac{a}{2} \right) - A_{sc} f'_y \left(d' - \frac{a}{2} \right) \qquad (2.15)$$

f_{ps} can be calculated as follows;

$$f_{ps} = f_{pu}1 - \frac{\gamma_p}{\beta_1}\left\{\rho_p \frac{f_{pu}}{f_c^{'}} + \frac{d_s}{d_p}\left(\omega_s - \omega^{'}\right)\right\} \quad (2.16)$$

Where,

$$\rho_p = \frac{A_{ps}}{b\,d_p}, \omega_s = \frac{A_s f_y}{bdf_c^{'}}$$

If compression steel is used, then

$$\rho_p \frac{f_{pu}}{f_c^{'}} + \frac{d_s}{d_p}\left(\omega_s - \omega'\right) \geq 0.17, d' \leq 0.15 d_p$$

and $\gamma_p = 0.4$ *for* $f_{py} \geq 0.85 f_{pu}$

$$\beta_1 = 0.85 - 0.05\left(\frac{f'_c - 4000}{1000}\right) \quad (2.17)$$

Ultimate load $P = \frac{4\phi M_n}{L}$

ϕ is taken as 1.0 because the load is exactly measured during the test.

L = the distance between the two supports of the beam.

The cracking load is given by $P_{cr} = \frac{4M_{cr}}{L}$ (2.18)

Where,

$$M_{cr} = A_{ps} f_{pe}\left(e_o + \frac{Z_b}{A_c}\right) - f_r Z_b \quad (2.19)$$

Where,

$f_{pe} = 0.55 f_{pu}$, $A_c = bh$, $Z_b = I / Y_t$ and,

the tensile stress in the conc*rete*, $f_r = 7.5\sqrt{f_c^{'}}$

2.5.2 Ultimate Strength of SFRPC Beams

2.5.2.1 Ultimate Strength Prediction for SFRC Beams (without rebar only with fibers)

Various researchers [e.g. Schrader and Lankard, 1983; Landkard, 1972; Swamy et al. 1972] have developed different methods to predict the flexural strength for small SFRC beams (reinforced only with steel fibers). Swamy et al. [1972] proposed equations based on theoretical derivation with coefficients obtained from regression analysis of test data. The equation for the first crack composite strength, in psi, is:

$$\sigma_{cf} = 0.845\, f_r V_m + 425 V_f \frac{l}{d_f} \qquad (2.20)$$

And the equation for ultimate composite flexural strength, in psi, is

$$\sigma_{cu} = 0.97\, f_r V_m + 494 V_f \frac{l}{d_f} \qquad (2.21)$$

Where,

f_r = stress in the matrix (modulus of rupture of the plain concrete mortar or concrete), in psi

V_m = *the volume fraction of the matrix = 1-*V_f

V_f = *the volume fraction of the fiber*

$\frac{l}{d_f}$ = *the ratio of the length to diameter of the fibers (aspect ratio)*

As those equations were developed based on laboratory testing or small scale testing it might not be extrapolated for larger beams. If these equations were used to

predict the strength of cast-in-place large beams; variations could be more than 50% as compared to the actual values [Swamy et al., 1972].

2.5.2.2 Ultimate Strength of SFRC Beams with Bars and Fibers

Henagar and Doherty (1976) developed a method for predicting the strength of beams with both reinforcement bars and steel fibers. The method is similar to the ACI ultimate strength method. The tensile strength computed for fiber concrete is added to that contributed by the reinforcing bars to obtain the ultimate moment. The basic assumptions made by Henagar and Doherty are shown in Figure 2.21.

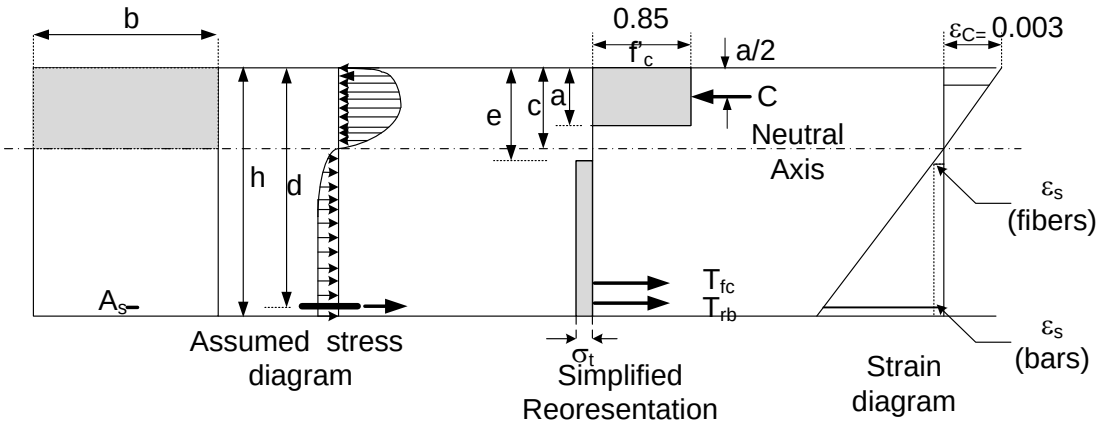

Figure 2.21 Design Assumptions for Analysis of Singly Reinforced Concrete Beams Containing Steel Fibers [Henagar and Doherty 1976]

Based on Figure 2.20, the equation for nominal moment, M_n, for a singly reinforced SFRC beam is given by;

$$M_n = A_s f_y \left(d_s - \frac{a}{2} \right) + \sigma_t b (h - e) \left(\frac{h}{2} + \frac{e}{2} - \frac{a}{2} \right) \quad (2.22)$$

$$e = [\varepsilon_s (fibers) + 0.003] c / 0.003 \quad (2.23)$$

Where

$$\sigma_t = 1.12\,\rho_f F_{be}\,(l / d_f)$$

l = the fiber length

d_f = the fiber diameter

*ρ_f = the percent by volume of steel fiber*s

F_{be} = the bond efficiency factor of the fiber, which varies from 1.0 to 1.2 depending on the fiber characteristics

a = the depth of the rectangular stress block

b = the width of the beam

c = the distance from the extreme compression fiber to the neutral axis found by equating the internal tension and compression forces

d = the distance from the extreme compression fiber to the centroid of the tensile reinforcement

e = the distance from the extreme compression fiber to the centroid of the tensile block of fibrous concrete (Figure 2.21)

ε_s = the tensile strain in the steel at the theoretical moment strength of the beam, for bars = f_y/E_s and for fibers = σ_f/E_s based on the fiber stress developed at pullout with dynamic bond stress of 333 psi [Henagar and Doherty 1976]

ε_c = the ultimate compressive strain in the concrete

f'_c = the compressive strength of the concrete

f_y = the yield strength of the reinforcement bar

A_s = the area of the tension reinforcement

C = the compressive force

h = the total depth of the beam

σ_t = *the tensile stress in the fiber concrete*

E_s = *the modulus of elasticity of steel*

T_{fc} = *the tensile force of the fibers concrete* = σ_t *b (h-e)*

T_{rb} = *the tensile force of the bar reinforcement* = $A_s f_y$

In the analysis above, the maximum usable strain at the extreme concrete compression fiber was taken as 0.003, which was conservative based on the data provided by various researchers, shown in Table 2.3.

Table 2.3 Usable Strain at Extreme Concrete Compression Fiber at ultimate Suggested by Different Researcher [ACI Committee 544, 1988]

S.N.	Researcher	Suggested concrete strain (ε_c)
1	Williabmson (1973)	0.0033
2	Pearlman (1979)	0.0033
3	Swamy and et al. (1979)	0.0035
4	Hossun and Sahebjam (1985)	0.0035 (V_f =1%)
5	Hossun and Sahebjam (1985)	0.0040 (V_f =1 to 4%)

Swamy et al. (1981) used 0.0035 ultimate strain values in concrete to predict the ultimate load for their study. The ultimate strength analysis was based on the conventional reinforced concrete beam theory taking into consideration of the contribution of fibers in the tension zone. The actual and assumed stress versus strain distributions are shown in Figure 2.22.

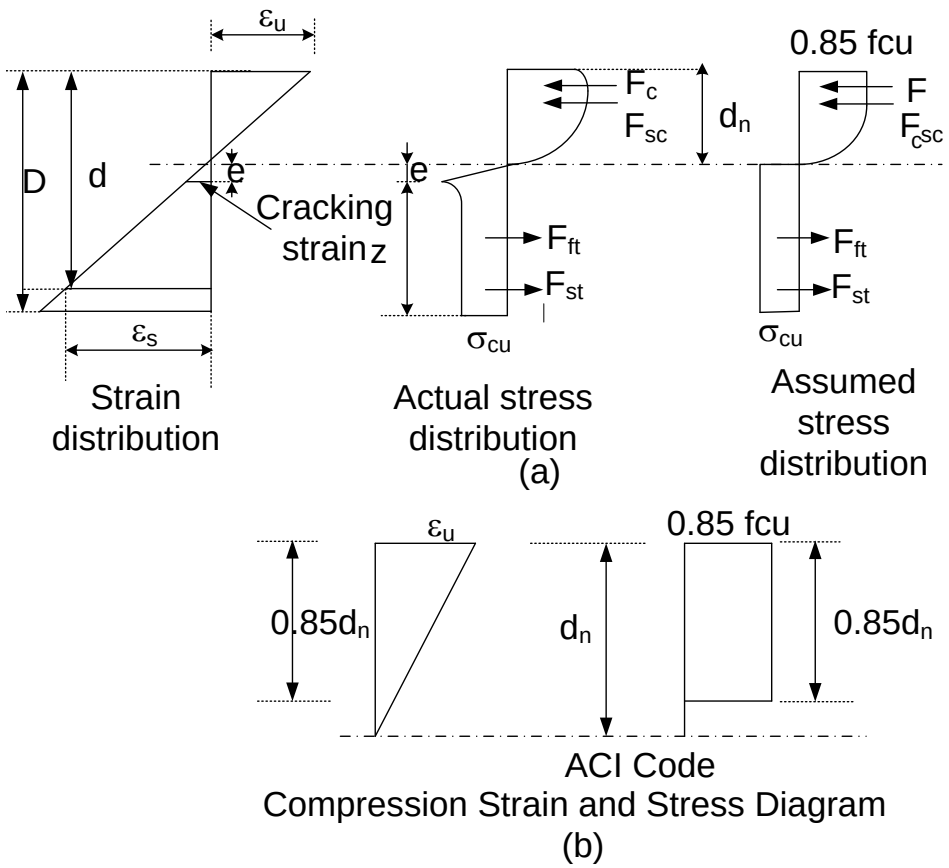

Figure 2.22(a) Stress and Strain Distributions at Failure and (b) Stress and Strain Diagram for Concrete in Compression Block [Swamy and et al., 1981]

The cracking stress of the steel fiber concrete composite in direct tension is given as;

$$\sigma_{cr} = \sigma_{mu} V_m + \sigma'_t V_f \qquad (2.24)$$

Where,

σ_{mu} = *the cracking stress of the matrix*

σ'_f = *the stress in fibers at the matrix cracking*

V_m = *the volume fraction of the matrix*

V_f = *the volume fraction of fibers*

In case of SFRC when the concrete cracks, it may be assumed that the entire stress is carried by the fibers. Hence the ultimate strength of the SFRC composite is given in terms of fracture strength of the fiber (σ_{fu}).

$$\sigma_{cu} = \sigma_{fu} V_f \tag{2.25}$$

If a perfect bond between the fibers and the matrix is assumed, then σ_{fu} is given by:

$$\sigma_{fu} = 2\tau \frac{l_f}{d_f} \tag{2.26}$$

where l_f and d_f are the length and diameter of fibers, respectively. Thus, σ_{cu} becomes;

$$\sigma_{cu} = 2\tau \frac{l_f}{d_f} V_f \tag{2.27}$$

To account for the several other factors such as uniform distribution and randomly oriented fibers [Swamy et al., 1974] Equation 2.27 becomes;

$$\sigma_{cu} = \eta_o \eta_L \eta_b 2\tau \frac{l_f}{d_f} V_f \tag{2.28}$$

Where η_o = the orientation factor, determined to be 0.41 for three dimensional random orientation [Romualdi and Mandel, 1964], and

η_b = the bond efficiency factor depending upon the shape of the fiber, such as smooth, hooked, crimped, or etc., (1.2 for crimped fiber) and

η_L = the length correction factor suggested [Cox, 1952] can be determined as follows;

$$\eta_L = 1 - \frac{\tan h\left(\beta l_f / 2\right)}{(\beta l_f / 2)} \tag{2.29}$$

where l_f is the fiber length and β factor is determined by

$$\beta = \sqrt{\frac{2\pi G_m}{E_f A_f ln\left(S / r_f\right)}} \tag{2.30}$$

Where G_m is the matrix shear modulus, A_f is the fiber cross sectional area, r_f is the fiber radius, and S is the mean centroid spacing in mm given by;

$$S = 25\sqrt{\frac{d_f}{\rho l_f}} \tag{2.31}$$

The equilibrium force in the tension zone and the compression zones are given by;

Tensile force due to steel fiber $F_{ft} = \sigma_{cu} b\left(D - d_n\right)$ (2.32)

Tensile force due to tensile reinforcement $F_{st} = A_s f_f$ (2.33)

Compression forced due to concrete $F_c = \frac{0.85 f_{cu}}{\epsilon_u}\left(\epsilon_u - \frac{\epsilon_0}{3}\right) b d_n$ (2.34)

Compression force due to compression reinforcement

$$F_{sc} = \frac{d_n - d'}{d_n} \epsilon_u E_s A'_s \tag{2.35}$$

Equating the values of the tension and compression forces, d_n can be determined by trial and error. Then the ultimate moment of resistance is given by;

$$M_u = F_c\left(d_n - k_2\right) + F_{sc}\left(d_n - d'\right) + F_{st}\left(d - d_n\right) + F_{ft}\left(\frac{D - d_n}{2}\right) \tag{2.36}$$

Where k_2 is the distance from the extreme compression face to the centroid of the compression block can be determined by:

For ACI, $k_2 = 0.425 d_n$

(2.37)

Finally stresses in compression and tension steel were calculated and checked for yielding.

$$f_s^{'} = \frac{d_n - d'}{d_n} 0.003 E_s \qquad f_s = \frac{d - d_n}{d_n} 0.003 E_s \qquad (2.39)$$

2.5.2.3 Ultimate Strength of SFPRC Beams

For steel fiber reinforced prestressed concrete (SFRPC) beams (used for this research), with the inclusion of the forces due to pre-stressing, Figure 2.21 has been slightly modified as shown in Figure 2.22.

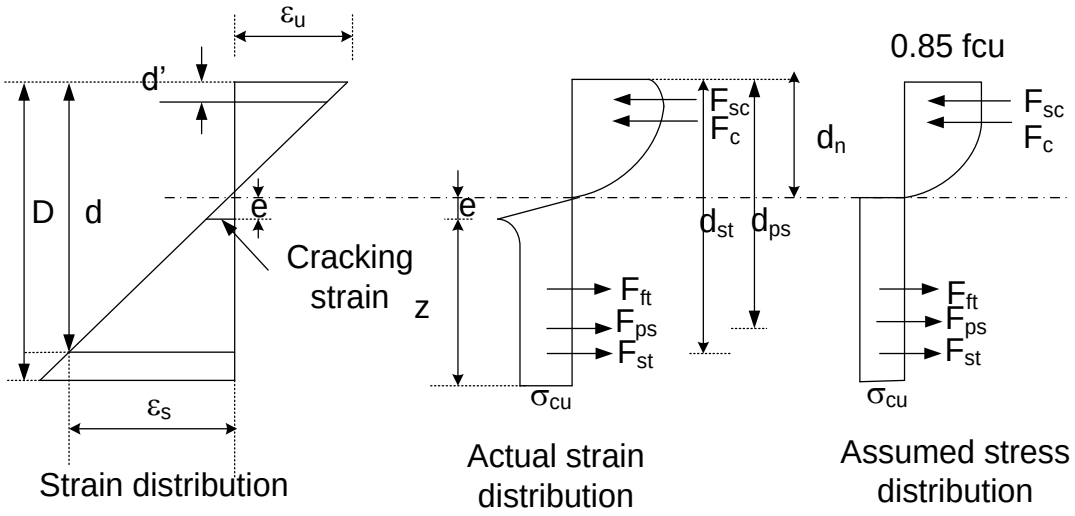

Figure 2.23 Modified Actual and Assumed Stress Strain Distributions at Failure for SFRPC Beams

The additional tensile force due to prestressing steel in SFRPC beams is determined by Equation 2.40.

$$F_{ps} = A_{ps} f_{ps} \quad (2.40)$$

Where f_{ps}, is the tensile stress in pre-stressing steel at ultimate and is determined in the similar manner as discussed in Section 2.5.1 by using Equation 2.16. Including this additional tensile force accompanied by prestressing force the value of d_n is determined equating tensile and compression forces as discussed earlier with trial and error. Then total ultimate moment of resistance for SFRPC is determined as follows:

$$M_u = F_c\left(d_n - k_2\right) + F_{sc}\left(d_n - d'\right) + F_{st}\left(d_{st} - d_n\right) + F_{st}\left(\frac{D - d_n}{2}\right) + F_{ps}\left(d_{ps} - d_n\right) \quad (2.41)$$

Various terms and parameters used in the above equations (2.30 to 2.41) are defined as follows:

D = the overall depth of the beam

d= the effective depth of the beam

b = the width of the beam

d'= the depth of the compression steel

d_n = the depth of the neutral axis

e = the depth of the elastic, un-cracked tension zone

F_{st} = the force in the tension steel

F_{ft} = *the force in the steel fibersin the tension zone*

F_{sc} = *the force in the compression steel*

F_c = *the force in the concrete in the compression zone*

f_s = *the stress in the tension steel*

f_y = *the yield stress of the tension steel*

f'_s = *the stress in the compression steel*

f_s = *the stress in the tension steel*

f'_c = *the cylindrical compressive strength*

A_s = *the area of the tensile reinforcement*

A'_s = *the area of the compressive reinforcement*

E_s = *the elastic modulus of the steel reinforcement*

E_{ps} = *the elastic modulus of the prestressing strands*

ε_0 = *the strain at the extreme fiber of the elastic, un-cracked tension zone*

ε_u = *the strain in the concrete at ultimate*

k_2 = *the depth of the centroid of the compression block*

M_u= *the ultimate moment of resistance*

F_{ps} = *the force in the pre-stressing steel*

A_{ps} = *the area of the pre-stressing steel*

f_{ps}= *the stress in the pre-stressing steel*

2.6 Material Test Methods

2.6.1 General

The standard material test methods have to be used to evaluate the material properties of the fiber reinforced concrete (FRC) in order to ensure that the FRC was batched properly. These tests should also give indications of the FRC's performance if it is used in structures. An ideal material test method for FRC needs to account for many factors. Mindess et al. (2003) suggested that the toughness and residual strength parameters obtained from the FRC material tests should satisfy the following criteria:

- It should have a physical meaning that is both readily understandable and fundamentally significant if it is to be used for the specification or quality control.
- The "end-point" used in the calculation of the toughness parameters should reflect the most severe serviceability conditions anticipated in the particular application.
- The variability inherent in any measurement of concrete properties should be low enough to give acceptable levels of both within-batch and between-laboratory precision.
- It should be able to quantify at least one important aspect of the FRC's behavior (e.g. strength, toughness, or crack resistance) and should reflect some characteristics of the load versus deflection curve itself.

- It should be as independent as possible of the specimen size and geometry.

2.6.2 Existing Material Test Methods

Various types of material tests are used to determine the fundamental properties of plain and reinforced concrete. A few of the material tests that were used, or compared and analyzed in the experimental investigations carried out during course of the research work are discussed in the following paragraphs.

2.6.2.1 ASTM C1609 Flexural Testing of Fiber Reinforced Concrete Beams

ASTM C1609 [ASTM, 2010] is the standard test method of fiber reinforced concrete beams for determining the flexural performance using a beam under a third-point loading system. This is the only suggested method by ACI 318-11 to evaluate the mechanical properties of FRC. However, experimental evidence shown by Bernard (2002) indicated that the residual strength of a third-point loaded beam is the least attractive parameter because of inconsistent results, which can be concluded because the coefficient of variation is generally greater than 20%. This large scatter in the residual strength can be a major problem if the characteristic values have to be determined. On top of that, ASTM C1609 requires the use of a closed-loop, servo controlled compression testing machine which makes test complex and time consuming.

Figure 2.24 shows a typical test setup to perform the ASTM C1609 test. It is a third-point loading fixture with two hinged supports and two loading points on the top of the beam. A rectangular jig surrounds the beam and is mounted on the beam's neutral

axis directly over the supports. Two displacement transducers, one on each side of the beam, are mounted at the mid-span to measure the beam's deflection. The output of each transducer is averaged. This configuration ensures an accurate measurement of the deflection at the mid-span and minimizes errors due to the concrete specimen twisting or seating in the supports.

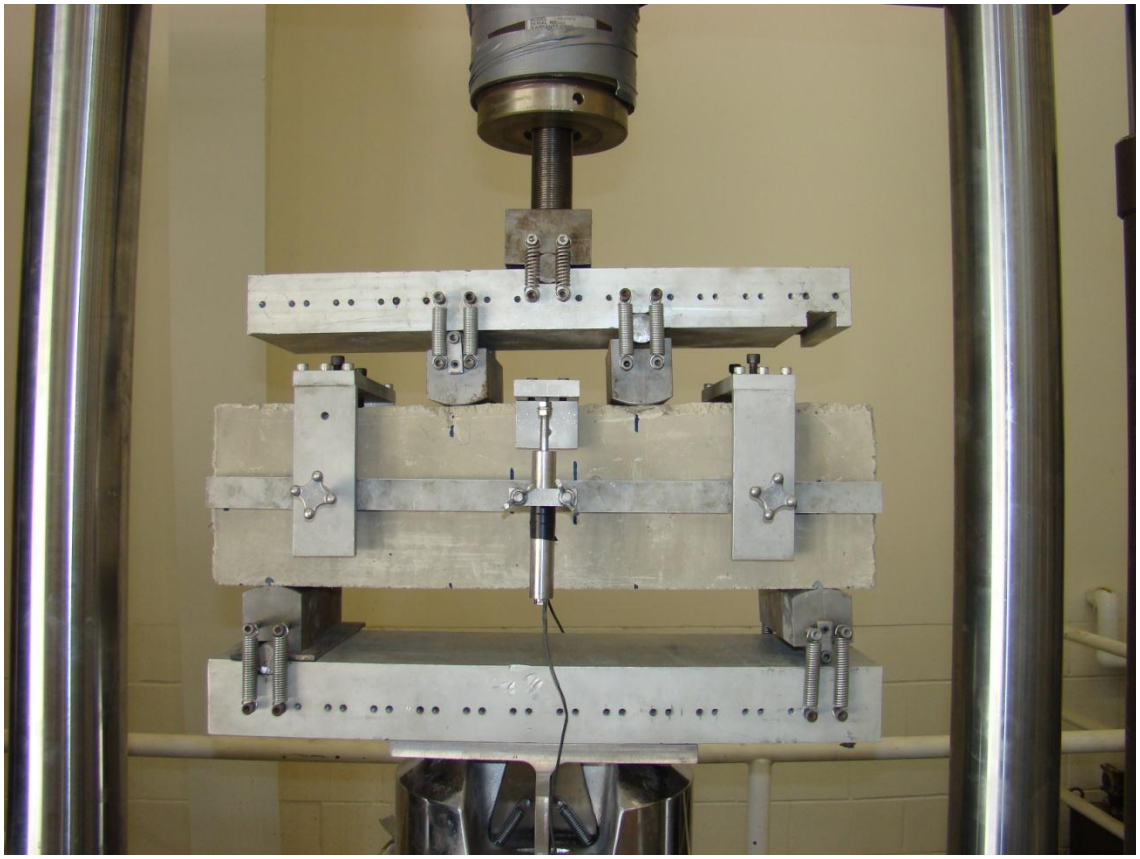

Figure 2.24 Typical ASTM C1609 Test Fixtures [ASTM 2010].

The test is run at a specified net deflection rate until a net deflection of L/600 (where L is the span distance between supports) is reached. After which it can be run at a higher specified net deflection rate until the test's specified endpoint (Table 2.4).

Table 2.4 ASTM C1609 Net Deflection Testing Rates [ASTM 2010]

Beam size	Net Deflection rate to L/600	Net Deflection rate for L/600 to end of test
14 × 4 × 4 (350 × 100 × 100) inches (mm)	0.002 to 0.004 in/min (0.05 to 0.12 mm/min)	0.002 to 0.008 in/min (0.05 to 0.20 mm/min)
20 × 6 × 6 (500 × 150 × 150) inches (mm)	0.002 to 0.005 in/min (0.05 to 0.12 mm/min)	0.002 to 0.010 in/min (0.05 to 0.24 mm/min)
L= Support Span 12 inches for 14 inches beam; 18 inches for 20 inches beam		

ASTM C1609 data analyses include the first peak strength, the peak strength, the residual strength at L/600, the residual strength at L/150, and the toughness, which is the area under the load versus net deflection curve from 0 to L/150 (Figure 2.26).

First curve is used when there exits both first peak load and peak load and second figure is used when first peak load and second peak load is same. The flexural strengths of the tested specimens at various stages; first peak load, the peak load, and the residual load (at deflections of L/600 and L/150); can be calculated as follows;

$$f = \frac{P L}{b d^2} \tag{2.41}$$

Where,

f = the flexural strength, psi

P= the load, kips

L= the span length, inches

b= the average width of the specimen at fracture, as oriented for testing, inches

d= the average depth of the specimen at the fracture, as oriented for testing, inches

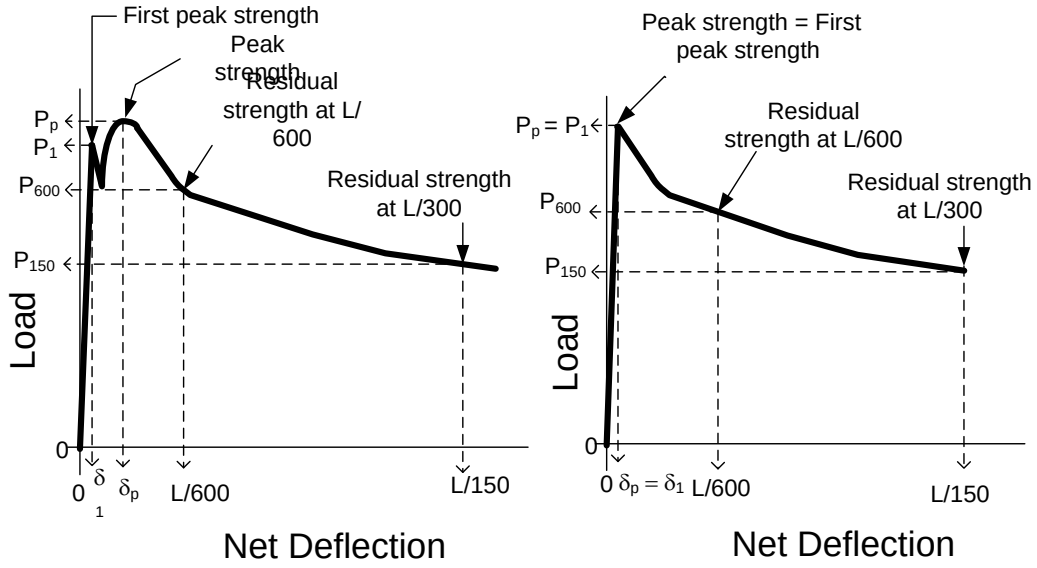

Figure 2.25 Ideal Load Versus Net Deflection Curve with ASTM C1609 Analysis Results [ASTM 2010].

2.6.2.2 Uniaxial Direct Tensile Test (Dog Bone shaped specimen)

The uniaxial direct tensile test method is the method by which one can identify the key properties of FRC; such as strain-hardening or strain-softening, the elastic modulus, and stress versus strain relationships under tension. These are the constitutive properties of FRC that are useful for the modeling and design of FRC structural members [Naaman, et al., 2007]. However, currently there is no standard method for this test is available in the U.S., in part because it is difficult to provide a gripping arrangement which will not lead to the specimen cracking at the grips.

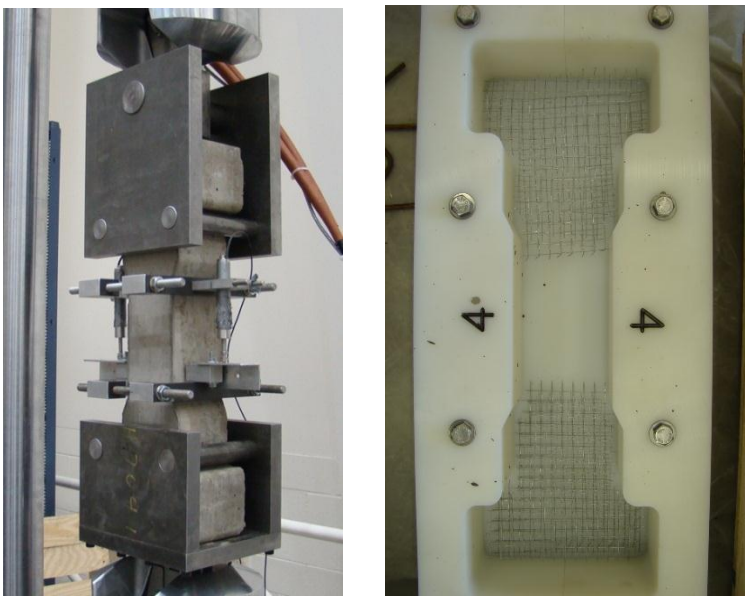

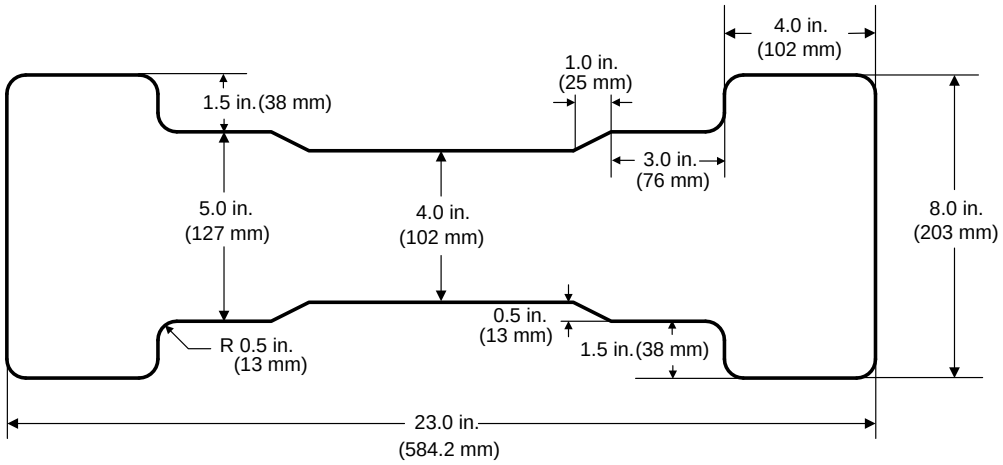

Figure 2.26 Geometry and Dimensions of the Direct Tensile Specimen Used at UT-Arlington [Chao et al, 2011]

Some uniaxial tensile tests were carried out at UT-Arlington [Chao et al, 2011]. The specimens were specifically designed so that a pin-pin loading condition is created at the ends (Figure 2.26). Both ends have double dog-bone geometry and are strengthened by the steel mesh to ensure that cracking would only occur in the central portion of the specimen, within the gauge length. The double dog-bone shape was used

to provide a better transition to avoid stress concentration which resulted from the reduction of cross-section. The central portion has a square cross-section with a dimension of 4 × 4 inches. This dimension was selected to ensure more uniformly distributed fibers while maintaining a suitable weight for laboratory handling. The strains were measured by a pair of linear variable differential transformers (LVDTs) with a gauge length of approximately 6 inches. Tests were carried out by a closed-loop, servo-controlled machine with a loading rate of approximately 0.002 inches/minute. Some of the drawbacks of this test method are as follows:

- Consistent location of cracks and propagation path cannot be well controlled. This is the major factors that led to variability in the post-cracking response.
- Some improvement was possible with the use of steel mesh reinforcement to locate the cracks with the gauge length still difficult to locate the cracks with the gauge length.
- Though the first cracking stresses of two replicate specimens were close, the post-cracking response and residual strength showed significant variability.

2.6.2.3 Round Panel Test (ASTM C1550)

This recently developed bending test method [ASTM, 2008] is based on extensive studies carried out by Bernard [2000, 2001a, 2001b, 2002,]. This test involves the central point loading of a large round panel, 31.5 inches in diameter and 2.95 inches thick, supported on three symmetrically arranged pivots, as shown in Figure 2.27.

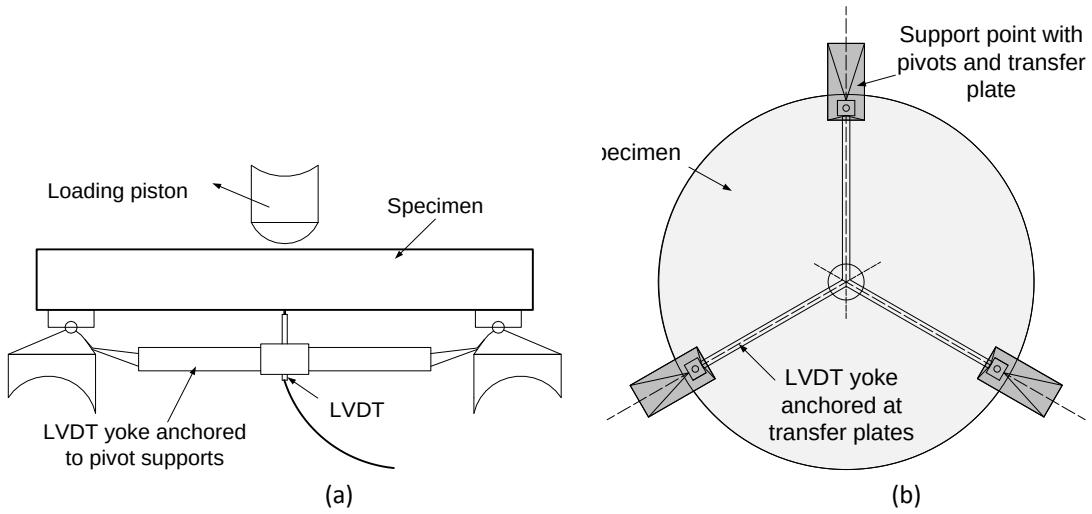

Figure 2.27 Setup and Specimen for ASTM C1550 Round Panel Test [Chao et al., 2011]

Although this method was originally developed for fiber reinforced shotcrete, it can also be used for evaluating plate-like members such as concrete slabs-on-grade. The test panel experiences bi-axial bending in response to the central point load. The performance of FRC specimens tested by this method is quantified in terms of the energy absorbed between the onset of loading and selected values of central deflection. Some suggested performance-based specification are [Bernard, 2002]: 1) Energy absorbed up to a deflection of 0.2 inches to indicate the performance for applications in which crack control is important; 2) Energy absorbed up to a deflection of 1.6 inches to evaluate the performance for applications where large cracks can be tolerated.

The radius of the hemispherical end of the loading piston and the supports were fabricated according to the dimensions and criteria given in ASTM C1550 [ASTM, 2008]. A closed-loop, servo-controlled machine is also required as per ASTM C1550 for performing this test.

Previous studies [Bernard, 2002] indicated that the variation in the first cracking load, peak load, or energy absorbed up to a specified central deflection from this test is generally low (coefficient of variation between 5% and 13%).

Due to large specimen sizes and heavy steel supports it is difficult to perform this test in small laboratories. Some of these tests were carried out at UT-Arlington [Chao et al., 2011] under a stiff reaction frame through a hydraulic cylinder that carefully controlled the loading rate, which was approximately 0.16 inches/min. as

specified by ASTM C1550. The load versus central deflection curves of two replicate panel specimens are shown in Figure 2.28. A scatter in the post-cracking response during the test is noticeable. This was probably the consequence of specimens not being cast from the same batch, eccentric loading, or complicated cracking propagation path.

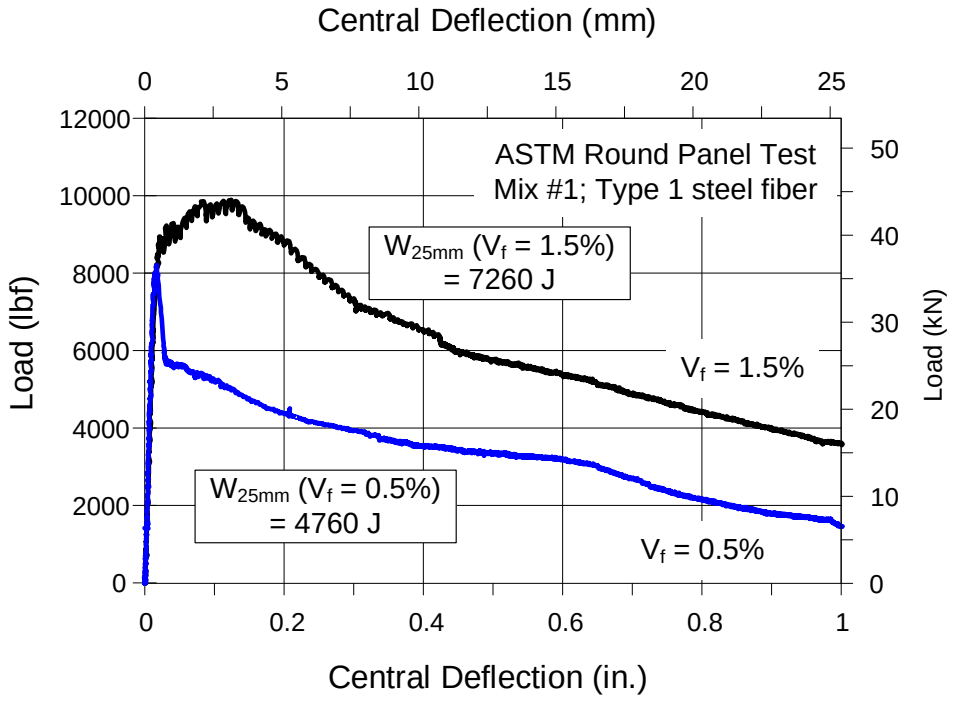

Figure 2.28 Load Versus Central Deflection Responses of Specimens with Different Fiber Fractions under Round Panel Test as well as Absorbed Energy up to 1 inch, (25 mm) Deflection [Chao and et al. 2011]

2.6.2.4 Compressive Strength Test

The standard cylinder test is the most commonly used, simple, relatively low cost test designed to measure the compressive strength of hardened concrete. Cylinders usually are tested in specially designed large capacity machine which is capable of recording the load required to crush the cylinder. Cylinder ends usually are capped to

ensure smooth contact with the testing machine loading heads (Figure 2.29). When a cylinder is loaded in compression, microscopic internal cracking begins at about 30% of the ultimate load. As these cracks grow, the cylinder gets shorter and fatter. Cracks initially form around the aggregate particles and eventually branch out and link together. ASTM C39 [ASTM, 2011] requires that cylinders be loaded at a rate of 20 to 50 psi per second; a higher load rate can be used up to 50% of the expected failure load.

The cylinder test is sensitive to the type of machine being used. Other factors that can affect the results of cylinder testing include capping, cylinder placement in the test machine, and moisture conditions. Test cylinders will not accurately represent the concrete if they have been made, handled, or cured improperly.

If a cylinder has tight, flat caps, then the friction between the caps and the testing machine will keep the cylinder's top and bottom from expanding during the test, causing the cylinder to become barrel shaped. The failure of well-capped cylinders is caused by splitting, which begins at the largest diameter of the barrel and leaves two concrete cones (Figure 2.28).

(a)

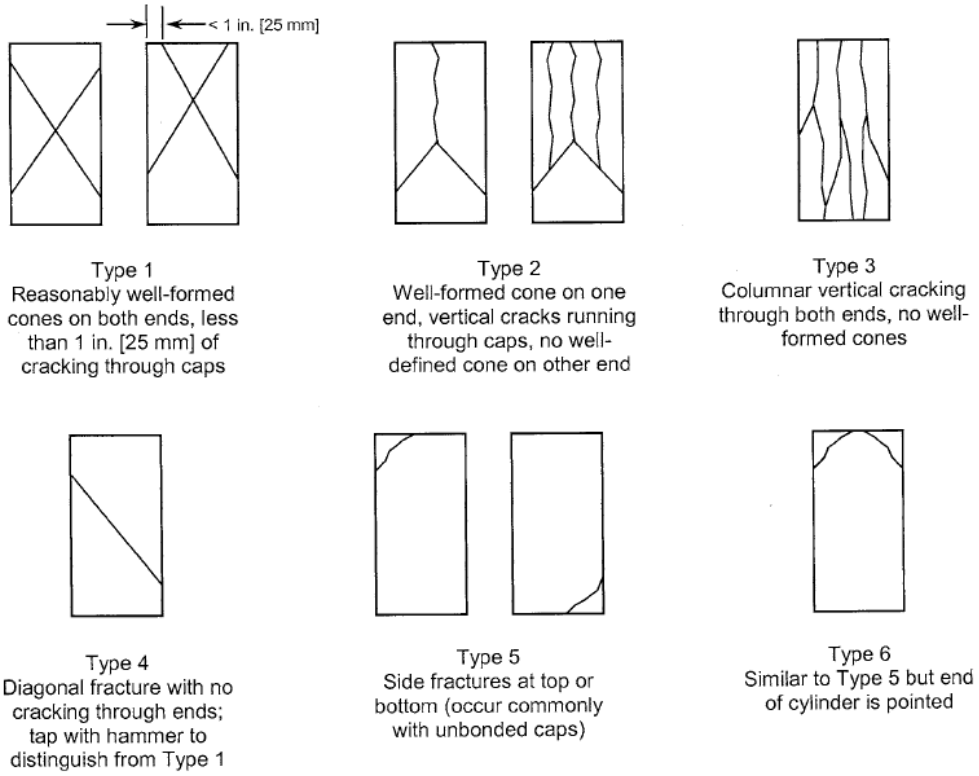

(b)

Figure 2.29 Compression Strength: (a) Test setup and (b) General Failure Pattern [ASTM C39-11]

The large cylinder (6 × 12 inches) with additional arrangement for measurement deformation as shown in Figure 2.30 can be used for determination various parameter such as elastic modulus, compressive stress-strain curves, residual strength, stress softening behavior and energy dissipation. Detail of this test is discussed in later chapters.

Figure 2.30 Test setup for obtaining Compressive Stress-strain relation

2.6.2.5 Split Cylinder Test (ASTM C496)

In the split cylinder test, the plain concrete actually fails by tensile stretching at the center of the cylinder. In this test the cylinder is laid it on its side and compression load is applied the on a "knife edge" along the entire length of the sample (Figure 2.31). Similar to the compression test, this load shortens the cylinder in the direction of the load, but causes it to grow wider in the other direction until it splits. This is called the *split cylinder test*, described in ASTM C496 [ASTM, 2011]. Split cylinder testing is a convenient way to measure the tensile strength because the specimens and testing equipment are basically the same as in compression testing. It is also possible to determine not just the failure strength of concrete cylinders but how much they deform during testing.

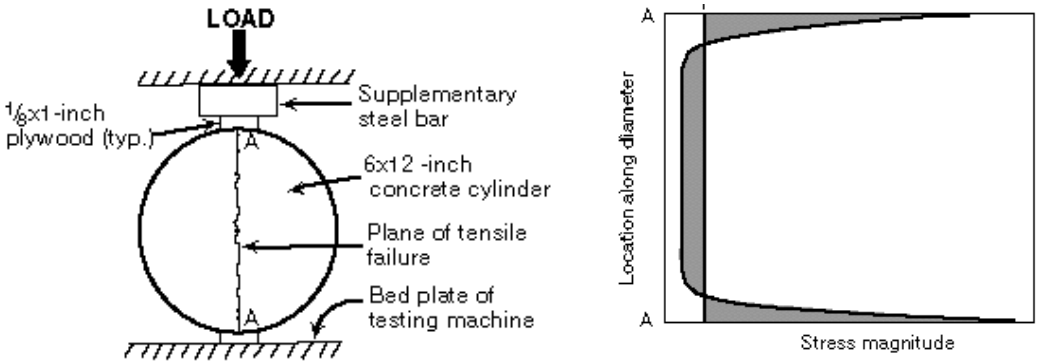

Figure 2.31 ASTM C 496 Split Cylinder Test [ASTM, 2011].

In this test the load is applied as a line load to the cylinder edges, as shown in Figure 2.30. Tensile stresses develop across most of the diameter A to A, then the cylinder cracks and fails along this line when the stress reaches the splitting strength.

The major drawback of this method is that it produces a predefined failure plane while loading. The specimen is forced to fail in the line of the application of the load. Therefore, the true properties of the material may not be reflected. Also, ACI has not recommended this method for the evaluation of the properties of FRC. Some of the previous tests carried out for plain concrete and FRC with this method are discussed in the following sections of this chapter.

2.6.3 Reintroduction of the Double Punch Test for Material Test of SFRC

As discussed earlier, it is well known that a material test method is very important technique to evaluate the mechanical properties of FRC. However, it has been recognized that none of the standard tests used for obtaining FRC toughness or residual strength and other properties with low variation. As discussed earlier each type of material test methods has some limitations. Some produce very scattered results, some require a sophisticated testing setup, and some require larger specimens and occupy a large space. Hence, development of a simple and reliable material test method is essential. In this context the reintroduction of double punch test method can be one of options.

The double punch test (DPT) was first introduced by Chen in the 1970s. A compressive load is applied to a cylinder, or cube, along the axis at the center of the specimen through two small steel punches on the specimen's top and bottom surfaces. In this case, nearly uniform tensile stress occurs over several diametric planes and

fractures occur along these diametric planes. Some of the important features of this test are [Chen, 1970]:

- The procedure for performing a double punch test on a cylinder or cube specimen is easier than other material test methods.
- The testing setup as shown in Figure 2.31 is simple and can be carried out by a smaller capacity compression testing machine.
- The calculated equivalent tensile strength from the double punch test gives an average value of tensile strength on several cracked diametric planes, rather than from one dominating cracked surface. This has been shown to be the reason for low variability for the ASTM C1550 round panel test (reference). .

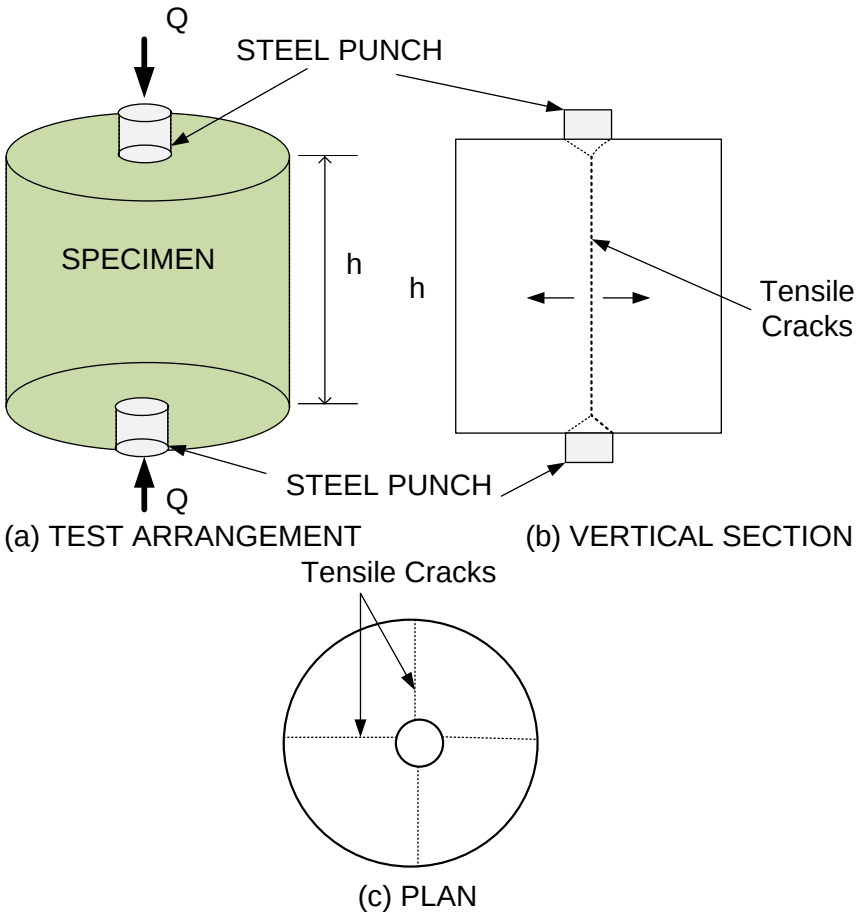

Figure 2.32 Testing Apparatus for the Double Punch Test [Chen 1970]

Chen and Yuan started evaluating the DPT with plain concrete in the 1980s. They tested several plain concrete specimens with different ages, water cement ratios, size, and aggregate types (normal and light weight). They used 1.0 inch thick steel punches with diameters of 0.75 inches to 1.5 inches. The ratio of the punch diameter to specimen diameter was 1:4. They recommended using 6 × 6 (diameter × height) inches specimens with steel punches 1.5 × 1 (diameter × thickness) inches.

2.6.4 Plasticity Theory of Plain Concrete

Chen (1970) derived equivalent tensile strength for DPT based on the theory of perfect plasticity using limit analysis techniques, which was found to be identical to the results derived from the theory of linear elasticity. Since the behavior of concrete during a bearing capacity test is closely related to the double punch test, the relevant formula of the double punch test can be obtained directly from a simple modification of the results from the bearing capacity test.

The ideal failure mechanism for a double punch test is shown in Figure 2.33 which consists of several simple cracks along radial direction and two cone-shapes rupture surface directly under loading punches. As per upper bound computation discussed by Chen in section 11.6.1 of his book (Limit Analysis and Soil Plasticity) [Chen, 1975], equating the external rate of work to the total rate of internal energy dissipation yields the value of the upper bound on the applied load Q^u can be expressed as

$$q = \frac{Q^u}{\pi d^2} = f_t^{'}\left[\frac{bh}{a^2}\tan(2\alpha+\varphi)-1\right] \qquad (2.42)$$

Where,

$$\cot\alpha = \left\{1+\frac{\frac{bh}{a^2}\cos\varphi}{\frac{f_c^{'}}{f_t^{'}}\left[\frac{1-\sin\varphi}{2}\right]-\sin\varphi}\right\}^{1/2} \qquad (2.43)$$

Where, a = radius of the punch, b and h are specimen dimensions, α and φ are angles to surfaces as shown in Figure 2.33) and $f_c^{'}$ and $f_t^{'}$ are compressive and tensile stress respectively.

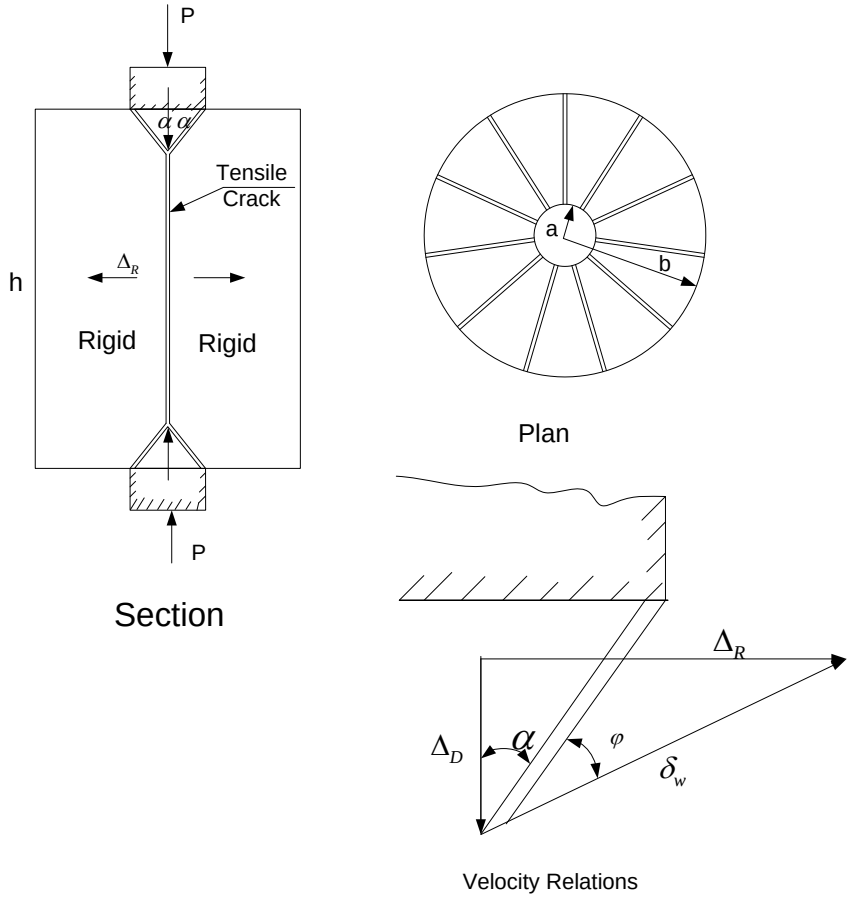

Figure 2.33 Bearing Capacity the Double Punch Test [Chen 1970]

As a typical case consider compressive stress as 10 time tensile stress and other considering other parameters as follow the maximum upper bound load is as given in Equation 2.44.

$f_c^{'} = 10\ \mathrm{f}_t^{'}$ and $\varphi = 30^0$ and $2a = 1.5\ in., 2b = 6\ in.$ and $h = 8\ in. \alpha = 10^0$

$$Q^u = \pi\left(1.19bh - a^2\right) f_t^{'} \qquad (2.44)$$

Based on this theory, Chen used Equation 2.45 to calculate the equivalent tensile strength from the ultimate load using the DPT;

$$f_t = \frac{Q}{\pi\left(1.2bh - a^2\right)} \qquad (2.45)$$

Where, Q is the ultimate applied load.

2.6.5 Size Effect

Marti (1989) conducted some studies on the influence of size effect in the double punch test for plain concrete. He carried out two series of experiments with twenty-three and nineteen double punch tests on plain concrete with different sizes (3 inches to 128 inches) in two series. He kept specimen size proportions as *d = h =4p*. Where p is punch diameter. He carried out the test at fifteen and twenty-one days for series 1 and series 2 respectively. He calculated the nominal stress with Equation 2.46 (developed based on Chen's approach) and predicted stress with Equation 2.47 based on Bazant's nonlinear fracture mechanic approach.

$$\sigma_N = \frac{0.40P}{d^2} \qquad (2.46)$$

$$\sigma_{\mathrm{N}} = \frac{f_t}{\sqrt{1 + \mathrm{d}/(\lambda \mathrm{d_a})}} \qquad (2.48)$$

Where, *P = the peak load, d = the diameter of the specimen, d_a= the maximum aggregate size, and λ = an empirical constant.* The ratios of the two equations were found varied from 0.92 and 1.14.

His experiment (Figure 2.34) exhibited a pronounced size effect, which was predicted with good agreement with Bazant's size effect relationship. He also concluded that the right hand side of Equation 2.46 provides a simple working formula for the approximate determination of f_t from a small scale double punch test.

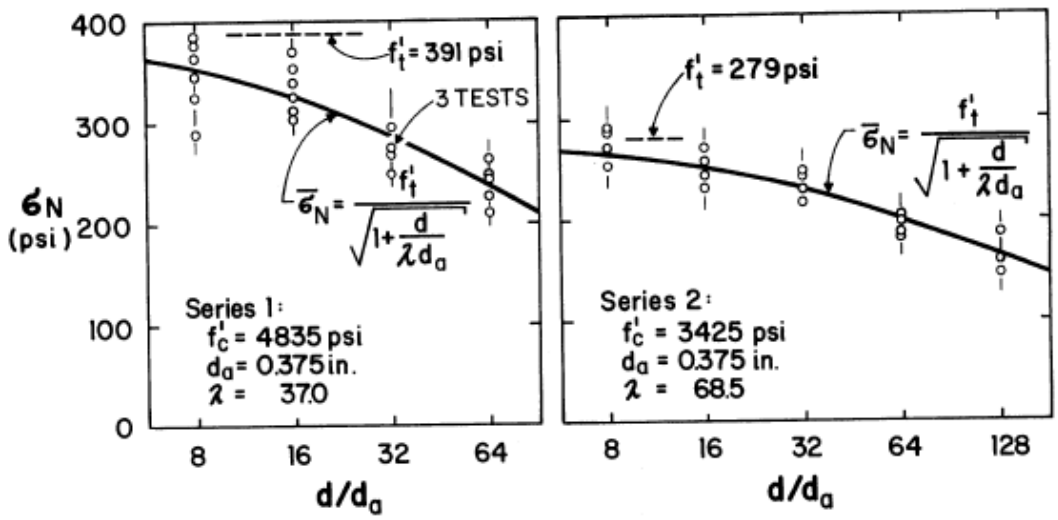

Figure 2.34 Effect of Specimen Size on Nominal Failure Stresses [Marti, 1989]

2.6.6 Comparison with Split Cylinder Test

Chen and Yuan (1980) performed double punch test on plain concrete and concrete with steel and polymer fibers (0.3%) for normal weight and light weight concrete and compared the results with the split cylinder test. The results showed good uniformity relationship between tensile strength determined from both test methods. The failure load from split cylinder test ranged from 40.5 to 78.7 kips (180 to 350 kN),

whereas these values ranged from 20.2 to 36 kip (90 to 160 kN) using the DPT. A smaller capacity testing machine was found to be sufficient for the DPT. They concluded that for the measurement of the tensile strength, the DPT was the best method. This is because the concrete's failure in the DPT occurred in the weakest section, as opposed to a pre-determined failure plane in the split cylinder test.

Marti (1989) also compared his results (discussed in Section 2.6.5) with the results obtained by Hasegawa's split cylinder test results for determining the size effect [Hasegawa, 1985];. Hasegawa's findings showed that the split cylinder test with plain concrete had no size effect for very large specimens [Hasegawa, 1985];;, however, he cautioned against the use of the test results due to his limited study, just two cylinders were tested. In the end, he recommended the DPT as a valid alternative for the split cylinder test.

Elices et al. [1982] also compared the two test method double punch test (DPT) and split cylinder test (SCT) by testing various plain concrete specimens of different geometries, ages, and moisture content at room temperature, 68^0 F (20^0C), to very low temperatures, down to - 321^0 F (-196^0 C). They used 3.51 × 7.1 inches cylinders for the compressive strength and 3.5 × 3.5 inches for the DPT and SCT. They compared the results from the two different test methods. They found average tensile strengths were varied from 2.1 to 5.8 N/mm^2 (305 to 834 psi) for DPT and from 2.0 to 6 N/mm^2 (283-863 psi) for SCT. Though both test methods gave similar results, they found that the DPT is much easier to perform than the SCT. So they concluded that the DPT is an easy

and suitable method for measuring the tensile strength of concrete at cryogenic temperatures.

2.6.7 Comparison with Bending Test

Climent et al. [2008] carried out the experimental program using both the DPT (they called it BCN or Barcelona test although it is exactly the double punch test) and the bending test [NBN B 15-238, 1992] with different types of fibers, concrete, and fiber contents. They compared the maximum loads between the two tests and the loads on different values of total circumferential opening displacement, TCOD (measured as a circumferential opening $\Delta\phi = 3W_{BCN}$, varying from 0.04 to 0.24 inches (1 to 6 mm) for the DPT and a vertical deflection value (δ) varying from 0.02 to 0.12 inches (0.50 to 3.0 mm) for the bending test (Figure 2.35). When comparing the BCN and NBN results in terms of energy and toughness, their results showed that the coefficient of variations (COVs) at peak loads from DPT tests are in typically lower as compared to the COVs from bending test. At residual loads (at different values of TCOD and δ as discussed above), the COVs from DPT test with steel fibers are still lower than those from bending test. However COVs at residual load from DPT test with Polyolefin fiber are greater than corresponding values from bending test (NBN).

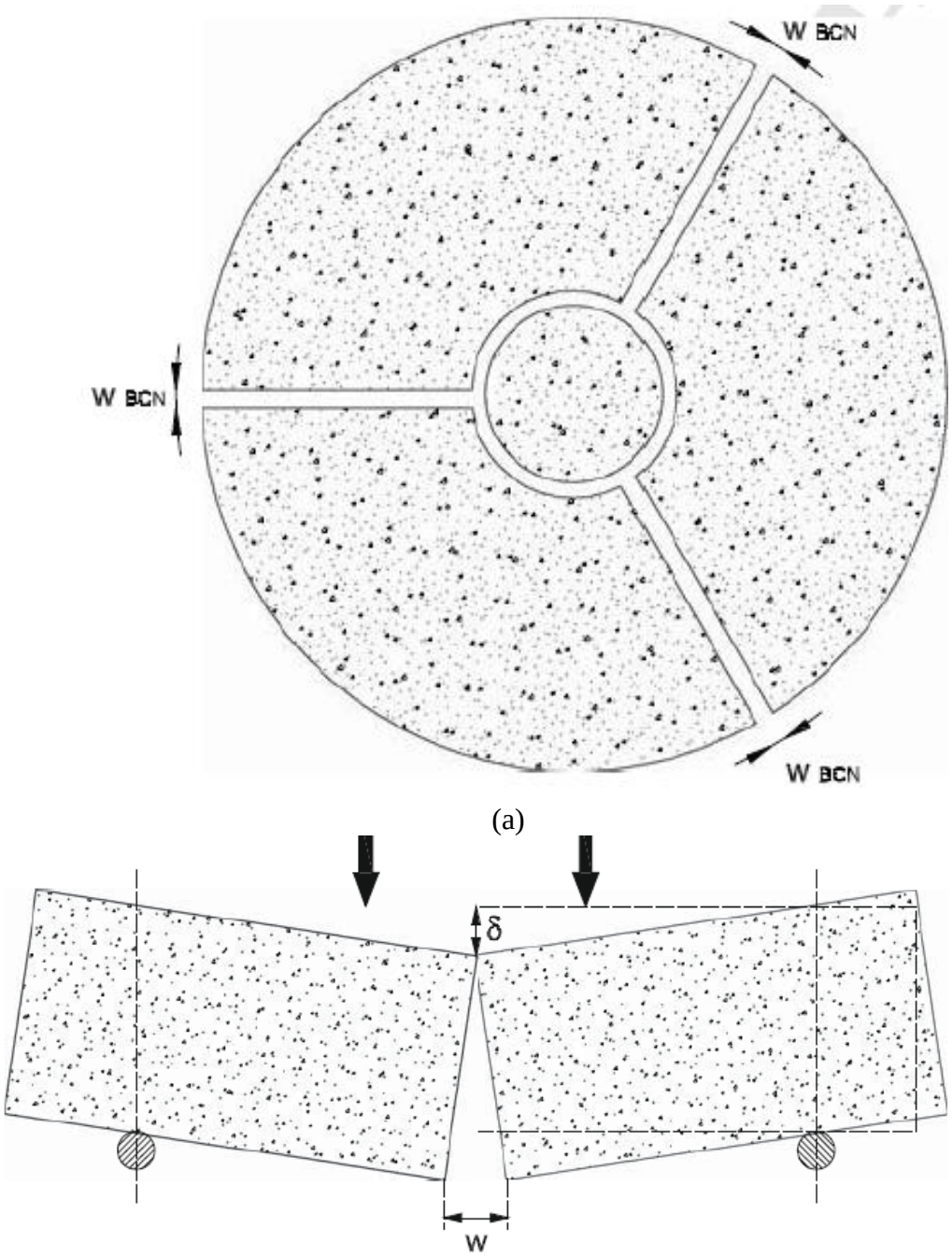

Figure 2.35 Ideal Cracking Layout Assumed: (a) BCN test (b) Belgium beam test [Climent et al., 2008]

2.6.8 Biaxial Loading Condition for SFRC

Demeke and Tegos (1994) carried out experiments in order to study the biaxial effect of SFRC. They developed a tension-compression test (applying load by pushing and pulling) to study the effect of biaxial stresses as shown in Figure 2.36. biaxial test started to decrease rapidly.

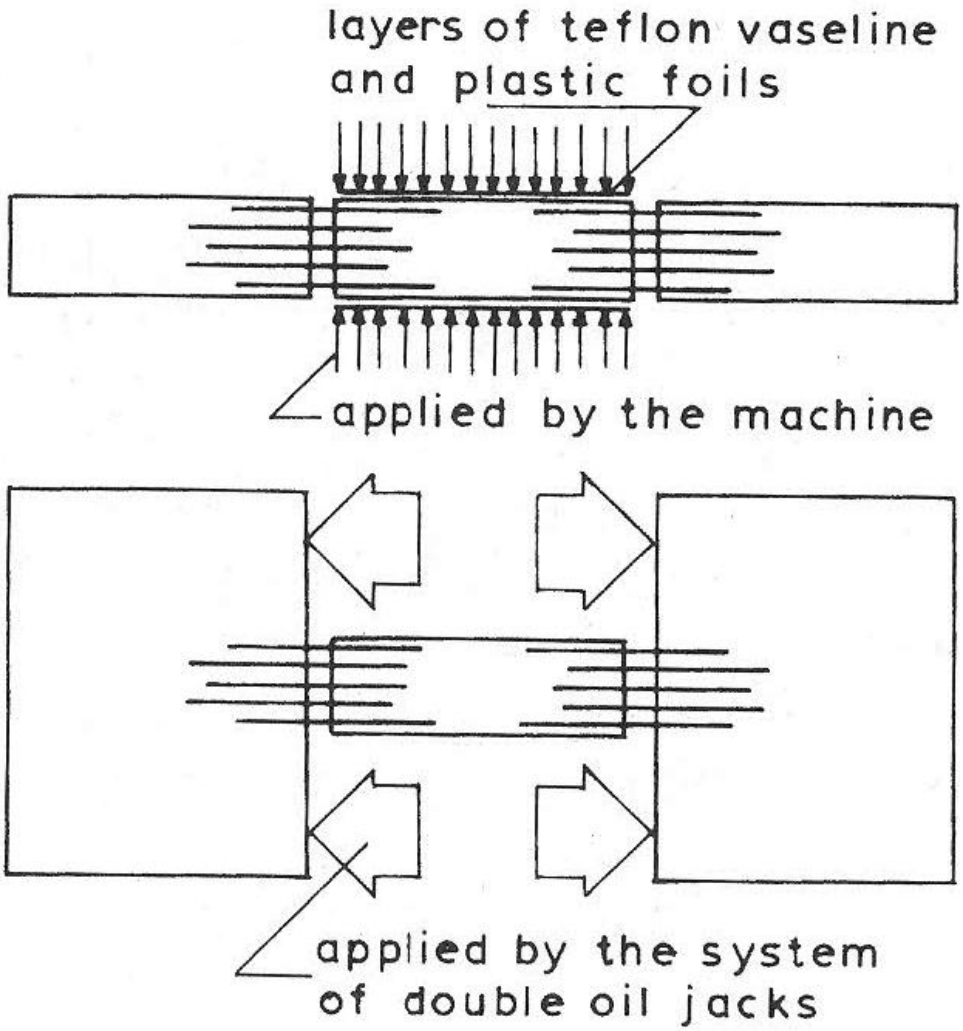

Figure 2.36 Biaxial Loading of Concrete Specimen [Demeke and Tegos, 1994]

They found that the tensile ultimate strength under biaxial loading was generally less than the strength from a uniaxial test, as shown in Figure 2.37. This usually depends on the ratio of the compressive principle stress to compressive strength. It can be shown in the figure, in the case of a PC specimen, that the tensile strength (f_1) reduced by 50% at the compressive strength (f_2) leaving a compressive strength ratio of $\left(\frac{f_2}{f_c} = 0.50\right)$. However, for SFRC with 1.5% volume fraction of fibers, the tensile strength was found to be almost constant until the point where this ratio is 0.5. For all specimens after the principal stress to compression strength ratio $\left(\frac{f_2}{f_c} \geq 0.75\right)$, the tensile strength from the biaxial test started to decrease rapidly.

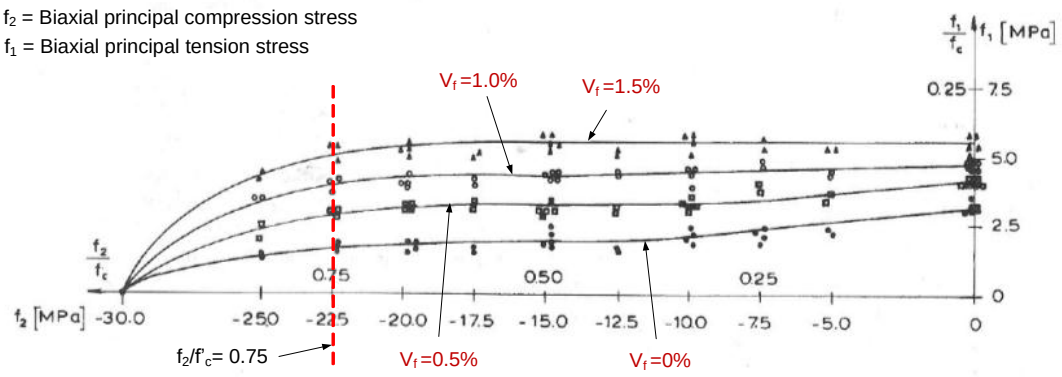

Figure 2.37 Ultimate Strength Envelopes of Principal Stress under Compression-Tension Condition [Demeke and Tegos, 1994]

They had concluded that the incorporation of steel fibers into the concrete matrix results smoothening the shape of versus biaxial stress curve to a large extent, approximating the uniaxial strength diagram as shown in Figure 2.39, which can be

important for application. As shown in the figure the tensile principal strength of SFRC can be considered as constant even with there is increase in principal compressive strength.

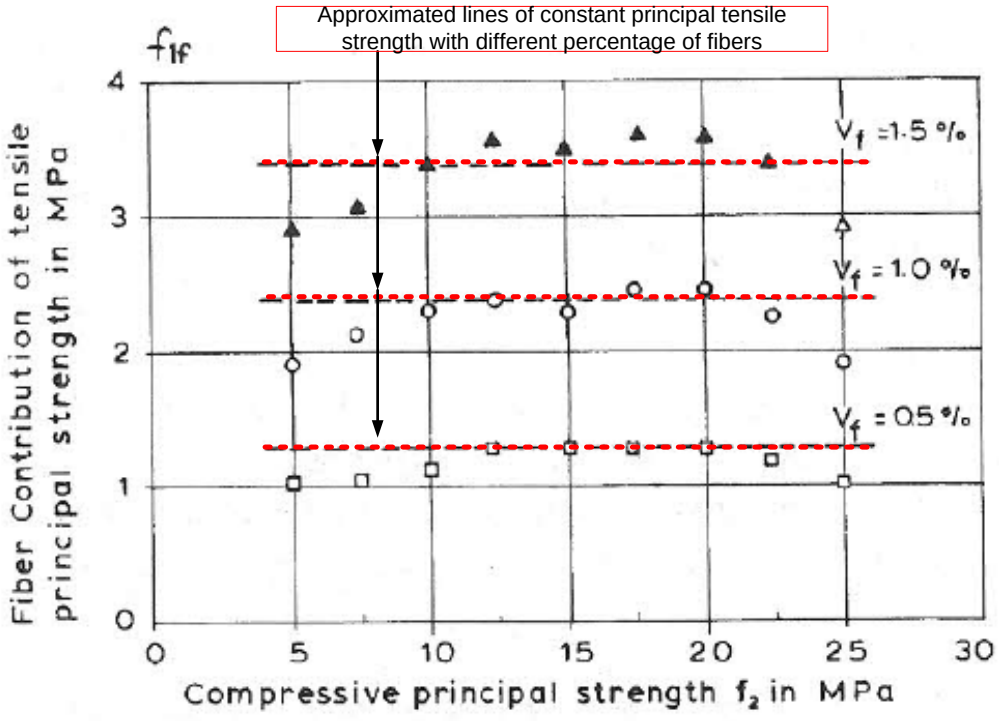

Figure 2.39 Relationships Between Fiber Contribution in Principal Strength and Volume Fraction V_f [Demeke and Tegos, 1994]

2.6.9 Finite Element Modeling

Pros et al. (2010) has discussed the validation of numerical models for the DPT with plain concrete. They used two types of models, the first one is a continuous model named as the Nonlocal Mazars Damage Model and the second one is a discontinuous model named as the Heusitic Damage Model. The latter consisted of three and four radial cracking planes, which were modeled as 2D joint elements. Experimental results from uniaxial compression test to determine the compressive strength and the split

cylinder test (Brazilian test) to determine the tensile strength were used. The values obtained from these tests were used in order to develop the input parameters for the models. For the peak load, the test results from the DPT were considered. Finally they compared the results of the numerical analysis with the results from different empirical equations, as shown in Table 2.4. It can be seen that the discontinuous model with 3 radial cracking planes have shown the lowest error among all of the models for plain concrete. So they mentioned this as most suitable model for DPT with plain concrete.

Table 2.5 Comparison of the Results from Numerical Analysis and Empirical Equations [Pros et al., 2010]

Description	P (N)	$\varepsilon_1 = \frac{P_{ref1} - P_i}{P_{ref1}}$	$\varepsilon_2 = \frac{P_{ref2} - P_i}{P_{ref2}}$	$\varepsilon_3 = \frac{P_{ref3} - P_i}{P_{ref3}}$
$f_t = \frac{P}{\pi\left(1.2bh - a^2\right)}$	1.51×10^5	P_{ref1} [Chen and Yuan, 1980]		
$f_t = \frac{0.75P}{\pi\left(1.2bh - a^2\right)}$	2.01×10^5		P_{ref2} [Chen and Yuan, 1980]	
$f_t = \frac{4P}{9\pi Ha}$	1.45×10^5			P_{ref3} [Saludes and et al., 2006]
Continuous model	3.50×10^5	1.3	0.74	1.4
Discontinuous Model 3 planes (h=3.5 $\times 10^{-2}$m)	1.25×10^5 1.50×10^5	0.006	0.25	0.03
Discontinuous Model 4 planes (h=3.0$\times$ 10^{-2}m)	1.25×10^5	0.17	0.38	0.14

CHAPTER 3

EXPERIMENTAL INVESTIGATION: LARGE-SCALE FIBER REINFORCED PRESTRESSED CONCRETE (SFRPC) BEAMS

3.1 General

As discussed in previous chapters, numerous researchers have demonstrated that adding steel fibers can improve the various properties of plain concrete. ACI 318 building code has recently adopted the use of steel fibers as an alternative to minimum shear reinforcement when certain specifications are satisfied with Section 11.4.6.1 (ACI 318-08, 2008). This provision is applied to both non-prestressed and prestressed concrete beams. However, the code does not specifically address the advantages of using steel fibers in flexural applications. In addition, previous studies on steel fiber reinforced prestressed concrete beams are limited and most of them were only on small scale specimens (depths of beams were less than 10 inches). Those results might not be applied to larger beams due to possible size effect.

As discussed in Chapter Two, in order to study more realistic flexural behavior of an SFRPC beam member including moment redistribution the testing of large-scale continuous beams is more appropriate. However testing of such large-scale continuous beams is not an easy job and it may not be economical. An inverted simply support beam can also represent the behavior of part near the interior support of a continuous beam [Mattock, 1964] as discussed in earlier chapter.

In view of these reasons, large-scale testing of six prestressed concrete beams with and without steel fibers was conducted in this research to investigate the flexural behavior and other properties.

The large-scale experimental programs mainly consisted of two phases. In the first phase, two specimens having longitudinal tensile reinforcement satisfying the tension-controlled requirements as per ACI 318-11, were prepared and tested. The first specimen was a steel fiber reinforced prestressed concrete (SFRPC) beam named as SFRPC#1-1, which was prepared without the minimum web shear reinforcement. For comparison purpose, a prestressed concrete (PC) beam namedPC#1-1 was prepared and reinforced with slightly less than the minimum web shear reinforcement as per the ACI 318-11 provision (reason is discussed later).

The second phase consisted of four specimens: two PC beams (PC#2-1 and PC#2-2) with longitudinal tensile reinforcement satisfying tension-controlled requirements as per ACI 318-11 and minimum web shear reinforcements, as required by ACI 318-11, and two SFRPC specimens. The first SFRPC specimen (SFRPC#2-1) had a high longitudinal tensile reinforcement ratio which made this specimen not qualified as tensioned-controlled, and with small amount of stirrups that is less than the design requirement for a plain concrete beam (the reason is discussed later). The second SFRPC specimen (SFRPC#2-2) had longitudinal tensile reinforcement satisfying the tension controlled requirement as per ACI 318-11 and only one stirrup at the center of the beam was used for fabrication purposes. All SFRPC specimens had the same volume fraction of steel fibers (0.75%).

All specimens in the large-scale experimental program had a height of 24 inches. This height is the upper bound limitation currently allowed by the ACI 318-11 building code if steel fibers are used as an alternative shear reinforcement to replace the minimum required conventional shear reinforcement. These beams with 24-inch height were much larger than that used in prior tests in which the beam height was only about 10 inches (see Chapter 2).

3.2 First Phase of Large Scale Experiments

3.2.1 Design of Specimens

In this phase, two specimens were prepared and tested. Both beams have identical geometries: 14 ft (168 inches) in length, 16 inches in width, 2 ft (24 inches) in height, and an effective depth of 21 inches. The span length between supports is 12 ft (144 inches). As shown in Figure 3.1, five strands (0.5 inches diameter pre-stressing strand, ASTM A416, Grade 270 and stress-relieved) were stressed by using the pre-stressing jack system at a local precast plant (Hanson Pipe & Precast Plant, Grand Prairie, Texas). The dial pressure gage was monitored while the pressure was applied by professional workers at the plant. Initial prestressing of 189 ksi was applied to each strand, which in turn gave an average initial prestress of 380 psi in each beam.

Figure 3.1 Pre-stressing Bed and Jacking in local precast plant (Hanson Pipe & Precast Plant, Grand Prairie, Texas)

In addition to the prestressing strands, two No. 3 mild steel bars were added at the bottom for ease of installation of strain gauges as installation of those in strands is difficult, and two No. 4 mild steel bars at the top for holding stirrups were provided. The percentage of tensile longitudinal bars (with respect to the gross area of the concrete section) including prestressing strands for both beams was about 0.29%, which satisfied the minimum longitudinal reinforcement for prestressed flexural member as per ACI 318-11 (See Appendix A) Slightly less web shear reinforcement than required as per ACI 318-11 was purposely provided for PC#1-1 in order to investigate whether the specimen would fail in shear or flexure (detail calculation are shown in Appendix A). Only two stirrups were provided along the span for SFRPC#1-1 for fabrication purposes. For both beams, five additional stirrups (as shown in Figure 3.2) were provided near the support in order to minimize possible cracking due to bursting pressure upon release of the strands. The detailed design parameters and dimensions of

the specimens are shown in Table 3.1 and Figure 3.2. Detailed design calculations of each beam are presented in Appendix A.

Table 3.1 Summary of Design Properties of Specimens Used in the First Phase of Experimental Program

Specimen	Total length (in.)	Total height (in.)	Effective depth (in.)	Shear reinforcement	Longitudinal reinforcement ratio (ρ)	Average prestress in concrete (psi)
PC#1-1	168	24	21	2-legged #3@14 inches c/c	0.29 % (2-#3 and 5 strands)	380
SFRPC# 1-1	168	24	21	2-legged 2-#3*	0.29 % (2-#3 and 5 strands)	380

*for construction purposes only

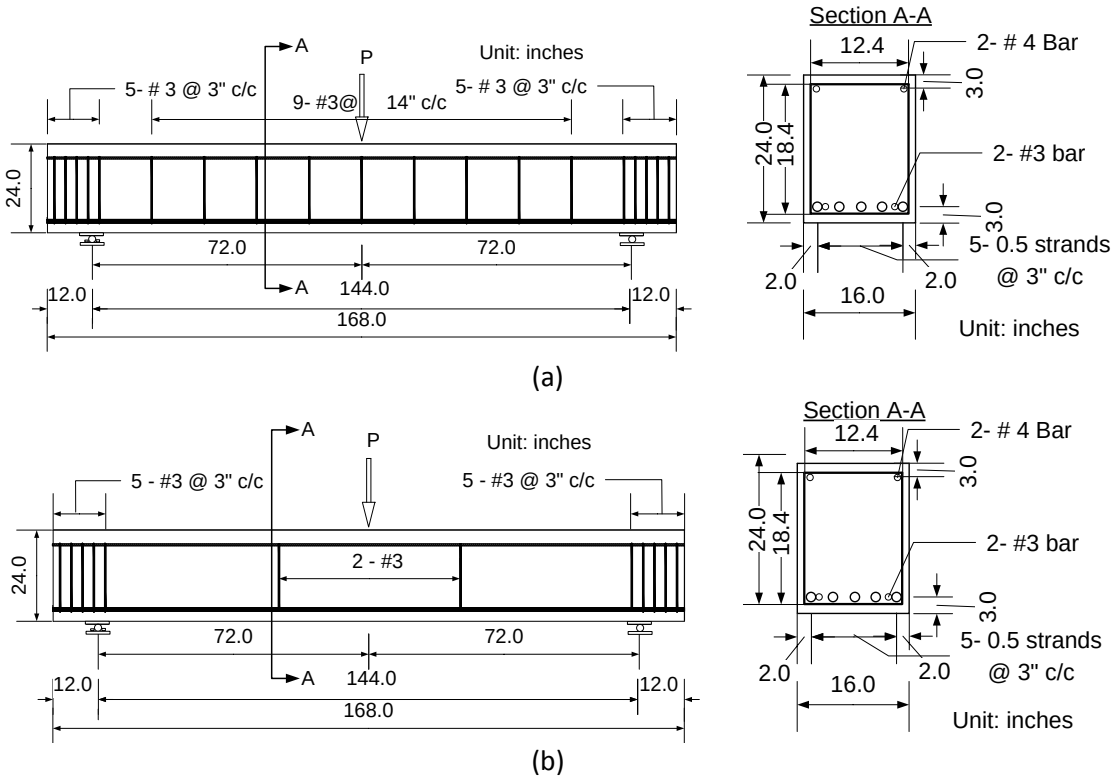

Figure 3.2 Dimensions of Specimens Used in the First Phase a) PC b) SFRPC

The volume fraction of steel fibers used for SFRPC#1-1 was 0.75%, which is the minimum required amount of deformed steel fibers specified by the ACI 318-11 building code.

3.2.2 Materials

3.2.2.1 Steel Fibers

The steel fibers used in the first phase of the experiment were Dramix RC-80/60-BN fibers manufactured by Bekaert Cooperation. The steel fibers are doubled-hooked at their ends and glued into bundles by dissolvable glue. The manufacturer advertised that the bundled steel fibers with dissolvable glue would help prevent balling, which is when the fibers stick together and create balls during mixing. This balling can impede the uniformity of the fiber distribution. The glue would be dissolved by the water used in a normal mix. The mechanical properties of the steel fibers used in this phase of the study are listed in Table 3.2.

Table 3.2 Mechanical Properties of Steel Fibers Used in the First Phase [1]

Shape	Length (L)	Diameter (D)	Aspect ratio (D/L)	Tensile strength
Doubled-hooked ends	2.37 inches	0.029 inches	82	152 ksi

[1]: All values are provided by manufacturer.

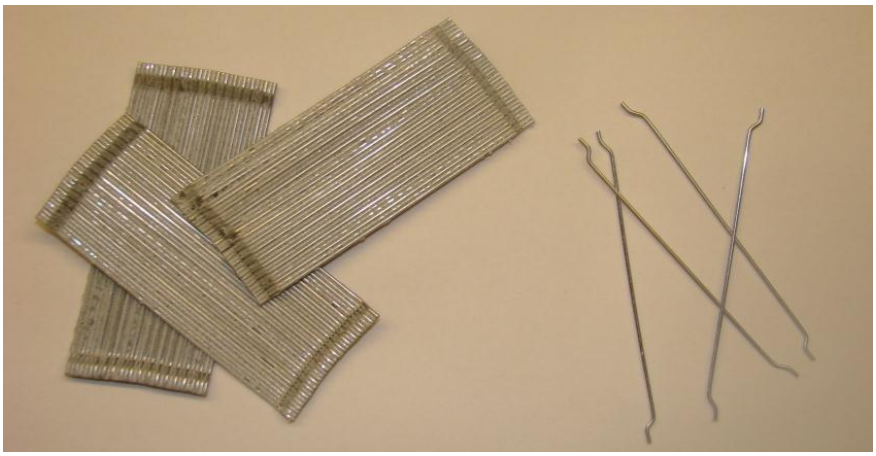

Figure 3.3 Dramix RC-60/80-BN Steel Fibers Manufactured by Bekaert Corporation

3.2.2.2 Concrete Mix

A trial mix was carried out at the University of Texas at Arlington's Civil Engineering Laboratory (CELB) to ensure workability and uniform distribution of steel fibers, as well as to check the designed compressive strength of 6000 psi, which is the maximum limitation of compressive strength allowed by the ACI 318-11 building code for SFRC.

All materials were provided by the local precast plant (Hanson Pipe & Precast Plant, Grand Prairie, Texas). Concrete was mixed using the local precast plant facilities (Figure 3.4) and transported to the prestressing bed. Type I cement, river sand, and crushed limestone of ¾ inches maximum size were used. The mix proportion used for the first phase is shown in Table 3.3.

Figure 3.4 Concrete Mixing Facilities in Local Precast Plan

Table 3.3 Mix Proportions and Compressive Strength of Concrete used in the First Phase

Types of concrete	Cement (Type 1)	Sand[1]	Coarse aggregate[2]	Water	Steel fiber	Compressive strength[3]
PC	1.00	1.13	0.67	0.40	-	5763 psi
SFRPC V_f = 0.75%	1.00	1.13	0.67	0.40	0.08	5470 psi

[1]: ASTM Natural River sand (Fineness modulus = 2.57)
[2]: Crushed limestone with maximum size of ¾ inches
[3]:The strength was measured by testing six 4×8 inches concrete cylinders cast simultaneously with large-scale beams

For the SFRPC mix, the steel fibers were simply added manually at the last stage of the mixing procedure. The weights of all the materials were measured and dumped into a mixing drum by an automation system, except for the steel fibers. Prior to mixing, the steel fibers were measured and placed beside the mixing drum. After the concrete mixture was well mixed as shown in Figure 3.5, the mixing hatch was opened and the steel fibers were added manually.

Figure 3.5 Typical Photos of Concrete Mixing

3.2.3 Internal Sensor Instrumentation

3.2.3.1 Steel Strain Gauges

For each beam, foil-type strain gauges were installed in the bottom and top reinforcing bars to measure the strains in the steel reinforcement. The reason for using tensile mild steel bars was because that the strain gauges can be easily mounted on the mild steel bars as compared to a seven-wire strand. It is assumed that both the strands and the mild steel bars beside the strands would undergo the same strains under loading.

The length of the steel strain gauge is 7/16 inch. The resistance of the strain gauge is 350 ± 0.6% ohm.. The ribs on the reinforcing bars were grinded to create a flat and smooth surface slightly greater than the size of the strain gauge. The area was cleaned with grease and other acidic and neutralizing chemicals. Each strain gauge was glued to a cleaned surface and protected by three layers of coating, namely polyurethane (coat A), nitrite (coat B), and a piece of rubber pad sealed by electric liquid tape, as shown in Figure 3.7.

Figure 3.6 Example of Steel Strain Gauge Installment

Two strain gauges were installed underneath the loading point on the compression reinforcing bars (one one each bar) and six strain gauges were installed on

the tension reinforcing bars for both specimens. The locations of the strain gauges are shown in Figure 3.8.

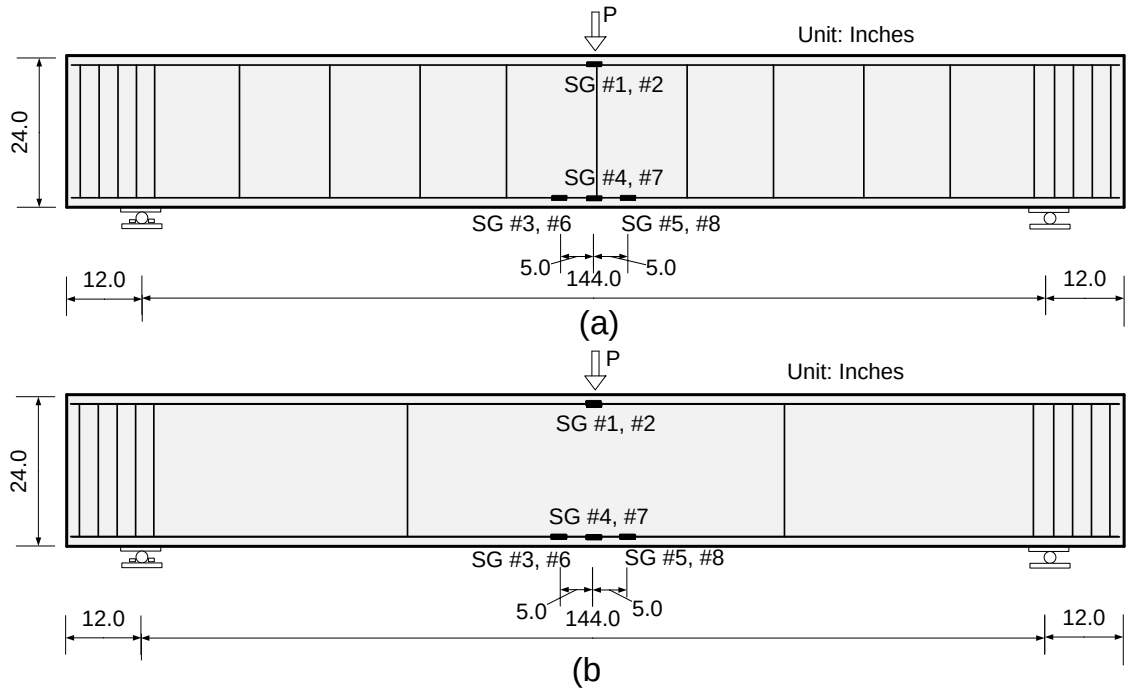

Figure 3.7 Locations of Steel Strain Gauges Used in the First Phase:
(a) PC#1-1 and (b) SFRPC#1-1

3.2.3.2 Concrete Strain Gauges

Internal concrete strain gauges (PFL-50-2LT, three wires, 2.25 inches long) were used to measure the concrete internal strains. The resistance of the gauge was 120.0 ohm, the gauge factor was 2.11, and the strain limit was 0.02 in./in. These internal concrete strain gauges were placed in mid-span, at side of beams (near the surface) and at the center of the beams, under the loading point, as shown in Figure 3.9 (b). The strain gauges were fixed with help of thin meshes and small rods so that the alignment of the strain gauges remained horizontal and straight.

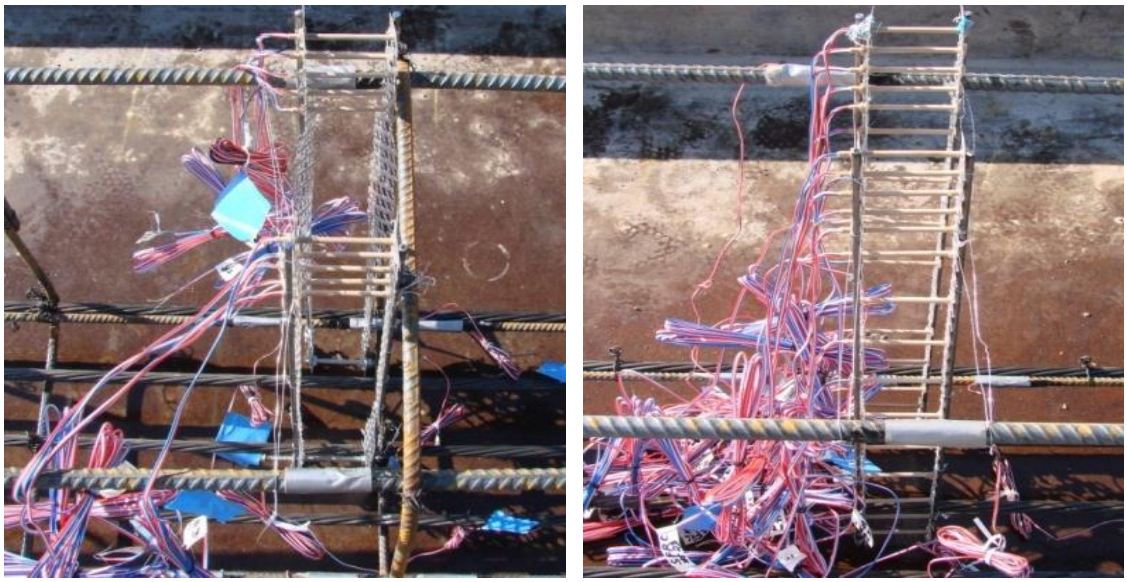

Figure 3.8 Embedded Concrete Strain Gauge for PC#1-1(left) and SFRPC#1-1 (right): Installation Photos

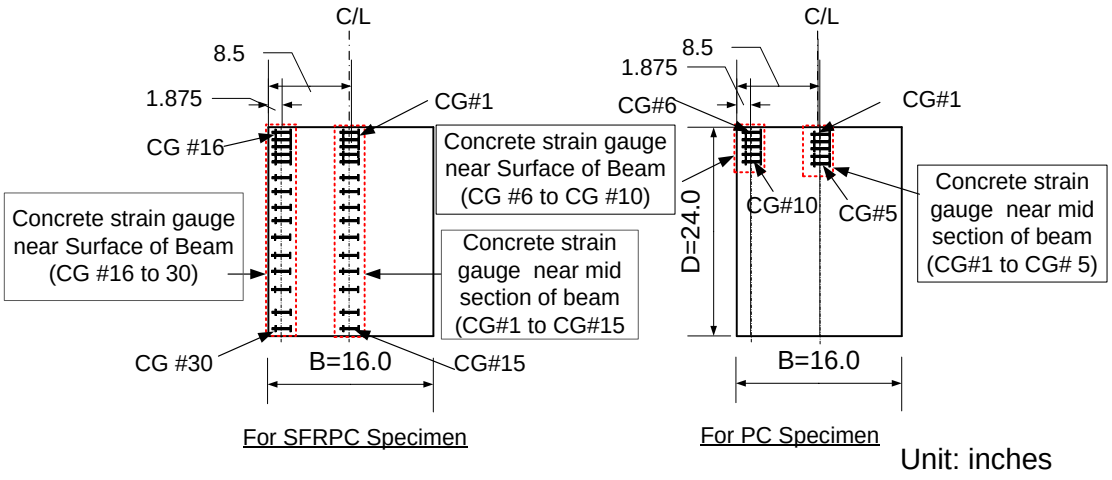

Figure 3.9 Locations of internal concrete strain gauges (cross-sectional view)

Table 3.4 Locations of Internal Concrete Strain Gauges Used in the First Phase

Mid-Section at 8.5 in. from left side (near center line)		Mid-Section at 1.875 in. from left side (near the surface)	
Strain gauge number	Distance from top fiber (in.)	Strain gauge number	Distance from top fiber (in.)
SFRPC#1-1 Specimen			
CSG #1	0.56	CSG #16	0.50
CSG #2	1.25	CSG #17	1.25
CSG #3	2.00	CSG #18	2.00
CSG #4	2.75	CSG #19	2.75
CSG #5	3.50	CSG #20	3.63
CSG #6	4.63	CSG #21	4.50
CSG #7	7.00	CSG #22	6.75
CSG #8	9.13	CSG #23	8.88
CSG #9	11.38	CSG #24	11.38
CSG #10	13.75	CSG #25	13.63
CSG #11	16.00	CSG #26	15.88
CSG #12	18.18	CSG #27	18.00
CSG #13	20.38	CSG #28	20.25
CSG #14	22.00	CSG #29	21.38
CSG #15	23.25	CSG #30	23.00
PC#1-1 Specimen			
CSG # 1	0.69	CSG # 6	0.75
CSG # 2	1.38	CSG # 7	1.50
CSG # 3	2.00	CSG # 8	2.25
CSG # 4	3.00	CSG # 9	3.00
CSG # 5	3.63	CSG # 10	3.50

The first strain gauge started to install from the compression fiber of concrete section (0.5 to 0.75 inches from the top of the beam). Details of the locations of the internal concrete strain gauges are as shown in the Table 3.4.

Additional external strain gauges were mounted on the surface of the concrete before testing. Those strain gauges were 1.25 inches in length and was a PFL-30-11-3L strain gauge. Among other properties, the resistance was 120.4 ± 0.5 ohm, the gauge factor was 2.13 ±1, and the transverse sensitivity was -0.70. Details of these strain gauges are described later on.

3.2.4 Fabrications of Specimens

3.2.4.1 Reinforcement Cages and Formworks

The initial step for the fabrication of the specimens was the fabricating of the formworks and reinforcement cages which was carried out by professional workers at local precast plant under the author's supervision. Five holes were made in the side wood pieces of the formwork for pre-stressing strands and then the pre-stressing strands and the required number of stirrups were placed. The pre-stressing force was applied using a pre-stressing jack. The reinforcement caging work included placing the longitudinal reinforcement and stirrups in position and binding them tightly, as shown in Figure 3.10. Before completing the assembly of the formwork, the formworks were oiled for ease of stripping the form later on. While doing this it was insured that the reinforcements were not stained with oil.

Figure 3.10 Example of Preparing Reinforcing Cages and Formworks

3.2.4.2 Casting of Beam Specimens

For casting the specimens, a fresh concrete mix was prepared as discussed in Section 3.2.2. It was then transferred from the mixing facilities to the pre-stressing bed using a concrete transporter truck (the "Tuckerbilt"). The concrete was poured into a ready formwork with reinforcement cages. Even though the concrete itself had a high

workability and flowability, vibration was applied to consolidate the mix. An example of the casting process is shown in Figure 3.11.

Figure 3.11 Example of Casting of Concrete Beam Specimens in the First Phase

In order to have uniform distribution of the fibers, the proper viscosity of the mix was required which was previously verified at the laboratory through trial mix. As shown in Figure 3.12, steel fibers did not segregate and sink such that these fibers were observed at the top surface and well distributed. Figure 3.13 shows the finishing of the surface to provide a smooth surface and avoid fiber stick-out.

Figure 3.12 Examples of Uniformly Distributed Steel Fibers in Fresh Concrete

Figure 3.13 Finishing Surface after Pouring and Compacting the Fresh Concrete

After casting, both specimens were covered, as shown in Figure 3.14, with plastic sheets for one day in order to facilitate the curing process. On the following day of casting, formworks of the beams were stripped out and pre-stressing strands were cut. Fabricated beams (Figure 3.15) were exposed to the natural environment until tested.

Figure 3.14 Casted Beam Covered with Plastic Sheets

(a)

(b)

Figure 3.15 Fabricated Beam Specimens (a) PC#1-1 and (b) SFRPC#1-1

3.2.5 Testing of Specimens

3.2.5.1 General

As discussed in beginning of this chapter in order to study more realistic flexural behavior of continuous beam member including moment redistribution, testing a large-scale continuous beam is more appropriate. However testing such beams in lab is difficult task and also can be more expensive. That is why a simply supported test setup was adopted in this study. As discussed earlier, the simply supported beam can represent the part of a continuous beam between internal support and two adjacent points of contraflexure [Mattock, 1964]. The moment induced by a point load at mid span of the simply supported beam can simulate the distribution of moment at internal support of a continuous beam due to the reaction force. As the mid span load was applied through a steel plate, some confining effect would be produced due to the applied compression. However this confinement could be reduced to some extent by using steel plate with small width (as used in second phase in experiment). The modification factor as discussed in Chapter Two was also used to calculate the expected failure load (given in Appendix A).

3.2.5.2 Test Frame

A steel reaction frame was used for the large-scale specimen testing. Steel frames are anchored onto a strong concrete floor. A hydraulic cylinder that is single-acting high tonnage with a 660-kip loading capacity and an 11.81-inch stroke (ENERPAC, model CLSG-30012) was mounted on the frame, as shown in Figure 3.16. This hydraulic cylinder is pressurized by a submerged electrical pump controlling the

oil pressure. A 600-kip load cell was placed between the hydraulic cylinder and a 6-inch wide load bearing plate. The oil pressure was controlled based on the intended loads.

Figure 3.16 Test Frame Used in the First Phase

The specimen was supported by two concrete blocks. The top of the concrete blocks were covered with a 0.5-inch thick steel plate to create a smooth surface. Steel plates of 1×6×20 inches and rods of 2-inch diameter were used to create the roller and hinge support conditions, as shown in Figure 3.16. These supports were placed between the concrete blocks and specimens. A 1×6×20 inches steel plate was placed at the loading point. To uniformly distribute the load under the load bearing plate, a non-shrink grouting was pasted on the loading point at the top of the specimen before placing the load bearing plate so that the load bearing plate was fully contacted with the concrete surface.

3.2.5.3 Sensor Instrumentation

In the first phase, some external concrete strain gauges were also placed on the side surface (south face) of the specimen (for PC#1-1 only) at different heights, as

shown in the Figure 3.17. These strain gauges were made of two wires. As discussed earlier in the PC specimen the internal concrete strain gauges were installed only up to depth of 3.5 inches from top of beam. Hence some more surface strain gauges and LVDTs were installed so that the strain of concrete for the entire depth of the beam could be measured. Three wired potentiometers (spring pots) were used to measure the deflection of the loading point and supports. One additional LVDT (Linear Variable Differential Transformer) was fixed at the loading point as a backup for central deflection measurement.

Additional four LVDTs were fixed with plexi-glass and mounted horizontally on the south face of the specimens as shown in Figure 3.17 to measure the strain in tension zone of the beam section for the PC specimen. The 600-kip load cell was used to measure the applied load. All the sensors were connected to a Vishay 5000 data acquisition system and all the sensors values were monitored in real time and recorded at a rate of five data points per second. The detail of the sensor instrumentation is shown in Figure 3.18.

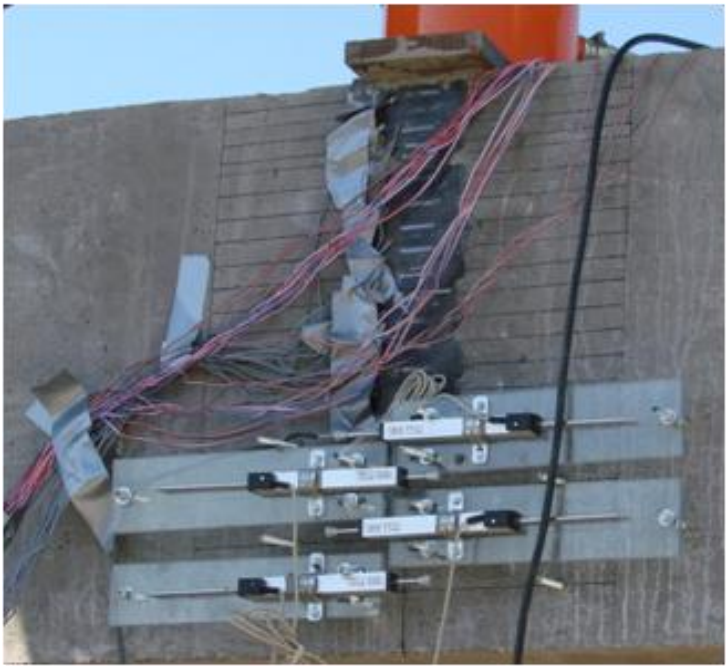

External Strain gauge	Distance from top (in.)
ESG#1	0.75
ESG#2	1.5
ESG#3	2.25
ESG#4	3
ESG#5	3.5
ESG#6	4.5
ESG#7	5.5
ESG#8	6.5
ESG#9	7.5
ESG#10	8.5
ESG#11	9.5
ESG#12	10.5
ESG#13	11.5
ESG#14	12.5
LVDT #1	14.5
LVDT #2	16.5
LVDT #3	18.5
LVDT #4	20.5

Figure 3.17 External Concrete Strain Gauges and Horizontal LVDTs

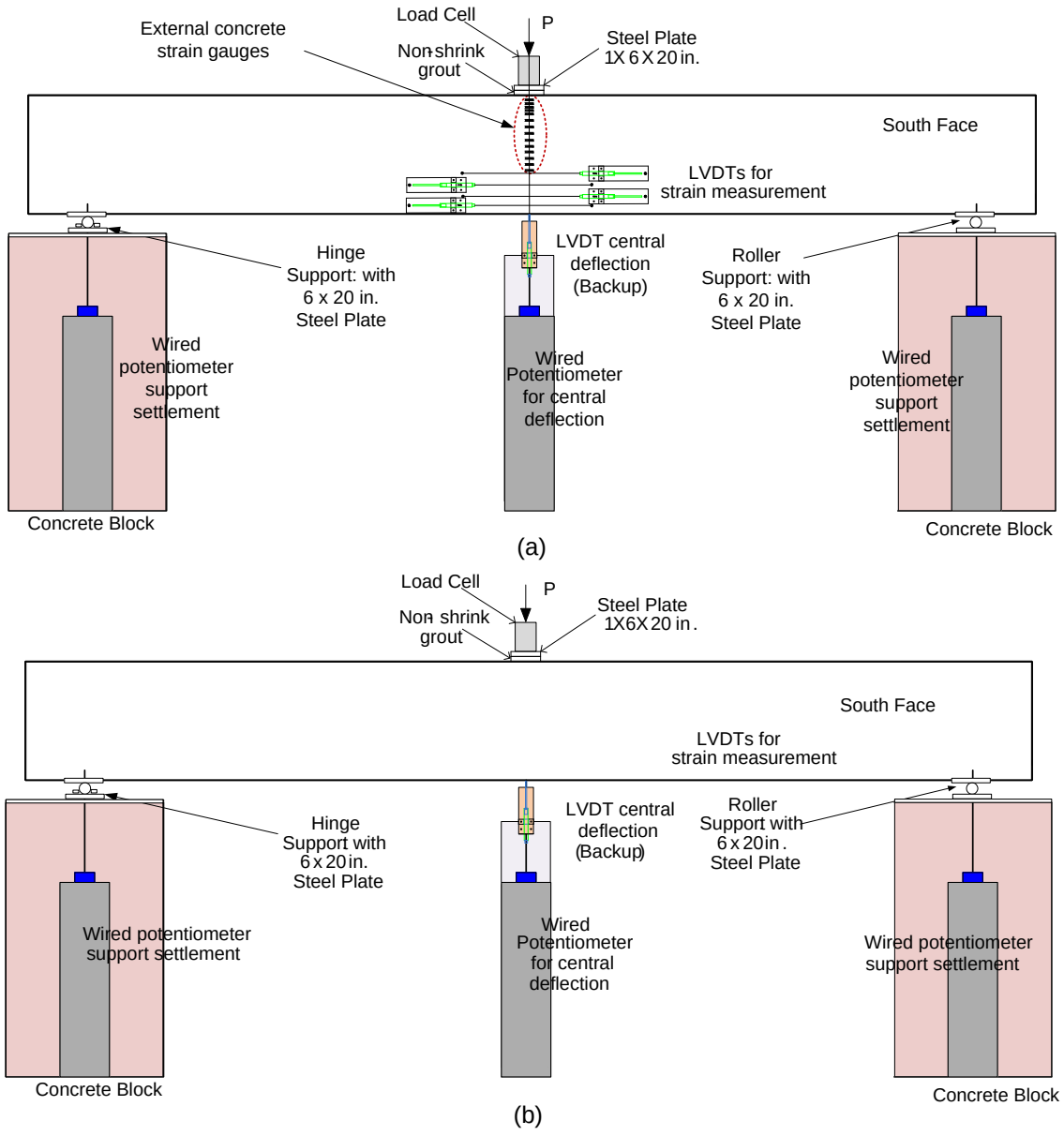

Figure 3.18 Sensor Instrumentation in the First Phase Experiment: (a) for PC#1-1 and (b) for SFRPC#1-1

3.2.5.4 Acoustic Emission Sensor

Acoustic Emission (AE), a non-destructive evaluation method, was used to measure crack initiation and propagation. Acoustic emission uses sensors that detect

acoustic waves created when cracks occurred upon increased load. It served as a very valuable tool, as it allowed analysis of energy dissipation in the form of crack formation, crack propagation, and reinforcing slippage and yielding (Colombo, et.al, 2003). Three sensors are generally required to locate exact location of the event (crack) occurring in the specimens. Hence location of AE sensors were so selected so that number events (crack) with accurate locations could be captured at area of interest. AE sensors were bonded with hot glue to the surface of both Specimens PC#1-1 and SFPRC#1-1 before testing, as shown in Figure 3.19. A total of seven AE sensors were used and radius of influence of each sensor was determined by the so-called lead pencil break test. This test consisted of breaking a 0.012 inches (0.3 mm) pencil lead in step by step to determine the effective radius of influence. Beyond this radius of influence, the system does not detect any signals. These sensors were connected to a central scanner box with in-line pre-amplifiers. The pre-amplifiers were set at 40 dB boost, which was determined before testing to be the most effective setting to eliminate unwanted noise associated with loading the concrete specimen. Installation of Acoustic emission sensor and scanner is illustrated in Figure 3.20.

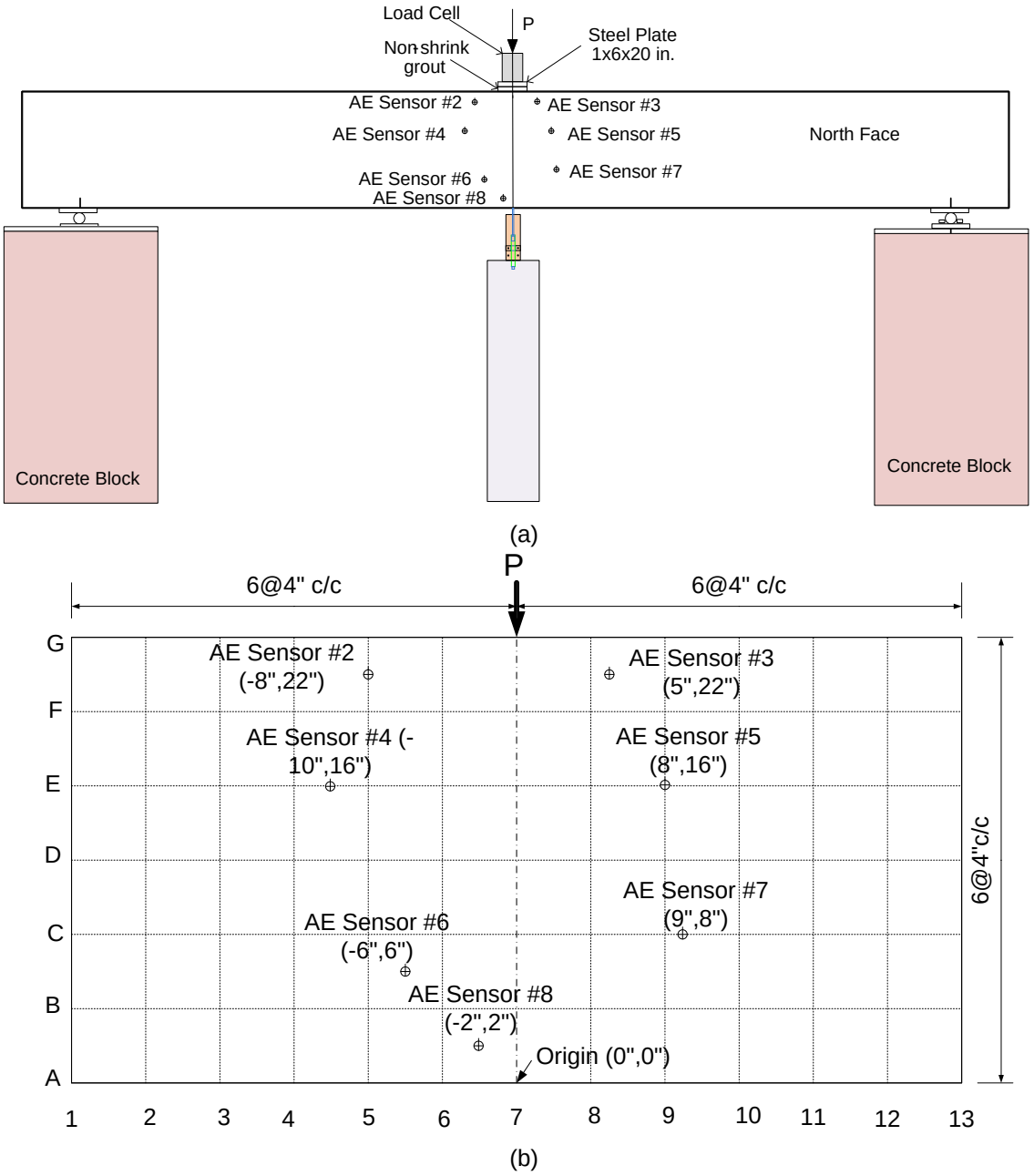

Figure 3.19 Acoustic Emission Sensors: (a) Overall Layout (b) Locations of AE Sensors

Figure 3.20 Installation of Acoustic Emission Equipments

The shear wave velocity for concrete was found to be 9.5-11.0 × 10^5 inches/s for reinforced concrete. The velocity was determined by recording the time between the detection of signal with two AE sensors and dividing by the known distance between the sensors, as shown in Figure 3.21. Sensor #4 and time required to travel the wave to closest sensor i.e. Sensor # 4(t_1) and (time required to travel the wave farthest sensor i.e. Sensor # 5(t_2) were recorded and Δt was calculated from equation 3.2. Again a pencil tip was broken near Sensor # 5 and time t_1 and t_2 (vice versa of earlier case) were recorded

and Δt was determined. The average of two values of Δt was used to determine the shear velocity from Equation 3.1.

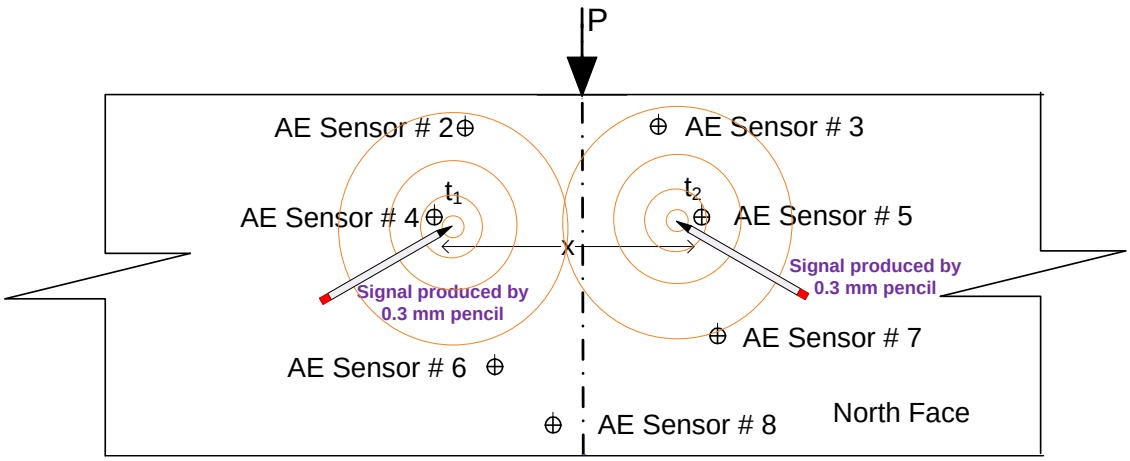

Figure 3.21 Method to Determine Shear Wave Velocity

$$v = x/\Delta t \qquad (3.1)$$

where:

v = shear wave velocity (inches/second)

$$\Delta t = t_2 - t_1\ (sec.) \qquad (3.2)$$

x is the distance in inches between the two AE sensors (# 4 and #5) and t_1 and t_2 are the time required to travel the wave produced by breaking of the 0.012 inches (0.3 mm) pencil tip to individual sensors.

3.2.5.5 Testing and Data Recording

By initially applying a load of one kip, all sensors and strain gauges were checked to find out if they were operating properly. Load was applied at 5 to 10 kip increments up to the first visible crack and then at 10 to 20 kip increments up to failure. When the load was paused at each load increment, cracks were marked and their widths

were measured, and testing pictures were taken. All data was recording using a data acquisition system (DAQ) attached to computers.

3.3 The Second Phase Experimental Program

3.3.1 Materials

3.3.1.1 Steel Fibers

In the second phase of the experimental program, different types of end hooked steel fibers (Maccaferri long, FF3) were used (Figure 3.23). The properties of the fibers are listed in Table 3.5. Compared to Bekaert RC-80/60-BN fibers, FF3 steel fibers have a shorter length, equivalent diameter, and a lower aspect ratio but higher tensile strength. The shape of the fibers is similar, round and end-hooked ended. The major reason of using of FF3 steel fibers in the second phase was that the dissolvable glue on the bundled fibers of Bekaert steel fiber used in the first phase were not completely dissolved as shown in Figure 3.22. This undissolved glue led to a non uniform distribution of fibers with uncertain quality control issue of fiber reinforced concrete. Thus, steel fibers used in the second phase were changed to discrete fibers; no glue was used with the steel fiber, as shown in Figure 3.23.

Figure 3.22 Example Photo of Glued Fiber (Remaining Intact)

Figure 3.23 Type of Steel Fiber Used: Macceferri Long (FF3)

During mixing it was observed that these fibers were well distributed without balling issue, which made easy for the concrete to mix and have a uniform fiber distribution. The better distribution was noticed during casting and after testing from a broken piece of concrete as shown in Figure 3.24.

Table 3.5 Mechanical properties of steel fibers used in the second phase experiment [1]

Shape	Length (L)	Diameter (D)	Aspect ratio (D/L)	Tensile strength
Doubled-hooked ends	2 inches	0.03 inches	67	159 ksi

[1]: All values are provided by manufacture

Figure 3.24 Uniformly Distributed Steel Fiber in the Second Phase Specimens

3.3.1.2 Concrete Mix

In this phase of the experiment, the concrete's target compressive strength was also 6000 psi, which was similar to the first phase of the experiment. There were some minor modifications in the mix design in the second phase as compared to first phase: Class C type fly ash was added in with Type I cement. Another mix as shown in Table 3.7 for PC#2-2 was also used. Mixing was done at the local precast plant using the same facilities and procedure as for the specimens in the first phase. The mix proportions and compressive strengths of the concrete used in the second phase are presented in Table 3.6.

Table 3.6 Mix Proportion and Compressive Strength of Concrete Used in the Second Phase

Types of concrete	Cement (Type 1)	Fly Ash Class C	Sand [1]	Coarse Aggregate [2]	Water	Steel Fiber	Comp. strength[3]
PC	1.00	0.50	1.70	1.0	0.60	-	5409
SFRPC V_f=0.75%	1.00	0.50	1.70	1.0	0.60	0.12	5250

[1]: ASTM Natural River sand (Fineness modulus = 2.57)
[2]: Crushed limestone with maximum size of ¾ inches
[3]: The strength was measured by testing six number of 4×8 inches concrete cylinders cast simultaneously with large-scale beams

Table 3.7 Mix Proportion and Compressive Strength of Concrete Used for PC # 2-2 in Second Phase

Types of concrete	Cement (Type 1)	Fly Ash Class C	Sand [1]	Coarse Aggregate[2]	Water	Steel Fiber	Comp. strength [3]
PC	1.00	0.50	1.3	1	0.40	-	6963

[1]: ASTM Natural River sand (Fineness modulus = 2.57)
[2]: Crushed limestone with maximum size of ¾ inches
[3]: The strength was measured by testing six number of 4×8 inches concrete cylinders cast simultaneously with large-scale beams

3.3.2 Design of Beam Specimens

In the second phase of the experimental program, four beam specimens were prepared and tested for further investigation on the flexural behavior of SFPRC beams. Specimens used in the second phase of the experiment had the same geometry as those used in the first phase of the experiment. The total length of the beams was 14 feet (168 inches). The height of the beams was 2 feet (24 inches). The effective depth of the beams was 21 inches.

Two PC specimens were prepared for comparison purposes. The first PC specimen (PC#2-1) was tested using single point loading at the center of the specimen

on a steel plate of 1×6×20 inches dimensions. The two SFRPC specimens were prepared with a 0.75% volume fraction of steel fibers. The first SFRPC specimen, SFRPC#2-1, had a 2.11% longitudinal reinforcement ratio. The other SFRPC specimen, SFRPC#2-2, had a 0.29% longitudinal reinforcement ratio. SFRPC#2-1, with a steel ratio of 2.11%, had $c/d_t = 0.41$ (see Appendix A) which is greater than 0.375, as per ACI 318-11, hence the section is not tension controlled. It lies within the transition zone. The first PC specimen (PC#2-1) and the two SFRPC specimens (SFRPC#2-1 and SFRPC#2-2) were prepared using the same mix, with a concrete compressive strength of approximately 5.3 ksi. However, the second PC specimen, PC#2-2, had a higher compressive strength, 6.93 ksi, because it was casted using a different concrete mix on a different date (mix proportion is shown in Table 3.7). PC#2-2, SFRPC#2-1, and SFRPC#2-2 were tested with a single point loading at the center of the beam over a steel plate of × 3× 16 inches dimensions (same as that used by Mattock [1964], as discussed in Chapter Two) to investigate the effect of smaller plate in reducing the confining area due to the applied load (which induces a bi-axial compression thus increasing the compressive strength as well as the ultimate strain of the concrete).

For both PC specimens, minimum web shear reinforcements were provided based on the requirements provided by ACI 318-11. No. 3 mild steel bars were used for the shear reinforcement in a hooped manner, at a spacing of 8 to 12 inches center to center. Based on previous shear tests results [Cho et al, 2010], SFRC can have an ultimate shear strength of approximately $5.6\sqrt{f_c'}$ (psi). The additional area of stirrups was computed assuming SFRC has this shear strength. Hence the area of stirrups

provided for SFRPC#2-1 was less than the area required based on current ACI provision for regular concrete beams. Note that this specimen was designed with a larger longitudinal steel reinforcement ratio, as a consequence in order to avoid premature shear failure, sufficient shear reinforcement would have to be provided if no fibers were used. As per ACI provisions for this type of beam the required spacing of No. 4 bar (in hooped form) would be 3 inches near the mid span and 5 inches near the support if there no fibers were used. However, the spacing of stirrups provided in the span of SFRPC#2-1 was only 8 inches center to center, which was slightly more than the required spacing of 6 inches (considering shear strength for SFRC as $5.6\sqrt{f_c'}$.)

Although the shear demand for SFRPC#2-2 is smaller, due to a lower longitudinal steel ratio used, the spacing of stirrup would have require was 8 inches (mid span) to 12 inches (near support) for plain concrete as is the case for PC#2-1. However, for SFRPC#2-2, only one stirrup (No. 3 bar) was provided at the middle of the beam for fabrication purpose.. Details of the design parameters of all of the specimens for the second phase are shown in Figure 3.25 and Table 3.8. The detail flexural and shear design calculations for all beams are shown in Appendix A.

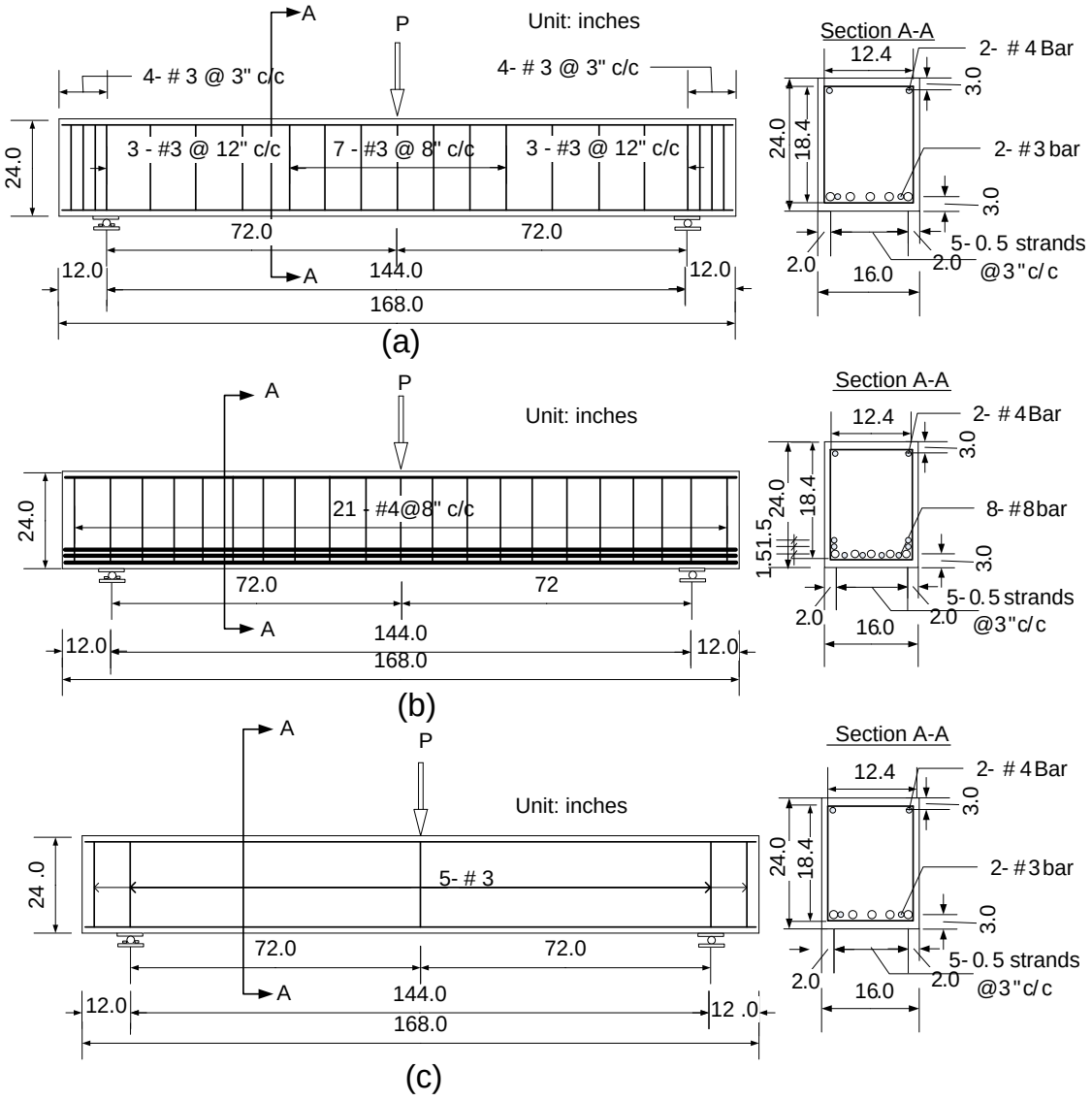

Figure 3.25 Dimensions of Beam Specimens Used in the Second Phase:
(a) PC specimens (PC#2-1 and PC#2-2) (b) SFRPC#2-1 and (c) SFRPC#2-2

Table 3.8 Summary of Design for the Beam Specimens of Second Phase

Specimens	Height (in.)	Length (in.)	Shear reinforcement	Longitudinal reinforcement ratio (ρ)	Average prestress in concrete (psi)
PC#2-1	24	168	2-legged #3@8-12”c/c	0.29% (2-#3 and 5-0.5-in. strands)	380
PC#2-2	24	168	2-legged #3@8-12”c/c	0.29% (2-#3 and 5-0.5-in. strands	380
SFRPC#2-1	24	168	2-legged #3@8”c/c	2.11% (8-#8 & 2-#3 and 5-0.5-in. strands)	380
SFRPC#2-2	24	168	2-legged 1-#3*	0.29% (2-#3 and 5-0.5-in. strands)	380

*for construction purposes

3.3.3 Internal Sensor Instrumentation

The strain gauges in both compression and tension steel in the second phase are installed in exactly the same manner as those installed in the first phase (Figure 3.24). Seven internal concrete strain gauges were placed only at the compression zone at 1.25 inches from top of the beam section as shown in Figure 3.25, for all four specimens. Locations of the embedded concrete strain gauges are shown in Table 3.9.

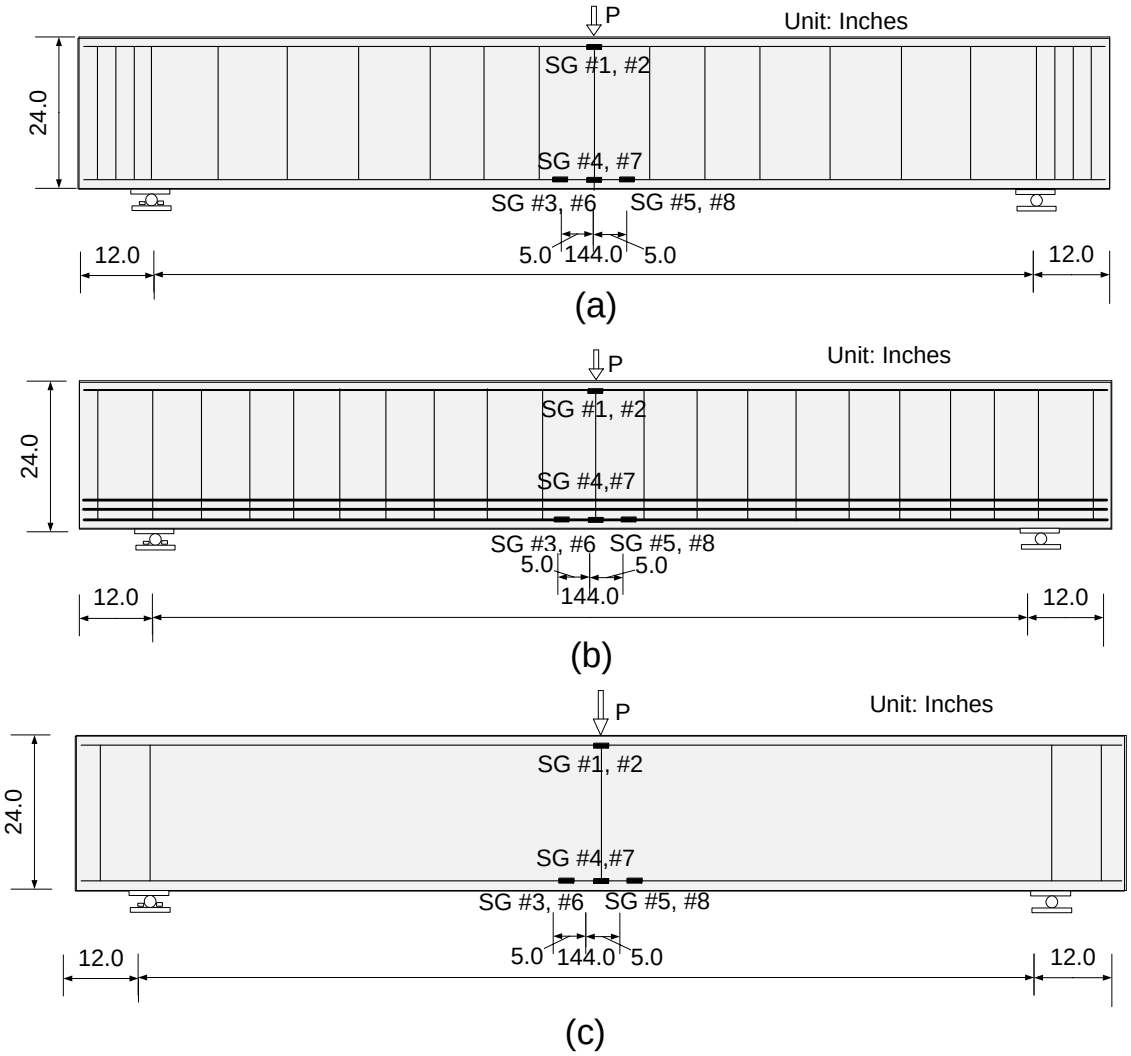

Figure 3.26 Steel Strain Gauges in Second Phase Experiment (a) PC#2-1and PC#2-2 (b) SFRPC#2-1 and (c) SFRPC#2-2

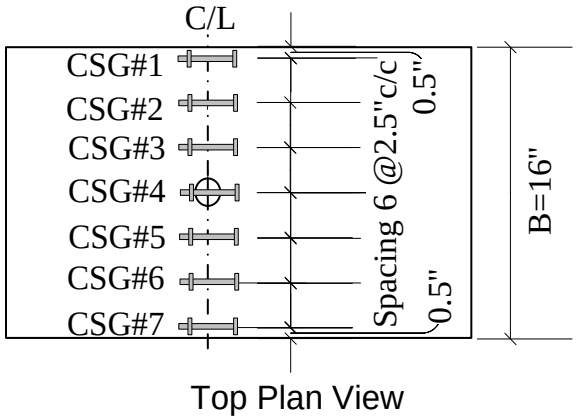

Figure 3.27 Concrete Strain Gauges Used in Second Phase of Experiment

Table 3.9 Location of Concrete Strain Gauges in Second Phase

Strain gauge #	PC#2-1	PC#2-1	SFRPC#2-1	SFRPC#2-2
	Distance from north face (inches)			
CSG# 1	0.50	0.50	0.50	0.38
CSG# 2	3.00	3.00	3.00	3.00
CSG# 3	5.50	5.50	5.25	5.25
CSG# 4	8.00	8.00	7.75	8.00
CSG# 5	10.50	10.50	10.25	10.50
CSG# 6	12.75	13.00	12.75	13.00
CSG# 7	15.75	15.50	15.25	15.63

3.3.4 Fabrication of Specimens

Fabrication of the specimens in the second phase included the preparation of formwork, reinforcement caging and casting. The work was carried out at the local precast plant under the author's supervision. Same facilities that were used in the first phase were also used for the fabrications of beams in the second phase. The manpower and time required for preparation the stirrups for PC#2-1 and SFRPC#2-2 was also recorded for comparison purpose. All specimens were covered by plastic sheets after casting to facilitate the curing process. After one day, the formworks were stripped out and prestressing strands were cut. The camber was measured and found negligible. All specimens were placed in the natural environment until tests were conducted. Examples of fabrication process of specimens in second phase are shown in the following photographs (Figures 3.28 and 3.29).

Figure 3.28 Typical Photos of Reinforcement Caging and Formworks in Second Phase

Figure 3.29 Typical Photos of Casting in Second Phase

3.3.5 Instrumentation and Testing of Specimens

In the second phase of the experiment, the same test frame was used as the first phase for the reason discussed earlier. The same Vishay 5000 DAQ system was used to collect data from all sensors: load cells, LVDTs, and strain gages recording five data points per second. In this phase, four concrete surface strain gauges were also installed

for PC#2-1 in the compression zone to compare the strains with those obtained internal concrete strain gauges, as shown in Figure 3.30.

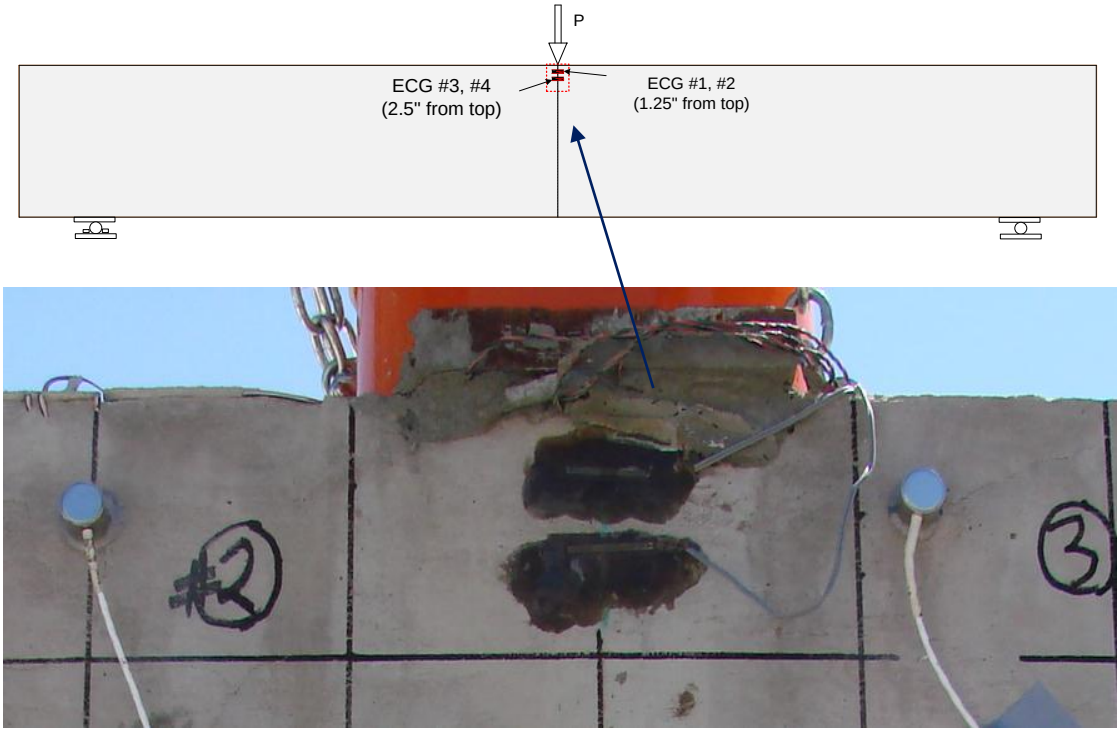

Figure 3.30 External Concrete Strain Gauge in the Second Phase

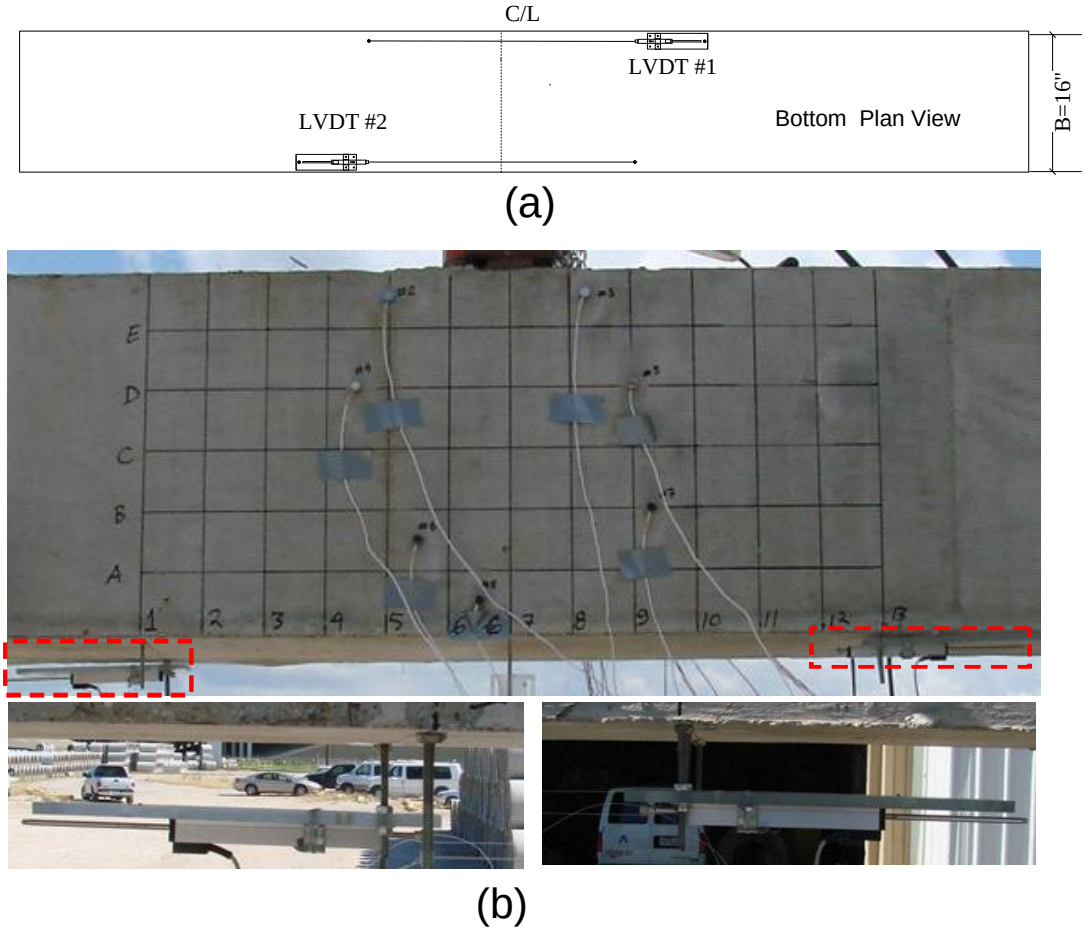

Figure 3.31 LVDT placed Underneath the Beam to measure the longitudinal deformations (a) Plan View and (b) Side View

Two LVDTs were mounted underneath the beam, as shown in Figure 3.31, to measure the deformations along the length of specimen at mid span with in range 24 inch from center line in order to determine the rotation.

Other instrumentation such as load cells, LVDTs, and AE sensors were installed as in the first phase of the experiment. However, for this phase, no spring pots were used for measuring deflection, which created some problems during testing in the first phase because the long string was usually disturbed during the blowing of the wind.

Hence, in this phase, all displacement sensors used were LVDTs, as shown in Figure 3.32.

(a) (b)

(c)

Figure 3.32 LVDTs for Measurement of Defection and; (a) at Mid Span (b) at Left Hinge Support (c) Right Roller Support

There was one modification in the loading point. For this phase, excluding PC#2-1, a 3-inch wide plate was used at the loading point in order to reduce the loading confinement area. Details of the instrumentation used in the second phase are shown in Figure 3.33.

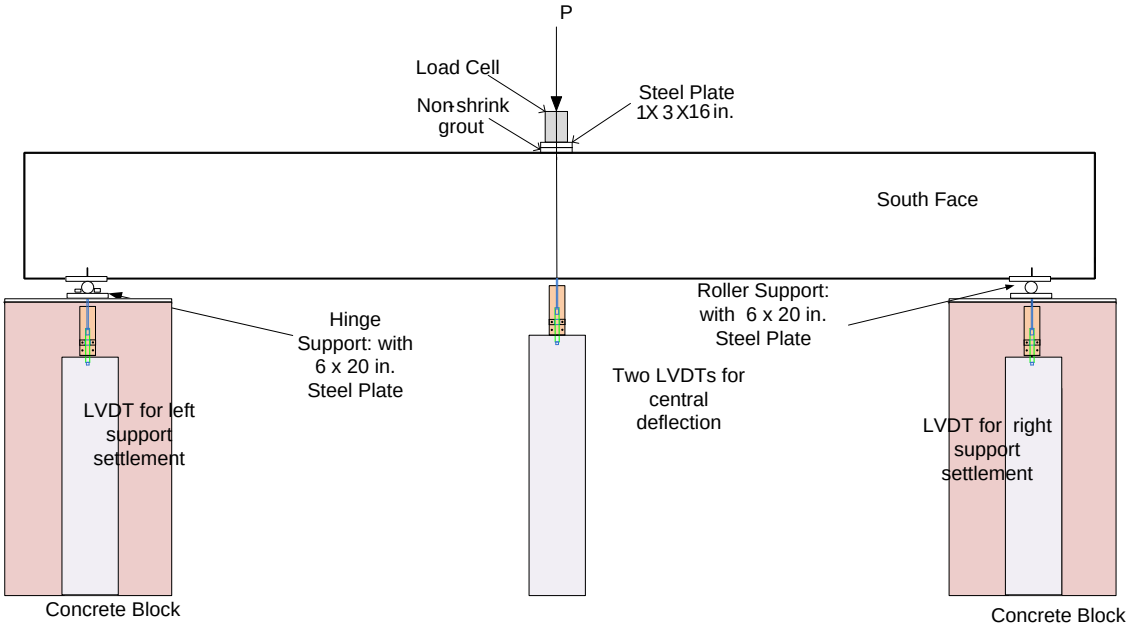

Figure 3.33 Instrumentation for Second Phase Experiment

In the second phase, seven acoustic emission sensors were installed and connected to the scanner to capture the events that occurred during the loading of the specimens (Figure 3.34). Locations of AE sensor were the same as those used in case of first phase.

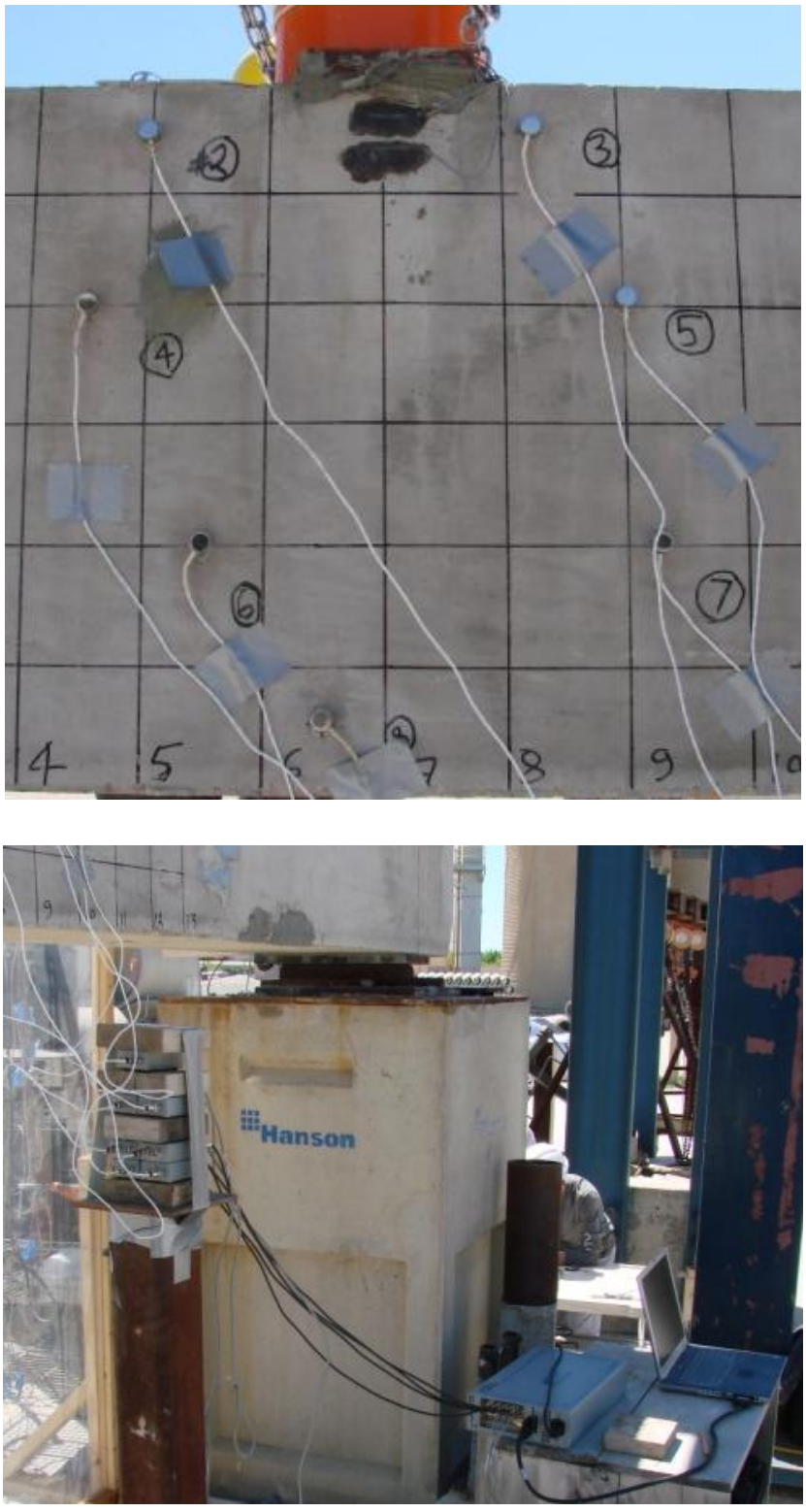

Figure 3.34 Acoustic Emission Sensors and Scanner Used in Second Phase Experiment

3.4 Material Testing for Large Scale Prestressed beams

3.4.1 Preparation of Specimens

Both in the first and the second phase of experiment, some small specimens for material testing were prepared and tested in order to evaluate various mechanical properties of the concrete. These specimens were small 4 × 8 inches cylinders for compressive strength test, large 6 × 12 inches cylinders for compressive stress strain curves (with large cylinder test), equivalent tensile strength for the peak load as well as residual strength of SFRC (Double Punch Test). As shown in Figure 3. 35 one concrete strain gauge was placed at the center of the large cylinder to measure the compressive train in concrete.

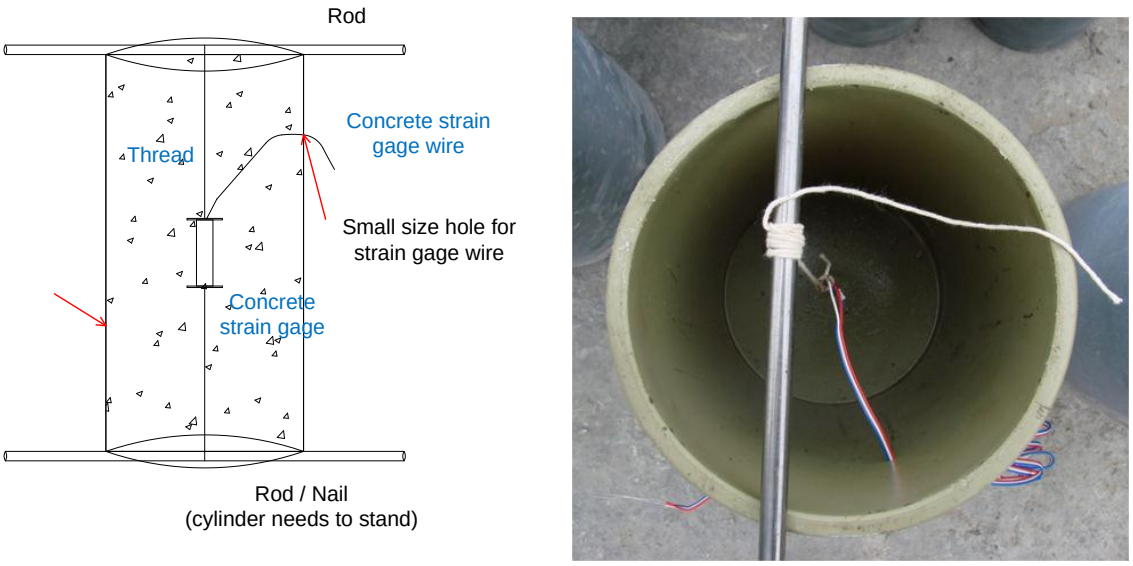

Figure 3.35 Typical Photos of Preparation of Specimens for Material Test

Beams for the third point bending test (ASTM C1609) and dog-bone shaped specimens for the direct tensile test were also prepared.

Examples of the preparation of different types of specimens are shown in Figures 3.36 and 3.37.

Figure 3.36 Preparations of Molds for Material Test Specimens

Figure 3.37 Typical Photos of Preparation of Specimens for Material Test

3.4.2 Compressive Strength Test

Concrete was sampled to prepare 4 × 8 inches cylinders. Six cylinders were prepared for each specimen and were tested one day after the large-scale specimen was tested. A 500-kip capacity hydraulic compressive machine was used for the cylinder test. The test procedure as per ASTM C39 (ASTM 2011), "Standard Test Method for Compressive Strength of Cylindrical Concrete Specimens" (discussed in Chapter Two) was followed.

All cylinders were well capped with a capping compound, which satisfies specifications required by ASTM C617 [ASTM 2003]. The capping provided a very flat surface and helped uniformly distributed the load through the cylinder's cross-section.

Steel fiber reinforced concrete cylinders had a ductile behavior developing multiple cracks. Only top and bottom portions were crushed during testing, as shown in Figure 3.38.

Figure 3.38 Typical Photos of Compressive Strength Test (Cylinder Test)

Figure 3.39 Testing Setup for Compressive Testing of Large Cylinders (6 × 12 inches)

Figure 3.40 Typical Photos of Compressive Testing of Large Cylinders (6 × 12 inches)

Along with small cylinders, some 6 × 12 inch large cylinders were tested as shown in testing setup (Figure 3.40). Large cylinders consisted of one internal concrete strain gauge at the middle of the cylinder as discussed above (Figure 3.35).. Two external strain gauges and two LVDTs were placed on each side, as shown in Figure 3.39 , during testing to measure the deformation. Results are discussed in Chapter Five.

3.4.3 Third Point Bending Test

These tests were carried out for both phases of the experiment. The test is carried out as per ASTM C1609 (ASTM 2010) for the third point bending test method (discussed in Chapter Two) using a closed-loop servo controlled machine (Figure 3.41). Six specimens were tested for each phase with fiber reinforced concrete.

Figure 3.41 Typical Photos from Third Point Bending Test (ASTM C1609)

3.4.4 Direct Tensile Test

Although six dog bone shaped tensile specimens were also prepared with the large-scale beams, they could not be tested as all specimens were cracked in the manner shown in Figure 3.42 during curing and handling. The specimens were kept in natural condition with large-scale beams. The outside temperature was high in day time which may produce the surface crack in narrowed section of the specimens. While demolding the specimens the crack widened and propagated for whole depth. This showed that great care is needed when handling these types of specimens.

Figure 3.42 Typical Example of Problem with Preparation Dog Bone Specimens

3.4.5 Double Punch Test

Some large cylinders (6 × 12 inches) were prepared with the large-scale beams for double punch test (DPT). A total of 6 specimens were prepared by cutting half from three 6 × 12 inches cylinders and were tested for both plain concrete (PC) and steel fiber reinforced concrete (SFRC). A detailed procedure is explained in the next chapter and was adopted to carry out these tests. Typical examples of DPT tests are shown in Figure 3.43.

Figure 3.43 Typical Photos from Double Punch Test

CHAPTER 4

EXPERIMENTAL INVESTIGATION (DOUBLE PUNCH TEST) AND FINITE ELEMENT ANALYSIS FOR DPT MODEL

4.1 General

As discussed in first two chapters, the evaluation of material properties should ensure that the fiber reinforced concrete (FRC) has been batched properly and can give indications of probable performance when used in structures. On the other hand, an ideal material test method for FRC needs to account for many factors. It should have low variability in the measurement of any property; it should be able to quantify certain criteria with regard to FRC mechanical performance in terms of strength, crack resistance, or toughness; and it should additionally reflect the characteristics depicted by a load versus deflection curve (Mindess et al. [2003]). There are various material test methods for the evaluation of the mechanical properties of FRC, such as third point bending test (ASTM C1609), direct tensile test, round panel test (ASTM C1550), and spilt cylinder test (ASTM C496).

Previous studies have indicated that the material test method recommended by ACI (third point bending test, ASTM C1609) and other methods have several limitations, as discussed in Chapter Two. The search for a simple and reliable material test method to determine the tensile performance of FRC is essential. That is why the reintroduction of the double punch test (DPT), which was first introduced by Chen in

1970s (reference), has come back into the picture. Hence the double punch test has been exclusively evaluated in this experimental investigation in order to develop a simple and reliable material testing method. The experimental program for the double punch test consists of different phases with the use of different types of steel fibers and mixed steel fibers (hybrid) with different volume of fractions and ages, as well as mixtures. Finite element analyses (FEA) were also carried for DPT models to observe stress distribution.

4.2 First Phase Experimental Program

4.2.1 General

In the first phase the double punch test was performed to investigate the load versus deformation response and the equivalent tensile strength of plain concrete and steel fiber reinforced concrete. In this phase, plain concrete and three different types of steel fibers with various volume fractions were prepared and tested. The volumes of fractions of fibers used in this phase were ranging from 0.5% (67 pound per cubic yard) to 2.0% (268 pound per cubic yard). Each set (with one type and one volume of fraction of fiber) had 10 specimens. A total of 126 specimens were tested. The tests were performed when the compressive strength was about 4 ksi (the reason for this is discussed later on in this chapterat age from 24 to 48 hours).

4.2.2 Steel Fibers

In the first phase, three types of steel fibers (both made in USA or outside of USA) were used in this phase of study. The properties of different steel fibers are

presented in Table 4.1. As shown in Figure 4.1, Type 1 fiber (Royal) has a single-bend hooked shape at the ends and Type 2 (Bekaert, Short) and Type 3 (Bekaert Long) fibers have double-bend hooked shapes at the ends. Type 1 has an aspect ratio (L/D) of 40 and Type 2 and Type 3 fibers have an aspect ratio of 53 and 83, respectively. All steel fibers have a tensile strength of approximately 150 ksi.

Table 4.1 Properties of Steel Fibers Used in First Phase

Fiber Type	Shape	Length (L)[1]	Diameter (D)[1]	Aspect ratio (L/D)[1]	Tensile strength[2]
Type 1 (Royal)	Hooked-end (single-bend)	1.525 in. (38.7 mm)	0.038 in. (0.97 mm)	40	150 ksi (1034 MPa)
Type 2 (Bekaert, short)	Hooked-end (double-bend)	1.171 in. (29.8 mm)	0.022 in. (0.56 mm)	53	152.3 ksi (1050 MPa)
Type 3 (Bekaert, long)	Hooked-end (double-bend)	2.427 in. (61.6 mm)	0.029 in. (0.74 mm)	83	152.3 ksi (1050 MPa)

[1] Measured; [2] Provided by manufactures

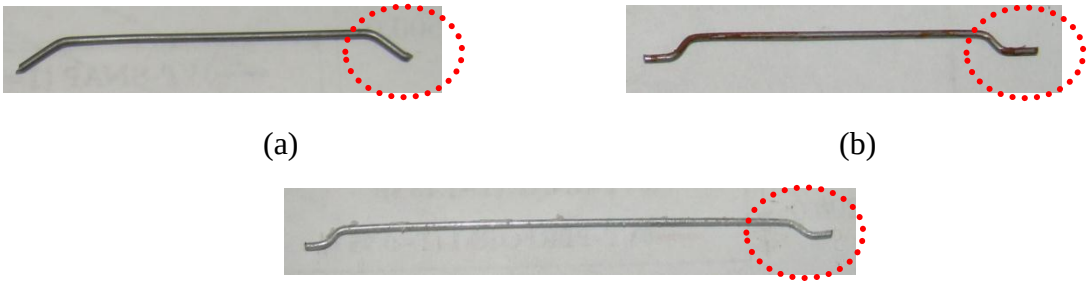

Figure 4.1 Types of Fiber Used in First Phase of Study for DPT: (a) Type 1 (Royal, Single-Bend Hooked at End) (b) Type 2 (Bekaert Short, Double-Bend Hooked at End) (c) Type 3 (Bekaert Long, Double-Bend Hooked at End)

4.2.3 Concrete Mix

The concrete mix design used for this phase of study as shown in Table 4.2 was provided by the Texas Department of Transportation (TxDOT). The trial mix demonstrated that the mix design generally work for the steel fiber reinforced concrete.

Table 4.2 Mix Proportion (By Weight) Used in the First Phase

Specimens	Cement (Type-I)	Sand	Coarse aggregate[3]	Water	Steel fiber	Super plasticizer[9]
PC (control)	1.00	1.96	2.72	0.34	0	0.013
SFRC-X*-050					0.101[4]	
SFRC-X-075					0.152[5]	
SFRC-X-100					0.204[6]	
SFRC-X-150					0.311[7]	
SFRC-X-200					0.422[8]	

[3] Maximum size = ¾ in; [4] 0.50% of volume fraction; [5] 0.75% of volume fraction; [6] 1.00% of volume fraction; [7] 1.50% of volume fraction; [8] 2.00% of volume fraction; [9] Super plasticizer: High Range Water Reducing Admixture;

* X: R for Type 1 fiber, BS for Type 2 fiber and BL for Type 3 fiber

All other materials such, as cement, sand, and coarse aggregate used for the concrete mix were donated by local precast concrete plant (Hanson Precast and Pipe, Grand Prairie). ASTM Natural River sand (Fineness modulus 2.57) and crushed lime stone aggregate with a maximum size of ¾ inches were used. Type I cement was used. The concrete was mixed by a drum mixer at the Civil Engineering Lab (CELB). During

mixing, first the sand and cement were mixed for about 1-2 minute. Then water was gradually added so that a good paste with was prepared. Then course aggregate was added and mixed again. When the concrete mix was ready, the steel fiber was gradually added and mixed again for a few minutes. Super plasticizer was initially added into the water. The steps for mixing the concrete are illustrated in Figure 4.2 and Figure 4.3.

(a)

(b)

Figure 4.2 Typical examples of concrete mixing (a)Preparation of Materials (b) Adding Water Gradually to Prepare Good Paste

(a)

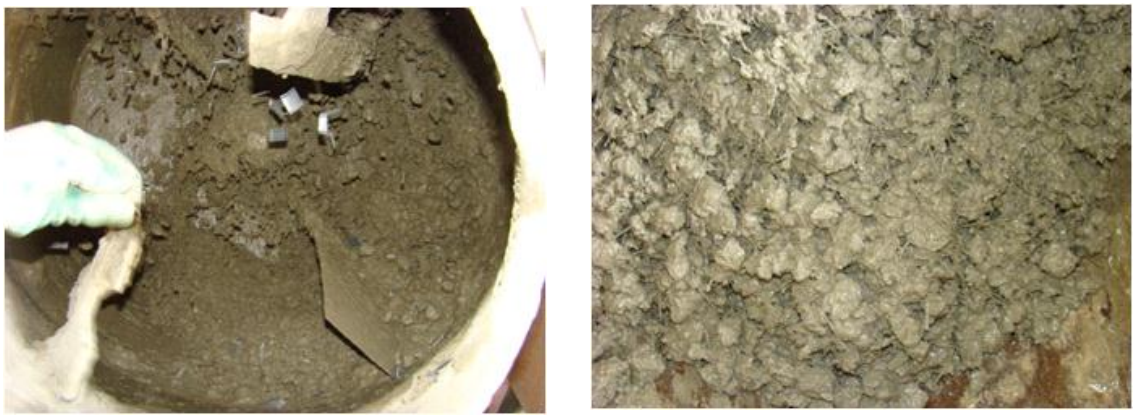

(b)

Figure 4.3 Typical Examples of Mixing Concrete:(a) Addintion of Course Aggregate in Cement Mortar Paste to Pprepare Plain Concrete Mix (b) Addition of Steel fibers to Prepare SFRC Mix

4.2.4 Preparation of Specimens

4.2.4.1 Specimen Information:

Specimens were named in the following fashion (Table 4.3): 1) PC: plain concrete; SFRC: steel fiber reinforced concrete; 2) the first number represents fiber type ; 3) the second number represents the volume fraction of fiber, 050 means 0.50% and 075 means 0.75% volume fraction of fibers and so on. Similarly R represents Royal fiber (Type 1), BS represents Bekaert short fiber (Type 2) and BL represents Bekaert

long fiber (Type 3). Each group of specimen consisted of 10 specimens, except SFRC BL-150 which had only six specimens. 126 specimens were in this phase.

Table 4.3 Specimen Information Used in the First Phase

<table>
<tr><th>Specimens name</th><th>Steel fiber type</th><th>Volume of fraction</th><th>Number of specimens</th></tr>
<tr><td>PC</td><td>-</td><td>-</td><td rowspan="12">10 for each set, total 120</td></tr>
<tr><td>SFRC R-050</td><td rowspan="5">Type 1
(Royal)</td><td>0.50 %</td></tr>
<tr><td>SFRC R-075</td><td>0.75 %</td></tr>
<tr><td>SFRC R-100</td><td>1.00 %</td></tr>
<tr><td>SFRC R-150</td><td>1.50 %</td></tr>
<tr><td>SFRC R-200</td><td>2.00 %</td></tr>
<tr><td>SFRC BS-050</td><td rowspan="3">Type 2
(Bekaert short)</td><td>0.50 %</td></tr>
<tr><td>SFRC BS-075</td><td>0.75 %</td></tr>
<tr><td>SFRC BS-100</td><td>1.00 %</td></tr>
<tr><td>SFRC BL-050</td><td rowspan="4">Type 3
(Bekaert long)</td><td>0.50 %</td></tr>
<tr><td>SFRC BL-075</td><td>0.75 %</td></tr>
<tr><td>SFRC BL-100</td><td>1.00 %</td></tr>
<tr><td>SFRC BL-150</td><td>1.50 %</td><td>6</td></tr>
<tr><td colspan="3">Total numbers of specimens</td><td>126</td></tr>
</table>

4.2.4.2 Casting of Cylinders

In the first phase, each of the 12 sets had 10 specimens and one set had 6 specimens with 0 to 2% volume fraction of fibers with three types of steel fibers, Type 1(Royal fiber), Type 2 (Bekaert short), and Type 3 (Bekaert long), as shown in Table 4.3, were prepared. Five 6×12 inches plastic molds were used for preparation of five or three cylinders for one set. Used molds which bulged at the bottom were not used to

make sure a smooth surface of the specimens. This is more critical for DPT since the load was applied through the central portion of the top and bottom faces. Concrete mix, prepared as discussed earlier, was poured into the 6×12 inches plastic molds. The concrete mix was poured in three layers and compacted with a table vibrator). Three 4×8 inches cylinders were also prepared for determining the compressive strength. After casting all specimens were placed in a curing room, as shown in Figure 4.4.

Figure 4.4 Preparation and Placing Speciemn in Curing Room

4.2.4.3 Preparation of Test Specimens

To prepare the test specimens for the double punch test, 6×12 inches cylinders were cut in half with a concrete saw, as shown in Figure 4.5. Then ten 6×6 inches cylindrical specimens were prepared for each set. The top and bottom surfaces were made smooth with sand stone and the centers of the surfaces were marked.

Figure 4.5 Typical Examples of Preparation of 6 × 6 Inches Test Specimens for DPT

4.2.5 Test Setup and Instrumentation

The simple apparatus suggested by Chen (year), as shown in Figure 4.6, was used for testing the specimen. The test setup consisted of a 60-kips compression machine (Baldwin), LVDTs (Linear Variable Differential Transformer), load cell (50-kips capacity), and two steel punches. The size of loading punches was 1.5 × 1 inches (diameter × height) .These punches were centered on the top and bottom surfaces. Tape was used to secure the position of the centered loading punches after they were placed on the top and bottom surfaces. A steel plate was placed between the bottom punch and the load cell in order to distribute the load. Two LVDTs were used to measure the vertical deformation of the specimens. The LVDTs and the load cell were connected to data acquisition box to record the data from the test. The overall view of the test setup is shown in Figure 4.6.

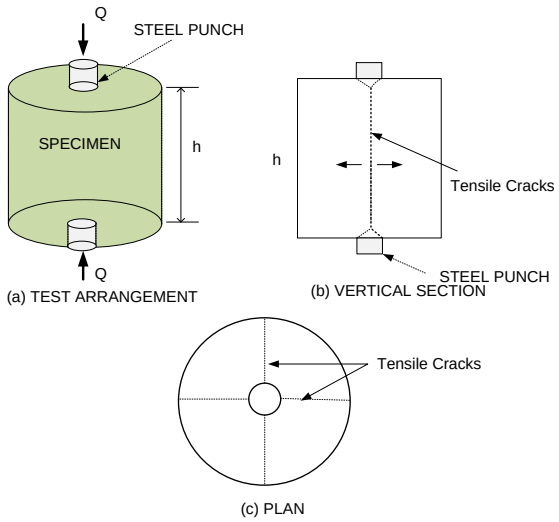

Figure 4.6 Test Apparatus Suggested by Chen [Chen, 1970]

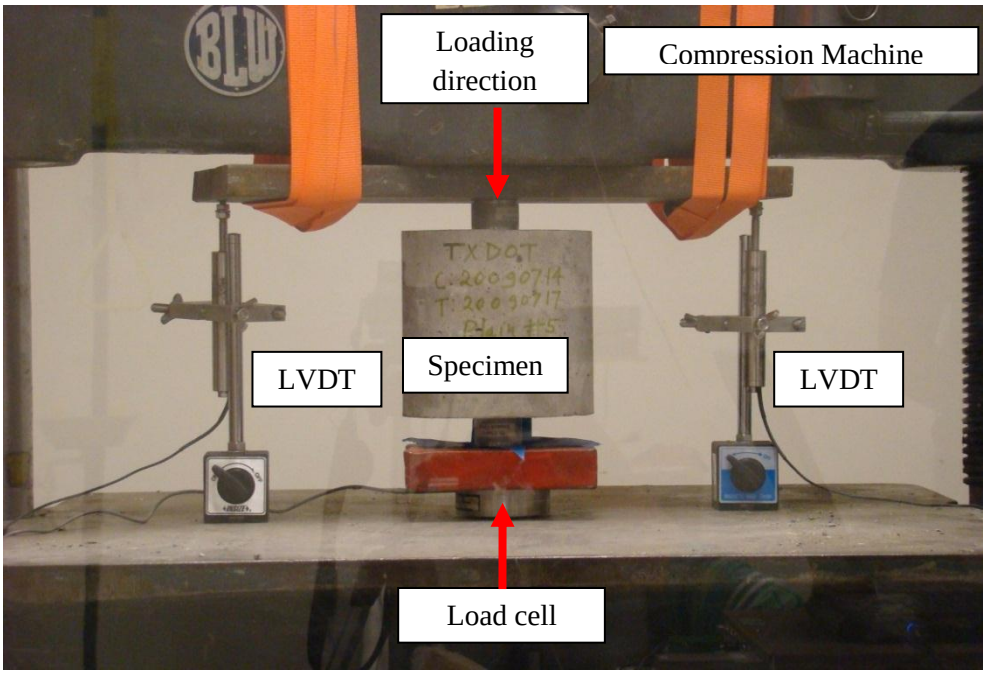

Figure 4.7 Double Punch Test Setup

4.2.6 Testing of Specimens

The 6×6 inches specimens were tested after 24 to 48 hours. The tests were performed when the compressive strength was approximately 4 ksi to represent the early age strengths of typical prestressed concrete members (especially the prestressed concrete panels). This stress corresponds to the initial stress at the time of the transfer of prestress (before prestress losses). The compressive strength of the concrete was determined by testing three 4×8 inches cylinders by a 500kips compressive machine.

Compressive force was applied by 60-kips Baldwin testing machine through with a loading rate of 100 lb/sec up to the peak load (ascending portion of the load deflection curve) the corresponding deflection rate was 0.002 inches/min. However after peak load it is hard to control with load rate as no load was increasing. So the

deflection rate of 0.006 inches/sec (three time fater than the rate during ascending portion) was adopted after the peak load has been reached (descending part of the load deflection curve) or the crack opening stage. The loading rate was manually controlled by monitoring the computer data. Photographs at different stages were taken. The test was stopped when the residual load reached approximately one fourth of the peak load . In the first phase, 10 specimens were tested for each set. Typical examples of the first phase of the double punch test and compressive strength test are shown in Figure 4.8.

Figure 4.8 Typical Examples for Testing of Specimens (DPT and Compressive Strength)

4.3 Second Phase Experimental Program

4.3.1 General

Based on first phase experimental result (see Chapter Six), the number of specimens were reduced from ten to four. From the first phase study, it was shown that the coefficient of variation (C.O.V) for peak loads was generally low (discussed in Chapter Six). In first phase since larger number of specimens (10 numbers) were prepared only for one batch (specimen with one type of steel fiber with one volume of fraction) could be casted at one time. In order to minimize the variability of concrete properties due to casting on different days, one group of specimens (i.e. all specimens with Type 1 fiber with different volume fraction) was prepared on the same day and tested after 48 hours. In this phase of the experimental program, mix proportions with volume of fraction and type of fiber was same as in case of phase one as shown in Table 4.3 above. However, each specimen set was casted on the same day. For example, SFRC -R-X series specimens (all specimen with Royal fiber in different volume of fraction) were prepared on the same day and were all tested after 48 hours.

The SFRC specimens with higher volume of fraction of Type 1 and Type 2 fiber (BS-200, and BL-200) were not prepared in this phase due to mixing issue observed in first phase of experiment (Figure 4.8). During the first of phase study, various trial mixes with higher volume fractions of steel fibers were prepared. A specimen with higher volume of fraction of fibers normally requires more cement paste and fewer amounts of coarse aggregates, and a high amount of water reducing admixtures could

help. Based on prior experiences, the mix design used in the experimental program was not suitable for high volume fractions of fibers, more than 1.5%, except the Royal fiber since no problem was noticed for this fiber. Hence, SFRC BS-200 and BL-200 series were excluded from further experimental programs. Also, from the first phase study, R-050 specimen showed good results compared to that of PC in terms of peak load. For this reason it was excluded from the rest of the experimental program.

Figure 4.9 Example of SFRC Mix Problem (observed During First Phase) with Higher Volume Fraction of Steel Fiber

4.3.2 Fabrication of Specimens and Testing

The details of specimens for the second phase are shown in Table 4.4. The casting of the cylinders, preparation of test specimens, test setup, instrumentation, and testing procedure were exactly the same as the first phase of the experimental program.

As discussed earlier each group (i.e. all specimens with one type of fiber) were casted in one day and tested after 48 hours.

Table 4.4 Specimen Information Used in Second Phase

Specimens name	Steel fiber type	Fiber volume fraction	Number of specimens
PC	-	-	3
SFRC R-075	Type 1 (Royal)	0.75 %	4 for each set, total 28
SFRC R-100		1.00 %	
SFRC R-150		1.50 %	
SFRC R-200		2.00 %	
SFRC BS-075	Type 2 (Bekaert)	0.75 %	
SFRC BS-100		1.00 %	
SFRC BS-150		1.50 %	
SFRC BL-075	Type 3 (Bekaert)	0.75 %	3 for each set, total 9
SFRC BL-100		1.00 %	
SFRC BL-150		1.50 %	
Total numbers of specimens			40

4.4 Third Phase Experimental Program

4.4.1 General

The third phase study was carried out in an attempt to: 1) verify reduction in the variability in specimens with the same type of fibers by casting and testing all of them on the same days; 2) investigate if fewer specimens would still give a reasonably small coefficient of variations; 3) improve test result to obtain the consistent initial ascending curve byslightly modifying the testing procedure : load was applied up to 2 kips and then unloaded to 0.5 kips, and from this load on the test was started. This way the entire setup was “shakedown” and consistent initial stiffness of specimens was obtained.

4.4.2 Material and Mix Proportion:

All the materials such as cement, sand, course aggregate and steel fiber used in this phase are exactly the same as those in the previous two phases of the experimental program. The steel fiber types and the volume of fractions are also the same as in the previous phases. There was, however, a slight modification in mix design from the first and second phases. The content of super plasticizer in the mix design was reduced from 0.013 to 0.0015 in order to reduce segregation and bleeding. The composition of the mix proportion is shown in Table 4.5.

Table 4.5 Mix Proportion (by Weight) for Third Phase

Specimens	Cement (Type-1)	Sand	Coarse aggregate[3]	Water	Steel fiber	Super plasticizer
PC (control)	1.00	1.96	2.72	0.34	0	0.0015
SFRC-X*-050					0.101[4]	
SFRC-X-075					0.152[5]	
SFRC-X-100					0.204[6]	
SFRC-X-150					0.311[7]	
SFRC-X-200					0.422[8]	

[3] Maximum size = ¾ in; [4] 0.50% of volume fraction; [5] 0.75% of volume fraction; [6] 1.0% of volume fraction; [7] 1.5% of volume fraction; [8] 2.0% of volume fraction;

* X: R for Type 1 fiber, BS for Type 2 fiber and BL for Type 3 fiber

4.4.3 Specimen Preparation and Testing

Detailed information on all of the specimens that were prepared and tested in the third phase is provided in Table 4.6. The casting procedure of concrete in this phase is also similar to second phase of the experimental program. All specimens in one specimen group (e.g. specimens with Type 1 steel fibers) were tested on the same day. In previous phases it was noticed that, due to the bulged bottom face of the used plastic molds. Some cylinders did not have smooth bottom surface . Hence, steel molds were used to cast the cylinder in this phase, which produced a smoother surface at bottom. The procedure for preparation of the test specimen was the same as in the previous phases.

Table 4.6 Specimen Information in the Third Phase Experimental Program

Specimens name	Steel fiber type	Fiber volume fraction	Number of specimens
SFRC R-075	Type 1 (Royal)	0.75 %	4 for each set, total 16
SFRC R-100		1.00 %	
SFRC R-150		1.50 %	
SFRC R-200		2.00 %	
SFRC BS-050	Type 2 (Bekaert, short)	0.50 %	4 for each set, total 16
SFRC BS-075		0.75 %	
SFRC BS-100		1.00 %	
SFRC BS-150		1.50 %	
SFRC BL-050	Type 3 (Bekaert, long)	0. 50%	4 for each set, total 16
SFRC BL-075		0.75 %	
SFRC BL-100		1.00 %	
SFRC BL-150		1.50 %	
Total numbers of specimens			48

The same 60 kips compression machine was used to test the specimens in this phase. As discussed earlier, a slight change in the testing procedure was made in order to check its effect on the initial slope of the load-deflection curve. So the load was applied up to 2 kips at first and then unloaded to 0.5 kips. The test then started from this

point and test data was recorded. After this modification, it was noticed that the consistent stiffness of the specimens could be gained in the early stages of the test.

4.5 Fourth Phase Experimental Program

4.5.1 General

A fourth experimental study was carried out in an attempt to: 1) verify the reduction in variability of specimens with different types of fibers after a 28-day as at in early age of concrete it was difficult to achieve quality control in some case., 2) investigate if less number of specimens would still give a reasonable small coefficient of variations after 28 days; 3) investigate if DPT could identify strain-hardening behavior as well as toughness properties of SFRC.

4.5.2 Specimen Preparation and Testing

The proportions of all materials were kept the same as those in the third phase. The composition of the mix proportion is shown in Table 4.7. One additional steel fiber, as shown in Figure 4.9, was used in this phase. The fiber brand name was Helix 5-25 (twisted fiber). Detailed properties of this fiber are shown in Table 4.8. Information for all specimens prepared and tested in this phase is shown in Table 4.9.

Table 4.7 Mix Proportion (by weight) Used in Fourth Phase

Specimens	Cement (Type-1)	Sand	Coarse aggregate[3]	Water	Steel fiber	Super plasticizer
PC (control)	1.00	1.96	2.72	0.34	0	0.0015
SFRC-X*-050					0.101[4]	
SFRC-X-075					0.152[5]	
SFRC-X-100					0.204[6]	
SFRC-X-150					0.311[7]	
SFRC-X-200					0.422[8]	

[3] Maximum size = ¾ in; [4] 0.50% of volume fraction; [5] 0.75% of volume fraction; [6] 1.0% of volume fraction; [7] 1.5% of volume fraction; [8] 2.0% of volume fraction;

* X: R for Type 1 fiber, BS for Type 2 fiber, BL for Type 3 fiber and H for Type 4 (Helix)

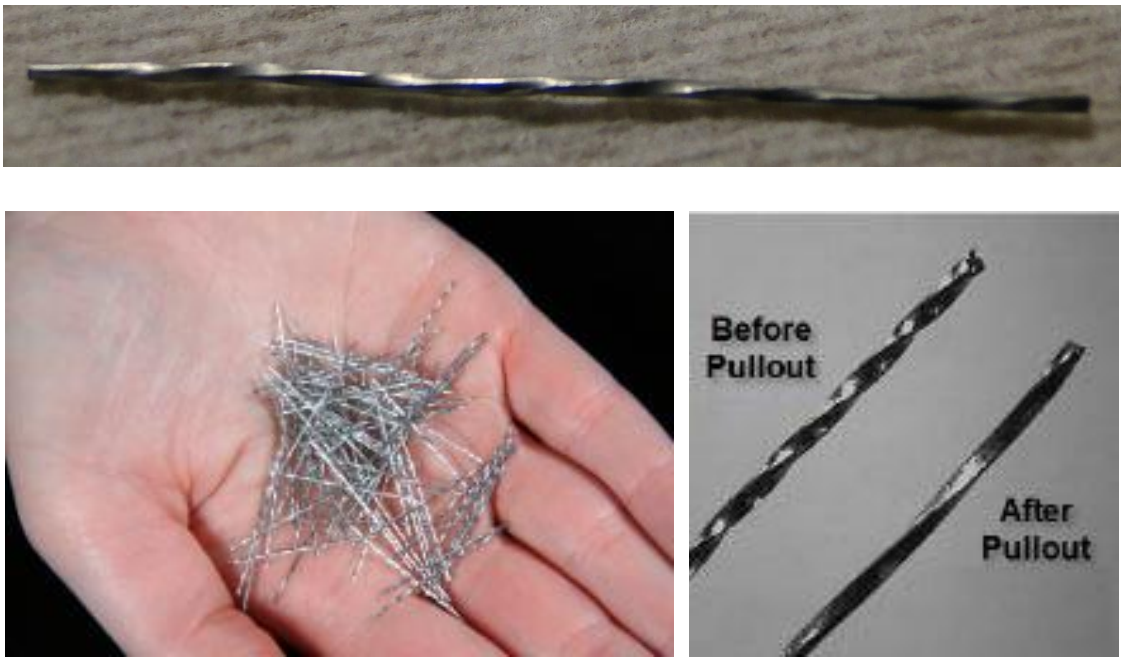

Figure 4.10 Helix (Twisted Fiber) Used in Fourth Phase

Table 4.8 Properties of Additional Helix Fiber Used in Fourth Study

Fiber Type	Shape	Length (L)[1]	Diameter (D)[1]	Aspect ratio (L/D)[1]	Tensile strength[2]
Type 4 (Helix 5-25)	Twisted	1.0 in. (25 mm)	0.02 in. (0.50 mm)	50	304 ksi (2000 MPa)

[1]: Measured, [2]: From manufactures profile

Table 4.9 Specimen Information of the Fourth Phase

Specimen name	Steel fiber type	Fiber volume fraction	Number of specimens
PC	-	-	4
SFRC R-075	Type 1 (Royal)	0.75 %	4 for each set, total 16
SFRC R-100		1.00 %	
SFRC R-150		1.50 %	
SFRC R-200		2.00 %	
SFRC BS-050	Type 2 (Short Bekaert)	0.50 %	4 for each set, total 16
SFRC BS-075		0.75 %	
SFRC BS-100		1.00 %	
SFRC BS-150		1.50 %	
SFRC BL-050	Type 3 (Long Bekaert)	0. 50%	4 for each set, total 16
SFRC BL-075		0.75 %	
SFRC BL-100		1.00 %	
SFRC BL-150		1.50 %	
SFRC H-075	Type 4 (Helix, twisted)	0.75 %	4 for each set, total 12
SFRC H-150		1.50 %	
SFRC H-200		2.00 %	
Total numbers of specimens			64

The specimens with Helix steel fiber were named as SFRC H-075, SFRC H-150, and SFRC H-200, as shown in Table 4.9. As in the previous case, all specimens in one specimen group (e.g. specimens with Type 1 steel fibers) of were prepared on the

same day and were all tested on the same day. After casting the specimens were kept in a curing room until testing.

In the fourth phase, the specimens were tested at 55-58 days. Some of the specimens (BL-150) had a peak strength higher than 50 kips. Hence the testing setup for this phase was slightly different than the previous phase. In this phase a 400-kips testing machine was used. The load cell used was also of higher capacity (200 kips). There was additional modification to the testing setup. The top steel plate was fixed to the testing machine with bolts, as shown in Figure 4.11, which was believed to be able to improve the variations in the ascending load-deflection curves.

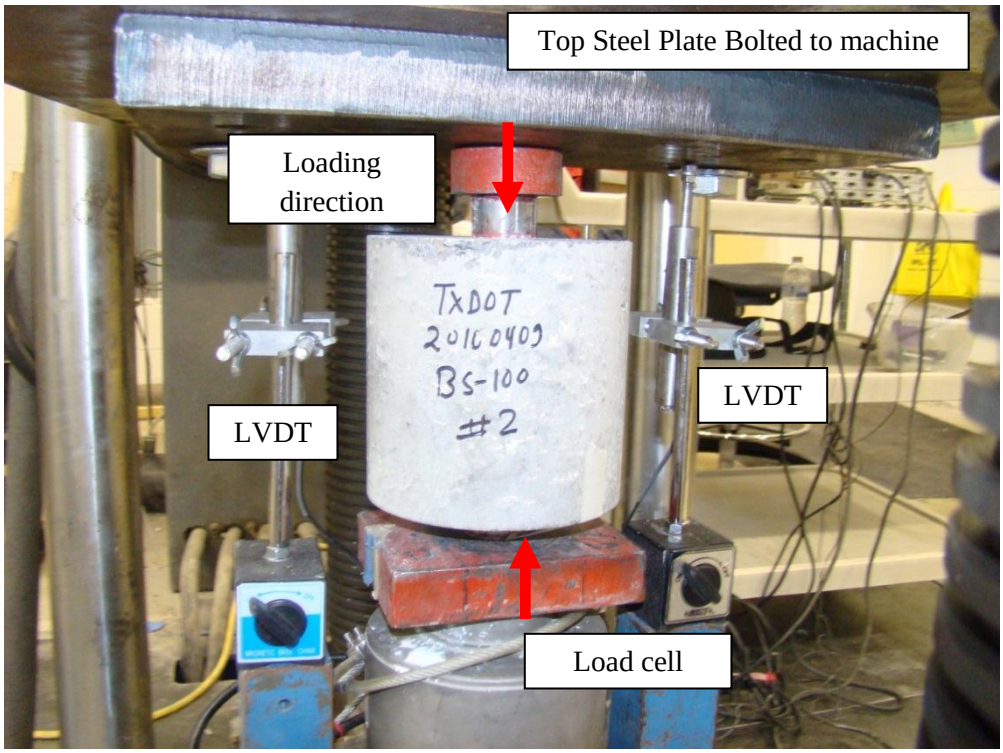

Figure 4.11 Double Punch Test Setup Used in the Fourth Phase

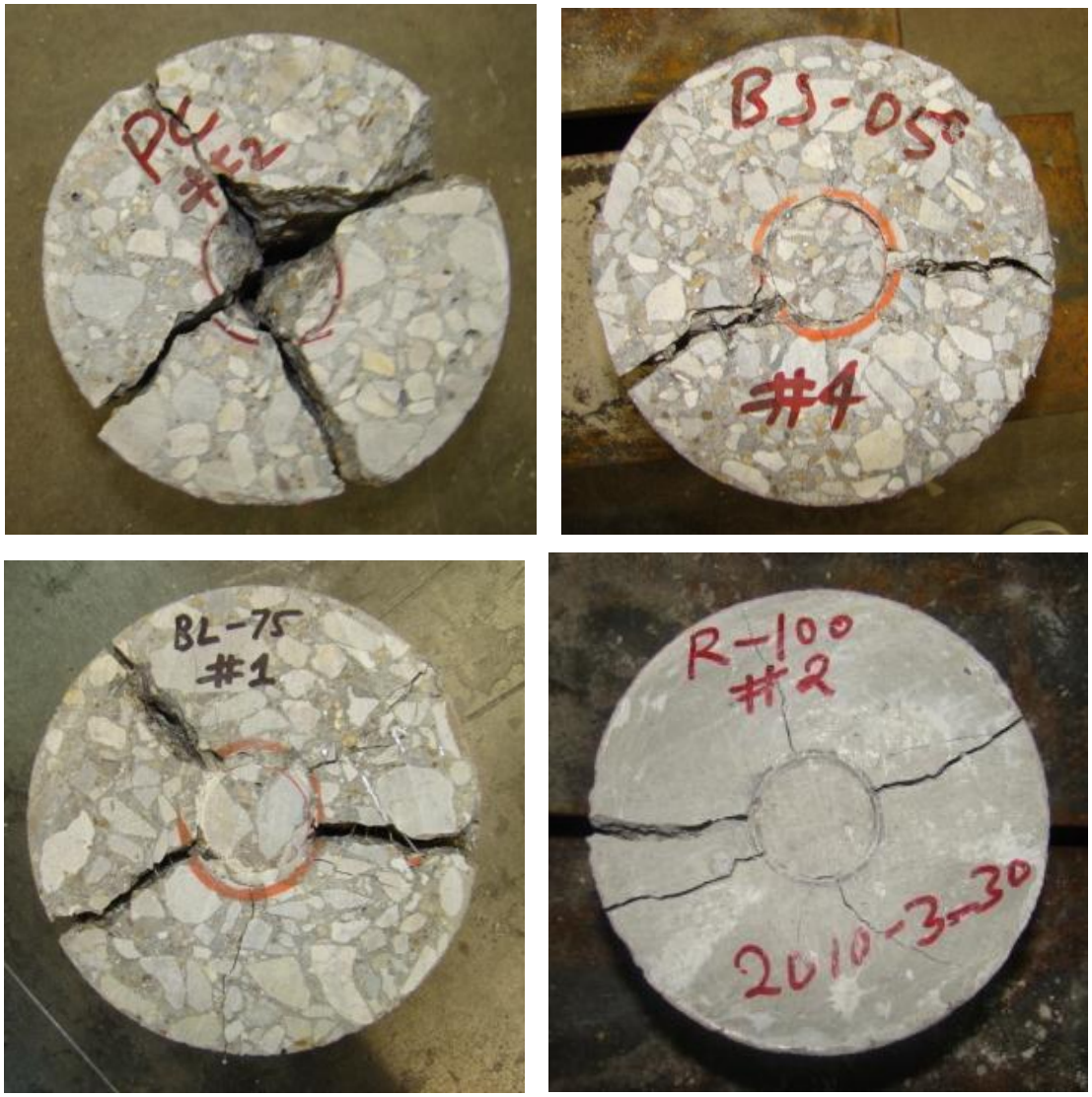

Figure 4.12 Typical Test Specimens with Various Fiber Volume Fractions in the Fourth+ Phase

Figure 4.12 shows the photographs of some tested specimens. As shown in Figure 4.12, while the plain concrete specimens broke into 4 pieces upon peak load, the SFRC specimens maintained their integrity due to the fiber bridging effect and produced more radial cracks.

4.6 Fifth Phase: Comparison of DPT Method with other Types of Material Test Methods and Post Crack Investigation

4.6.1 General

In this phase of the study, the double punch test was compared with the third point bending test (ASTM C1609) and the direct tensile test. Similarly, the post crack behavior of the SFRC tested by DPT was also studied. Twisted fibers, micro steel fibers, and a mix of these two types of fibers (hybrid) were used to evaluate the strain hardening and post cracking behavior SFRC with the double punch test.

4.6.2 Materials and Specimen Preparation

Three additional steel fibers and combinations of those fibers (hybrid) were used in this phase of study, as shown in Figure 4.13-15. Table 4.10 gives the properties of these steel fibers. Different volume of fractions of 0.75%, 1.5%, and 1.5% with mixed (hybrid fiber), were used. Six DPT specimens, six ASTM beams, and six tensile specimens were prepared with three different types of mixes for comparison of different material test methods. Three small cylinders (4×8 inches) were also prepared with each concrete mix.

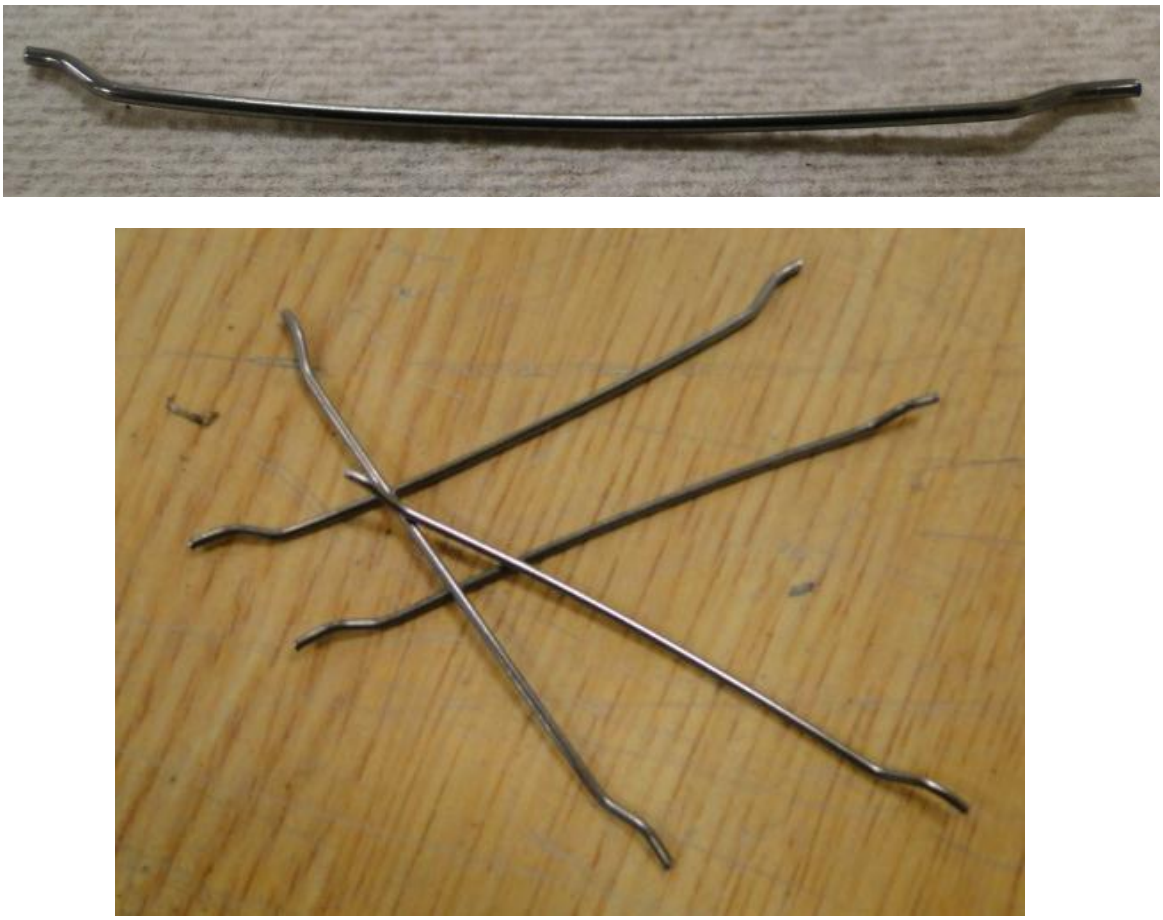

Figure 4.13 Steel Fiber Used in Further Study Type 5: Maccaferri Long Steel Fiber (Double Bend Hook at End, FF 3)

Figure 4.14 Steel Fiber Used in Fifth Phase of Study Type 6: Twisted Steel Fiber

Figure 4.15 Steel Fiber Used in Fifth Phase of Study Type 7: Maccaferri Micro Steel Fiber

Table 4.10 Properties of Steel Fibers Used for Comparison between Different Material Test Methods and Post Crack Evaluation

Fiber Type	Shape	Length (L)[1]	Diameter (D)[1]	Aspect ratio (L/D)	Tensile strength[2]
Type 5	Maccaferri Long (FF3)	1.87 in. (47.5 mm)	0.031 in. (0.76 mm)	60	166 ksi (1100 Mpa)
Type 6	Twisted	1 in. (25.4 mm)	0.008 in. (0.20 mm)	125	304 ksi (2000 Map)
Type 7	Maccaferri micro	0.5 in.[1] (12.7 mm)	0.007in[2]. (0.175 mm)	71	328 ksi (2200 Mpa)

[1]: measured; [2]: provided by manufacture;

In previous phases the concrete mix high percentage of course aggregate compare to cement and sand. Hence the mix has lower cement paste produce low compressive strength. Also use of larger size of coarse aggregate (3/4 in.) can produce the segregation. In this phase the size and volume of coarse aggregate decrease and volume of cement and sand was increased as shown in Table 4.11. The preparation of one group of specimens (with one type of mix proportion as shown in Table 4.11) was carried out on the same day with two batches due to the capacity limitation of the drum mixer used. All specimens were then moved to the curing room with a controlled environment set at 80^{o}F (27^{o}C) and 100% RH. Tests were conducted 21 to 30 days after casting.

Table 4.11 Mix Proportions by Weight Used for Comparison between Different Material Test Methods

Mix type	Cement Type 1	Fly ash (class C)	Sand[9]	Coarse Aggregate[10]	Water	SP[11]	Steel Fiber	f_c'[12] psi
ML-075	1.00	0.50	1.7	1.0	0.35	0.001	0.114	9.23
ML-150	1.00	0.50	1.7	1.0	0.35	-	0.232	7.75
Hybrid	1.00	0.50	1.7	1.0	0.35	0.001	0.232	9.72

[9] ASTM natural river sand (Fineness Modulus = 2.57); [10] ASTM C33 Size Number 8), 95% of mass finer than 3/8 in., nominal maximum size =3/8; [11] Super Plasticizer: High Range Water Reducing Admixture; [12] compressive strength average of three 4 × 8 in. cylinders, tested on the same day when the specimen was tested;

* Note: with 0.75% Type 5 (maccaferi long steel fiber) and 0.75 % Type 6 (twisted steel fiber)

Six other mixes, as shown in Table 4.12, were used to prepare additional DPT specimens to study more in the post crack properties specially as crack width, strain hardening. Along with other properties were also studied. In previous phases only single long steel fibers were used. However in this phase the hybrid fiber combination longer and short tiny fiber were used to study the development of crack and strain hardening to achieve high performance concrete It was expected that a cement mortar mix with a 3% volume fraction of twisted and micro fibers would able to achieve a high performance matrix.. For these six types of mixes, specimens were prepared using manual compaction; (use of temping rod) vibrators were not used in order to reduce the settlement of fibers to the bottom portion of the cylinders during compaction.

4.6.3 Specimen Information

Specimens were named in the following fashion: 1) The first word represents the type of material test method, such bending, tensile, or DPT; 2) the second character represents the type of fiber; 3) the third number represents the volume fraction of fibers, 075 corresponds to a 0.75% volume fraction and 150 corresponds to a 1.5% volume fraction of fibers. ML means Maccaferri long. The mixed fiber Maccaferri and twisted fiber specimen was named as hybrid. For example, Bending: ML-150 means the specimen was tested with the third point bending test (ASTM C1609) with Maccaferri fibers with a 1.5% volume fraction of fibers. Each set had 6 specimens. The specimens prepared with hybrid steel fibers used for the post crack evaluation of the DPTs are named as follows:

- HYB1 represents a combination of 2% Type 6 fiber (twisted steel fiber) and 1.0% of Type 7 fiber (micro Maccaferri fiber),
- HYB2 represents a combination of 1% Type 6 fiber (twisted steel fiber) and 0.50% Type 5 fiber (Maccaferri long (FF3)) fiber,
- HYB3 represents a combination of 0.75% of Type 5 fiber (Maccaferri long steel fiber) and 0.75% Type 7 fiber (Micro Maccaferri fiber) (mix with 3/8 inches aggregate).
- HYB4 represents a combination of 0.75%of Type 5 fiber (Maccaferri long fiber) and Type 7 fiber (0.75% Micro Maccaferri fiber) (mix with ¾ inches coarse aggregate and $f_c^{'} = 6\ ksi$).

Detailed information of the specimens used for post crack evaluation of the DPT method is provided in Table 4.12.

Table 4.12 Mix Proportions by Weight Used for Study of Post Crack Evaluation and Strain Hardening

Mix type	Cement Type 1	Fly ash (class C)	Sand[9]	Coarse Aggregate[10]	Water	SP[11]	Steel Fiber	f_c'[12] psi
HYB1	1.00	0.50	1.7	-	0.32	0.002	0.312	12140
HYB2	1.00	0.50	1.7	1.0	0.35	0.001	0.232	7375
HYB 3	1.00	0.50	1.7	1.0	0.35	0.001	0.232	7846
HYB 4	1.00	-	1.3	0.67	0.40	0.001	0.165	6030
ML-075	1.00	0.50	1.7	1.0	0.35	0.001	0.114	7047
R-075	1.00	0.50	1.7	1.0	0.35	0.001	0.114	7520

[9] ASTM natural river sand (Fineness Modulus = 2.57); [10] ASTM C33 Size Number 8, 95% of mass finer than 3/8 in., nominal maximum size =3/8; [11] Super Plasticizer: High Range Water Reducing Admixture; [12] compressive strength average of three 4 × 8 in. cylinders, tested on the same day when the specimen was tested;

Table 4.13 Specimen Information in the Used for Comparison between Different Material Test Methods

Specimens name	Steel fiber type	Fiber volume fraction	Number of specimens
Bending: M-075	Type 5	0.75%	6
Tensile: ML-075			6
DPT: ML-075-1			6
Bending: ML-150		1.50%	6
Tensile: ML-150			6
DPT: ML-150			6
Bending : Hybrid	Type 5 + Type 6	(0.75%+0.75%)	6
Tensile : Hybrid			6
DPT : Hybrid			6
Total numbers of specimens			60

Table 4.14 Specimen Information Used for the Study of Post Crack Evaluation and Strain Hardening

Specimens name	Steel fiber type	Fiber volume fraction	Number of specimens
HYB1	Type 6 + Type 7	(2%+1%)	4
HYB2	Type 5 + Type 6	(0. 50%+1.0%)	4
HYB3	Type 5 + Type 7	(0.75%+0.75%)	4
HYB4	Type 5 + Type 7	(0.75%+1.75%)	4
ML-075	Type 5, FF3	0.75%	4
R-075	Type1, Royal	0.75%	4
Total numbers of specimens			24

Note: FF3 represents for, Maccaferri long double bend hook at end steel fiber

4.6.4 Testing of Specimens

The specimens, shown in Table 4.13, were tested between 21 to 28 days using an MTS machine for the third point bending test (ASTM C1609) and the direct tensile test (dog bone test) and a 60 kips compression machine was used for the DPT. The test procedures for the third point bending test and dog bone test earlier two material tests were described in Chapter Two, were adopted. The specimens shown in Table 4.14 were tested with the DPT in a 400 kip compression machine after 28 days.

Previous experimental investigation of DPT with hybrid (mixed fibers) specially with large volume of content with short and tiny fiber has shown that some strain hardening after first crack. However large post peak strength variation was noticed. So six more DPT mortar specimens with mix proportion as shown in Table 4.15 were tested to study post peak strength variation. VMA was added in mix to increase the viscosity of the mix.

Table 4.15 Mix Proportions by Weight Used for Mortar Specimen

Mix type	Cement Type 1	Fly ash (class C)	Sand[9]	CA [10]	Water	BMA[11]	SP[12]	Steel Fiber	f_c'[13] psi
HYB5*	1.00	0.50	1.7	-	0.40	0.002	0.023	0.312	10.47

[9] ASTM natural river sand (Fineness Modulus = 2.57); [10] Coarse aggregate ASTM C33 Size Number (8), 95% of mass finer than 3/8 in., nominal maximum size =3/8; [11] Viscous material; [12] Super Plasticizer: High Range Water Reducing Admixture; [13] compressive strength average of three 4 × 8 in. cylinders, tested on the same day when the specimen was tested;

* Note: HYB5 represents a combination of 2% Type 6 fiber (twisted steel fiber) and 1.0% of Type 7 fiber (micro Maccaferri fiber),

4.7 Finite Element Analysis for DPT Model

4.7.1 General

Finite element (FE) analysis was carried out verify stress distribution for concrete specimen (cylinder) used in the double punch test (DPT) method. The equivalent ultimate strength determine by the equation developed by Chen (1970) based on plasticity theory of concrete (discussed in Chapter Two) were also compared with principal tensile stress obtained from FE analysis. With the accurate modeling of the specimen under monotonic and repeated loading the nonlinear response can be predicted.

A fiber reinforced concrete is composite material made with cement sand aggregate and fibers. This composite possess number of micro cracks during loading. When loading is increased these micro cracks increase and widen then concrete composite become nonlinear. After cracking the strength and durability of a concrete

specimen can increase until the fiber get pulled out or fractured depending upon type of fibers, volume of content and composite mix.

In case of DPT specimens the concrete material does not remain elastic after the crack occurs after certain stage of loading. Hence while modeling the double punch test for concrete cylinder the material nonlinearity which arise from a nonlinear constitutive model (that is, progressively disproportionate stresses and strains) was considered to observe the behavior of the specimens after the crack occurs.

For the FE analysis various software such as ABAQUS, SAP2000, ANSYS and LUSAS are available. Among them the LUSAS academic software was selected because of its flexibility in geometric and material modeling.

Finite element modeling in LUSAS consists of three main steps: modeling, running the analysis and viewing the results. Modeling is a pre-processing and viewing the results is a post-processing step of LUSAS analyses.

Modeling includes the process of geometric representation and defining physical properties such as geometries, materials, meshes, loading and support. Running the **a**nalysis is carried out by LUSAS Solver after completion of model and creates the results. Then the results can be viewed in terms of plots and tabular forms.

4.7.2 Model Geometry and Meshes

The geometries and meshes of the DPT model used in FEM analyses are as shown in Figure 4.17. For both concrete section and steel punches the stress hexahedral elements were used. A nonlinear concrete cracking material model is applied with solid elements for concrete cylinder and model with elastic stain steel material properties used for steel punches. A 3D isoparametric solid element with an incompatible strain field (Figure 4.16) was used. This mixed assumed strain element is a much superior performance to that of the regular H×8 element. Each node has three translational degree of freedom where as no rotations are considered. Mesh size has to be chosen properly as fine mesh can predict lower strength and coarser mesh can over estimate the strength. Mesh size of 0.75 inches were used based on trial meshing and checking with convergence of the results at selected point (center point in mid section of the model) as shown in Table 4.16

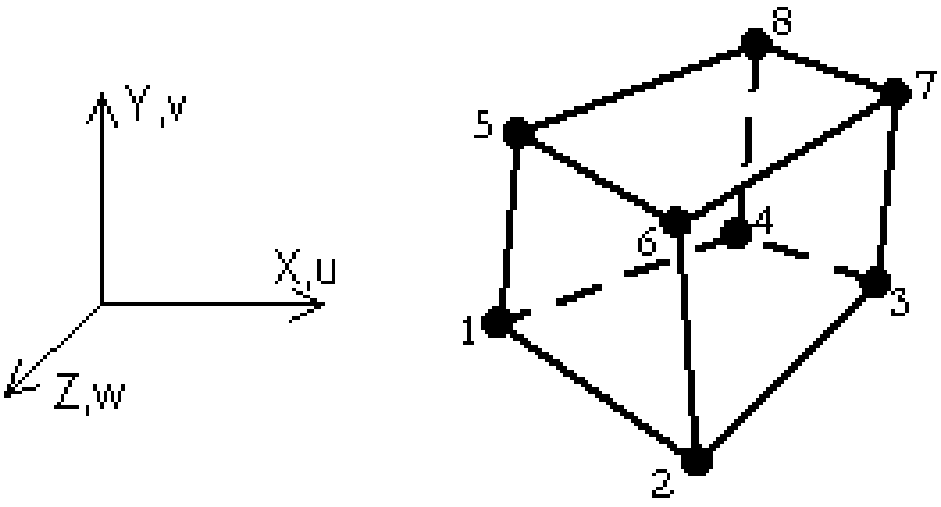

Figure 4.16 H × M8 Solid Stress Element Used for the FEM Analysis

Table 4.16 Various Results at Selected Point (Mid Span) at Different Mesh Sizes of the Model

Mesh size	Displacement (inches)	Tensile stress(psi)	Compressive stress (psi)
0.25	0.000711	699	3210
0.5	0.000691	649	3060
0.75	0.000583	518	3000
1	0.000583	531	2960
1.5	0.000582	512	2320

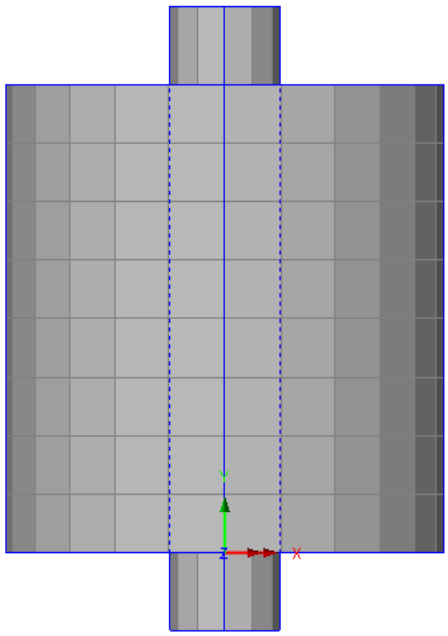

Figure 4.17 Geometry and meshes of the concrete cylinders and punches

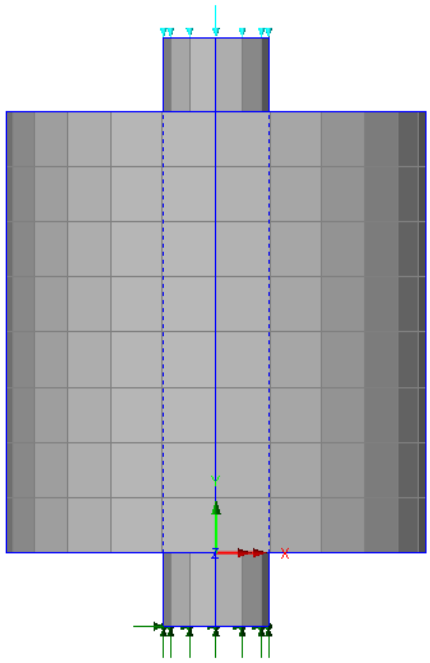

Figure 4.18 Load and boundary conditions

4.7.3 Load and Boundary Conditions

The model was supported at one end and loaded with point load at other end as shown in Figure 4.18. One of the surfaces of the steel punch was considered as pin support. Unit load per unit area was applied as shown. Weight of specimen is negligible compared with the applied load.

4.7.4 Material properties

4.7.4.1 Concrete Cylinder Model

Development of a model for the behavior of concrete is a must difficult task. As the concrete is brittle material and it has different behavior in compression and tension. The tensile strength of concrete is typically 8-15% of the compressive strength (Shah, et al. 1995). Figure 4.19 shows a typical stress-strain curve for normal weight concrete.

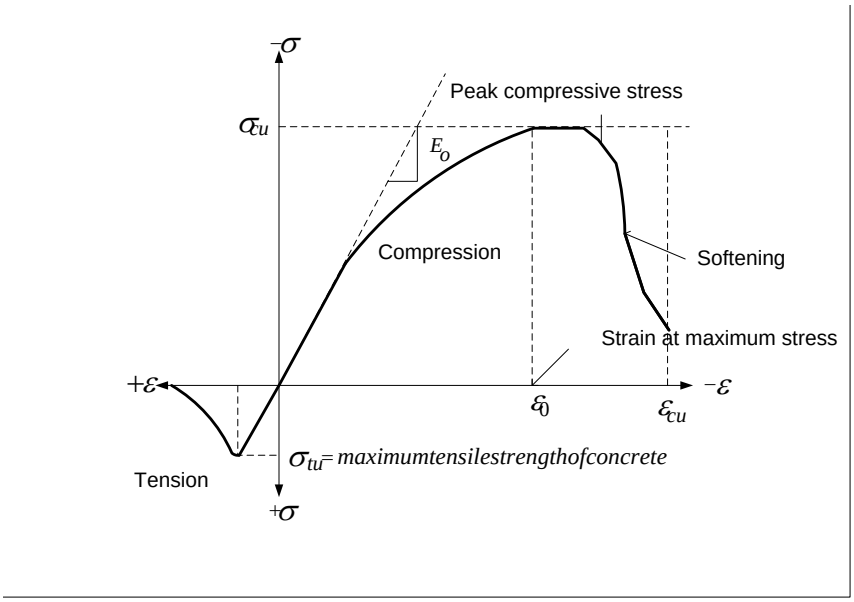

Figure 4.19 Typical Uniaxial compressive and Tensile Stress-Strain Curve for Concrete

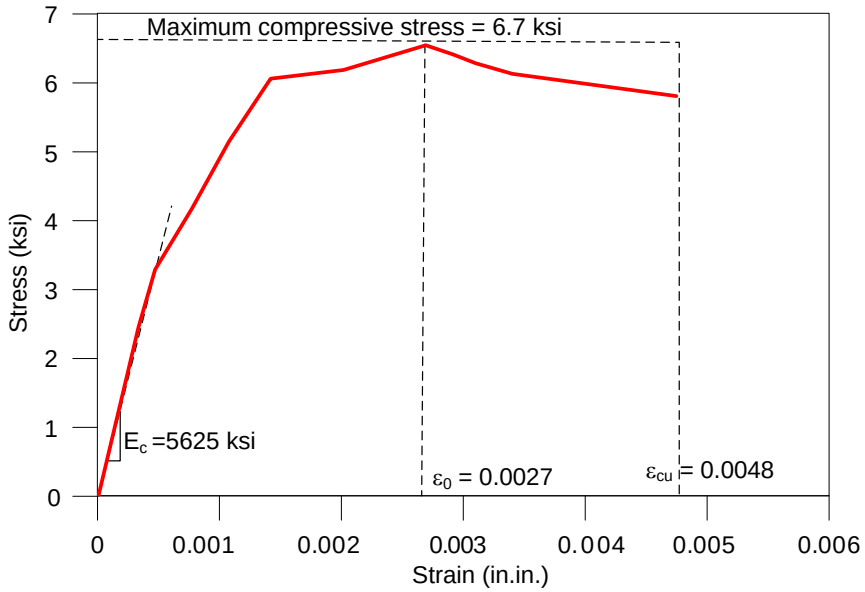

Figure 4.20 Typical Compressive Stress-Strain Curve for SFRC (Compression Test)

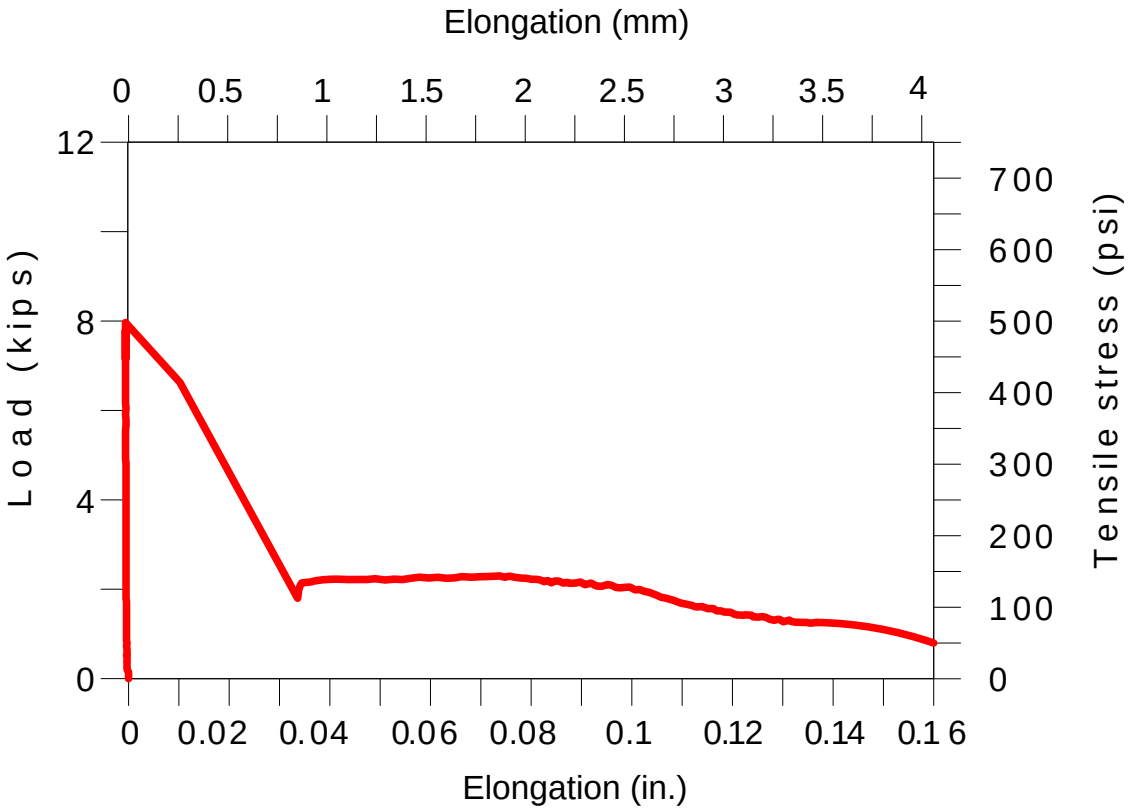

Figure 4.21 Typical Tensile Stress-Strain Curve for SFRC (Direct Tensile Test)

Generally in compression, the stress-strain curve for concrete is linearly elastic up to about 30 percent of the maximum compressive strength. After this the stress increases gradually up to the maximum compressive strength. When it reaches the maximum compressive strength σ_{cu}, the curve descends into a softening region, and crushing failure occurs at an ultimate strain ε_{cu}. In tension side, the stress-strain curve for concrete is approximately linearly elastic up to the maximum tensile strength. Then ultimately the concrete cracks and the strength decreases gradually to zero.

A nonlinear with LUSAS's Multi-Crack Concrete (94) plastic model was adopted for the concrete material properties. Based on LUSAS manual this multi-crack concrete model is a plastic-damage-contact model in which damage planes form according to a principal stress criterion and then develop as embedded rough contact planes. The basic softening curve (Figure 4.22) used in the model may be controlled via a fixed softening curve or a fracture-energy controlled softening curve that depends on the element size. The function is in terms of the fracture stress (f_s) and the strain parameter (ζ), has (as control parameters) the stress at first damage (f_{ti}), the associated strain (ε_{ti}), the uniaxial strength (f_t), the strain at peak stress (σ_k) and the strain at the effective end of the curve as (ε_0).There is no special provision for FRC concrete in LUSAS.

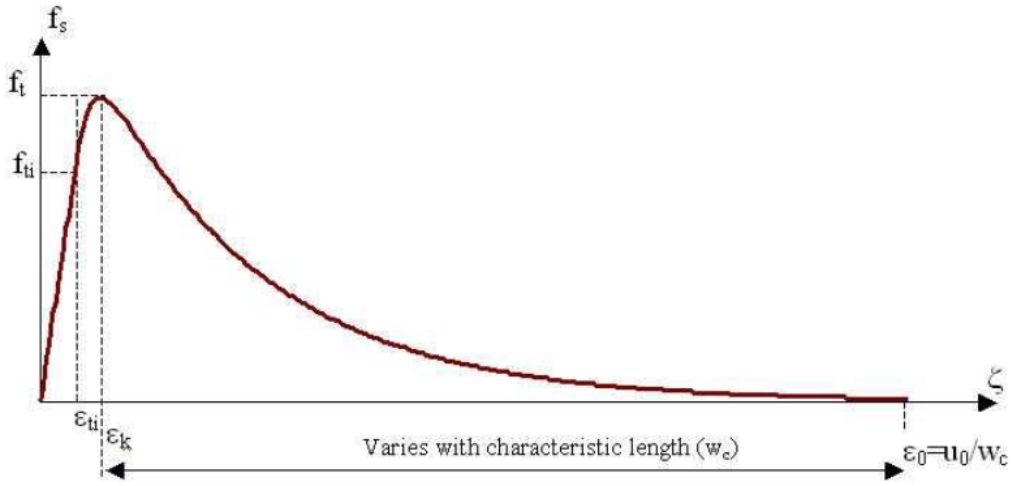

Figure 4.22. Damage evaluation function-softening curve. (LUSAS v14.6-3 user manual, 2011)

The strains will tend to localize in crack zones in case of SFRC. The mass concrete option was selected the value for ε_{t0} is set to zero and fracture-energy per unit

area, G_f is given a positive value. If the effective end of the softening curve parameter, ε_{t0} is set to zero, it will be calculated from $5G_f / W_c$, where W_c is a characteristic length for the element. Fracture energy for SFRC specimens was used based on previous studies Barros and Cruz, 1990 and Kazemi (2007). The detailed material properties of the concrete are summarized in Table 4.15. (Note: the units are in inch-kips system)

Table 4.17 Concrete Material Properties

	Value
Young's modulus	5625
Poisson's ratio	0.2
Mass density	0.22457E-3
Uniaxial compressive strength	9.2
Uniaxial tensile strength	0.560
Strain at peak uniaxial compression	0.0027
Maximum Strain	0.0048
Fracture energy per unit area	0.03

4.7.4.2 Steel punches

For steel, the model can be assumed to behave as an behave as elasto-plastic material in both and compression as shown in Figure 4.23 The hardening behavior is defined using plastic strain values, which have zero value at yield stress, corresponding to stress in steel at that particular point. The steel can be been treated as an elastic perfectly plastic material for analysis.

The maximum failure load obtained in most of the double punch test is less than 60 kips. For 60 kips load the maximum stress in steel punch is only about 34.0 ksi. This value is less the yield strength of stain less steel (41 ksi). Hence the material properties

for the steel punch can be assumed as linearly elastic material for the FE modeling and the corresponding properties are as follows:

Elastic modulus, E_s =28,282 ksi

Yield stress, f_y =41,000 psi

Poisson's ratio, ν = 0.3

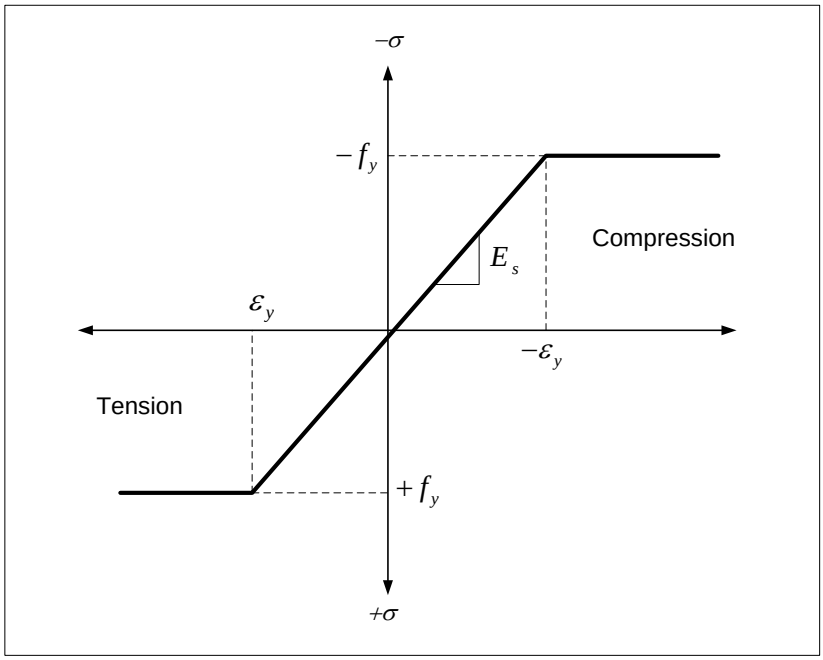

Figure 4.23 Typical stress-strain curve for steel

4.8 Results from LUSAS Analysis

The Results obtained from the FE analyses are presented and discussed in following paragraphs. The solid compression and tensile principal stresses at the mid-section, plan, and elevation (in contour form) are presented.

Figure 4.24 and 4.25 shows the radial principal tensile stress obtained from the analysis at the mid height and 1.5 inches above the mid height of the specimens. From

Figure 4.25 it can be seen that the values of stresses decrease outward from the center of the model. At ultimate load the values of tensile stresses vary from 0.437 to 0.553 ksi.

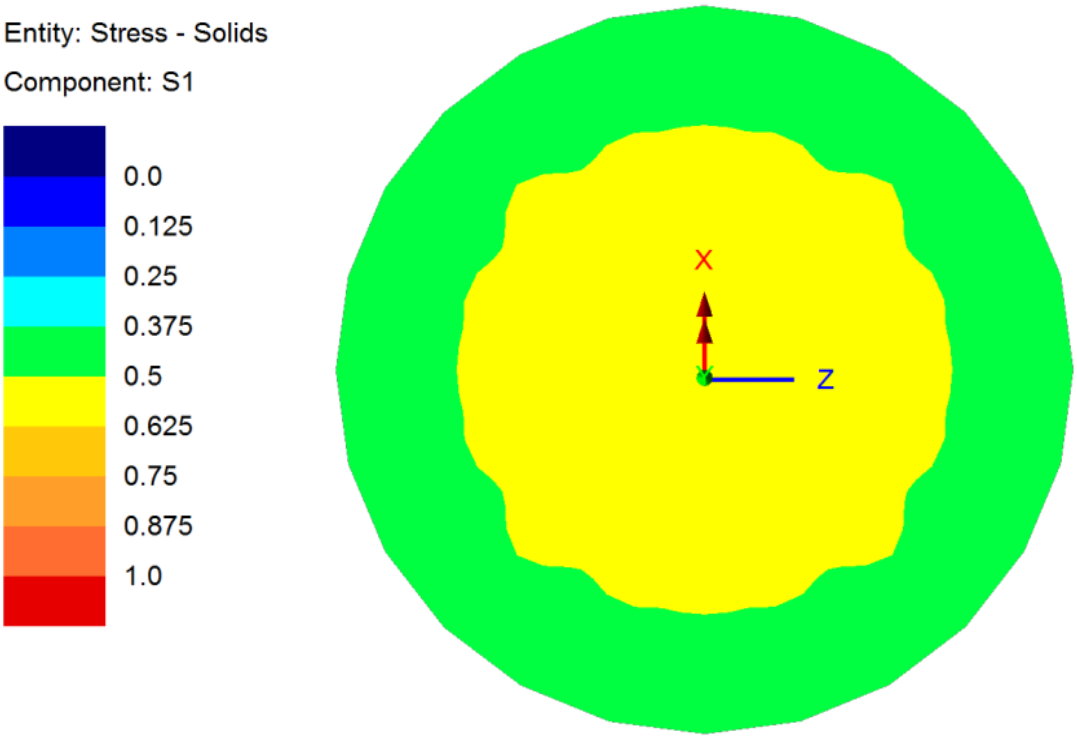

Figure 4.24 Principal Stress Contour in Tension of Concrete Cylinder at Mid Height (Plan)

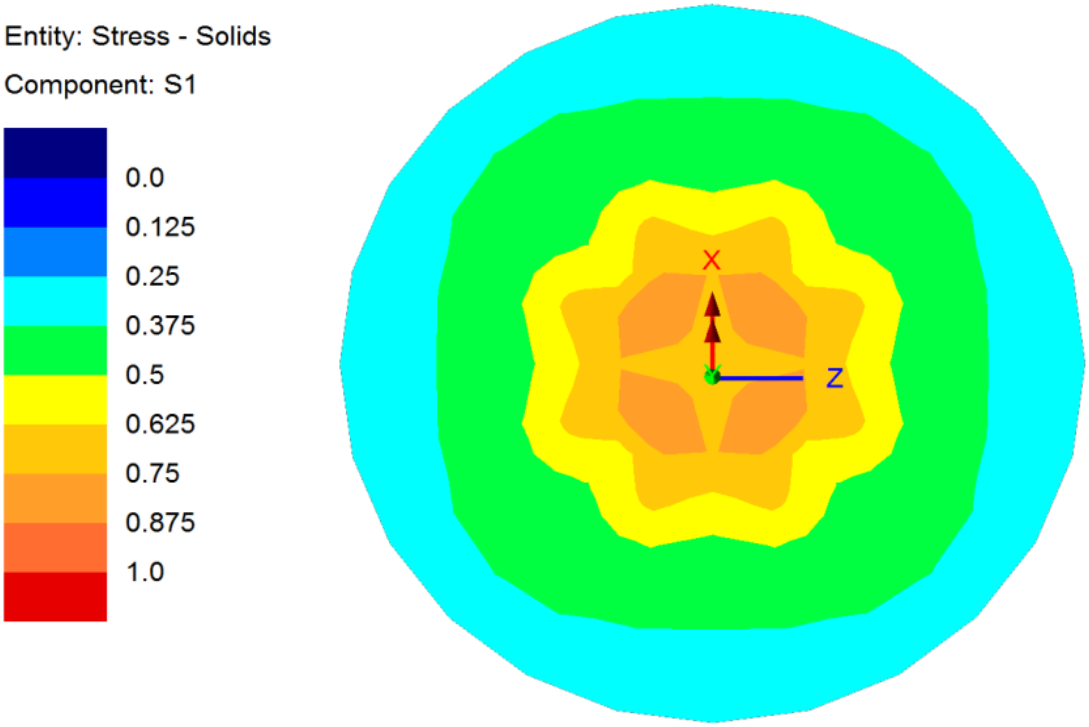

Figure 4.25 Principal Stress Contour in Tension of Concrete Cylinder at 1.5 inch Top from Height (Plan)

Figure 4.26 and 4.27 show the variation of principle stress in tension along the height at the center line of the concrete cylinder and 1.5 inches away from the center line. Near support and loading point there high stress concentration is seen and stresses are compressive. Two wards the mid depth of the cylinder the principal stresses are tensile and found more uniform.

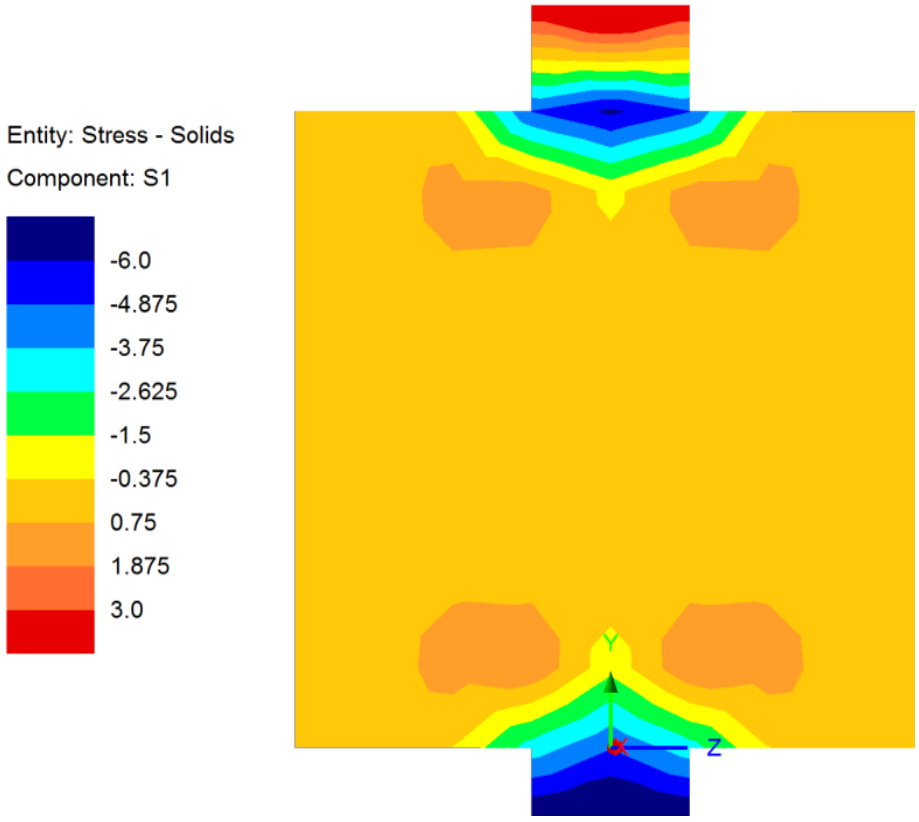

Figure 4.26 Principal Stress Contour in Tension of the Concrete Cylinder along Height of Cylinder at Center Line (Elevation)

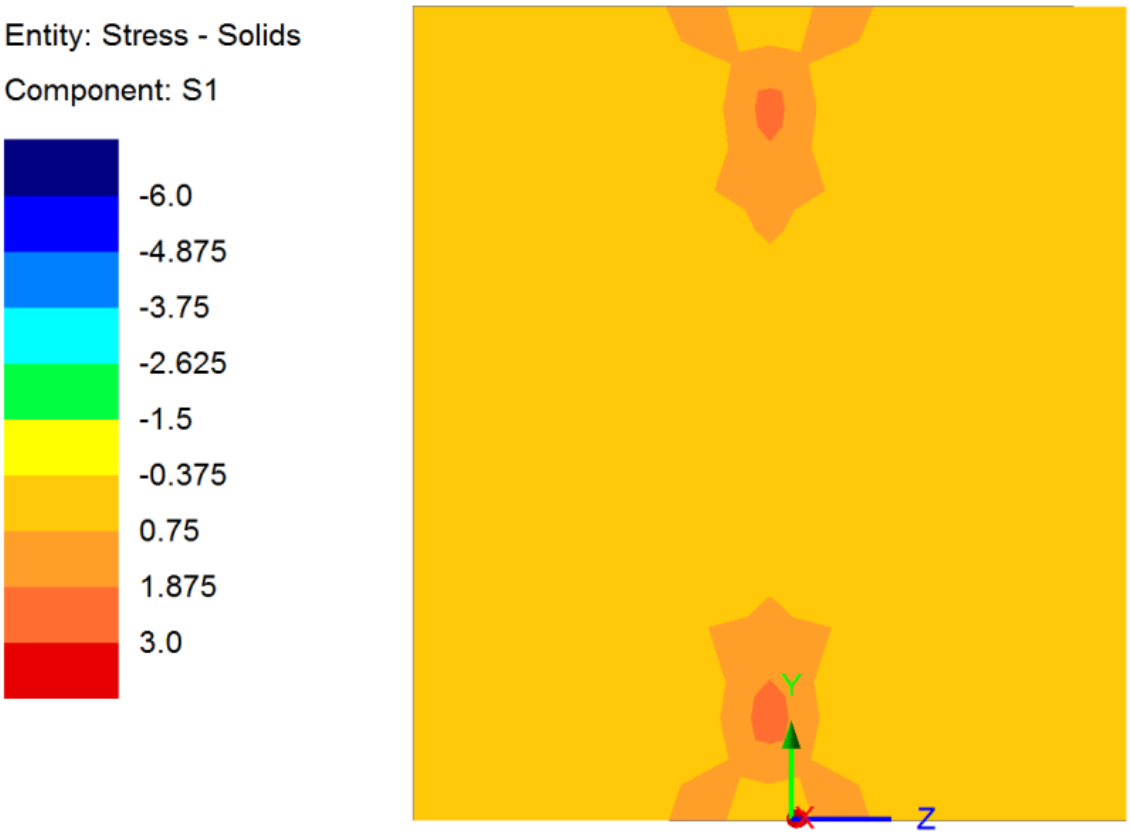

Figure 4.27 Principal Stress Contour in Tension of the Concrete Cylinder along Height of Cylinder at 1.5 inches from Center Line (Elevation)

Table 4.18 shows the comparison of ultimate load and tensile stress obtained from the different FE analysis of the DPT models with different volume of fractions of steel fibers and results obtained from DPT. It can be seen that ultimate load obtained from nonlinear analyses were slightly lower than maximum load obtained from the DPT tests. The tensile stress obtained from FE analyses are found slightly lower as compared with equivalent tensile strength obtained from the DPT.

Table 4.18 Comparisons of Results from FE analyses and DPT Test.

Specimen /Model	Finite Element Analysis		From Double Punch Test	
	Ultimate Load	Tensile Stress	Max. load	Tensile Stress
	kips	psi	kips	psi
ML-150	41.59	576	41.59	629
ML-075	38.98	574	38.98	589
Hybrid	43.98	660	43.98	685

Note: ML-150: with V_f = 1.5% Type 5 Steel Fiber, ML-075: with V_f = 75% Type 5 Steel Fiber and Hybrid: with Mixed fiber (0.75% Type 5 Steel Fiber + 0.75% Type 6 Fiber)

More FE analyses were carried out for plain concrete and SFRC with Type 3 (Bekaert Long) steel fibers. The volume of fraction was 0.5% (BL-050) to 1.5% (BL-150%). Concrete properties were same as those used in fourth phase of DPT experiment. The equivalent tensile strength for peak load obtained from fourth phases was compared with tensile stress obtained from FE analyses. Table 4.19 compares tensile principal stress obtained from FE analyses and equivalent tensile strength from DPT. The values principle stress at 0.75 inch from center line is slightly higher than those values in center line. From Table 14.7 it can be seen that the difference between principal tensile stress and equivalent tensile strength are small.

Table 4.19 Comparison of FE analyses the results from DPT test for Change in Volume of Fractions of Steel Fiber

Specimen/ Model	Tensile Stress (psi)			Difference
	From FE Analysis		From Double Punch Test	
	At Center	At 0.75 in. From center	DPT	
PC	533	654	585	11.79%
BL-050	534	655	586	11.77%
BL-075	600	737	659	11.84%
BL-100	600	747	667	11.99%
BL-150	742	911	815	11.78%

Figure 4.28 also shows the comparison of the principal stresses at compression and tension along the height cylinder at the center line. It can be seen that the tensile stresses are uniform for 3/4th of depth. Compression stresses vary rapidly from top to bottom when it goes away from the center. As discussed in Chapter Two, previous study [Demeke and Tegos, 1994] had shown that the biaxial stress in the tension–compression condition or the biaxial loading case, the variation in tension stress remains almost constant as compare to the compressive stress in case of SFRC.

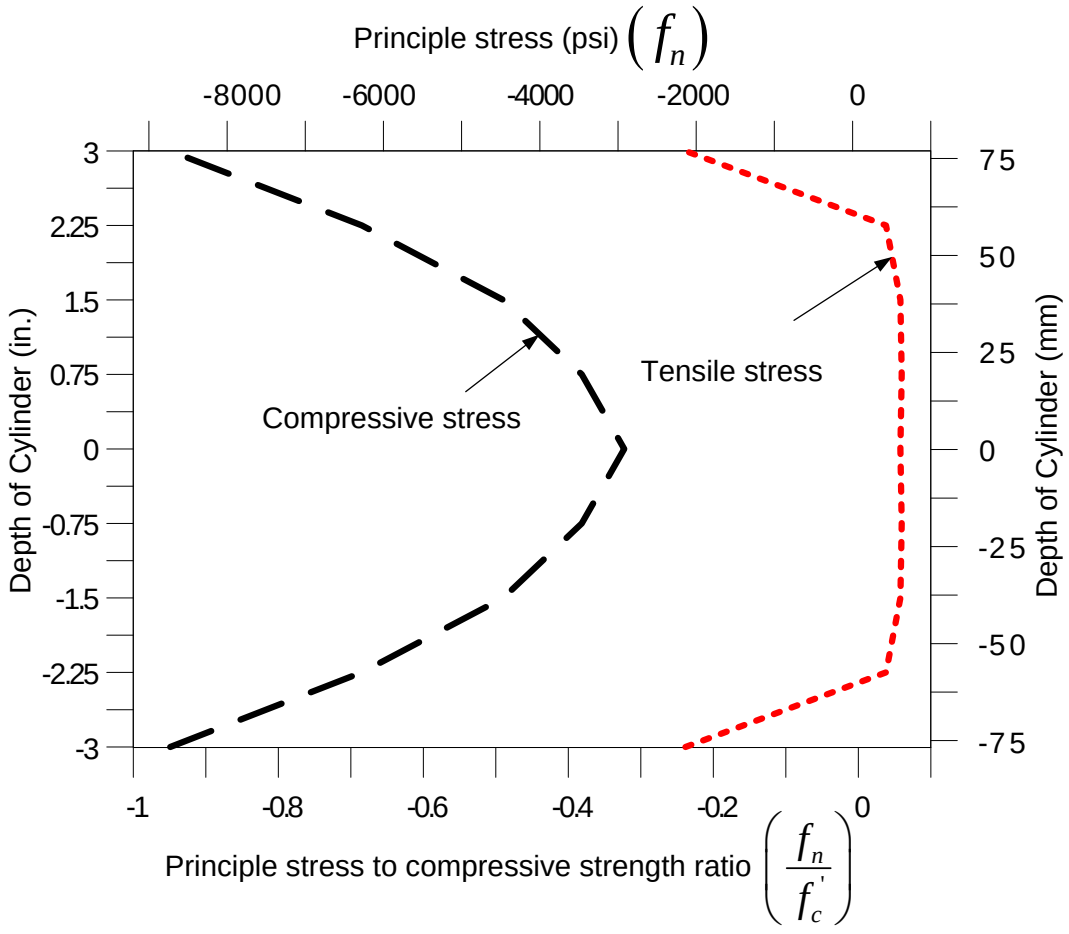

Figure 4.28 Stress Distributions along the Depth of the Cylinder Section through the Center Line

Figure 4.29 shows the variation of principal tensile stress along the height of the concrete cylinder model at different distance from the center line. It can be seen that beyond line at edge of punch (0.75 in from the center line), whole height has tensile strength which is almost uniform. Similarly, Figure 4.30 shows the variation of principal tensile stress along the diameter of the model at different sections (top, 1.5.in. from top and mid height). It can be seen that at top of the concrete model which was in contact with steel punch, the stress is compressive and varying. At section below that 1.5 in. from top and mid height the stress is tensile and more uniform.

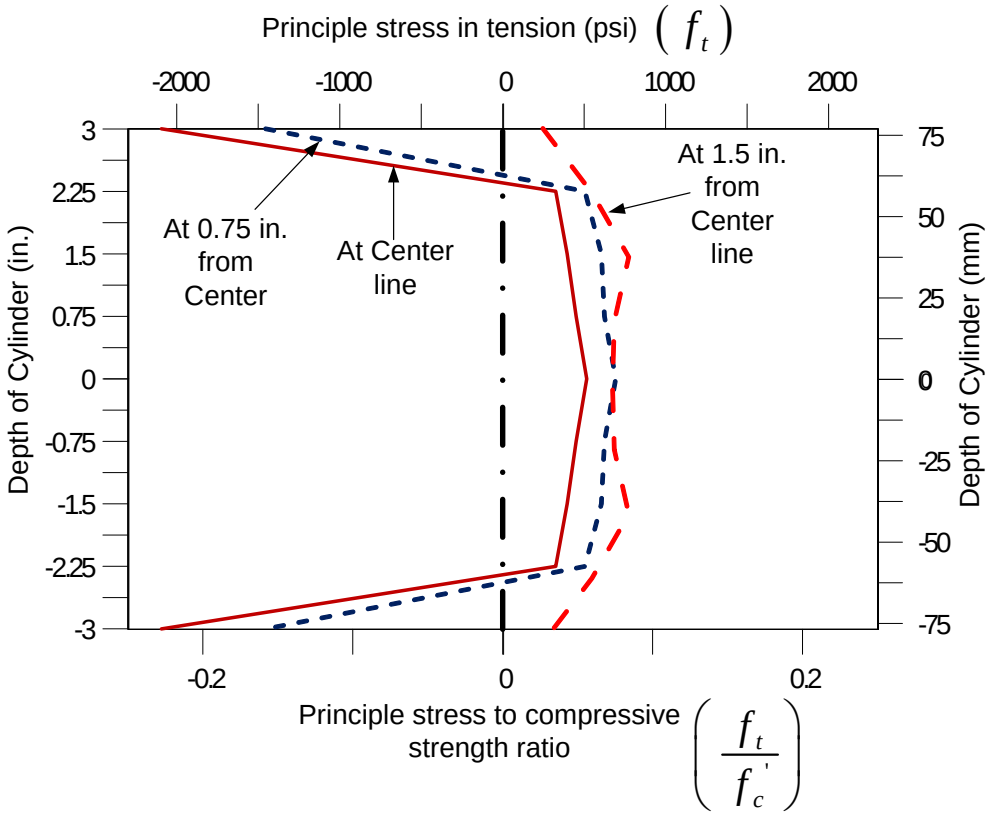

Figure 4.29 Stress Distributions along Height of the Cylinder at Different Distance from centerline

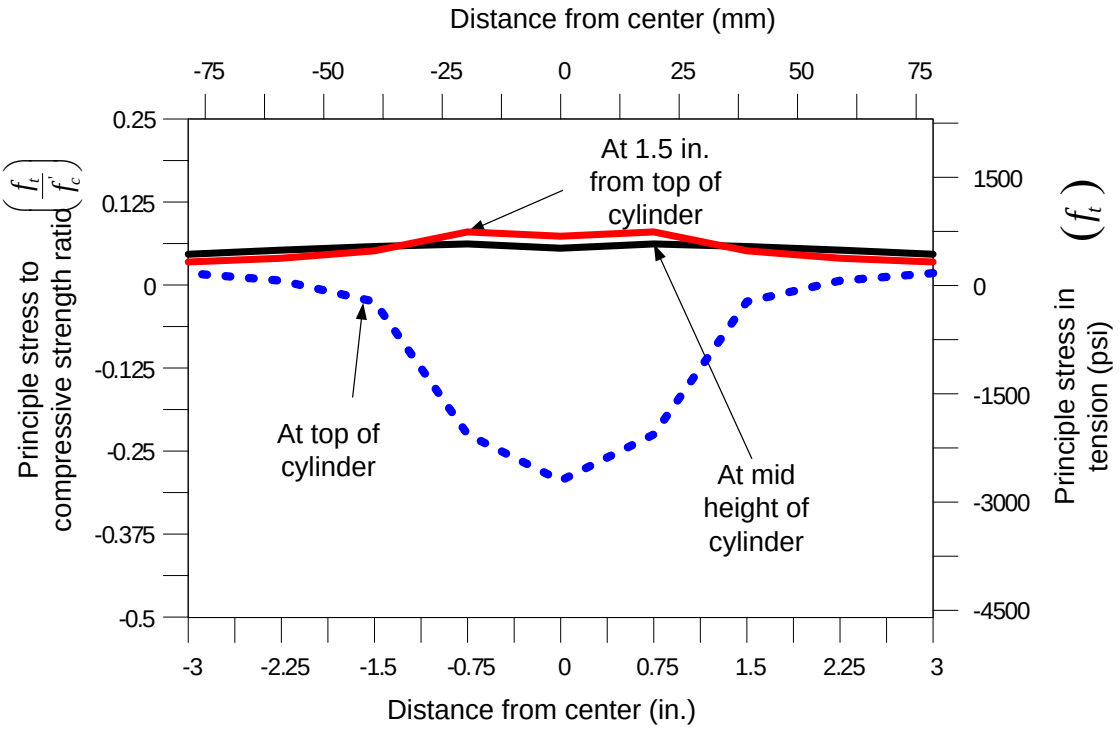

Figure 4.30 Stress Distributions along Diameter of the Cylinder at Different Distance from Top of Cylinder

From the finite element analyses results it can be concluded that even though there is biaxial stress condition will be developed while testing a specimen with DPT setup, the DPT method is still valid to use for determination of equivalent tensile strength. This is because even though there large variation of compression stress the variation in tensile stress is almost constant except near contact of the steel punch and concrete, where compressive force are very high. The results also indicated that the use of equation developed by Chen in 1970 based on plasticity theory of concrete to determine the equivalent tensile strength is reliable.

CHAPTER 5

EXPERIMENTAL RESULTS: LARGE SCALE PRESTRESSED CONCRETE BEAMS

5.1 General

As discussed in Chapter Three, the experimental investigation was carried out in two phases. In the first phase, two large-scale prestressed concrete beam specimens with longitudinal reinforcement satisfying the minimum reinforcement for prestressed concrete flexure member as per ACI 318-11 were tested. First specimen was prestressed concrete beam with minimum web shear reinforcement and the second specimen was SFRPC beam without minimum web shear reinforcement. For SFRPC specimen, 0.75% volume fraction of steel fibers was used. The second phase consisted of four large scale prestressed concrete beam specimens, two PC beams with longitudinal reinforcement satisfying the minimum reinforcement for prestressed concrete flexure member as per ACI 318-11 and minimum required web shear reinforcements by ACI 318-11 and two SFRPC specimens. The first SFRPC specimen was a beam with high longitudinal tensile reinforcement ratio and less web shear reinforcement. The second SFRPC beam specimen consisted of longitudinal reinforcement satisfying the minimum reinforcement for prestressed concrete flexure member as per ACI 318-11 and with just one web shear reinforcement at center for fabrication purpose. All SFRPC beam specimens consisted of 0.75% volume fraction of hooked at end steel fiber.

5.2 First phase specimen: PC#1-1

In first phase one PC beam specimen (PC#1-1) was prepared and tested for comparison purpose with the second SFRPC beam specimen (SFRPC#1-1).

5.2.1 Load versus Deflection, Crack Pattern, Failure Mode

The load versus deflection response for the first phase PC specimen, PC#1-1 is shown in Figure 5.1. The first visible crack was formed at flexure at 80 kips, which initiated from the bottom of specimen and then propagated towards the loading point vertically. This crack is exhibited as tensile strength of concrete at bottom fiber exceeds the limit. As the load increased, more cracks were developed. As can be seen in Figure 5.1, stiffness of the beam started to degrade after first crack as more cracks were developed.

Figure 5.2 illustrates crack pattern at various loading stages from first crack (80 kip) to up to failure. We can see that as load increased the crack pattern also changed. The cracks which originated as vertical became inclined toward the loading point. After 125 kip, the beam turned to deflection control. With slight increase in load, there was a large increase in the deflection. The failure occurred at 134 kip. The deflection at ultimate load was about 1.8 inches. As discussed in Chapter Three, PC#1-1 specimen was purposely under-designed so that the stirrup spacing of 14 inches was slightly larger than the required, 12 inches at potential shear failure region (at 1.5 feet from the face of support). It is interesting to see from Figure 5.3 that the failure of PC#1-1 was

induced by a shear crack after significant flexural yielding. Figure 5.3 shows the photographs of specimens just before failure and after failure. At failure stage, shear crack propagated such that crushing in reduced compression zone and significant sliding led to fail as seen in Figure 5.3.

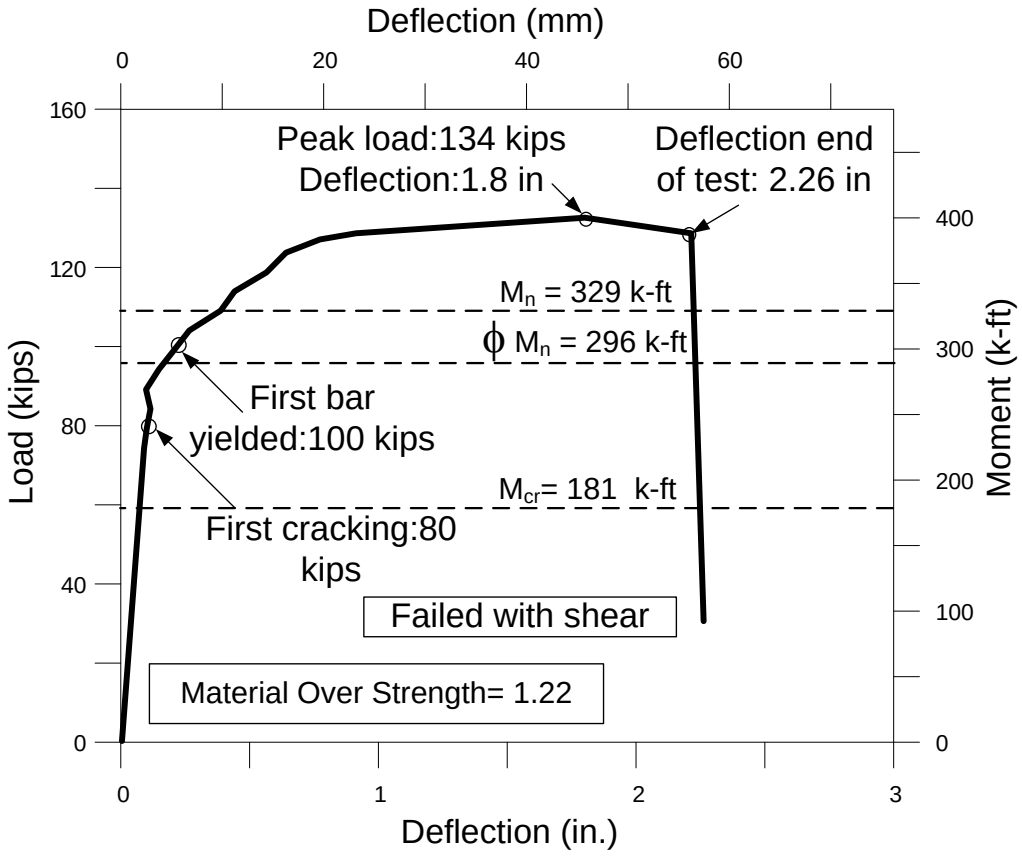

Figure 5.1 Load versus Deflection Curve for Plain Concrete Specimen (PC#1-1) from First Phase of Experimental Program

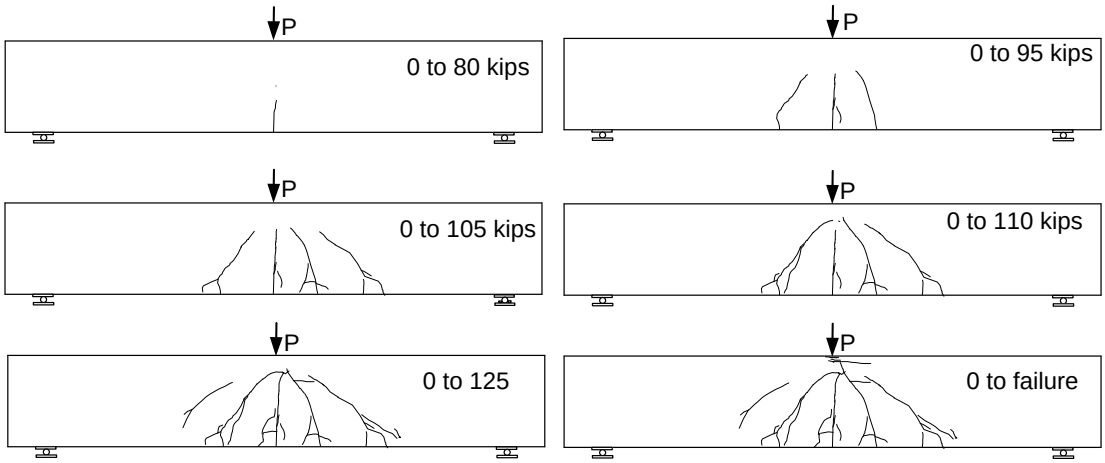

Figure 5.2 Crack Pattern of PC#1-1 Specimen at Different Stages of Loading

(a)

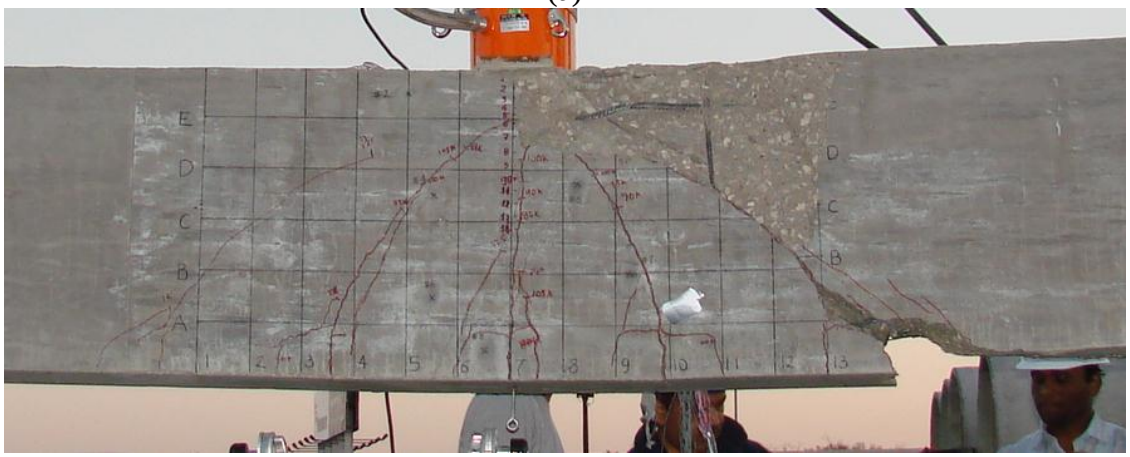

(b)

(c)

Figure 5.3 Typical Photos of Testing of PC#1-1 Specimen; (a) Prior to Failure; (b) At Failure; (c) Crushing in Compression Zone

5.2.2 Strain in Steel and Concrete

Eight strain gages were installed in longitudinal reinforcements; two in the compression reinforcement and six in tension reinforcement at mid sections of the specimens. The strains measured by those strain gages are presented in Figures 5.4 and 5.5. As can be seen in the Figure 5.5, the most of longitudinal reinforcements reached and passed yield strain, 0.002. However, the strain at the maximum compression steel was found only 0.00053 which is below yield strain. That means the compression bar did not yield at ultimate load. The strain from compression reinforcement showed skeptical data as shown in Figure 5.4. The strains increased in compression up to 100 kip, and then suddenly decreased. While load was increased, the strains were continuously decreased and went to positive side prior to fail. One of the possible reasons is that compressive strain may lose due to possible buckling of compression reinforcement at the specific location, where the strain gages were installed.

After first cracks, there were rapid increments of the strain values of strain gauges in tension steel. The first bar yielded at load of 95 kips. Up to load of 125 all most all bars were yielded. Maximum strain was shown by SG #5 of a value of 0.0055.

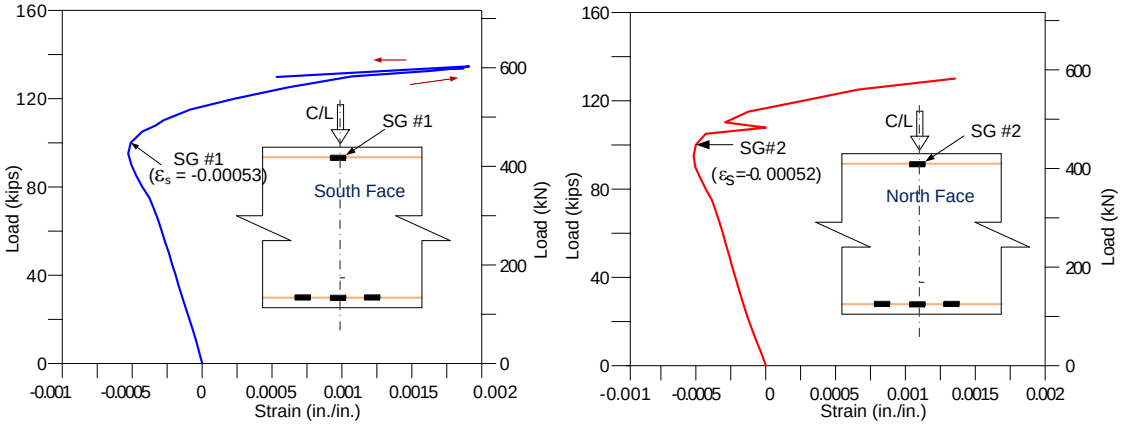

Figure 5.4 Load versus Strain in Compression Steel for PC#1-1 Specimen

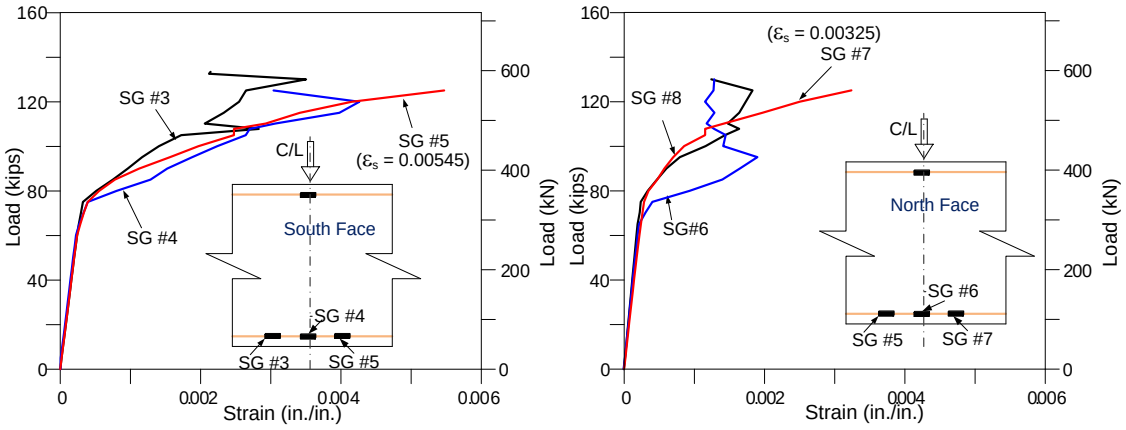

Figure 5.5 Load versus Strain in Tension Steel for PC#1-1 Specimen

Several embedded and surface concrete strain gauges were installed in different locations as discussed in Chapter Three. Load versus strain curves were shown in Figures 5.6 and 5.7. From figure 5.6 it can be shown that the strain gauge CG #1 which close to compression fiber exhibited maximum strain value of 0.0031 at applied load of 130 kips. All other strain gauges which were installed farther from the compression zone (at lower depth) have shown smaller values, which is reasonable. It can be seen from Figure 5.7 that values of all surface concrete strain gauges are well below the theoretical ultimate value of concrete strain (0.003) as per ACI code. Maximum strain

shown by the surface strain near top concrete fiber is order of 0.0019 (negative), whereas strain at mid depth is order of 0.00176 (positive). In between strain values are even lower. Data recorded by horizontal LDVTs installed at lower depth after surface concrete strain gauges gave very low and unreliable values, hence not presented here.

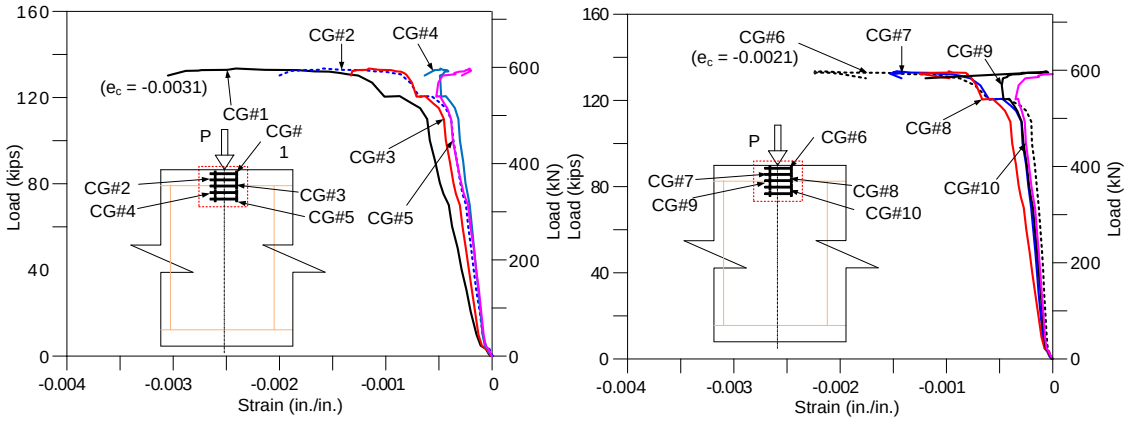

Figure 5.6 Load versus Strain in Concrete (with Embedded Strain Gauges) for PC#1-1 Specimen: (a) at Center of Section of Beam and (b) Near Surface of the Section

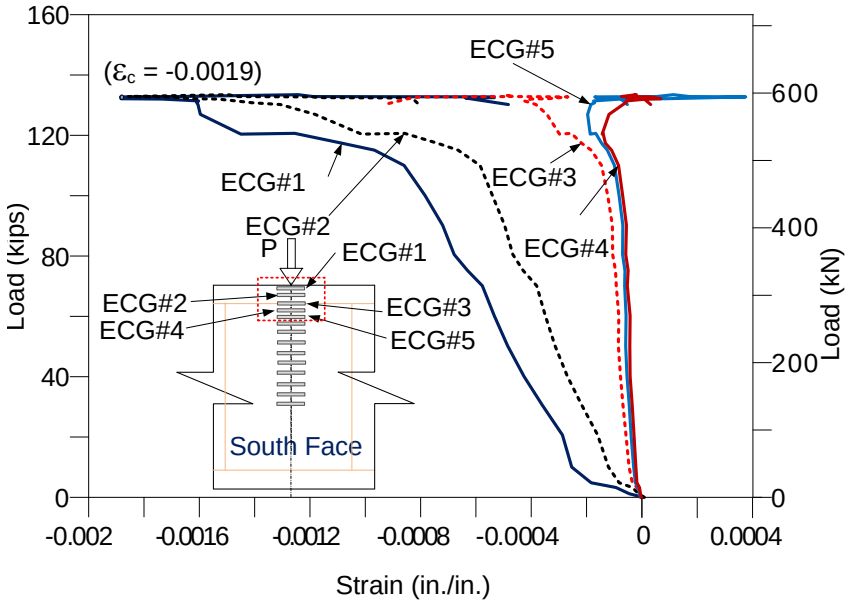

(a)

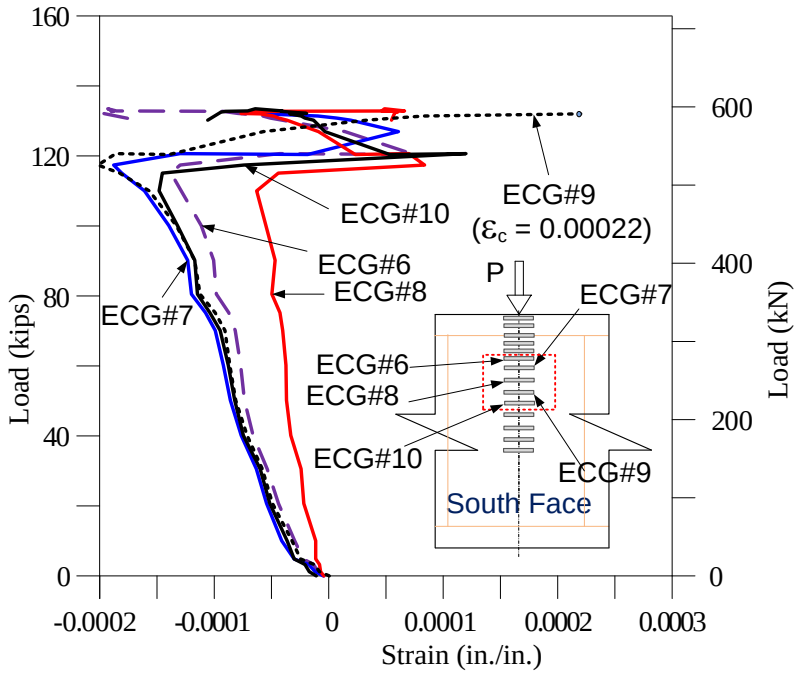

(b)

Figure 5.7 Load Versus Strain in Concrete with Strain Gauges (at South Surface along Depth of beam for PC#1-1 Specimen: (a) Upper Part (b) Lower Part

5.2.3 Ductility and Toughness

Figure 5.8 shows the load deflection curve with energy absorption at first yielding of the tensile and energy absorption at ultimate deformation. The areas under the curve at deflection at yield and ultimate deformation are the energy absorption or toughness at respective deformation. The values of yield deflection and toughness were 0.268 inches and 10.14 k-in and ultimate deflection and toughness were 2.26 inches and 271.5 k-in respectively.

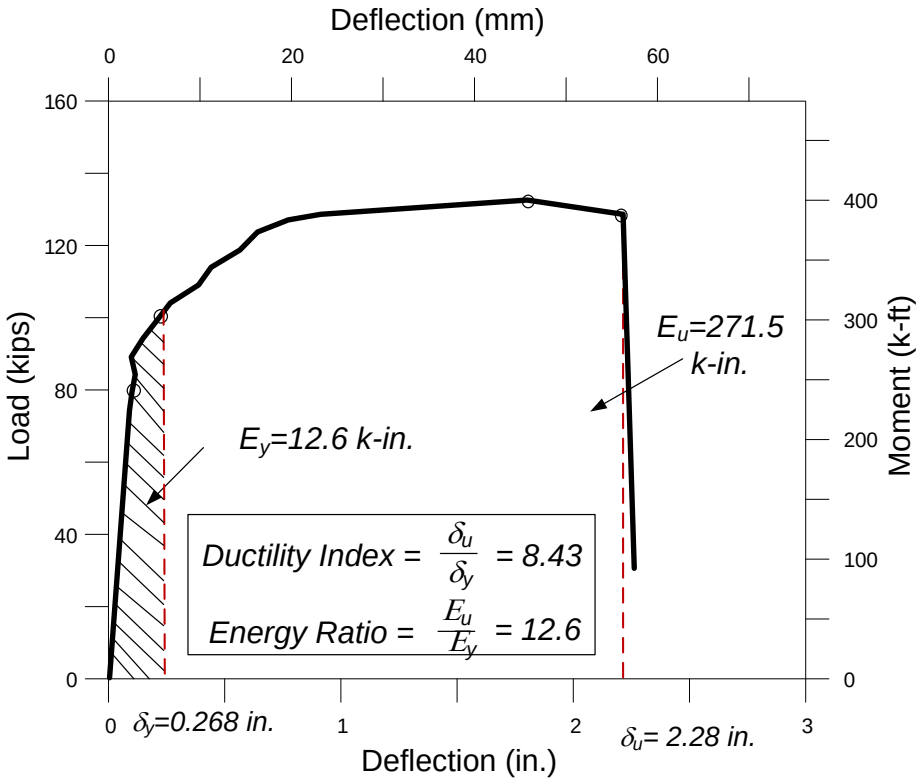

Figure 5.8 Load versus Deflection of PC#1-1 Specimen Showing Energy Dissipation and Ductility

The ductility index which is the ratio of the ultimate deflection to deflection at first yield of bar is computed as 8.43 and indicated at the same curve. Similarly, energy ratio which is the ratio of toughness at ultimate deflection to toughness at yield deflection was also computed as 12.6 and indicated in the Figure 5.8.

5.3 First Phase: SFRPC#1-1 Specimen

5.3.1 Load versus Deflection, Crack Pattern, Failure Mode

The load versus deflection curve for the First phase SFRPC#1-1 specimen is presented in Figure 5.9. As in case of PC specimen, the load was applied with 5 to 20 kips increment. At each loading step, applying of load was stopped and a specimen was inspected to mark any crack. As in case of PC specimen the first visible crack was observed near 80 kips for this SFRPC specimen. The stiffness of the specimen was slightly decreased after first crack. But unlike in PC specimen this variation is very less up to 130 kips. After 130 kip the specimen was controlled by deflection. Even slight increase in load produced large increase in deformation.

Figure 5.10 shows the crack patterns at different stages of loading. After first visible crack up to 90 kips, there were only few cracks which were vertical, and then some of the cracks started to incline. More inclined shear cracks were developed when specimen became to deflection control.

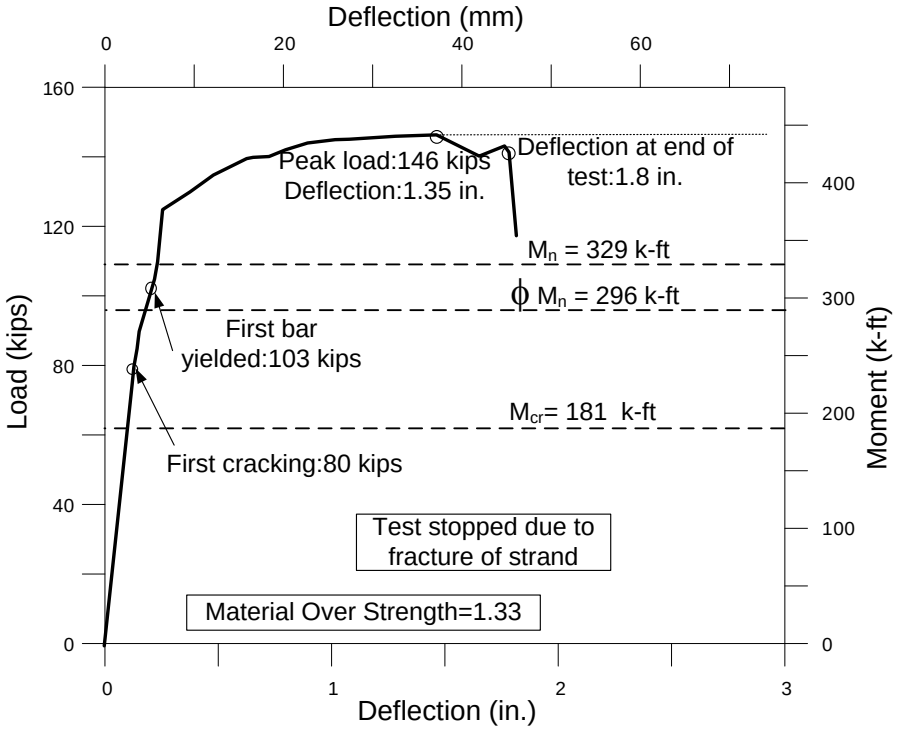

Figure 5.9 Load versus Deflection Curve for SFRPC Specimen (SFRPC#1-1) from First Phase

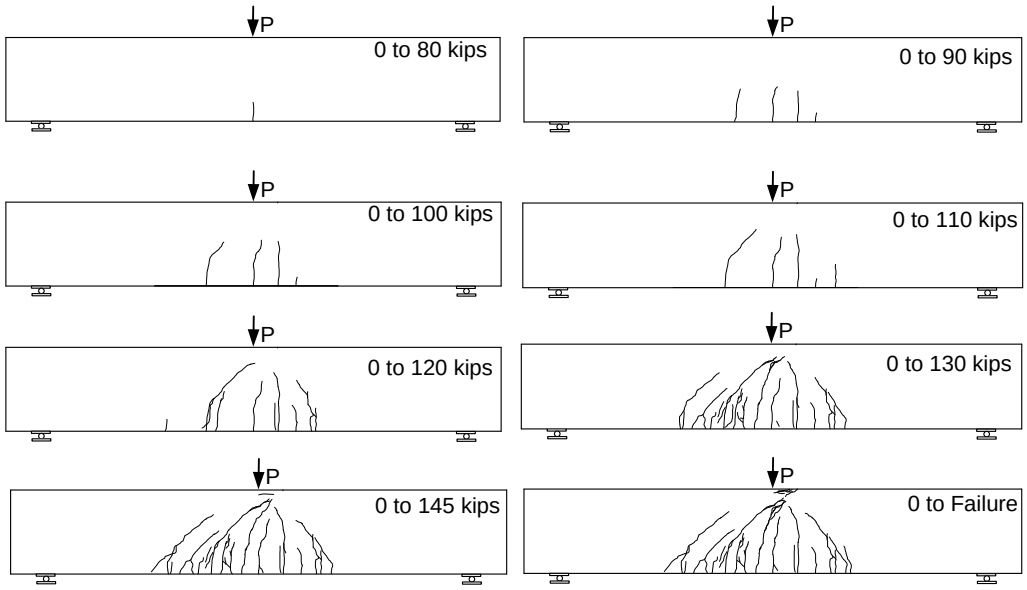

Figure 5.10 Crack Pattern of SFRPC#1-1Specimen at Different Stages of Loading

(a)

(b)

(c)

Figure 5.11 Typical Photos during Testing of SFRPC#1-1: (a) Prior to Failure, (b) after Failure and (c) Crushing in Compression Zone

While further load was applied, the cracks were propagated with inclined angles. When the crack reached the vicinity of loading point creating 3.5 inches depth of compression zone, further propagation was not observed even though the applied load increased. That may be due to higher compression stress. At the stage when the load reached 145 kips, this acted as a confinement, and prevented the crack propagation. Prior to failure, concrete crushing under loading point was observed as can be seen in Figure 5.10. Finally, with the fracture of one of the tensile reinforcement the load dropped and the test was stopped for safety reasons. Even without the required web shear reinforcement, the SFRPC#1-1 beam was failed by a gradual crushing of the concrete (Figure 5.10 (c)) in the compression zone and fracture of the tension reinforcement after a flexural crack became excessively wide. The ultimate load reached was 146 kips and ultimate deflection end of test was 1.8 inches.

5.3.2 Strain in Steel and Concrete

As in case of PC#1-1 specimen, eight strain gages were installed in longitudinal reinforcements; two in the compression reinforcement and six in tension reinforcement at mid sections of the specimens. However, out of six installed strain gauges in tensile reinforcement only two strain gauges were in working condition while testing. So, steel strain gauges data could be recorded only with those two strain gauges. The strains measured by those strain gages are presented in Figures 5.12 and 5.13 in from of load versus strain curves. As in case of PC specimen, figure shows that longitudinal reinforcements reached and passed yield strain (0.002). The maximum value of steel

strain gauge shown by SG#3 was 0.0034 which lower than 0.005 (required for tension controlled). However, the maximum strain at the compression steel was 0.0019 which is slightly less than yield strain. But these values are quite higher than in case of PC specimens. That means the compression reinforcement close to yield at ultimate load in case SFRPC specimens. After first cracks, there were rapid increments of the strain values. The first tension bar yielded at load of 100 kips. Up to load of 130 all bars were yielded. Maximum strain was shown by SG #3 of a value of 0.0034. As out six only two steel strain gauges were working the strain value obtained may not be demonstrated as true value of strain at tensile steel.

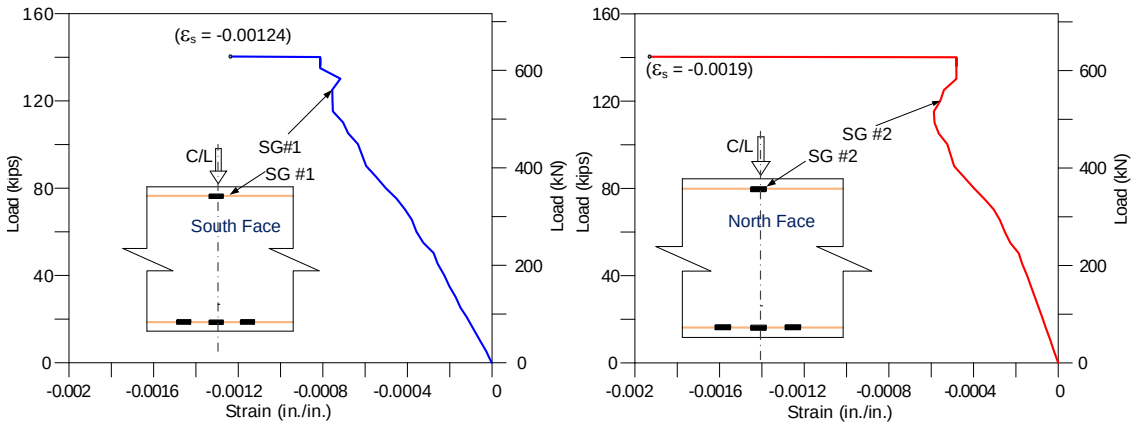

Figure 5.12 Load versus Strain in Compression Steel for SFRPC#1-1 Specimen

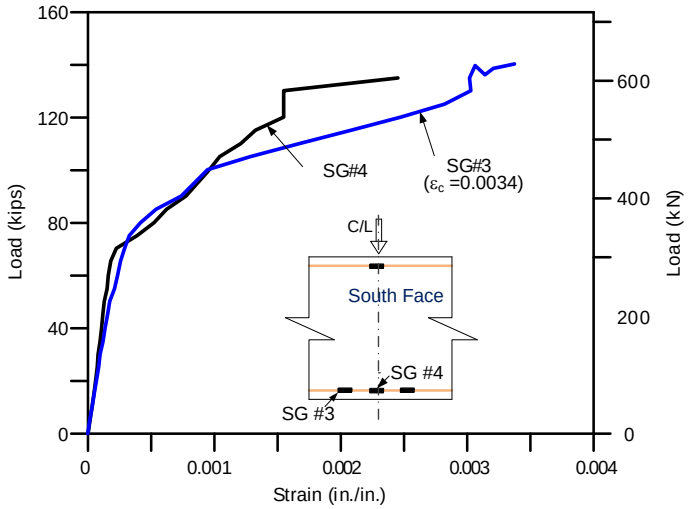

Figure 5.13 Load versus Strain in Tension Steel for SFRPC#1-1 Specimen

Several embedded concrete strain gauges were installed in different locations as discussed in Chapter Three. Load versus concrete strain curves were shown in Figures 5.14 and 5.15. From Figure 5.14 it can be shown the strain gauge CG #1 which close to compression fiber exhibited maximum strain value of 0.0044 at applied load of 141 kips. CG #2 and CG #3 have shown strain value of 0.0048 and 0.0031 respectively which are higher than ultimate design concrete strain (0.003) as per ACI code. All other strain gauges which were installed at lower depth of the beam have shown smaller values as expected.

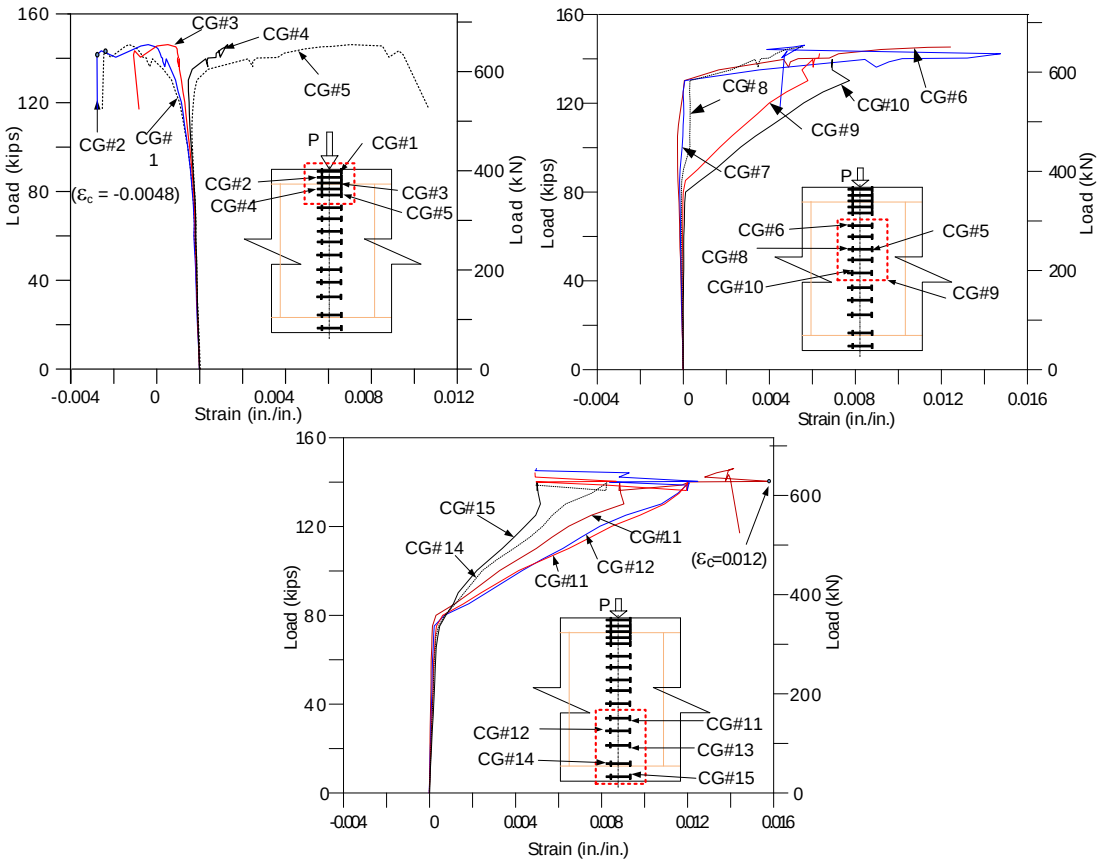

Figure 5.14 Load versus Strain in concrete (with Embedded Strain Gauges) at Mid Span for Specimen SFRPC#1-1

Concrete strain gauges installed below neutral axis such as CG #7 to CG #15 (at mid-section of the beam) exhibit positive values of strain which are of order 0.0058 to 0.0198 (positive). These indicated net tensile strain at c.g. of tensile longitudinal reinforcement (0.0082) is greater than steel strain gauge data recorded by SG #3 (0.0035). From Figure 5.14 it can be seen that the strain values shown by corresponding strain gauges near to the surface of the concrete section are smaller than those exhibited by concrete strain gauge at mid-section. The maximum value of concrete strain in this case was 0.003 (CG #16, near compression fiber). Other strain gauges showed even lower strain values as compared to strain gauge at mid-section.

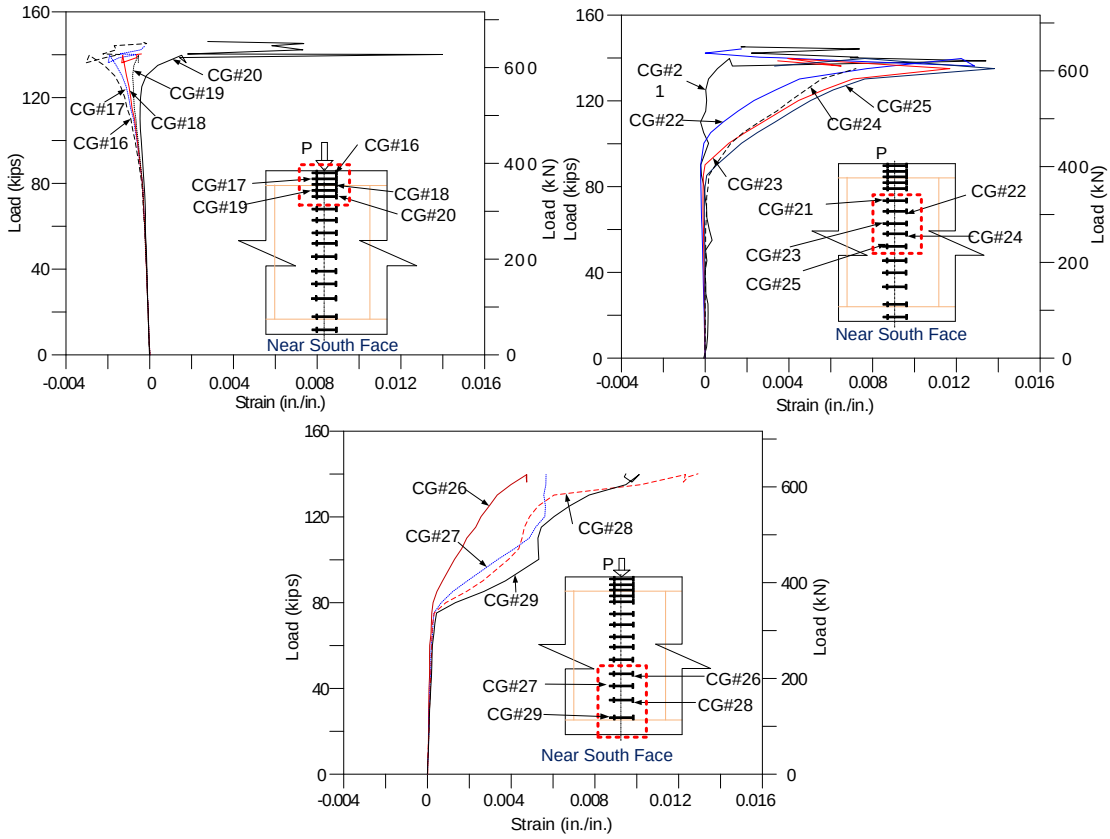

Figure 5.15 Load versus Strain in Concrete (With Embedded Strain Gauges) Near Surface for SFRPC#1-1Specimen

5.3.3 Ductility and Toughness

Figure 5.16 shows the load deflection curve with energy absorption at first yielding of the tensile bar and energy absorption at ultimate deformation for SFRPC#1-1 specimen. The deflection and toughness at first yielding of tensile reinforcement are 0.13 inches and 10.50 k-in respectively. Similarly, values of toughness at ultimate deflection of 1.80 inches were 229.6 k-in respectively. The ductility index and energy ratio were computed as 9 and 21.9 respectively. These values are larger as compared to PC specimen.

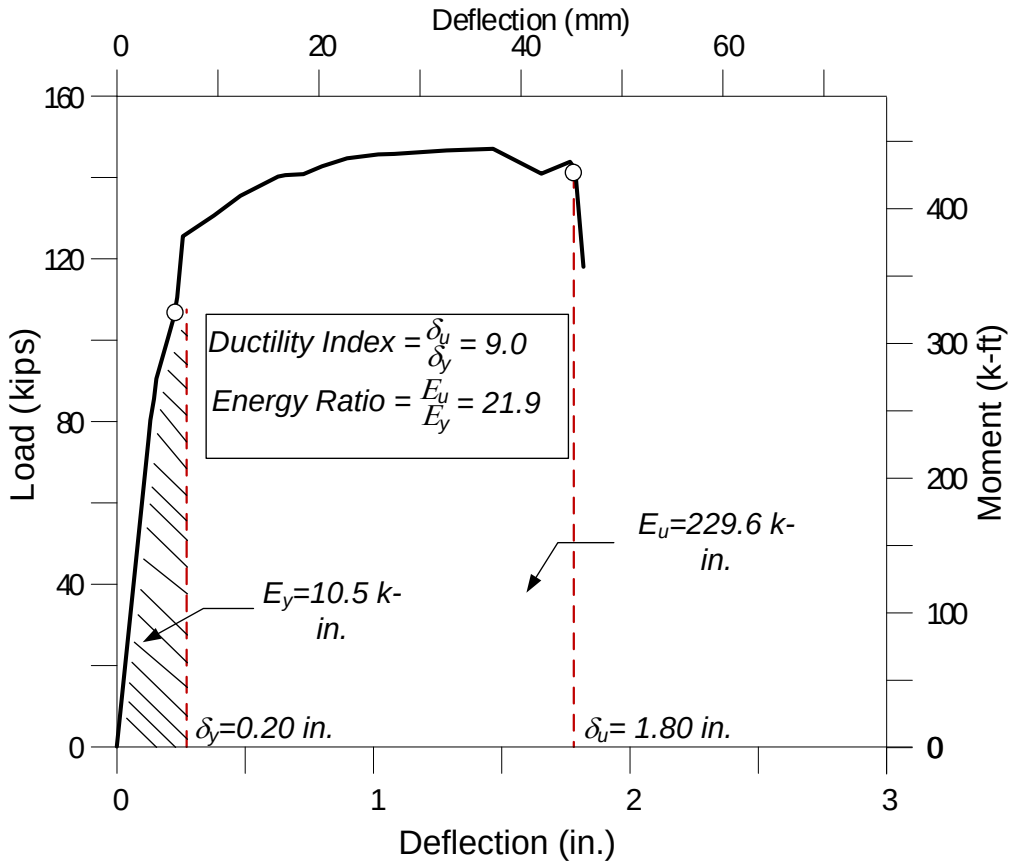

Figure 5.16 Load versus Deflection of SFRPC#1-1 Specimen Showing Energy Dissipation and Ductility

5.4 Second Phase: PC#2-1 Specimen

5.4.1 Load versus Deflection, Crack Pattern and Failure Mode

As in case of first phase, load was applied monotonically with increment of 5 to 20 kips. Figure 5.17 shows the load versus deflection curve. First visible crack was found in 75 kips, which was slightly less than first phase. Similar to earlier phase the stiffness of the specimen was reduced after first visible cracks.

Figure 5.18 shows various crack patterns in different stage of loading from 75 kips to failure. More flexural cracks were developed after first visible crack. Most of

the cracks developed up to 100 kip load were straight and vertical. After 110 kip existing cracks and new cracks developed were inclined and propagated toward loading point. These cracks stopped to propagate near depth of 4 inches compression zone and became wider and wider. Around 130 kip of load, the crushing of the concrete near compression fiber was started.

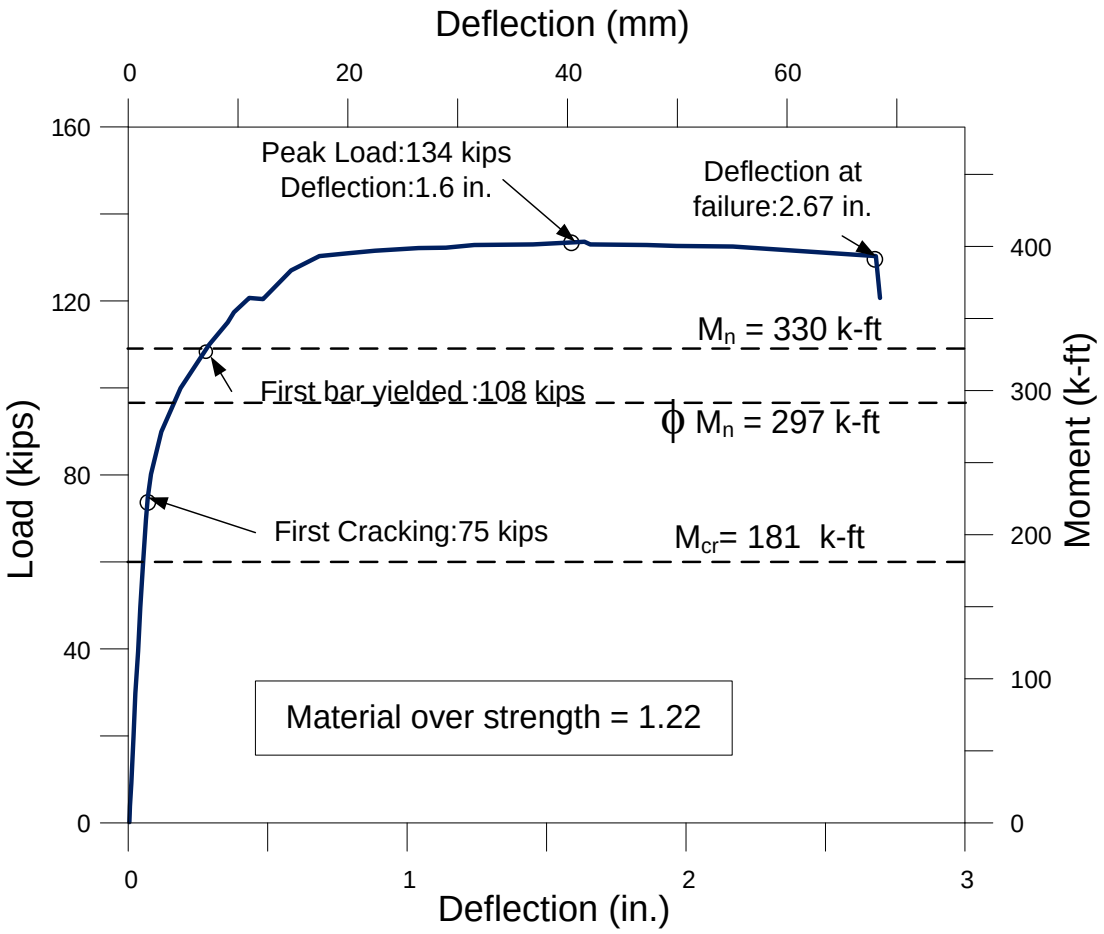

Figure 5.17 Load versus Deflection Curve for PC Specimen (PC#2-1) from Second Phase

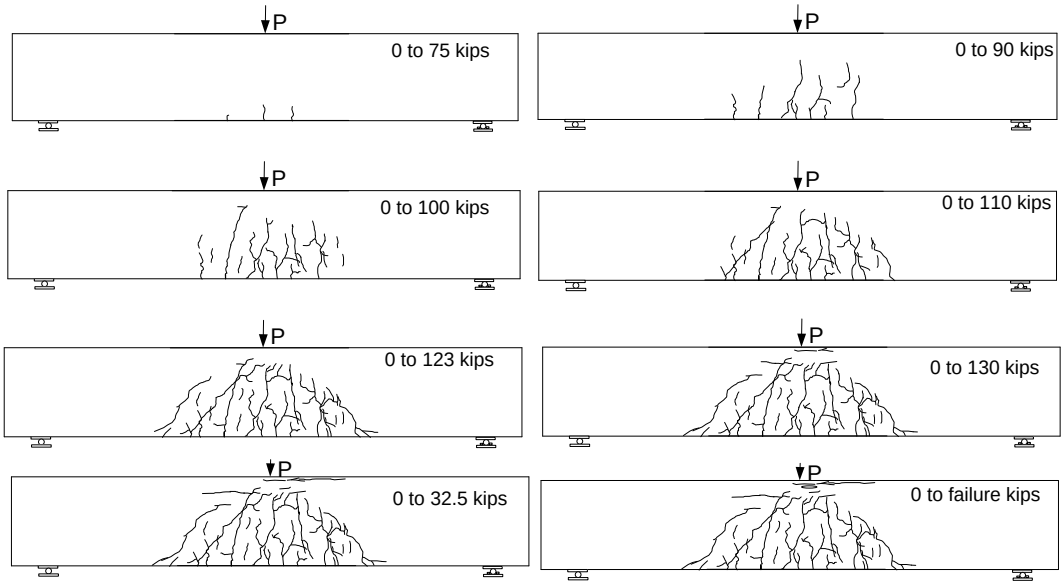

Figure 5.18 Crack pattern of PC#2-1 specimen at different stages of loading

Because the beam consisted of sufficient shear reinforcement, specimen failed in flexure with crushing of the concrete at load of 134 kips as shown in Figure 5.19.

(a)

(b)

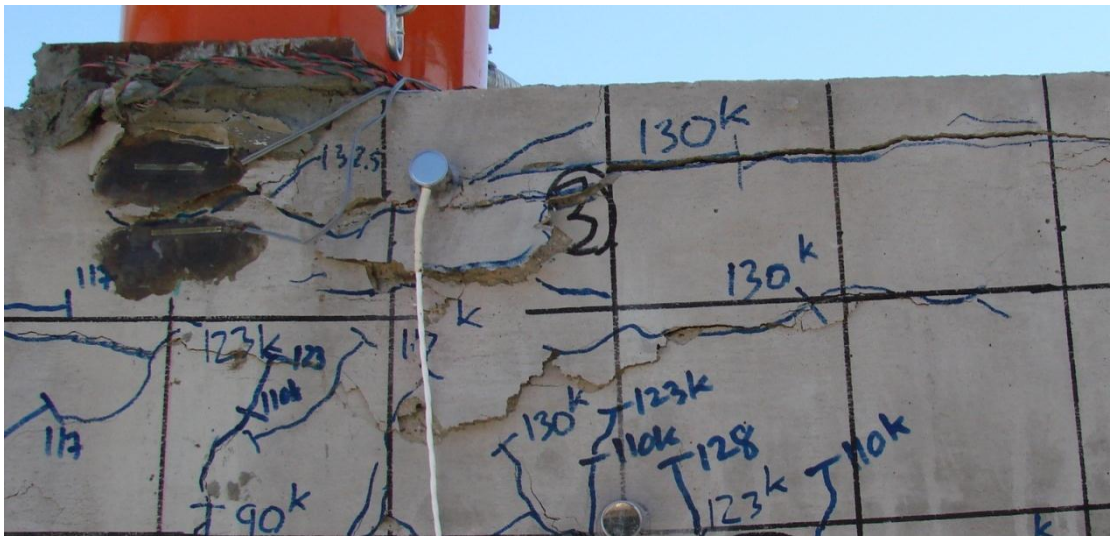

(c)

Figure 5.19 Typical Photos during of PC#2-1 Specimen: (a) Prior to Failure, (b) at Failure and; (c) Crushing in Compression Zone

5.4.2 Strain in Steel and Concrete

Similar to first phase, eight strain gauges were installed in compression and tensile reinforcement as discussed in chapter three. Results are presented in Figures 5.20 to 5.21. Load versus strain curve (Figure 5.20) shows that the values of strain in compression steel are order of 0.0004 and 0.0011 (negative), which are lower than the yield strain (0.002). This indicated that the compression bar did not yield at ultimate load. However, all strain gauges installed in tension reinforcement exhibited the strain values more than 0.002 indicating that reinforcement yielded before failure. SG #3 exhibited maximum value of strain 0.0089. Figure 5.21 shows that strain values increased very rapidly after the first crack occurred. Most of bars were yielded up to load of 100 kips. These indicate that failure was as tension controlled as expected.

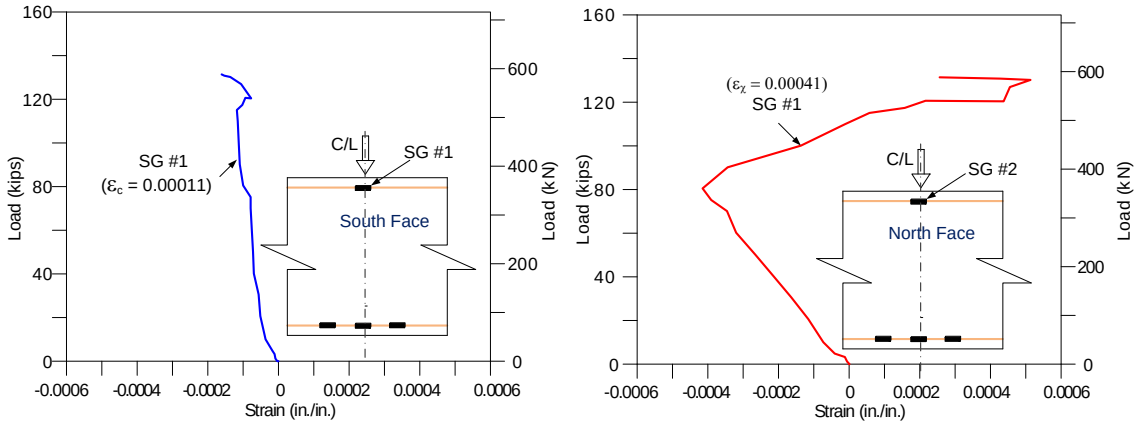

Figure 5.20 Load versus strain compression for PC#2-1 specimen

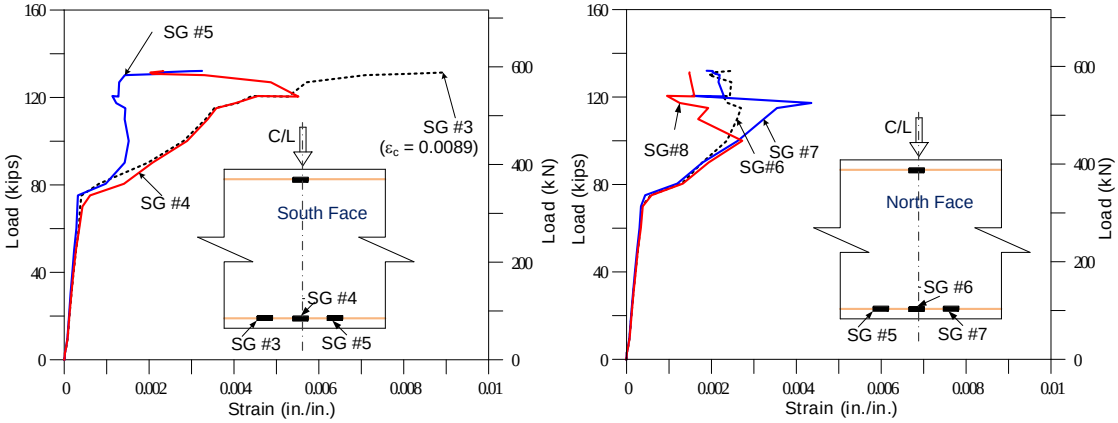

Figure 5.21 Load versus Strain in Tension Steel for PC#2-1 Specimen

As it has been seen that the strain values obtained from concrete strain gauges which were installed at lower depth of beam specimens in the case of first phase did not indicated reliable and appropriate data, so for second phase concrete strain gauges were installed only near the compressing fiber of beam section. A total of seven concrete strain gauges were installed at a depth of 1.25 in from top of the beam as discussed in Chapter Three. Besides these four more surface concrete strain gauges (two each face of beam) were also installed. Results are presented in form of load versus strain curves as shown in Figures 5.22 and 5.23. Except a few strain gauges, all strain gauges exhibited the strain values more than 0.003. From Figure 5.22, it can be seen that the maximum value of concrete strain is 0.0057. And from Figure 5.23, it can be seen that the concrete strain values exhibited from surface strain gauges were of lower order as compared to embedded strain gauges. Strain gauge ECG #1 shows maximum strain of 0.0052. Similar to the steel strain gauges, all concrete strain gauge values increased rapidly after loading of 80 kips (first crack).

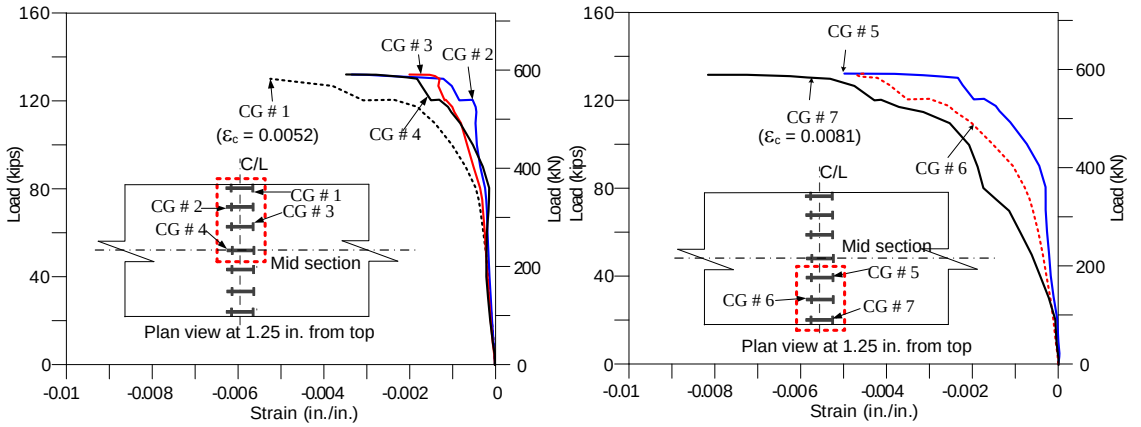

Figure 5.22 Load versus Strain Concrete (with Embedded Strain Gauges) for PC#2-1 Specimen

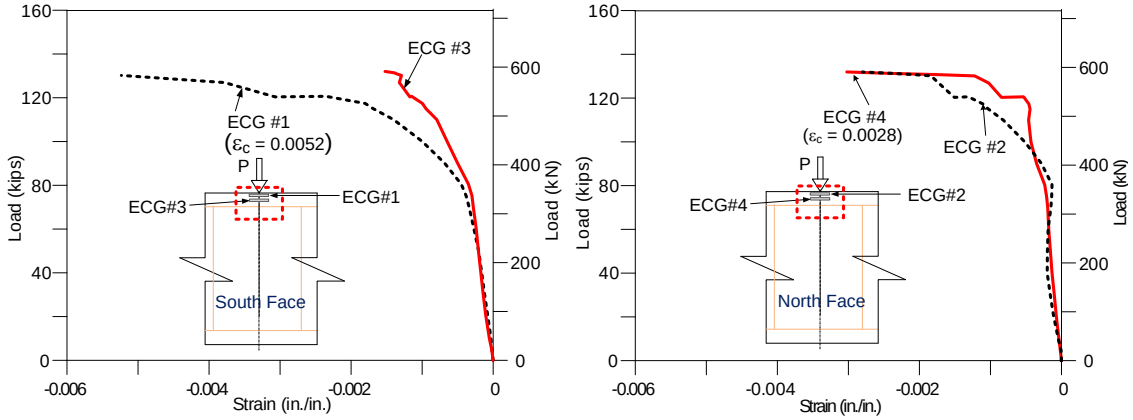

Figure 5.23 Load versus Strain Concrete (with Surface Strain Gauges) for PC#2-1 Specimen

5.4.3 Ductility and Toughness

As previous specimen, Figure 5.24 shows the load deflection curve with energy absorption at first yielding of the tensile bar and energy absorption at ultimate deformation for PC#2-1 specimen. The deflection and toughness at first yielding of tensile reinforcement are 0.268 inches and 25.2 k-in respectively. Similarly values of

toughness at ultimate deflection of 2.67 inches were 333.9 k-in respectively. The ductility index and energy ratio were computed as 9.3 and 13.3 respectively.

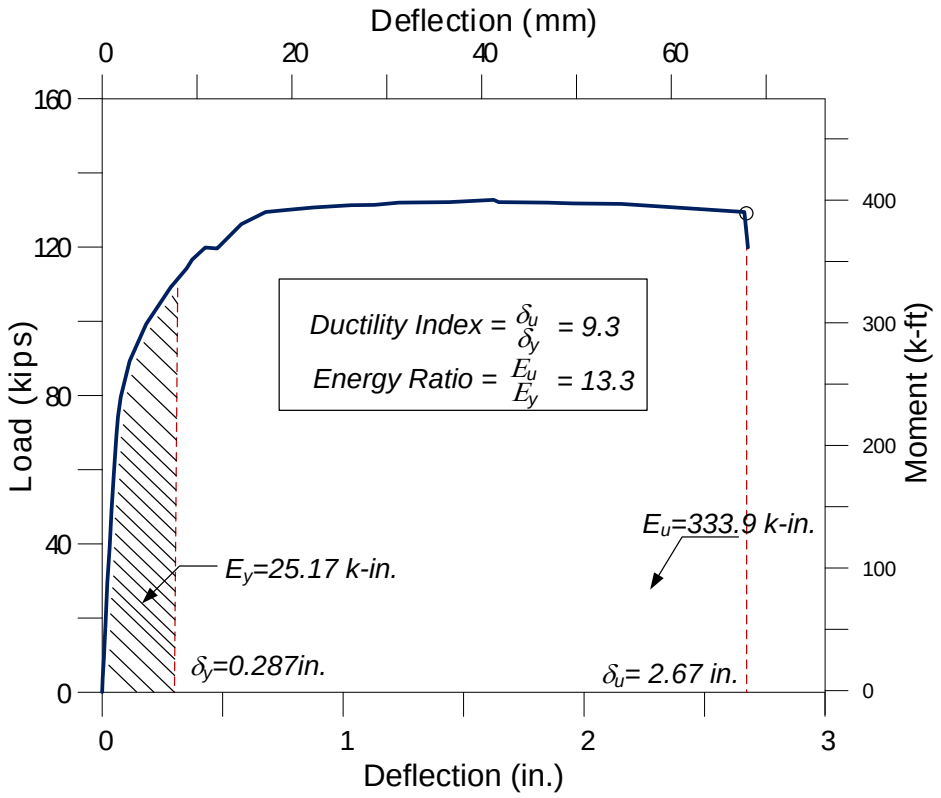

Figure 5.24 Load versus Deflection of PC#2-1 Specimen Showing Energy Dissipation and Ductility

5.5 Second phase: PC#2-2

5.5.1 Load versus deflection, crack pattern, failure mode

All first specimens from first phase and PC#2-1 specimen were tested using single point loading at center over a 1 × 6 × 20 inches steel plate. However, in order to find out the effect of reduction of the confining area due to the applied loading (which induces a bi-axial compression thus increasing the compressive strength as well as the

ultimate strain of the concrete) remaining specimens including PC#2-2, SFRPC#2-1 and SFRPC#2-2 specimens were tested with a single point load at the center of the beam over a 1 × 3 × 16 inches plate (same as that used by Mattock,1998), as discussed in Chapter Two). As discussed in case of previous specimens, the load was applied monotonically with increment of 5 to 20 kips. Figure 5.25 shows the load versus deflection curve. First visible crack was found in 70 kips, which was slightly less than PC#2-1. But this may be the very minor crack because the stiffness of the specimen started to reduce only after around 80 kips as shown in Figure 5.25.

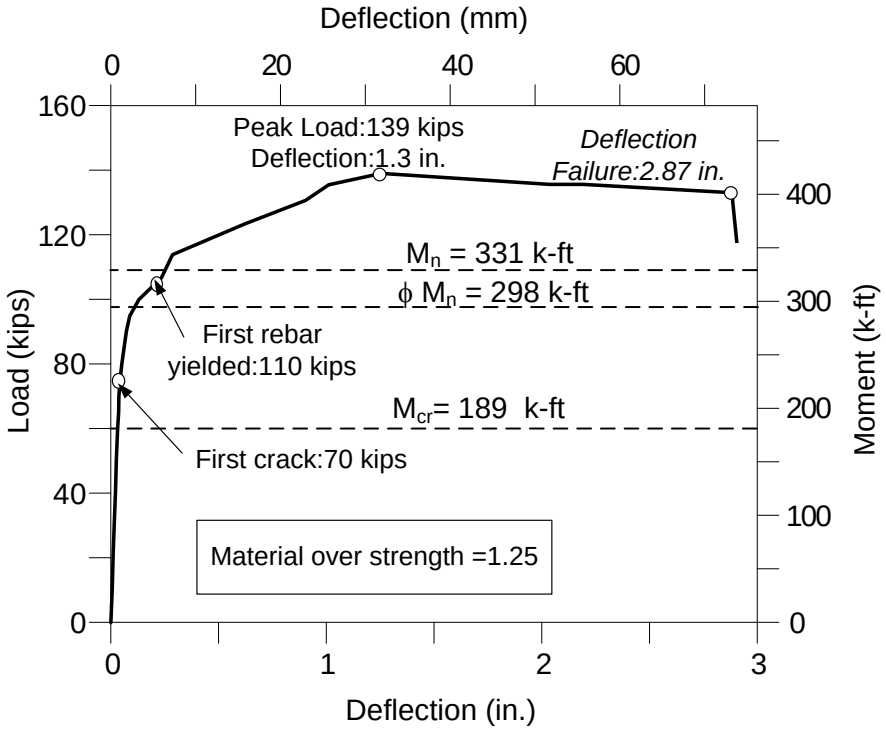

Figure 5.25 Load versus Deflection Curve for PC Specimen (PC#2-2) from Second Phase

Figure 5.26 shows various crack patterns in different stage of loading from 70 kips to failure. Up to 95 kips there only three flexural cracks. More flexural cracks

were developed after that. After 100 kip, existing cracks and new cracks developed were inclined and propagated towards loading point. These cracks stopped to propagate near depth of (2-3 inches) and became wider and wider. The reduction in this depth may be due to the use of 3-inch wide plate for loading which able to reduce the biaxial compression.

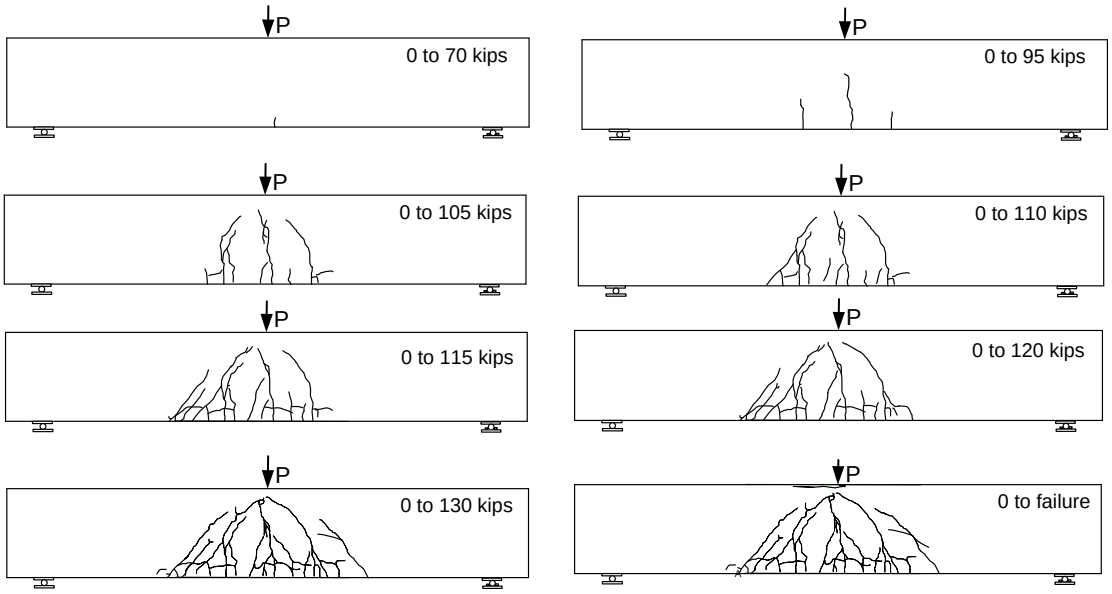

Figure 5.26 Crack patterns of PC#2-2 specimen at different stages of loading

Around 135 kip of load, the compression concrete started to crush. As shown in Figure 5.27 similar to PC#2-1 this also beam ultimately failed in flexure at load of 139 kips after crushing of the concrete at compression fiber, because the beam consisted of sufficient shear reinforcement.

(a)

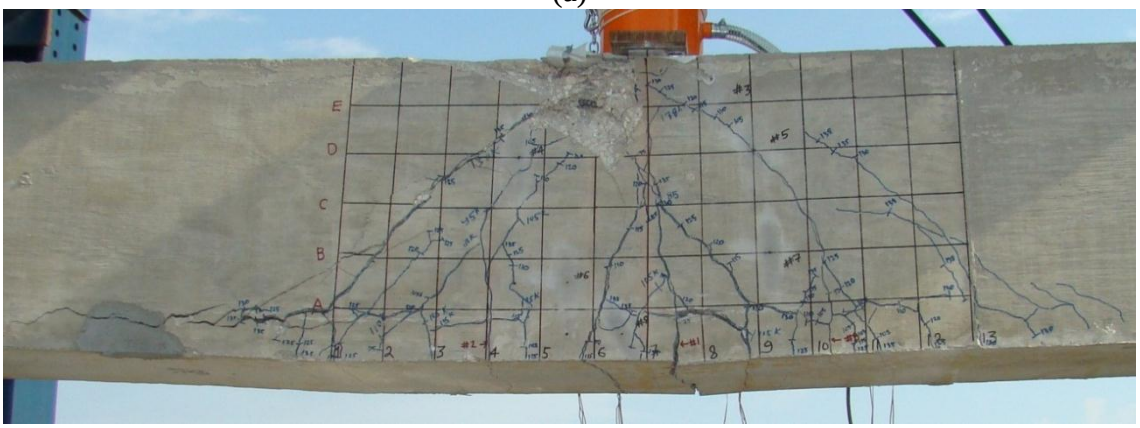

(b)

(c)

Figure 5.27 Typical Photos during Test for the PC#2-2 Specimen: (a) Prior to Failure, (b) at Failure and (c) Crushing in Compression Zone

5.5.2 Strain in Steel and Concrete

Similar to previous specimens, eight strain gauges were installed in compression and tensile reinforcement as discussed in Chapter Three. Results are presented in Figures 5.28 to 5.29. Load versus strain curves (Figure 5.28) show that the values of strain in compression steel are order of 0.00033 (negative) and 0.00043 (negative), which are again lower than the yield strain (0.002). The compression strain gauge kept on showing reduction of strain values and went to positive values. That indicated the compression bar did not yield at ultimate load. However, all strain gauges installed in tension reinforcement exhibited the strain values more than 0.002 indicating that reinforcement yielded before failure. SG #6 exhibit maximum value of strain 0.0096. Figure 5.29 shows that strain values increased very rapidly after the first crack occurred. Most of bars were yielded up to load of 100 kips. These indicate that failure was tension controlled as expected.

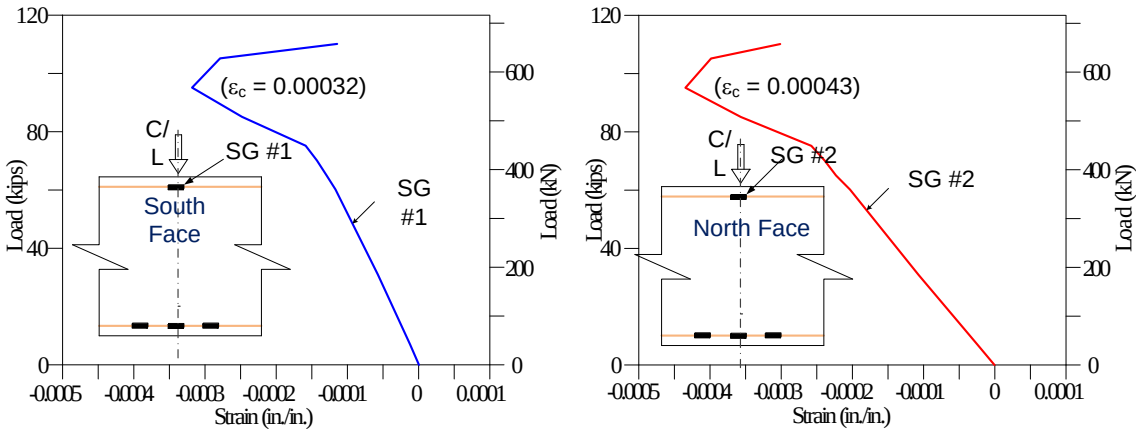

Figure 5.28 Load versus Strain at Compression Steel for PC#2-2 Specimen

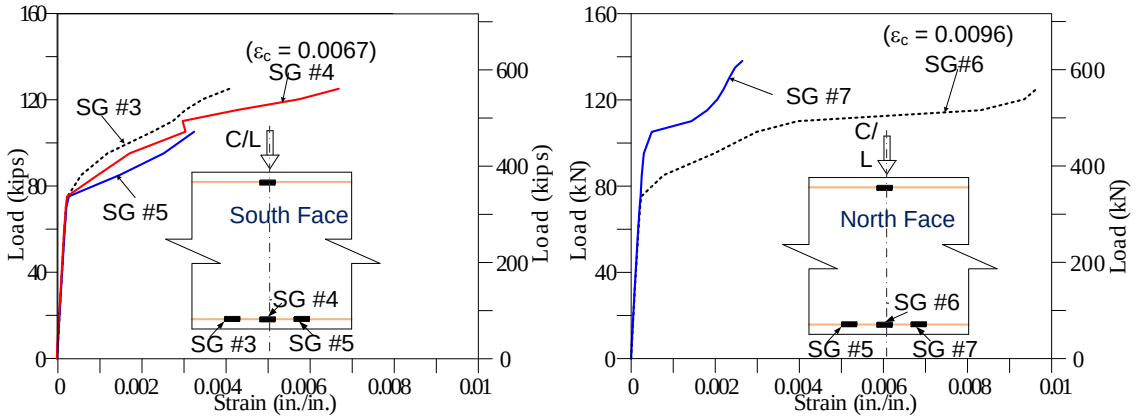

Figure 5.29 Load versus Strain in Tension for PC#2-2 Specimen

As in case of PC# 2-1, a total of seven concrete strain gauges were installed at depth of 1.25 inches from top of the beam as discussed in chapter three. As most of the surface concrete strain gauges in case of PC#2-1 specimen showed lower compressive strains as compared to embedded strain gauges, these type strain gauges were not used for remaining specimens (PC#2-2, SFRPC#2-1 and SFRPC#2-2). Results were presented in form of load versus strain curves as shown in Figure 5.30. All strain gauges exhibited the strain values more than 0.003. From Figure 5.30 it can be seen that the maximum value of strain at concrete was 0.0071. Similar to steel strain gauges, all concrete strain gauge values increased rapidly after loading of 80 - 100 kips.

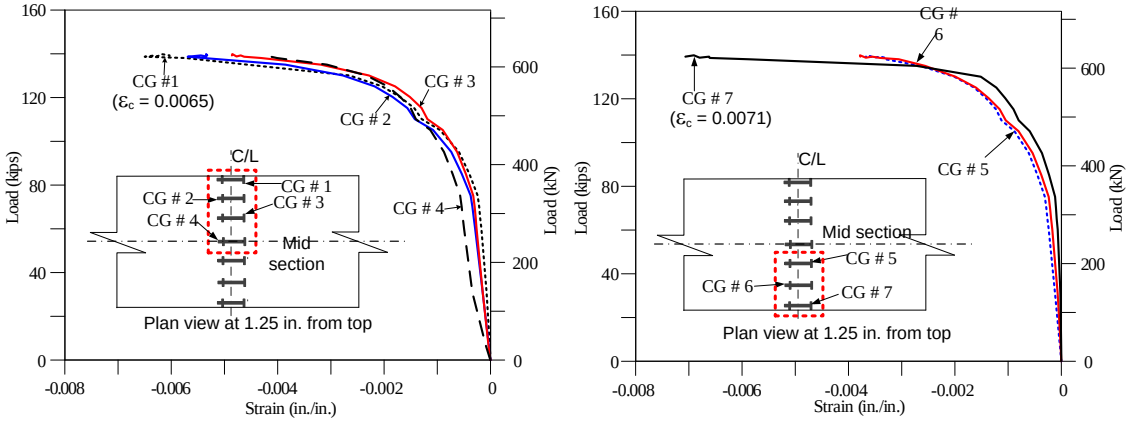

Figure 5.30 Load versus Strain in Concrete (with Embedded Strain Gauges) for PC#2-2 Specimen

5.5.3 Ductility and Toughness

Figure 5.31 shows the load deflection curve with energy absorption at first yielding of the tensile bar and energy absorption at ultimate deformation for PC#2-2 specimen. The deflection and toughness at first yielding of tensile reinforcement are 0.24 inches and 21.1 k-in respectively. Similarly, values of toughness at ultimate deflection of 2.87 inches were 373.0 k-in respectively. The ductility index and energy ratio were computed as 11.96 and 17.7 respectively.

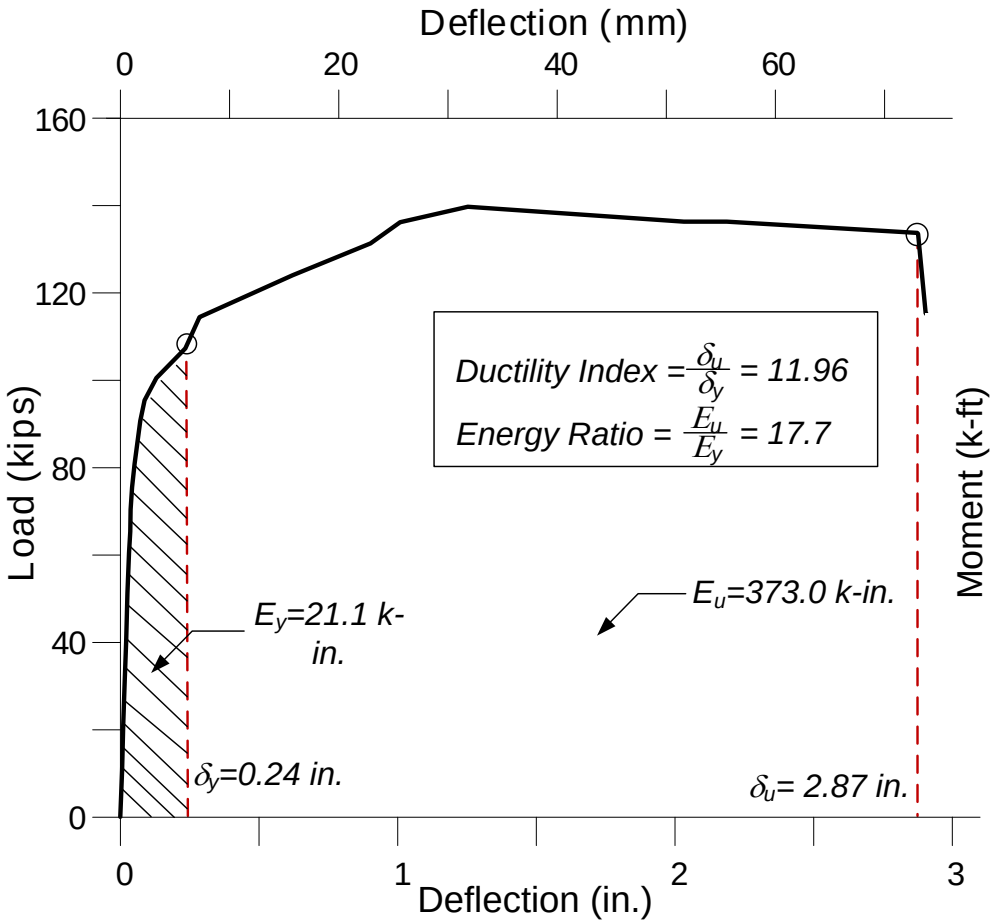

Figure 5.31 Load Versus Deflection of PC#2-2 Specimen Showing Energy Dissipation and Ductility

5.6 Second Phase: SFRPC#2-1

5.6.1 Load versus Deflection, Crack Pattern, Failure Mode

As discussed in case of previous specimens, load was applied monotonically with increment of 5-20 kips. Figure 5.32 shows the load versus deflection curve. First visible crack was found in 70 kips. Actually only three minor cracks were seen at that load. The stiffness of the specimen started to reduce only after applied load of 90 kip.

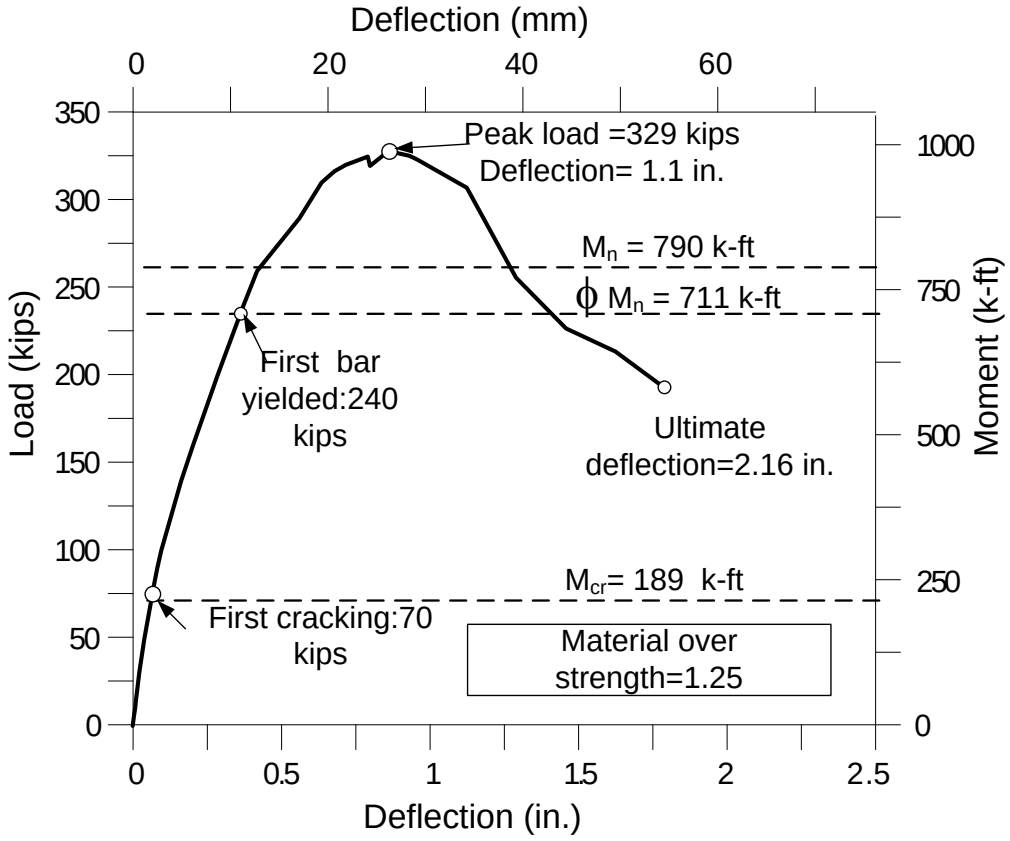

Figure 5.32 Load versus Deflection Curve of SFRPC specimen (SFRPC#2-1) from second phase

Figure 5.33 shows various crack patterns in different stage of loading from 70 kips to failure. Up to 120 kips several flexural and straight cracks were developed after that. Around 150 kips, more cracks developed and some newer cracks were inclined and propagated toward loading point. Most of the cracks stopped around 5-8 inches depth of compression block. Around 290 kip of load the crushing of the concrete started. Maximum load reached was around 1.1 inches deflection. Before failure large numbers of cracks developed and some of the cracks became wider.

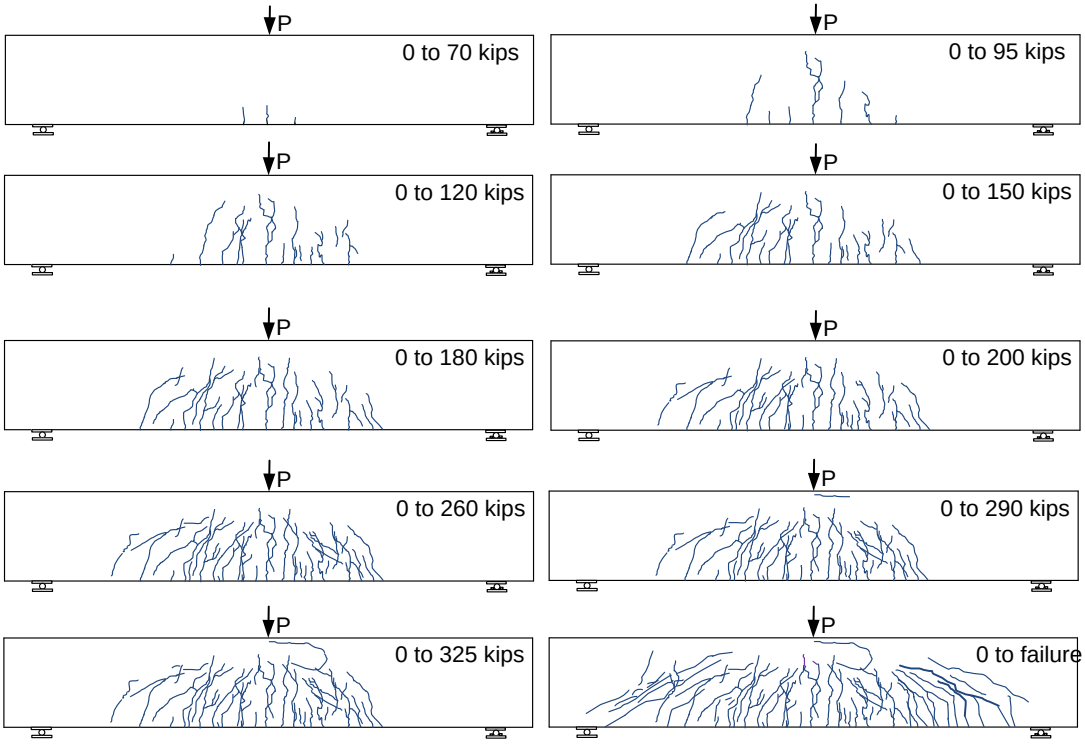

Figure 5.33 Crack pattern of SFRPC#2-1 specimen at different stages of loading

Though less than the required shear reinforcement as per by ACI code was provided as discussed in Chapter Three, the SFRPC #2-1 beam failed in flexure after crushing of the concrete near loading point as shown in Figure 5.34. The ultimate deflection reached at end of test was 2 inches.

(a)

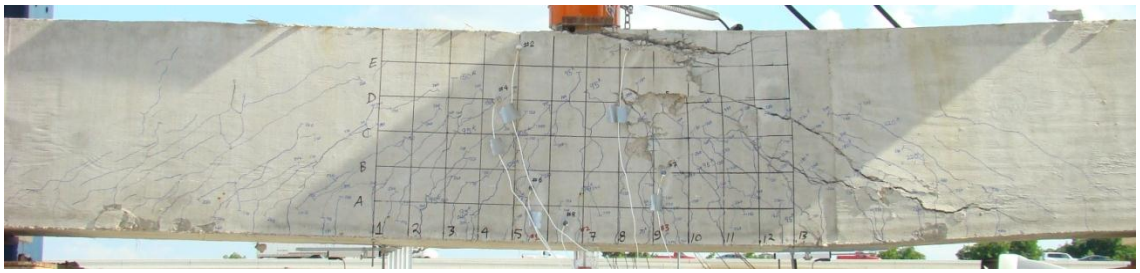

(b)

Figure 5.34 Typical Photos during Testing of SFRPC#2-1 Specimen: (a) Prior to Failure, (b) at Failure and (c) Crushing in Compression Zone

5.6.2 Strain in Steel and Concrete

Similar to previous specimens eight strain gauges were installed in compression and tensile reinforcement as discussed in Chapter Three. Results are shown in Figure 5.35 and Figure 5.36. Out of two installed strain gauges in compression steel, only one (SG #1) was working and data could be recorded. The maximum strain value obtained

was 0.00245 as shown in load versus strain curves (Figure 5.35). Strain value increased up 288 kips and then decreased when load was further increased. It looks like the compression bar also yielded at 288 kips of applied load. One of the six strain gauges for tension reinforcement bar one strain gauge was also found to be not working. Rest of strain gauges installed in tension reinforcement exhibited the strain values more than 0.002 indicating that reinforcement yielded before failure. SG #7 exhibit maximum value of strain 0.0086. Figure 5.25 shows that strain values increased very rapidly after the first crack occurred. Most of bars yielded up to load of 260 kips. These indicate that failure was occurred as tension controlled as expected even though the steel content in section was larger (2.11%) more than criteria required by the ACI code for a tension control member as discussed in first two chapters.

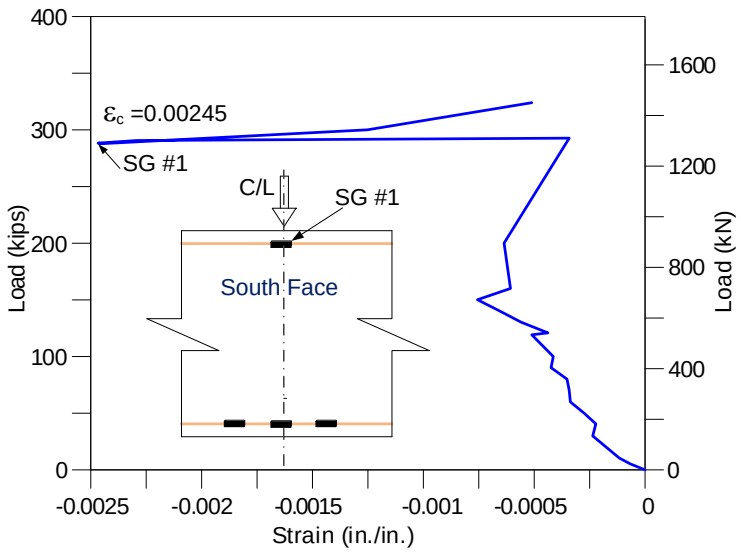

Figure 5.35 Load versus Strain in Compression Steel for SFRPC#2-1 Specimen

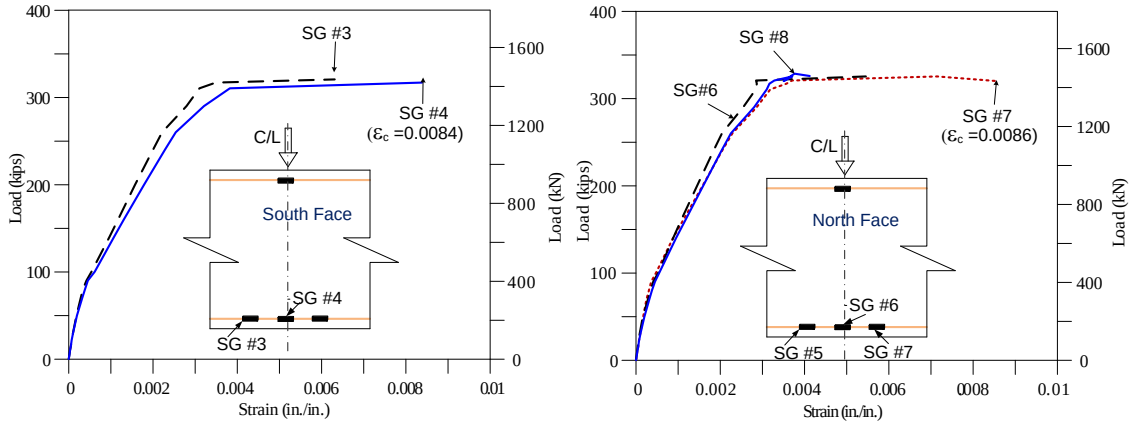

Figure 5.36 Load versus Strain in Tension Steel for SFRPC#2-1 Specimen

As in case of PC#2-2, a total of seven concrete strain gauges were installed at depth of 1.25 in from top of the beam as discussed in chapter three. Out of seven one strain gauge (CG #4) was not working properly after first crack loads. Results were presented in form of load versus strain curves as shown in Figure 5.36. Except one strain gauge (CG #1) all other strain gauges exhibited the strain values more than 0.003.

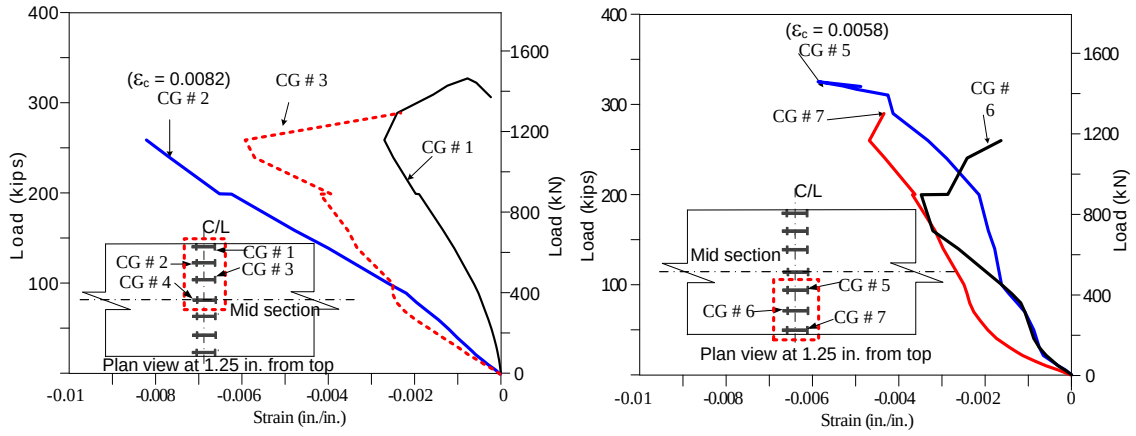

Figure 5.37 Load versus Strain in Concrete (with Embedded Strain Gauges) for SFRPC#2-1 Specimen

The concrete strain gauges showed the maximum value around load of 230 to 325 kips after reaching the peak load. The maximum shown by CG #2 was 0.0082 and

load of 260 kips. After reaching peak values strain gauges either stopped working or started to sudden change in the sign of the readings (change negative suddenly to positive).

5.6.3 Ductility and Toughness

As in previous specimen, Figure 5.38 shows the load deflection curve showing energy absorption at first yielding of the tensile bar and energy absorption at ultimate deformation for SFRPC#2-1 specimen. The deflection and toughness at first yielding of tensile reinforcement are 0.45 inches and 68.6 k-in respectively. Similarly, values of toughness at ultimate deflection of 2.16 inches were 532.6 k-in respectively. The ductility index and energy ratio were computed as 5.02 and 7.80 respectively.

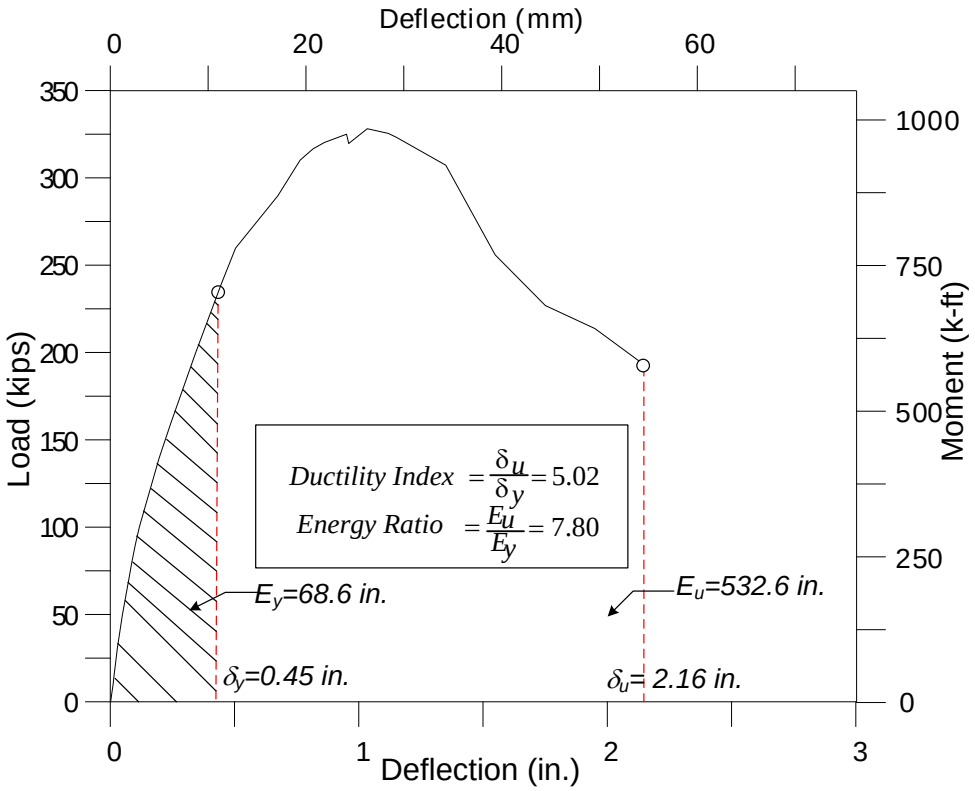

Figure 5.38 Load versus Deflection of SFRPC#2-1 Specimen Showing Energy Dissipation and Ductility

5.7 Second Phase: SFRPC#2-2

5.7.1 Load versus Deflection, Crack Pattern, Failure Mode

As discussed in case of previous specimens, load was applied monotonically with increment of 5-20 kips. Figure 5.39 shows the load versus deflection curve. Few very small visible cracks were found in 70 kips. However, these cracks were very minor cracks because it can be see that the stiffness of the specimen started to reduce only after around 80 kips after first visible crack.

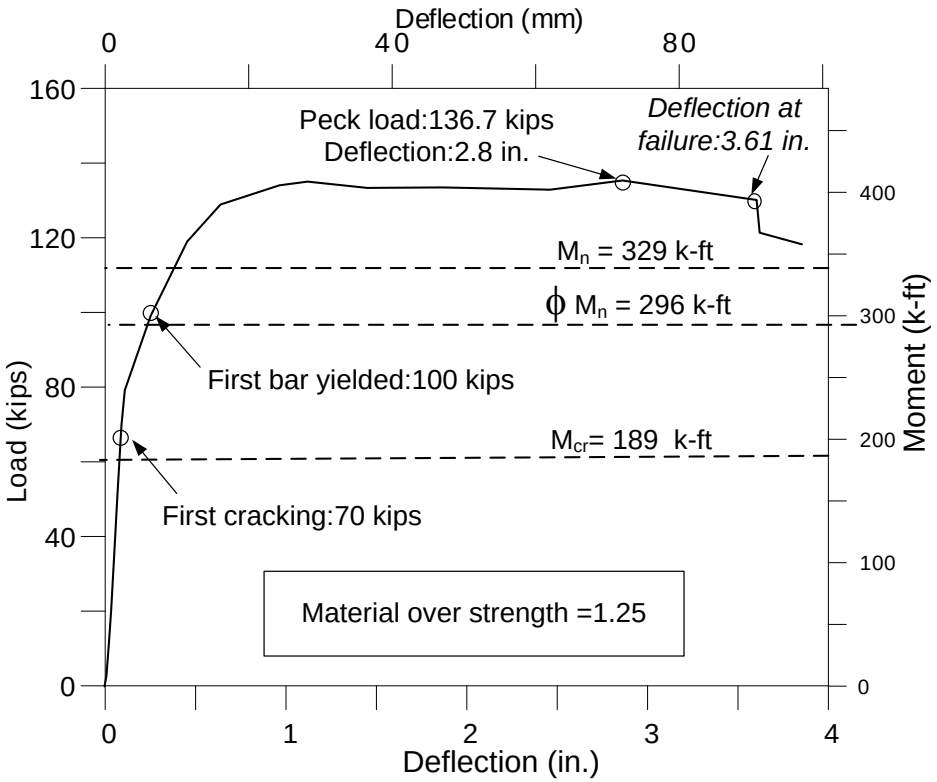

Figure 5.39 Load versus Deflection Curve for SFRPC Specimen (SFRPC#2-2) from Second Phase

Figure 5.40 shows various crack patterns in different stages of loading from 70 kips to failure. Up to 80 kips, there were few flexural cracks. More flexural cracks developed after that. After 100 kip existing cracks and new cracks developed were inclined and propagated towards the loading point. These cracks stopped to propagate near depth of (2-3 inches) and became wider and wider. The reduction in this depth may be due to use of 3-inch wide plate for loading which was able to reduce the biaxial compression. Around 135 kip of load, the compression concrete started to crush.

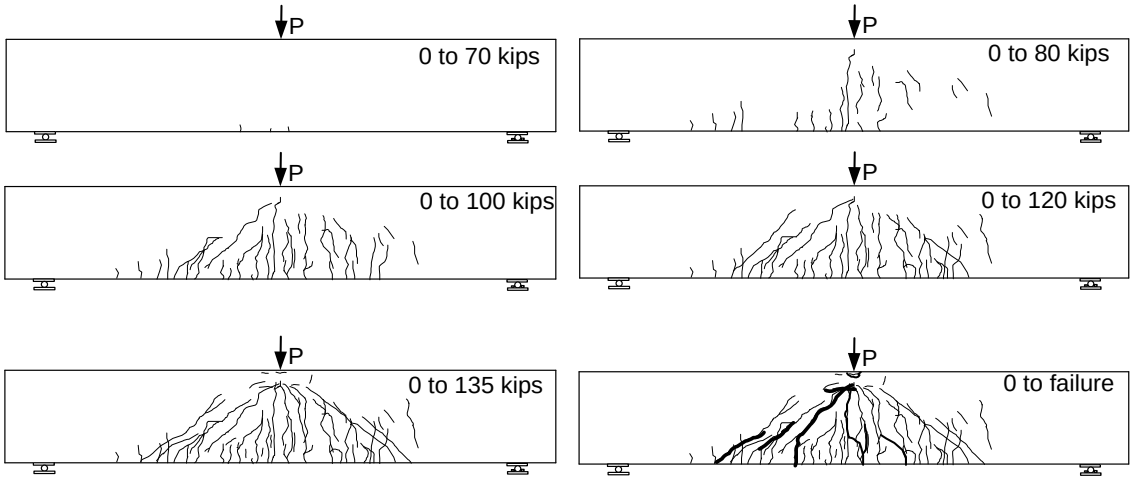

Figure 5.40 Crack Pattern of SFRPC#2-2 Specimen at Different Stages of Loading

(a)

(b)

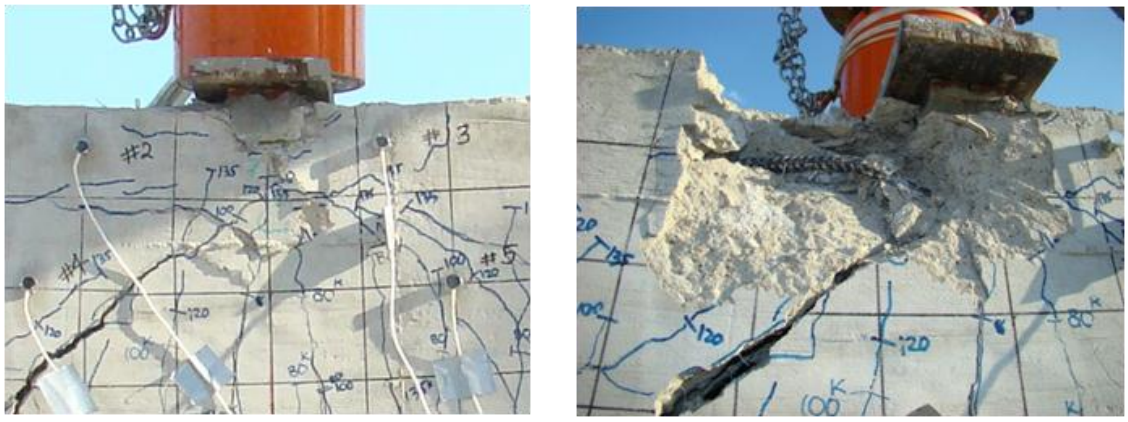

(c)

Figure 5.41 Typical Photos during Test of SFRPC#2-2 Specimen: (a) Prior to Failure, (b) at Failure, (c) Crushing in Compression Zone

Even though the beam was provided with no web shear reinforcement except one at center for fabrication purposes, this specimen failed in flexure with large crushing of the concrete at load of 137 kips as shown in Figure 5.41. The beam went to very large (3.6 inches) deformation before failure.

5.7.2 Strain in Steel and Concrete

Similar to previous specimens, total eight strain gauges were installed in compression and tensile reinforcement as discussed in Chapter Three. Results are shown in Figures 5.42 and 5.43. Load versus strain curves (Figure 5.42) shows that the values of strain in compression steel are order of 0.00123 and 0.00056, which are again lower than the yield strain (0.002) as previous specimens. This shows that the compression did not yield at ultimate load, which was also proved and satisfied as per design. However, all strain gauges installed in tension reinforcement exhibited the strain values more than 0.002 indicating that reinforcement yielded before failure. SG #5 exhibit maximum value of strain 0.014. Figure 5.43 shows that strain values increased very rapidly after the first crack occurred. Most of bars were yielded up to load of 100 kips. These indicate that failure was tension controlled as expected.

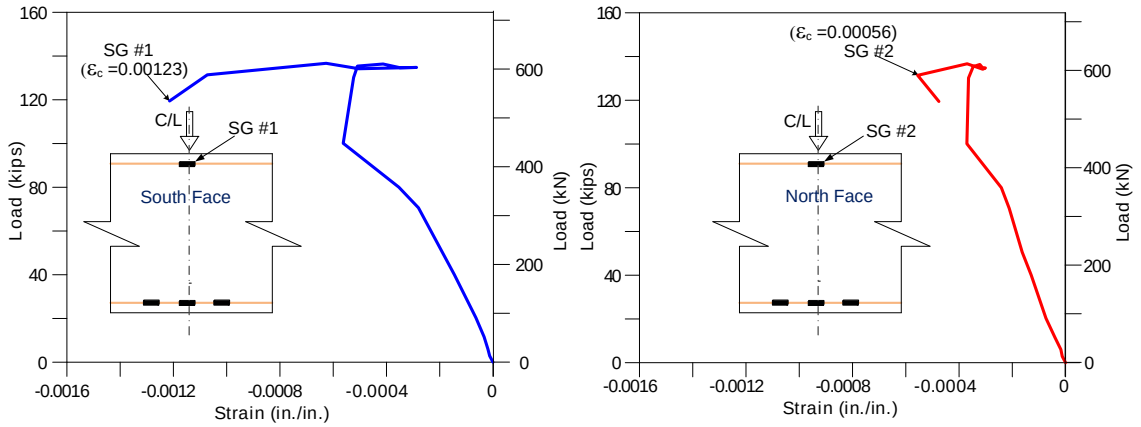

Figure 5.42 Load versus Strain in for SFRPC#2-2 Specimen

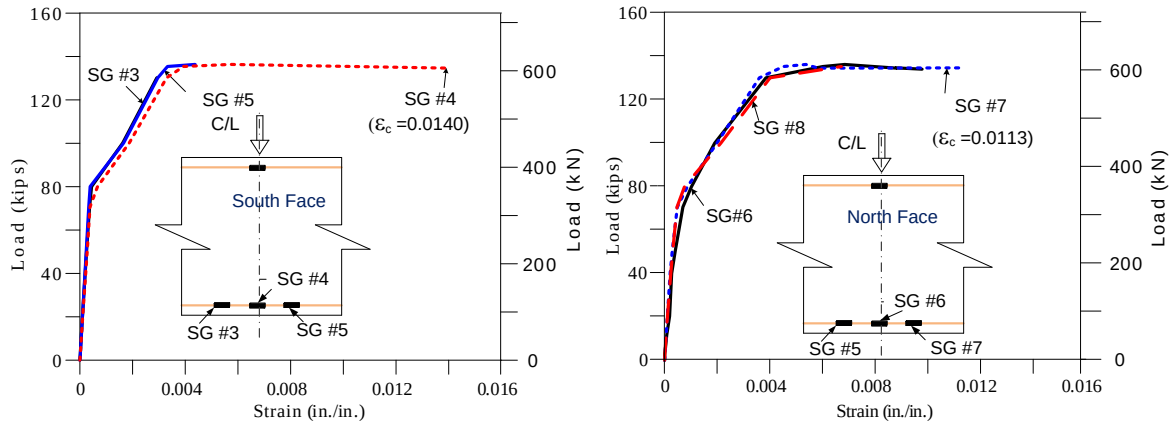

Figure 5.43 Load versus Strain in Tension Steel for SFRPC#2-2 Specimen

As in case of previous specimens, a total of seven concrete strain gauges were installed at depth of 1.25 inches from top of the beam as discussed in Chapter Three. Results were presented in form of load versus strain curves as shown in Figure 5.44. All strain gauges exhibited the strain values more than 0.003. From Figure 5.44, it can be seen that the maximum value strain at concrete was 0.0152. Similar to steel strain gauges all concrete strain gauge values increased rapidly after loading of 125 kips except strain gauge (CG # 7) value increased at load 90 kips.

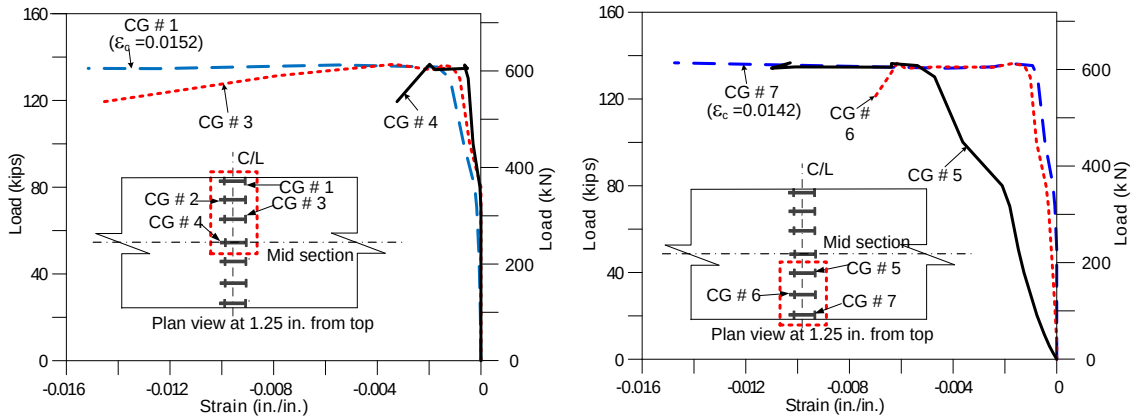

Figure 5.44 Load versus Strain in Concrete (with Embedded Strain Gauges) for SFRPC#2-2 Specimen

5.7.3 Ductility and Toughness

Figure 5.45 shows the load deflection curving with energy absorption at first yielding of the tensile bar and energy absorption at ultimate deformation for SFRPC#2-2 specimen. The deflection and toughness at first yielding of tensile reinforcement are 0.26 inches and 18.86 k-in respectively. Similarly values of toughness at ultimate deflection of 3.61 inches were 462.94 k-in respectively. The ductility index and energy ratio were computed as 14.16 and 24.5 respectively.

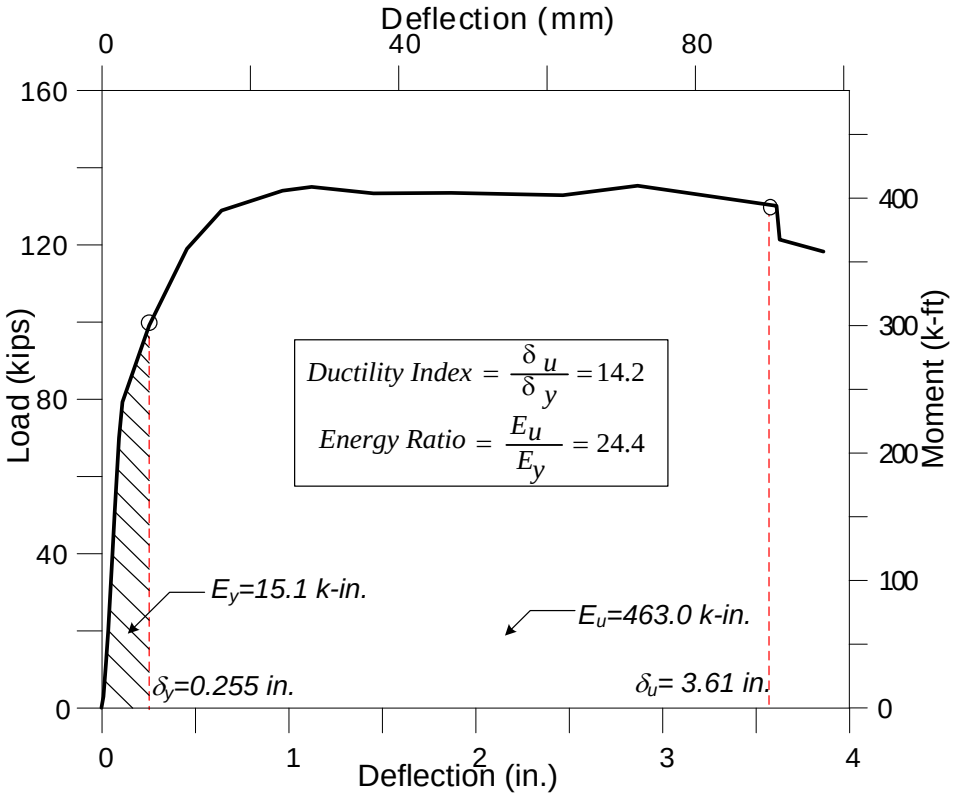

Figure 5.45 Load versus Deflection SFRPC#2-2 Specimen Showing Energy Dissipation and Ductility

5.8 Acoustic Emission Results

5.8.1 First Phase Study

Acoustic Emission results showed where strain energy was released relative to the location of the test specimens. Time-versus-hits were synchronized with loading increments to determine the specific time when energy was released within the specimen. The shear wave velocity was found about as 9.5 to 11× 10^4 inches/s for steel fiber reinforced concrete according change was made in material for the default value given for concrete in the AE software.

Figures 5.46 to 5.49 showed the AE results in terms of cumulative events occurred due to applications of load in different stages. Figures indicated that in each stage of the loading SFRPC#1-1 specimen had more hits than the PC#1-1 specimen. The PC specimen showed little activity near the loading point and bottom surface of beam near center as the first flexural crack occurred near mid span in bottom fiber.

AE revealed that more energy was dissipated on the area under the loading point in case of the SFRPC specimens. Compared to PC, the SFRC specimen showed more hits in this area (see Figure 5.46). Comparing the PC specimens as shown in Figure 5.49, the SFRPC showed energy dissipated in a more wide area. The inclusion of steel fibers in the concrete mix causes energy to be dispersed into smaller, discrete amounts, which AE captures as hits. The PC specimen had the same amount of energy dissipated, although in more concentrated amounts. Hence, the figure shows that fewer hits in the same region than the SFRPC specimen. This agrees with crack observations that the SFRPC specimen had smaller, thinner cracks that branch out in random directions up to peak load. Steel fibers serve as a "bridge," that enables forces to be redistributed from one area to the next. This overcomes concrete's weak tensile strength capacity and brittle nature. Also, the expanding cracking towards loading point could be delayed due to the higher tensile strength of SFRPC compared to plain concrete.

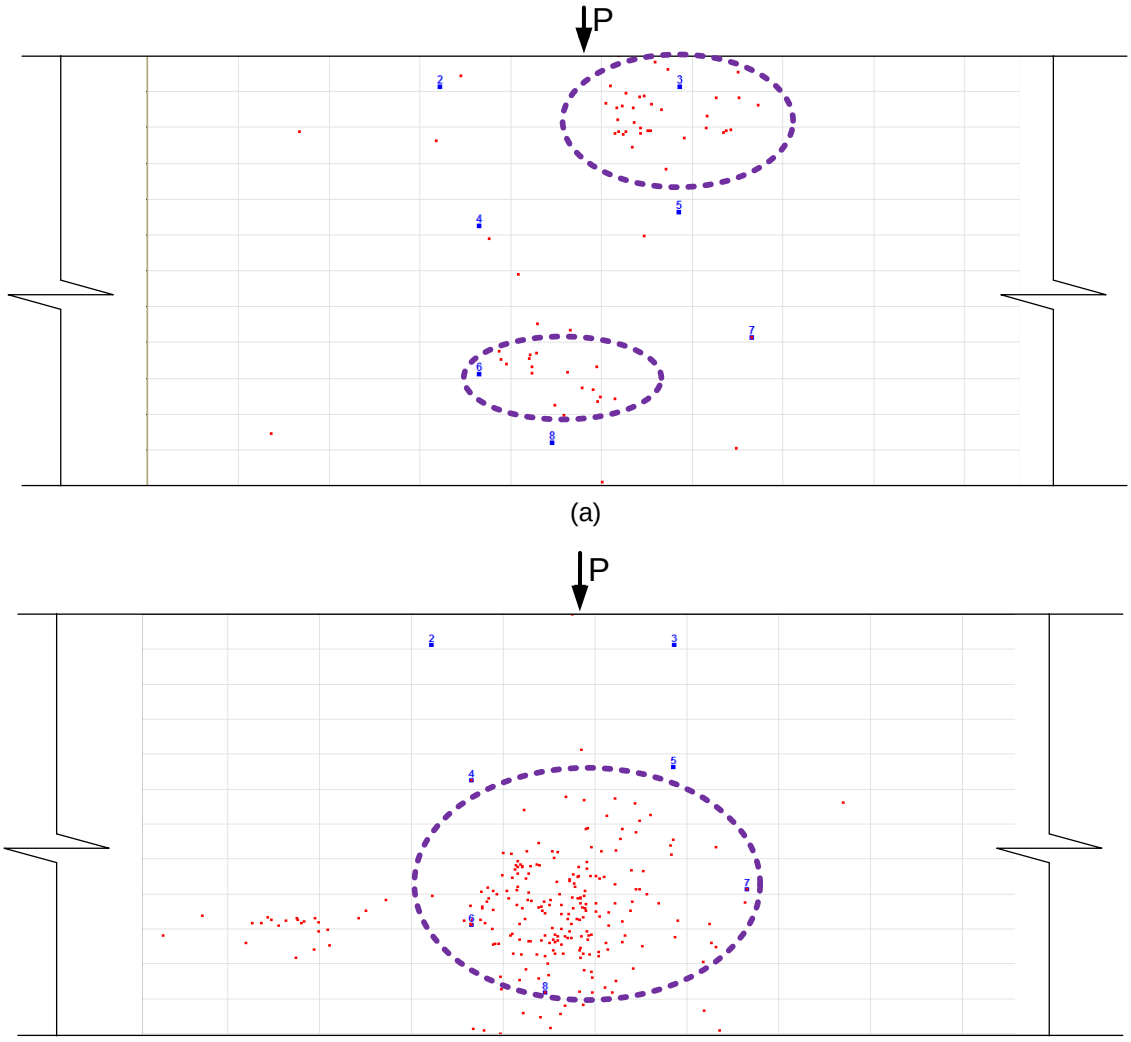

Figure 5.46 Acoustic Emissions Cumulative Events at First Crack Load of (a) PC#1-1 and (b) SFRPC#1-1 Specimen

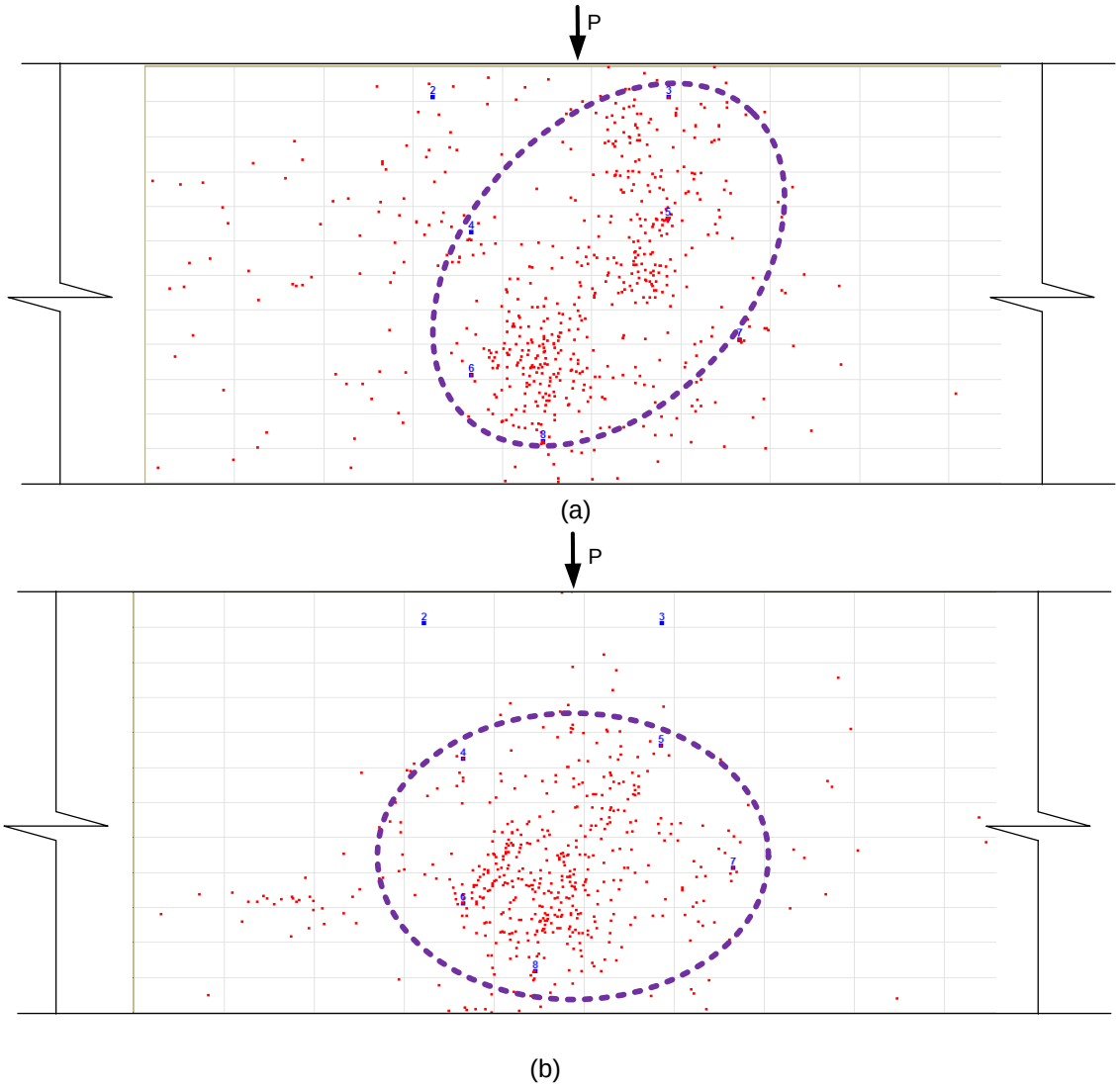

Figure 5.47 Acoustic Emission Cumulative Events at Load of 110 kips for (a) PC#1-1 and (b) SFRPC#1-1 Specimens

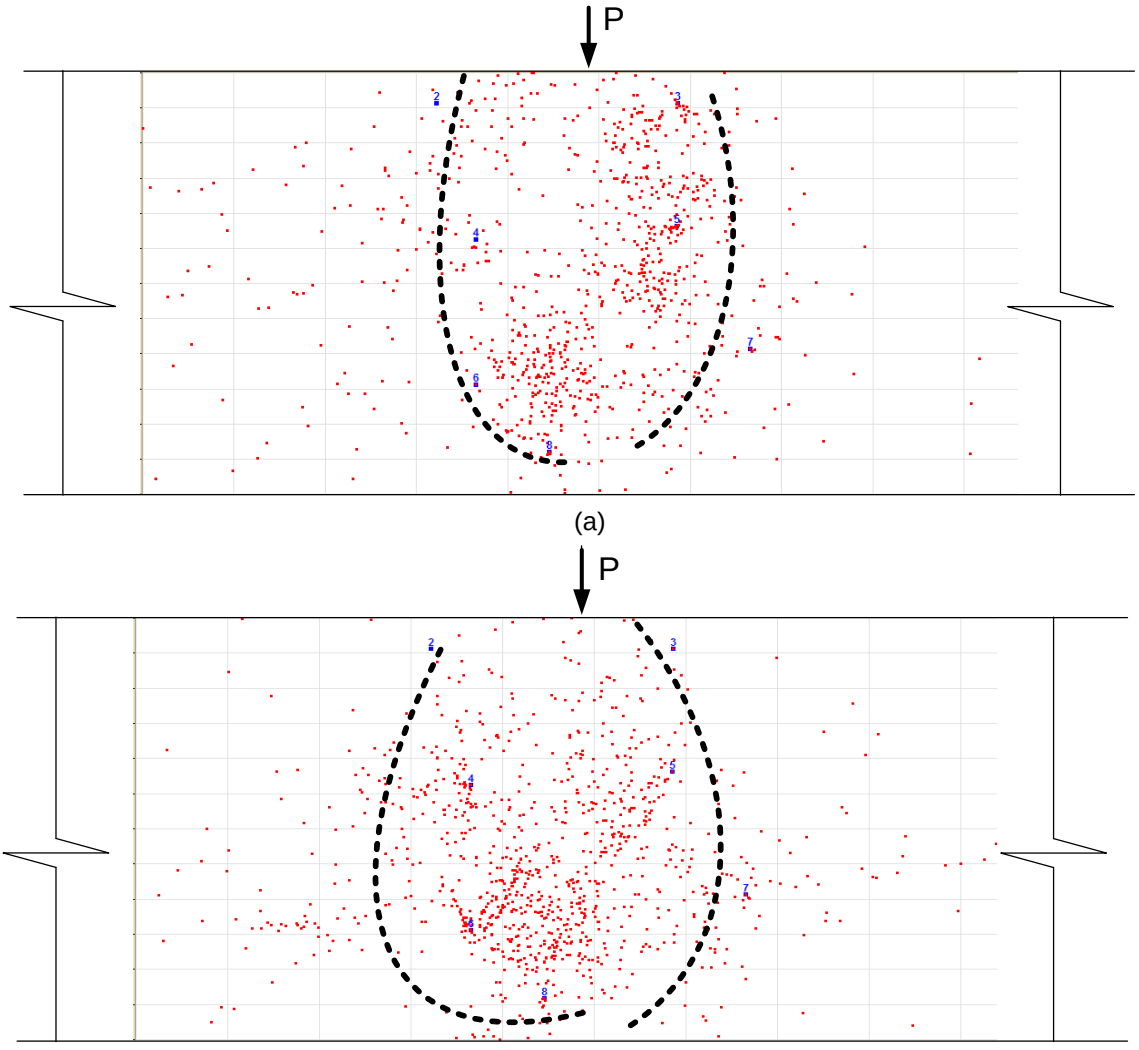

Figure 5.48 Acoustic Emission Cumulative Events at Load of 130 kips for (a) PC#1-1 and (b) SFRPC#1-1 Specimens

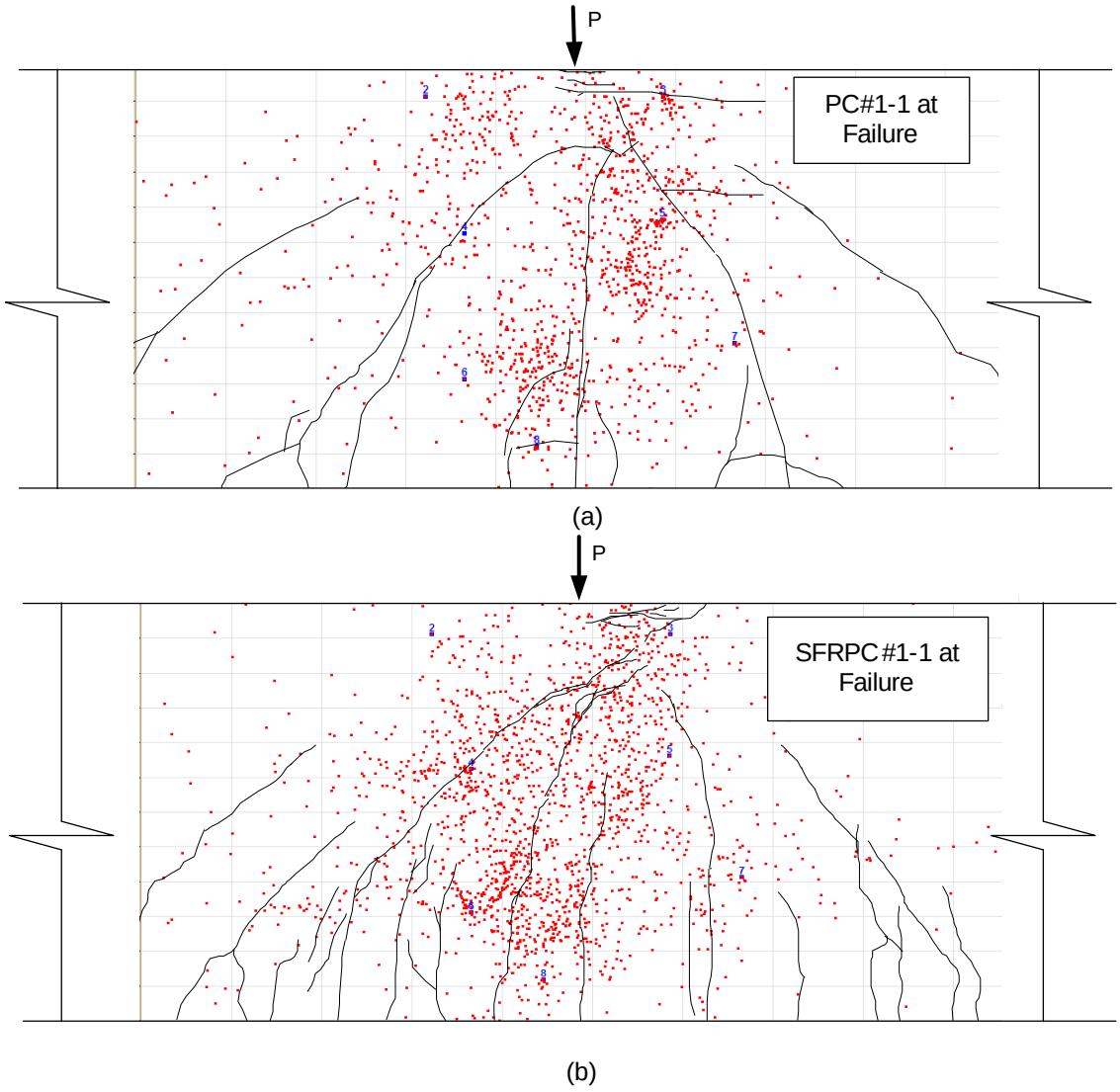

Figure 5.49 Acoustic Emission Cumulative Events at Failure of (a) PC#1-1 and (b) SFRPC#1-1 Specimens After Superimposed with Crack Patterns

5.8.2 Second Phase Study

Similar to first phase, results from Acoustic Emission results at various stage of loading starting first crack loading for both PC and SFRPC specimens are presented from Figure 5.50 to 5.54. Results showed where strain energy was released relative to the location of the test specimens. Time-versus-hits were synchronized with loading

increments to determine the specific time when energy was released within the specimen. Figure 5.50 shows that even though the first crack loads in case of SFRPC specimens are slightly less as compare to PC specimens, less numbers of events (red dots) was found in case of SFRPC. This indicates fewer internal cracks were developed in case of SFRPC specimen up to first cracking load.

Figure 5.52 shows crack patterns super imposed with AE results for both PC and SFRPC specimens at failure stages. It can be seen from the Figure 5.52 that large amount of cracks were formed before failure in case of SFRPC, which was proved with AE results as more events were found to have occurred in that case.

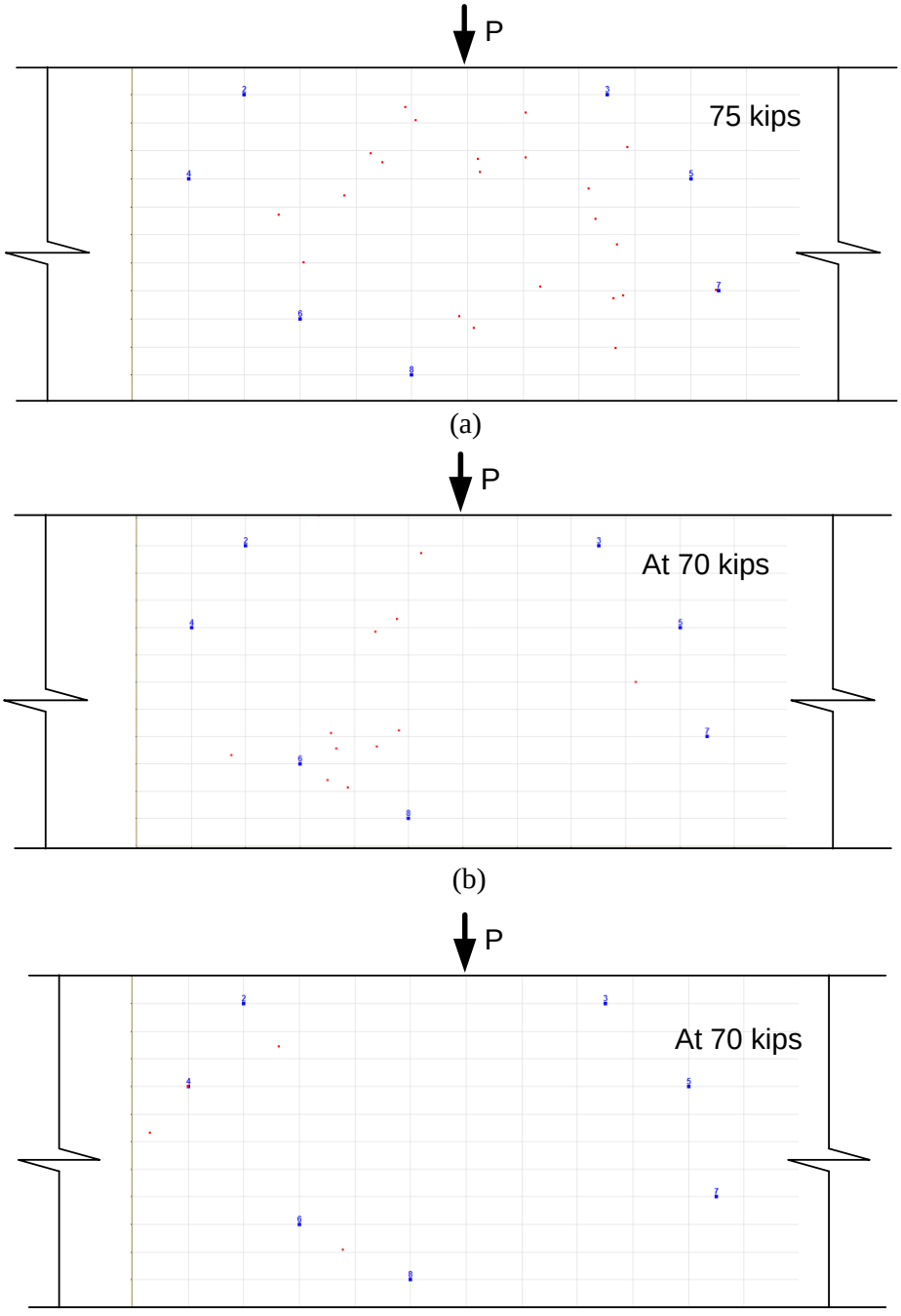

Figure 5.50 Acoustic Emissions Cumulative Events at First Crack Load of (a) PC#2-1, (b) SFRPC#2-1 and (c) SFRPC# 2-2 Specimens

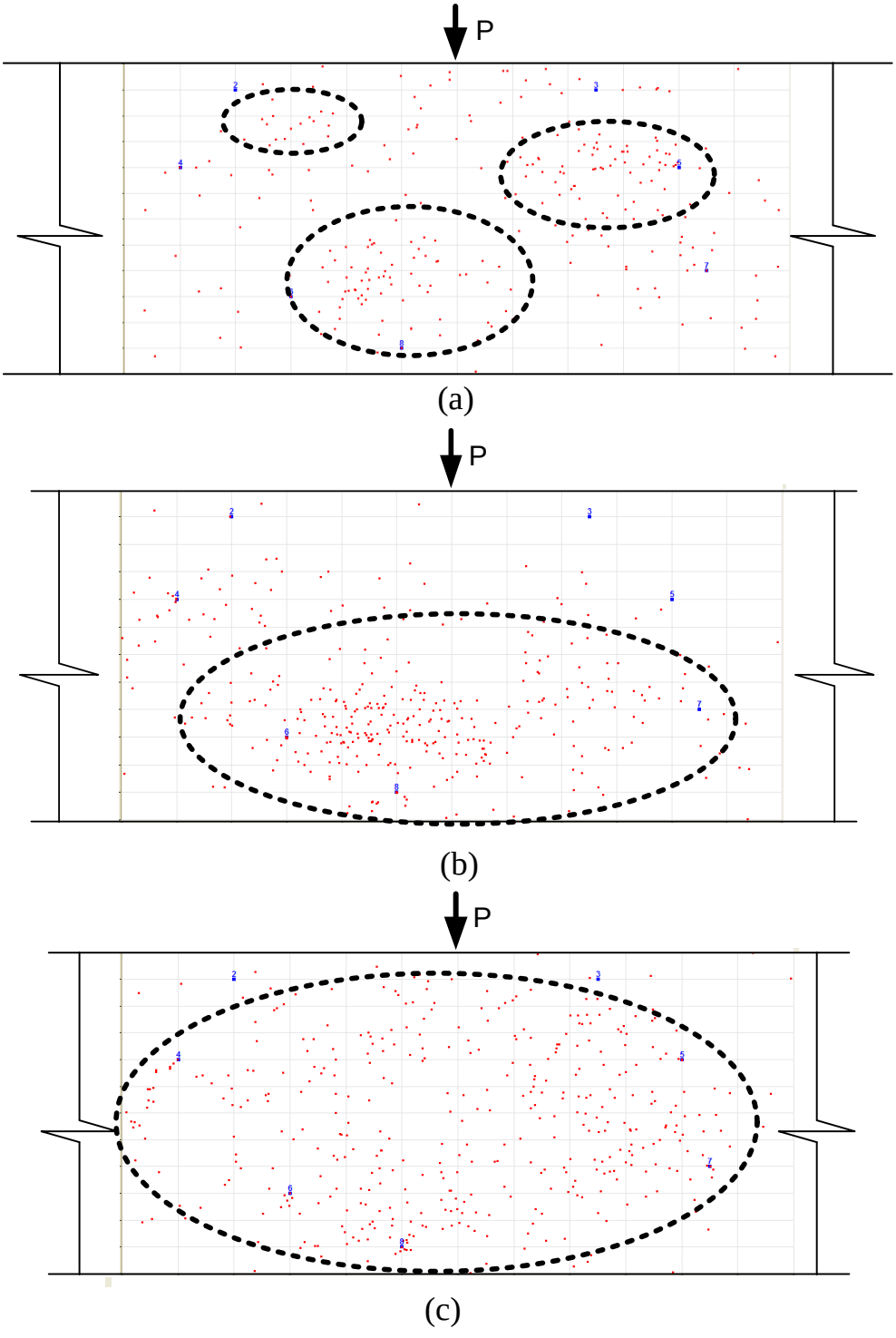

Figure 5.51 Acoustic Emissions Cumulative Events at 110 kips for (a) PC#2-1 and (b) SFRPC#2-2 specimens and at 290 kips for (c) SFRPC# 2-1 Specimen

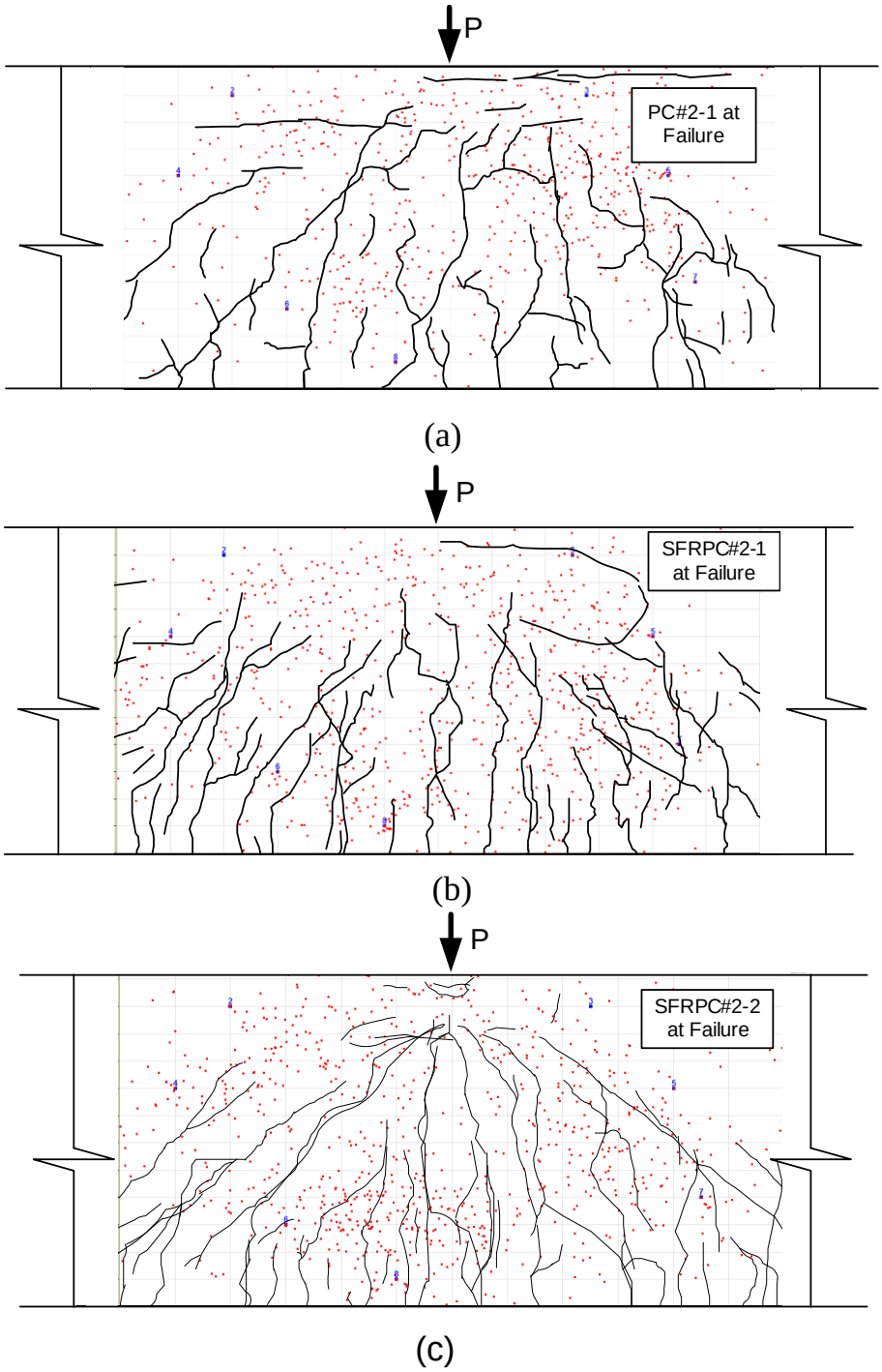

Figure 5.52 Acoustic Emissions Cumulative Events at Failure of (a) PC#2-1 and (b) SFRPC#2-1 and (d) SFRPC#2-2 Specimens after Superimposed with Crack Patterns

5.9 Discussion of Results from Large Scale Beam Test

5.9.1 Load versus Deflection Curves

Comparing the load deflection curves (Figure 5.53) for all six specimens, all beams went to large deformation before collapse showing large ductility. SFRPC#2-2 has shown large ductility compared to all specimens. In case of SFRPC#1-1, the test had to stop after broken down of one of the strand for security reason, hence showing slightly less deflection as compared to PC#1-1.

It can seen from Figure 5.53 (b) that the ultimate strength of PC specimens and SFRPC speciemns (except SFRPC#2-1) insecond phase were found quite close. This shows that the contribution of steel fibers (with 0.75% volume of frcation) is not found siginificant.. By examining the crack widths at the tension zone at failure and comparing with the stress versus elongation response from the direct tensile tests for the SFRC materials, it can be said that the tensile stresses at the tension zone can be contributed less effeted in contribution while calculating of the nominal flexural bending strength. The contribution from SFRC, however, could be used if fiber volume fraction is much greater.

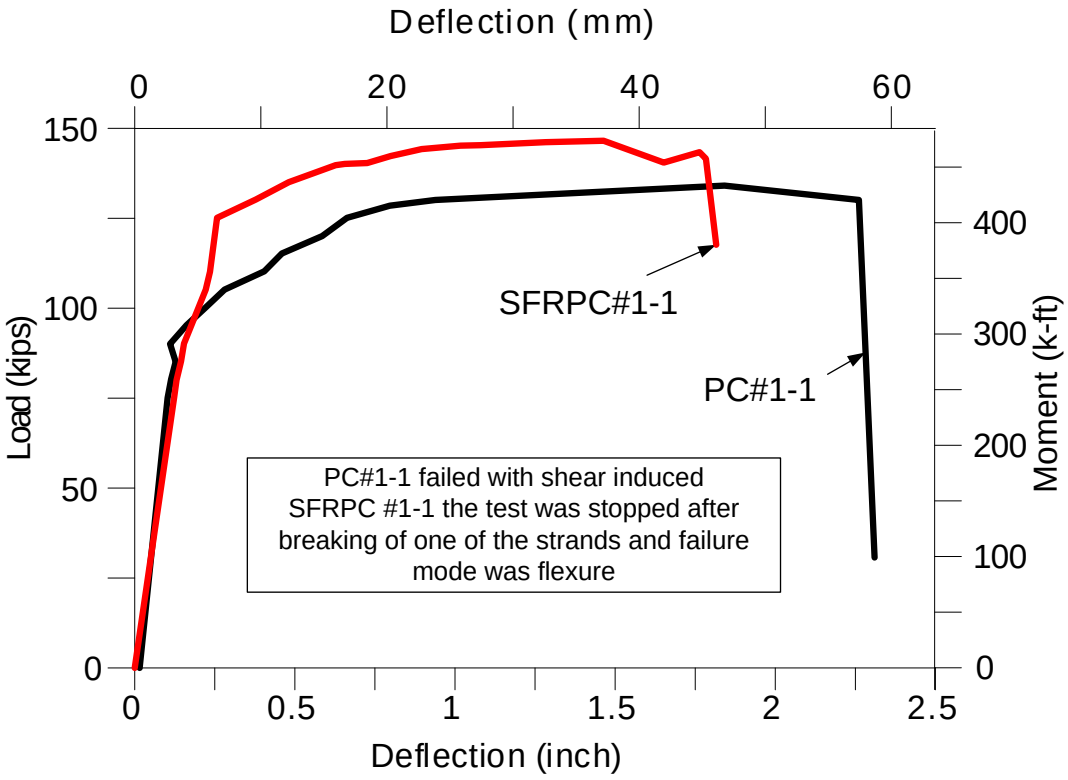

(a)

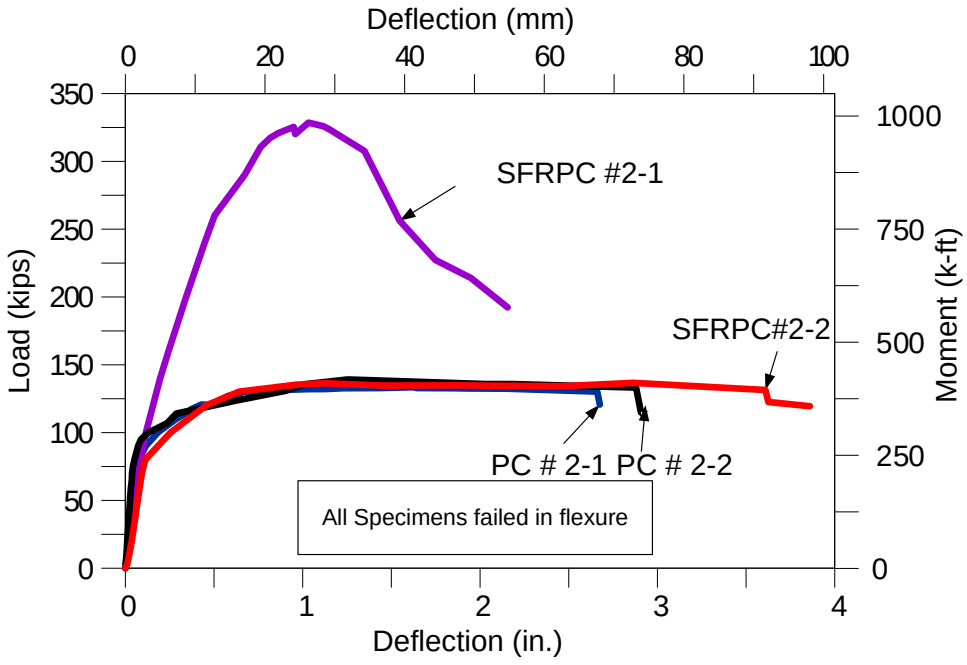

(b)

Figure 5.53 Comparisons of Load Deflection Curves (a) First Phase (b) Second Phase

From Table 5.1 it can be seen that except SFRPC #2-1 the difference in ultimate loads between PC and SFRPC specimens are not large. This indicates that there was only marginal contribution of steel fiber to increase ultimate strength of concrete in flexure. SFRPC#2-1 having the more tensile longitudinal steel area (than required for tension controlled failure) did not showed a brittle failure, but showed sufficient ductility with more than 1 inch of deformation at ultimate load.

Table 5.1 Summary of the Key Results

Specimen	First crack load (kips)	Ultimate load (kips)	Flexural strength (k-ft	Nominal flexural strength (k-ft)	Compressive strength (psi)	Normalized shear stress $\frac{V_u}{\sqrt{f_c'}bd}$	Deflection At failure(in.)
PC#1-1	80	134.8	392	330	5763	2.6	2.28
SFRPC#1-1	80	146.2	427	330! 402#	5470	2.9	1.8
PC#2-1	75	135.7	390	330	5405	2.7	2.67
PC#2-2	70	139.9	412	331	6963	2.5	2.87
SFRPC#2-1	70	328.6	935	821! 879#	5127	7.5	2.1
SFRPC#2-2	70	136.9	406	330! 383#	5130	2.8	3.61

!The contribution due to SFRC is ignored; #considered the contribution of SFRC, based on similar approach used by Swamy and Al-Ta'an. [1989]; shear stress due to self-weight is neglected

Normalized shear stress at peak load of SFRPC beams are larger than those of PC. Table 5.2 shows the comparison of flexural strength (moment) based on tested load and predicated or nominal flexural strength (calculated moments) based on ACI 318-11 and modified method as discussed in Chapter Two. It can be seen that ratios of ultimate moments (tested to predicted values) are slightly more in case of PC as compared to SFRPC. However there ratios of moments (tested to predicted) at first yield strain of steel for SFRPC and PC specimens are almost similar

5.9.2 Strain at Steel and Concrete

Table 5.2 shows that compression bars showing strains lower than yield strain (0.00207) for all specimens except SFRPC#2-1. However these values are higher in case of SFRPC specimens compared to PC specimens. It looks that there is also some contribution of fiber in increasing of compressive strain in steel. However the results show that compression bar did not yield in most of the specimens except in SFRPC#2-1 specimen.

Table 5.2 Strains in Compression Steel (Top Bars)

Specimen	Location		Average	Maximum
	left - mid	right - mid		
	SG #1	SG #2		
PC#1-1	0.00053	0.00052	0.0005	0.0005
SFRPC#1-1	0.00124	0.00193	0.0016	0.0019
PC#2-1	0.00011	0.00041	0.00026	0.00041
PC#2-2	0.00032	0.00043	0.0004	0.0004
SFRPC#2-1	0.00245	NW	0.00245	0.00245
SFRPC#2-2	0.00125	0.00056	0.0010	0.00125

*Note: NW means strain gauge was not working.

Table 5.3 shows the values of ultimate strains exhibited by different strain gauges installed in tensile reinforcement for all tested specimens. Both average and ultimate strain values and maximum ultimate strain values are more than yield strain (0.002) for all specimens. Average values of ultimate strain for tensile steel for SFRPC

specimens (except for SFRPC#1-1) are larger than PC specimens. In case SFRPC#1-1 specimen, most of the installed (four out of six) was not found working, hence strain values obtained from only two strain gauges may not be reflect true values. This is also verified by strain value obtained the concrete strain gauges installed at tension side of the section near the c.g. of tensile reinforcement as discussed in section 5.3.2. The value was 0.086, which more than 0.005, required for tension controlled members as per ACI code.

Table 5.3 Strains in Tension Steel (Bottom Bars)

Specimen	Location						Average	Maximum
	5 in left	left mid	5 in rt.	5 in left	right mid	5 in rt.		
	SG #3	SG #4	SG #5	SG #6	SG #7	SG #8		
PC#1-1	0.00350	0.00426	0.00547	0.00184	0.00191	0.00325	0.0034	0.0055
SFRPC#1-1	0.00245	0.00337	NW*	NW*	NW*	NW*	0.0029	0.0034
PC#2-1	0.00893	0.00427	0.00552	0.00395	0.00437	0.00274	0.0050	0.0089
PC#2-2	0.00411	0.00326	0.00671	0.00964	0.00264	NW*	0.0053	0.0096
SFRPC#2-1	0.00631	0.00838	0.00412	0.00857	0.00545	NW*	0.0066	0.0086
SFRPC#2-2	0.00292	0.00438	0.01389	0.00975	0.01137	0.00670	0.0082	0.0139

*Note: NW means strain gauges were not working.

For SFRPC#2-1 specimen the strain in tensile steel was found more than 0.005, which was the required ultimate strain for tension failure. That means SFRPC beams with larger tension steel area could fail in tension with use of steel fiber. This allows better utilization of concrete sections, with reduction in self-weight of large girders used for prestressed bridges.

Table 5.4 shows that the strain in concrete at compression fiber for SFRPC #1-1 in first phase is about 0.0048 which is more than that of ultimate strain 0.003 used by ACI code. Similarly such strain in concrete of compression fiber for SFRPC specimens

of second phase is higher as compared to PC specimens as given in Table 5.6. The average compression strain in concrete for SFRPC#2-1 is 0.0052 which is larger than ultimate crushing strain in concrete.

Table 5.4 Strains in Concrete from First Phase

Specimen	At 0.75 in from top	At 1.5 in from top	At 0.75 in from top	At 1.5 in from top	Average	Maximum
	Center		Near side face			
PC#1-1	0.0031	0.0020	0.0020	0.0015	0.0025	0.0031
SFRPC#1-1	0.0045	0.0048	0.0030	0.0020	0.0047.5	0.0048

Table 5.5 Strain in Concrete at Compression Zone from Second Phase

Specimen	Location: at 1.25 from top of beam section							Average
	7.5 in. left	5 in. left	2.5 in. left	center	2.5 in. right	5 in. right	7.5 in. right	
	CG # 1	CG # 2	CG # 3	CG # 4	CG # 5	CG # 6	CG # 7	
PC#2-1	0.0052	0.0033	0.0028	0.0035	0.0047	0.0058	0.0081	0.0046
PC#2-2	0.0065	0.0057	0.0049	0.0042	0.0037	0.0038	0.0071	0.0051
SFRPC #2-1	0.0027	0.0082	0.0059	NW*	0.0058	0.0047	0.0036	0.0052
SFRPC #2-2	0.0152	0.0145	0.0045	0.0148	0.0071	0.0114	NW*	0.0112

*Note: NW means strain gauge was not working.

5.9.3 Crack Width

Table 5.7 shows the comparison of crack widths measured at different stages of loading among six tested specimens. Up to the first crack load, the widths of cracks are similar for all specimens. At 100 kips of applied load width of cracks in case of PC is

larger than the crack width of SFRPC in same load. This may be due to presence of steel fibers which arrest the cracks and controls widening. Near peak load, (around 130 kips) the crack widths in SFRPC specimens are lower. For SFRPC#2-1 the crack width at 260 kips is only 0.25 inch.

Table 5.6 Comparison of Crack Width at Different Stage of Loading

Specimen	Crack width at different loads (mm)			
	Crack load (70-80 kips)	100 kips	130 kips	260 kips
PC#1-1	0.1	0.5	2.25	
SFRPC#1-1	0.1	0.2	0.9	
PC#2-1	0.1	0.4	1.6	
PC#2-2	0.1	0.5	2.5	
SFRPC#2-1	0.05	0.1	0.12	0.25
SFRPC#2-2	0.1	0.3	0.95	

5.9.7 Ductility and Toughness

Table 5.7 shows the comparison of docility index and energy ratio. These ratios were calculated as discussed in Chapter Two. It can be seen from the table that in first phase SFRPC#1-1 showed larger value of both ratios as compared to PC#1-1. Similarly in second phase both PC specimens showed lower value of ductility index and energy ratios as compared to SFRPC#2-2. Even for SFRPC#2-1 (specimen with high longitudinal steel ratio) show ductility ratio of 5.02 and energy ratio of 7.8 which larger than the ductility ratio (3.8) calculated based Naaman's text book (Namaan, 2004). This shows that even with small volume of fraction the fibers can contribute to increase the toughness and ductility.

Table 5.7 Comparison of Ductility Index and Energy Ratio

Specimen	Deflection at first yield of tension bar	Deflection at failure	Ductility Index: δ_u / δ_y	Ductility Ratio [Namaan,, 2004]	Energy at first yield of tension bar	Energy up to failure deflection	Energy Index: E_u/E_y
	δ_y	δ_u			E_y	E_u	
	First Phase						
PC#1-1	0.268	2.260	8.43	13.57	21.6	271.5	12.6
SFRPC#1-1	0.200	1.800	9.00	12.15	10.5	229.6	21.9
	Second Phase						
PC#2-1	0.287	2.670	9.30	13.57	25.2	333.9	13.3
PC#2-2	0.240	2.870	11.96	18.83	21.1	373.0	17.7
SFRPC#2-1	0.430	2.160	5.02	3.96	68.6	532.3	7.8
SFRPC#2-2	0.255	3.610	14.16	13.91	18.9	462.9	24.5

Note: Detailed calculation are given in Appendix A

Table 5.8 Comparison of Rotation with Experimental and Analytical

Specimen	Rotation (rad.)			
	Experimental			Analytical
	At yield	At Peak Load	At Load of Ultimate Deflection	[Namaan, 2004]
First Phase				
PC#1-1	0.0020	0.0241	0.0300	0.019
SFRPC#1-1	0.0017	0.0230	0.0233	0.017
Second Phase				
PC#2-1	0.0014	0.0214	0.0355	0.019
PC#2-2	0.0022	0.0160	0.0387	0.025
SFRPC#2- 1	0.0025	0.0105	0.0246	0.005
SFRPC#2-2	0.0024	0.0383	0.0485	0.019

Note: Detailed calculation are given in Appendix A

The values of rotation values obtained from experimental results for both peak load and at load at ultimate deflection were found larger than the theoretical values. Even for SFRPC#2-1 which has larger longitudinal steel ratio has shown larger values of rotation. This indicated that for SFRPC beam, there can be possibility of moment redistribution even the section has larger longitudinal steel ratio than the values specified by the code for moment redistribution. This is really important because the distribution of moment in mid span of simply supported beam can represent the distribution of moment at inverted internal support of continuous beams (plastic hinging section) as discussed in Chapter two.

Table 5.9 Depth of Compression Bock

Specimen	Thickness of Compression Block (in.)	
	Measured	As per Design
PC#1-1	4.3	3.24
SFRCP#1-1	3.5	3.34
PC#2-1	4.5	3.24
PC#2-2	2.7	2.64
SFRPC#2-1	6.5	7.16
SFRPC#2-2	2.9	3.21

The depth of compression block was measured for all specimens as shown in Table 5.9. The measured compression block depth for the specimens in which the load was applied through a 6-inch wide steel plate was found larger than the design values of compression depth (see appendix A), whereas the that measured depths for specimens in which the load was applied through a 3-inch wide plate was close to the design values.

The application of load through 3-inch wide steel plate in place of 6-inch plate should help to reduce load confinement area, which ultimately should reduce the biaxial stress near loading point. The depth of compression block was reduced by from 3.5 inches to 2.9 inches for SFRPC specimens (SFRPC #1-1 and SFRPC#2-2). For PC specimens (PC#2-1 and PC#2-1) this depth was reduced from 4.5 inches to 2.7 inches. The corresponding peak load was found reduced from 146 kips to 137 kips for SFRPC beams. However the flexural strength was increased from 134 kips to 139 kips in case of PC specimens. One of the possible reasons for this increase is may be due to increase in compressive strength (5.4 ksi to 6.9 ksi).

5.10 Constructability

One of the major concerns of using steel fibers in concrete members is the higher initial material cost as compared to conventionally reinforced concrete. However, labor and cost savings realized by using SFRC has been rarely studied and discussed. This subject was investigated in some extent during this research work. As discussed in Chapter Three all preparation work including steel cage fabrication was carried out by professional workers at a local precast plant.

Table 5.10 Comparisons of Time and Labor Required for Placing and Tightening of Stirrups (From the Second Phase)

PC#2-1			SFRPC#2-2		
Labor	Time	Man-min	Labor	Time	Man-min
Nos.	min		Nos.	min	
5	10	50	5	2	10
	Total	50		Total	10

Table 5.11 shows the required time required for the workers to tie all the stirrups for specimens PC#2-1 and SFRPC#2-2. Both specimens had the same amount of longitudinal reinforcement. It was found that while five workers spent approximately 10 minutes finishing the stirrups for specimen PC#2-1 (Figure 5.54 a), where as it only took the same five people about 2 minutes to tie all the stirrups for specimen SFRPC#2-2. In other word, preparation of the stirrups for conventional PC beams would take about five times the time required by SFRPC beams. It should be noted that the additional time and labor cost needed for cutting and bending stirrups for a PC beam were not included in the above analysis. Moreover, during casting, stirrups could interfere with the vibration and concrete placement process. In SFRPC beam, however, the steel fiber reinforcement will not affect the vibration in the least. The concrete placement can be easily performed as shown in Figure 5.54(b).

(a) (b)

Figure 5.54 Construction of Specimens (a) Preparation of the Steel Cage for PC#2-1(b) Concrete Pouring for SFRPC#2-2

As a consequence, it can be justified that the increased initial materials cost due to steel fibers is able to be more than offset by lesser labor hours and costs as well as

enhanced constructability. This advantage can be even more significant when congested stirrups need to be used as per design.

5.11 Material Tests with Large Scale Prestressed Concrete Beam Test

5.11.1 General

As discussed in Chapter Three several material tests were carried out with large scale beam test in order to determine compressive strength, bending strength and equivalent tensile strength. They were cylinder tests, third point bending test (ASTM C1609) and double punch test. The results from these tests are presented and discussed in following paragraphs.

5.11.2 Compressive Strength

Table 5.11 shows the results from compressive strength test carried out with 4 × 8 inches cylinders from first phase of experimental investigation for PC and SFRC specimens.

Table 5.11 Results for Compressive strength from Cylinder Test (First Phase)

Specimen	SFRC#1-1		PC#1-1	
	Ultimate Load	Compressive strength	Ultimate Load	Compressive strength
	(lbf)	(psi)	(lbf)	(psi)
Cylinder #1	66590	5299	72160	5742
Cylinder #2	66560	5297	69700	5547
Cylinder #3	68900	5483	69680	5545
Cylinder #4	65710	5229	71860	5718
Cylinder #5	70130	5581	73670	5862
Cylinder #6	74520	5930	77480	6166
Mean	68735	5470	72425	5763
STDEV	3284	261	2914	232
COV	4.78%	4.78%	4.02%	4.02%

Table 5.12 shows that the average compressive strength from first phase for PC and SFRC specimens were found as 5763 psi and 5470 psi respectively. Table 5.12 shows the compressive strength from cylinder test of second phase of experimental investigation. The compressive strength for SFRC specimens were found as 5127 psi and 5130 psi, whereas of these values for PC specimens were 5405 psi and 6963 psi respectively. Except for PC#2-2 all compressive strength were found less than the design compressive strength of 6000 psi. For PC#2-2 the mix design was different from rest hence the compressive strength was also found as 6963 psi.

Table 5.12 Results for Compressive Strength from Cylinder Test (Second Phase)

Specimen	SFRPC#2-1		SFRPC#2-2	
	Ultimate Load	Compressive strength	Ultimate Load	Compressive strength
	(lbf)	(psi)	(lbf)	(psi)
Cylinder #1	58730	4674	62730	4992
Cylinder #2	52070	4144	49770	3961
Cylinder #3	53940	4292	73400	5841
Cylinder #4	77200	6143	69230	5509
Cylinder #5	70050	5574	55720	4434
Cylinder #6	74540	5932	75930	6042
Mean	64422	5127	64463	5130
STDEV	10883	866	10290	819
COV	16.89%	16.89%	15.96%	15.96%

Table 5.12 continued

Specimen	PC#2-1		PC#2-2	
	Ultimate Load	Compressive strength	Ultimate Load	Compressive strength
	(lbf)	(psi)	(lbf)	(psi)
Cylinder #1	76171	6061	96030	7642
Cylinder #2	78524	6249	94470	7518
Cylinder #3	68223	5429	80930	6440
Cylinder #4	74245	5908	79130	6297
Cylinder #5	54569	4342	92110	7330
Cylinder #6	55760.6	4437	82350	6553
Mean	67915	5405	87503	6963
STDEV	10457	832	7514	598
COV	15.40%	15.40%	8.59%	8.59%

Figure 5.55 shows the load versus deflection curves from large (6 × 12 inches) cylinder tests for SFRC specimens from first and second phases of experimental program. From Figure 5.54 it can be seen that there is only small strain softening seen with small residual strength. The average compressive stress was about 5785 kip. Though the compressive strength of the concrete was not increased with steel fiber, it shows some small residual strength. These may be because of use of low volume of fraction of steel fiber (only 0.75%).

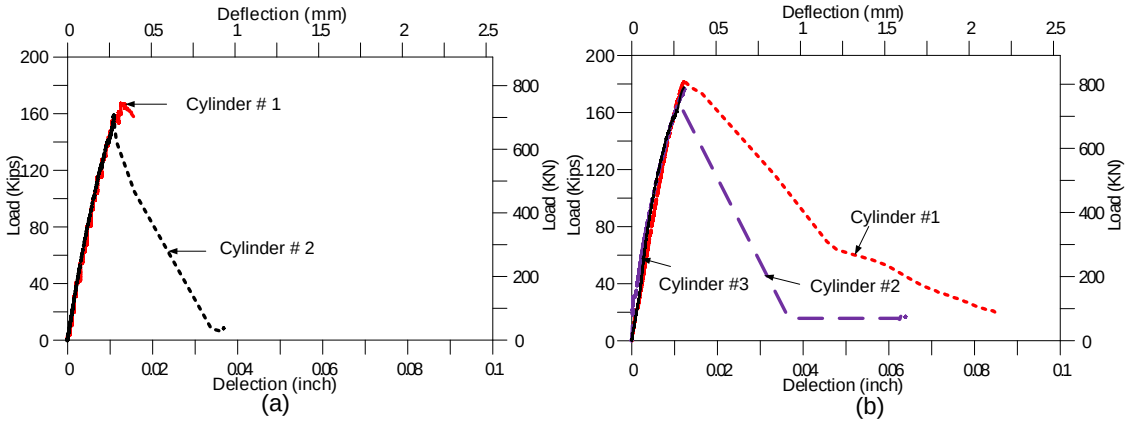

Figure 5.55 Load versus Deflection from Compression Test (Large Cylinder Test) for SFRC Specimens (a) First Phase and (b) Second Phase

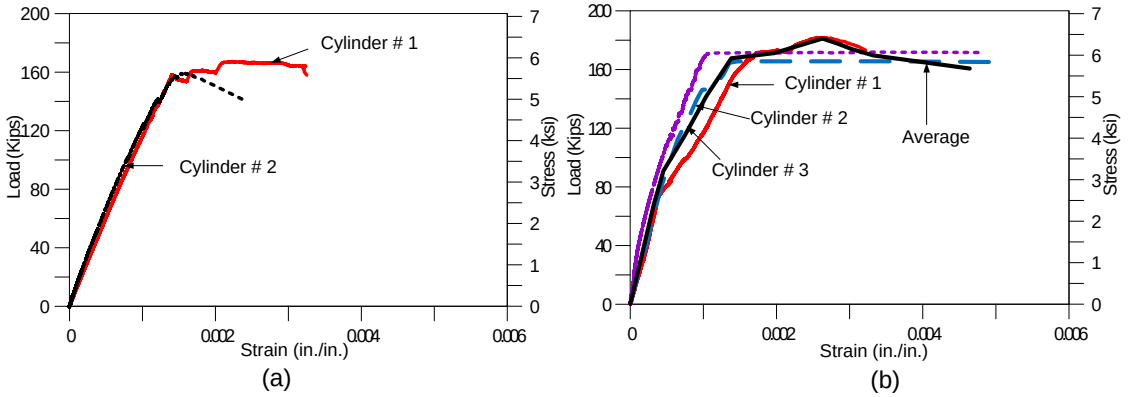

Figure 5.56 Load versus Concrete Strain from Compression Test for SFRC Specimens (a) First Phase and (b) Second Phase

Figure 5.56 shows load versus strain in concrete curves for SFRC specimens. It can be seen that the value of ultimate compressive strain concrete were found to be more than 0.003 which is maximum strain in concrete assumed by ACI Code. The maximum value of compressive strain in concrete with steel fiber was order of 0.005. It can also be seen from the large scale beam test results (Table 5.6) the ultimate strain in concrete fiber was more than 0.005 in case of SFRPC beams.

5.11.3 Flexural Strength

Tables 5.13 to 5.14 show the results from third point bending test (ASTM C1609), which is the only recommended material test method for FRC by ACI. Tables 5.14 and 5.15 show the peak and residual strength values along with their corresponding coefficients of variation (COV) from first and second phases of experimental programs. The COVs for peak strength are around 10% whereas COVs for residual strength are quite high (order of 25%).

Table 5.13 Results from Third Point Bending (ASTM C1609) Test (First Phase)

Specimen	First-Peak Load, P_1	Peak Load, P_p	Load at 0.03 in. (L/600) Deflection	Load at 0.06 in. (L/300) Deflection	Load at 0.12 in. (L/150) Deflection	First Peak Strength	Peak Strength
	(lbf)	(lbf)	(lbf)	(lbf)	(lbf)	psi	psi
ASTM #1	7441	8198	8110	7734	6538	620	683
ASTM #2	8216	8216	5616	4883	3705	685	685
ASTM #3	6983	6983	5518	4902	3852	582	582
ASTM #4	7862	7862	7191	6812	5567	655	655
ASTM #5	7777	9474	9297	8741	6696	648	790
ASTM #6	7765	7765	7557	6312	4157	647	647
Mean	7674	8083	7215	6564	5086	640	674
Standard Deviation	419	816	1462	1538	1358	35	68
COV		10.09%	20.27%	23.42%	26.71%		

Table 5.14 Results from Third Point Bending (ASTM C 1609) Test (Second Phase)

Specimen	First-Peak Load, P_1	Peak Load, P_p	Load at 0.03 in. (L/600)[10] Deflection	Load at 0.06 in. (L/300) Deflection	Load at 0.12 in. (L/150) Deflection	First Peak Strength	Peak Strength
	(lbf)	(lbf)	(lbf)	(lbf)	(lbf)	psi	psi
ASTM #1	5414	5414	3064	3094	2371	451	451
ASTM #2	6660	6660	4169	3650	2900	555	555
ASTM #3	5378	5378	3574	3550	2872	448	448
ASTM #4	5797	5797	5640	5561	4401	483	483
Mean	5812	5812	4112	3964	3136	484	484
Standard Deviation	596	596	1114	1092	878	50	50
Coefficient of Variation	10.25%	10.25%	27.10%	27.55%	27.99%	10.25%	10.25%

Table 5.15 Summary of ASTM C1609 Test: ACI Requirement Comparison (First Phase)

Specimen	90% of the first peak load (lbf)	Load at 0.06 in. (L/300) Deflection (lbf)	Difference	Note
ASTM #1	6696.9	7734	1037.1	Pass
ASTM #2	7394.4	4883	-2511.4	Not Pass
ASTM #3	6284.7	4902	-1382.7	Not Pass
ASTM #4	7075.8	6812	-263.8	Not Pass
ASTM #5	6999.3	8741	1741.7	Pass
ASTM #6	6988.5	6312	-676.5	Not Pass
Specimen	75% of the first peak load (lbf)	Load at 0.12 in. (L/150) Deflection (lbf)	Difference	Note
ASTM #1	5580.75	6538	957.25	Pass
ASTM #2	6162	3705	-2457	Not Pass
ASTM #3	5237.25	3852	-1385.25	Not Pass
ASTM #4	5896.5	5567	-329.5	Not Pass
ASTM #5	5832.75	6696	863.25	Pass
ASTM #6	5823.75	4157	-1666.75	Not Pass

Table 5.16 Summary of ASTM C1609 Test: ACI Requirement Comparison (Second Phase)

Specimen	90% of the first peak load (lbf)	Load at 0.06 in. (L/300) Deflection (lbf)	Difference	Note
ASTM #1	4873	3094	-1778	Not Pass
ASTM #2	5994	3650	-2343	Not Pass
ASTM #3	4840	3550	-1290	Not Pass
ASTM #4	5217	5561	344	Pass
Specimen	75% of the first peak load (lbf)	Load at 0.12 in. (L/150) Deflection	Difference	Note
ASTM #1	4061	2371	-1690	Not Pass
ASTM #2	4995	2900	-2095	Not Pass
ASTM #3	4033	2872	-1161	Not Pass
ASTM #4	4348	4401	53	Pass

The Tables 5.15 and 5.16 give the comparisons of residual loads (at 0.06 inches and 0.12 inches of deflection) with percentage (90% and 75% of first peak loads) as per ACI provisions. (ACI 318-11 section 5.6.6.2). It can be seen from the Tables that only few specimens (two in first phase and one in second phase) satisfied the criteria set by the ACI code.

Figure 5.57 shows the load deformation curves for third point bending test from first and second phase of experimental programs. From both curves (Figure 5.56 (a) and (b), it can be seen the results are much scattered especially in case of residual strength.

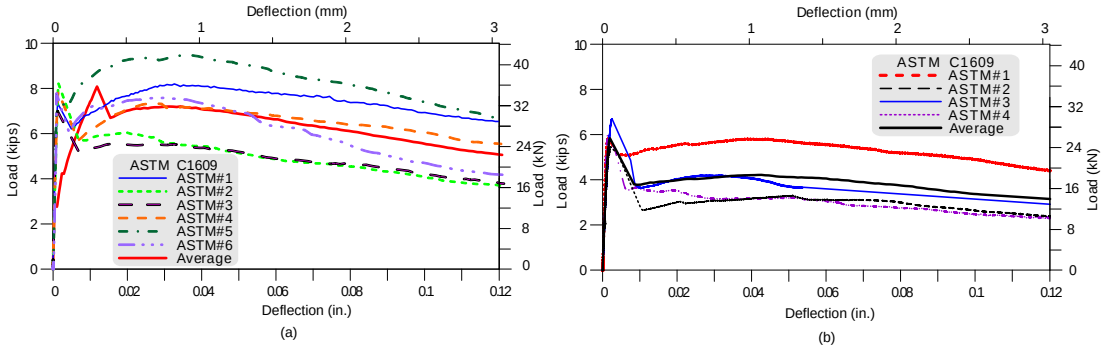

Figure 5.57 Load versus Deformation from Third Point Bending Test (ASTM C1609) for SFRC Specimens (a) First Phase and (b) Second Phase

5.11.4 Results from Double Punch Test

Table 5.17 and Figure 5.57 give the results from double punch test carried out along with large scale beam testing in second phase of experimental program. Table 5.18 provides the equivalent peak tensile strength and residual strength at 0.10 inches of deflection (reason discussed in chapter 6) with their COVs.

Table 5.17 Results from Double Punch Test (DPT) in Second Phase

SFRC-075					PC		
Ultimate Load			Residual load at 0.10 inches deflection		Ultimate Load		
Specimen	Load	Equivalent Tensile strength	Load	Tensile strength	Specimen	Load	Tensile strength
	(kips)	(psi)	(kips)	(psi)		(kips)	(psi)
SFRC#1	26.50	401.0	7.6	115.3	PC#1	25.70	388.9
SFRC#2	27.20	411.6	7.5	113.8	PC#2	22.90	346.5
SFRC#3	29.20	441.9	11.4	171.8	PC#3	22.80	345.0
SFRC#4	28.70	434.3	9.6	144.8	PC#4	25.60	402.5
Mean	27.90	422.2	9.01	136.4	Mean	24.3	367.0
STDEV	1.26	19.1	1.82	27.6	STDEV	1.62	24.5
COV	4.52%	4.52%	20.22%	20.22%	COV	6.67%	6.67%

The ultimate strength of SFRC specimens were found higher than PC specimens. The peak equivalent tensile strength for SFRC specimen was found about 15% more than PC specimen.

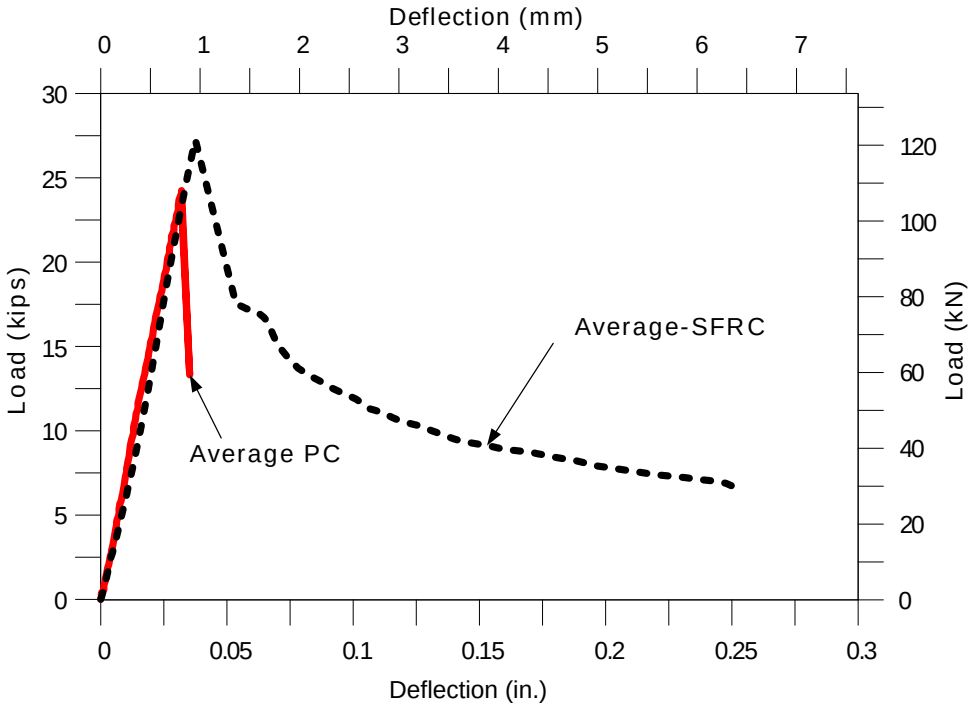

Figure 5.58 Comparison of Average Load versus Deflection from DPT

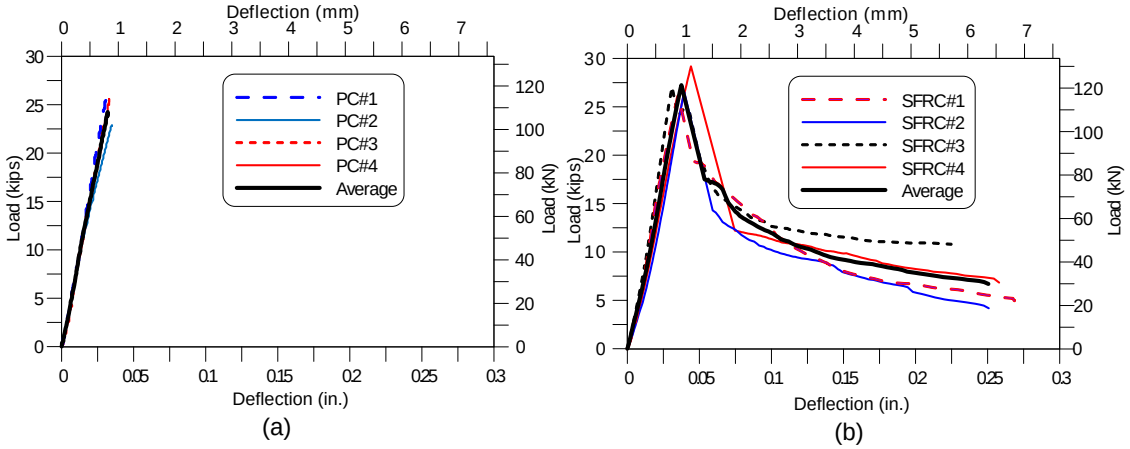

Figure 5.59 Load versus Deflection from Double Punch Test (DPT) for (a) PC Specimens and (b) SFRC Specimens

The values of COV for SFRC specimens from DPT for both peak and residual strength are lower compared with third point bending test (ASTM C1609). In Chapter Six, comparison between two tests was explained in detail with different volume of fraction of steel fibers.

CHAPTER 6

EXPERIMENTAL RESULTS: DOUBLE PUNCH TEST

6.1 General

Main parameter evaluated from double punch test (DPT) were peak equivalent tensile strength, residual strength at 0.10 inches deflection and coefficient of variation of these properties, deflection hardening and deflection softening, stiffness, crack opening and total energy dissipation (toughness). Various results obtained from different phases of the experimental studies are presented and discussed in following sections.

6.2 First Phase Experimental Results

6.2.1 Equivalent Tensile Strength

Equivalent tensile strength was calculated from the ultimate load based on Equation2.47. developed by Chen (1970) as discussed in Chapter Two. The results from the equation was also compared with the results from FE analyses and found that difference is small (less than 10%) (see Chapter Four). As shown in Table 6.1, SFRC specimens showed higher tensile strength compared to PC except SFRC BL-075. This might be due to the fact that the compressive strength of SFRC BL-075 was lower, approximately 17% less than PC since the ultimate tensile strength is related to compressive strength. SFRC BL-075 was tested after 24 hours whereas PC was tested at

48 hours. Compressive strength of SFRC-BL was slightly lower than 4 ksi and far lower than that of PC. However, SFRC BL-075 showed better performance in terms of residual strength. The behavior of residual strength at 0.10 inches deflection is discussed more in the following section. SFRC BL-150, in which 1.5% of Type 3 (Bekeart long, BL) steel fiber was used and had shown the highest equivalent tensile strength; 18.5% higher as compared to PC. Various properties including average equivalent tensile strength of different specimens are presented in Table 6.1. The bar charts in Figure 6.1 gives more clear comparison of peak equivalent tensile strength of different types of specimens .

Table 6.1 Average Maximum Load, Equivalent Tensile Strength and COV from the First Phase of Experiment

Specimens	Compressive strength (ksi)	Peak load (kips)	Equivalent tensile strength (psi)	Comparison with PC	Coefficient of variation	Tested hours after casting
PC	4.7	27.1	410	-	5.2 %	48
SFRC R-050	4.5	27.4	414	1.0 %	7.5 %	48
SFRC R-075	5.9	32.4	491	16.4 %	6.2 %	48
SFRC R-100	4.4	28.0	423	3.1 %	4.2 %	24
SFRC R-150	5.6	33.2	502	18.2 %	3.8 %	24
SFRC R-200	5.6	30.9	467	12.2 %	6.9 %	24
SFRC BS-050	5.5	32.8	496	17.3 %	3.9 %	48
SFRC BS-075	5.1	31.2	472	13.1 %	8.5 %	42
SFRC BS-100	4.9	32.4	490	16.3 %	3.1 %	24
SFRC BL-050	5.8	29.3	444	7.5 %	7.2 %	48
SFRC BL-075	3.9	23.8	361	-13.7 %	4.7 %	24
SFRC BL-100	4.9	33.7	509	19.5 %	8.2 %	24
SFRC BL-150	4.6	36.9	559	26.6 %	18.5 %	24

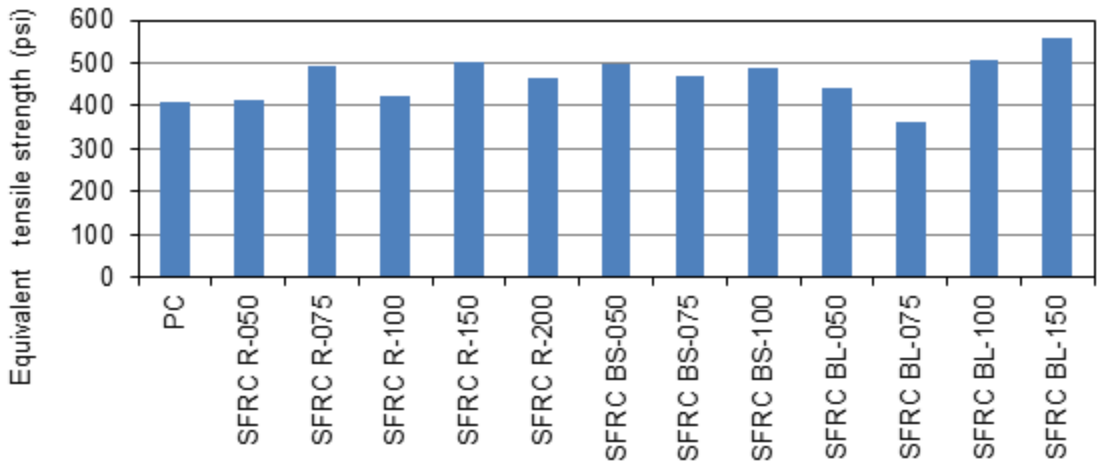

Figure 6.1 Comparisons of Equivalent Tensile Strengths (First Phase)

Specimen with Type 1 (Royal, SFRC-R) and Type 2 (Bekaert short, SFRC-BS) were compared to Type 3 fiber (Bekaert long , SFRC-BL) and result showed that SFRC-BL specimens were found with higher average equivalent tensile strength for each volume fraction of fiber expect 0.75% as shown in Table 6.2. Table 6.2 shows that when SFRC-BL specimens were compared to SFRC-R specimens, equivalent tensile strength increased by 7.3%, 20.3%, and 11.4% for fiber volume fractions of 0.5%, 1.00%, and 1.50%, respectively.

In the case of SFRC-BS, equivalent tensile strength was increased by 3.9% for fiber volume fraction of 1.50%. The equivalent tensile strength decreased by 10.5% and 23.5% for fiber volume fraction of 0.50% and 0.75%, respectively. As given in Chapter Four the Type 3 steel fiber has 2.4 inches length and it caused slightly difficult mixing with this particular concrete mixture. Even though Type 1 fiber has longer length than Type 2 fiber, the reason why Type 2 fiber showed higher strength than Type 1 can be

attributed to the double-hooked at ends of Type 2 fibers, which provide better mechanical bonding.

Table 6.2 Comparison of Peak Strength of Specimens using Type 3 Fibers (SFRC-BL) with Specimens using Type 1 Fibers (SFRC-R) and Specimens using Type 2 Fiber (SFRC-BS) (First Phase)

Volume fraction	Equivalent tensile strength of SFRC-BL (ksi)	Equivalent tensile strength of SFRC-R (ksi)	Difference with SFRC-R (ksi)	Equivalent tensile strength of SFRC-BS (ksi)	Difference with SFRC-BS (ksi)
0.50 %	444	414	30 (7.3% ↑)	496	-52 (10.5% ↓)
0.75 %	361	491	-130 (26.5% ↓)	472	-111 (23.5% ↓)
1.00 %	509	423	86 (20.3% ↑)	490	19 (3.9% ↑)
1.50 %	559	502	57 (11.4% ↑)	-	-

6.2.2 Residual Strength at 0.1 inches Deformation

PC specimens failed immediately after peak load so there was no residual strength. For SFRC specimens, residual strength at deflection of 0.10 inches has been selected to compare the post-peak performance of different FRC mixtures. To compare the mechanical performance of various FRC mixtures two points are required: one is the *peak strength* and the second one is *the residual strength at 0.1 in*. The reason being that characteristics of the descending portion of the load-deformation response can be quickly identified as long as information of these two points are known (for example, see Figure 6.2):

1. If the descending curve could not reach 0.1 in., then it tells that the ductility beyond peak strength (or first cracking) is generally minor;
2. A straight line connecting these two point can roughly represent the curve in the descending part;
3. FRC mixtures with higher strengths at these two points generally have higher strength throughout the entire curve.
4. Comparison between the residual strengths at 0.1 in. for different SFRC materials generally gives the relative toughness (energy absorption ability) beyond cracking.

It should be noted that, however, if a mixture has significant lower ascending slope (which means lower modulus of elasticity), using the 0.1 in. deformation might lead to unconservative results and unfair comparison with a FRC having stiffer ascending branch. In such a case the second point can be taken at the point 0.05 in. beyond the deformation at the peak strength. This criterion could also be applied to FRC mixtures with ultra high performance when the 0.1 in. deformation is still within its ascending branch of the load versus deformation curve.

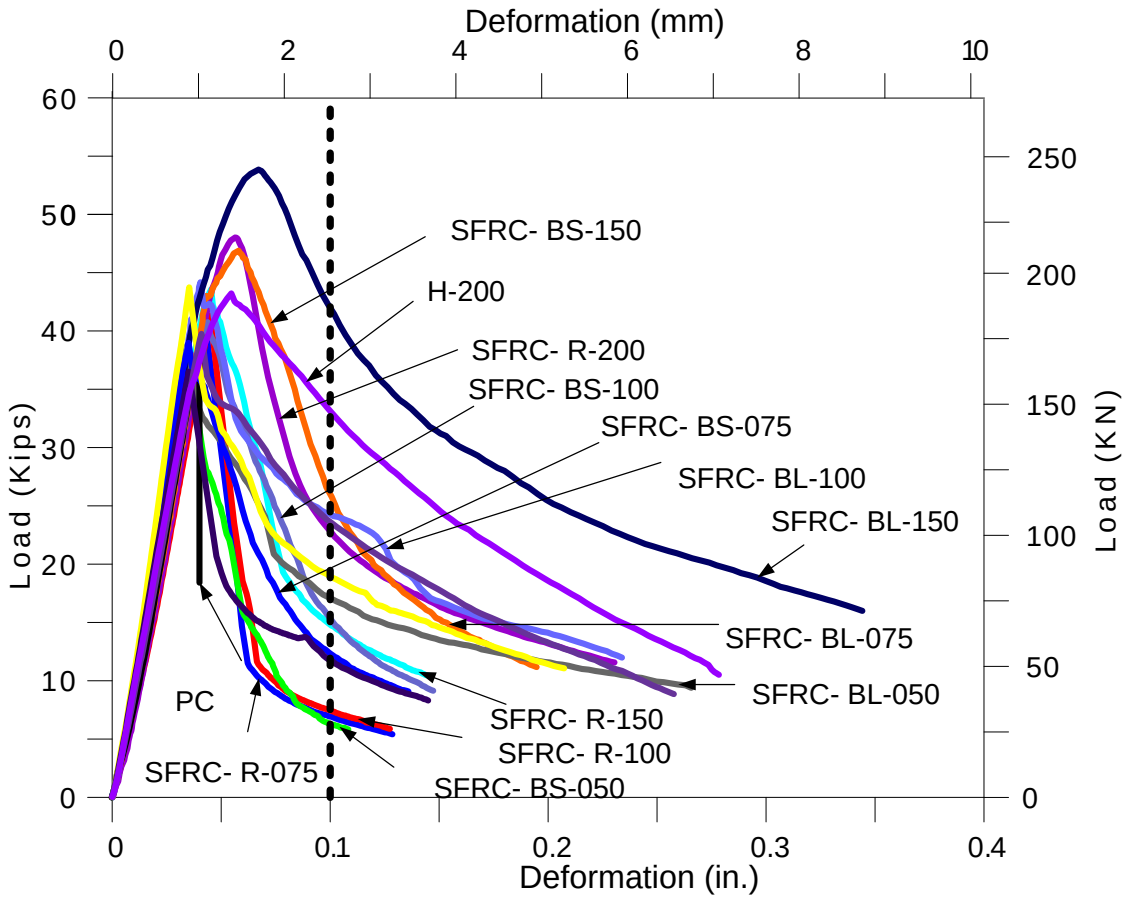

Figure 6.2 Selection of Deflection Limit (0.10 inch) to Determine Residual strength.

A few things could also be observed from Figure 6.2:

- The peak loads were generally occurred about 0.045 to 0.055 inches of deflections. (In case of strain hardening this value could be more.)
- For SFRC mix with less fiber volume fraction of (0.50%), some of the specimens exhibited very low residual loads at 0.10 inches deformaiton. Beyond this values are negligible.
- For SFRC mix with higher volume of fraction (>1.5%), residual loads at 0.10 inches deformation could be even more than 75% of peak load.

As discussed in Chapter Two, residual strength is an important parameter for SFRC because the major role, i.e. bridging the cracks, played by steel fibers was generally seen after the occurring of the first crack in the concrete.

As expected, there was no residual strength for plain concrete. In contrast, SFRC showed significantly higher residual strength. In order to observe tensile residual behavior of SFRC, the tests did not stop until the residual strength reduced to approximately 25% of the peak strength. Residual strengths at deformation diformationof 0.1 inches were observed for the reasons discussed earlier. The summary of residual strength is presented in Table 6.3 and Figure 6.3.

Table 6.3 Residual Strength at 0.1 inches deformation (First Phase)

Specimens	Residual load at 0.10 in. deformationdiformation (kips)	Coefficient of variation
PC	-	-
SFRC R-050	6.5	13%
SFRC R-075	7.4	17%
SFRC R-100	11.5	22%
SFRC R-150	15.2	20%
SFRC R-200	17.6	25%
SFRC BS-050	11.2	24%
SFRC BS-075	14.8	8%
SFRC BS-100	17.3	16%
SFRC BL-050	12.9	16%
SFRC BL-075	12.5	20%
SFRC BL-100	25.2	20%
SFRC BL-150	32.1	36%

It is clear that SFRC-BL specimens with Type 3 fibers showed better performance in terms of residual strength except 0.75% volume fraction of fiber (reason

already discussed earlier). The residual strengths were found larger for the specimens with high volume of fractions of fiber and for longer fiber with double bend hooked at ends.

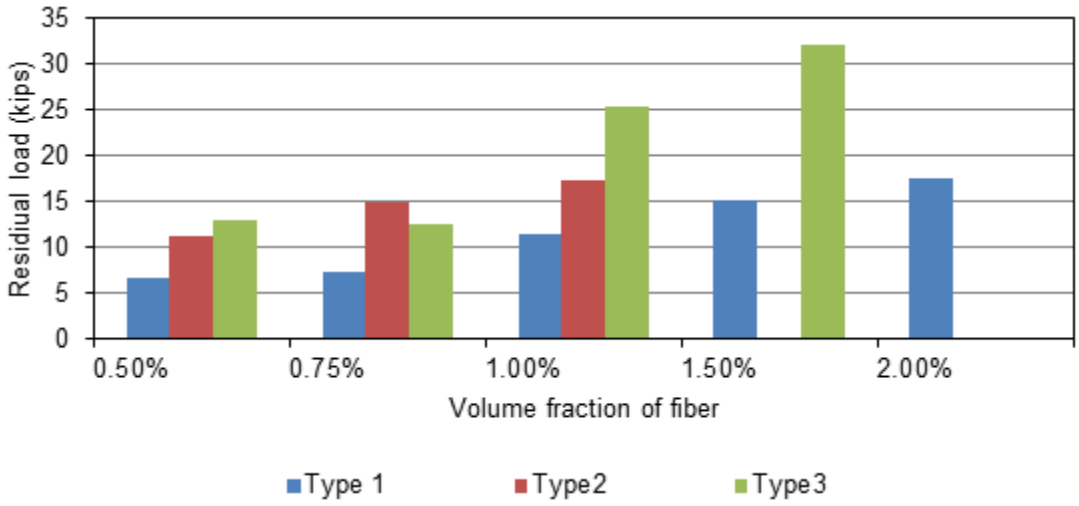

Figure 6.3 Comparison of Residual Strength at 0.10 inches Deformation (First Phase)

Table 6.4 shows comparison of residual strengths between Type 3 fiber and Type 1 and 2 fibers. As shown in Table 6.4 when SFRC-BL specimens with Type 3 fiber were compared with SFRC-R specimens with Type 1 fiber, residual strength was increased from 70 to 120% with different volume of fraction fibers.

Table 6.4 Comparison of Residual Strength of Specimens with Type 3 Fibers (SFRC-BL) with Specimens with Type 1 Fibers (SFRC-R) and Specimens with Type 2 Fiber (SFRC-BS) (First Phase)

Volume fraction	Corresponding load at diformationdeformation 0.1 in. for SFRC-BL (kips)	Corresponding load at diformation 0.1 in. for SFRC-R (kips)	Difference with SFRC-R (kips)	Corresponding load at diformation 0.1 in. for SFRC-BS (kips)	Difference with SFRC-BS (kips)
0.50 %	12.9	6.5	6.4 (98.2% ↑)	11.2	1.8 (16% ↑)
0.75 %	12.5	7.4	5.1 (69.3% ↑)	14.8	-2.4 (15.9% ↓)
1.00 %	25.2	11.5	13.7 (119.5% ↑)	17.3	8.0 (46.1% ↑)
1.50 %	32.1	15.2	16.95 (111.0% ↑)	-	-

6.2.3 Coefficients of Variation

The coefficient of variation (COV) for both peak and residual strength from the test were one of the major factor to justify the reliability of a standard test method. Table 6.1 shows that the values of COV for peak load are less than 10% expect SFRC BL-150. The COV is relatively lower compared to that of the third point flexural test (ASTM C1609) which typically showed values of approximately 20%. The details comparisons are presented in later part of this chapter. Similarly, Table 6.3 shows COV for the residual strength at 0.10 inches deformation. The COVs are varied from 8 to 36% for the test conducted in this first phase.

Figure 6.4 shows the comparison of the average load versus deformation curves of PC specimens and SFRC specimens with the same type butdifferent volume fractions

of fiber. Figure 6.5 compares specimens withwith different types of fibers but same volume fraction of fibers.

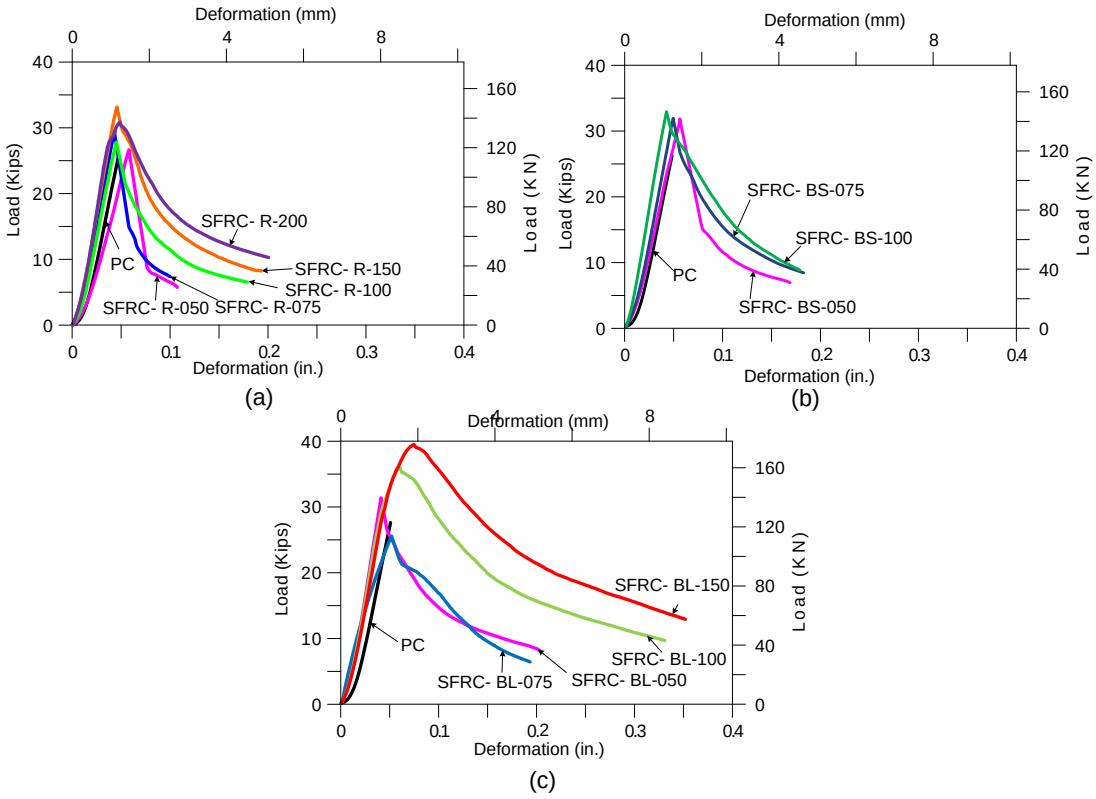

Figure 6.4 Comparisons of Average Curves for PC with SFRC Specimens with Different Types of Fibers (a) SFRC-R (b) SFRC-BS and (c) SFRC-BL in DPT First Phase

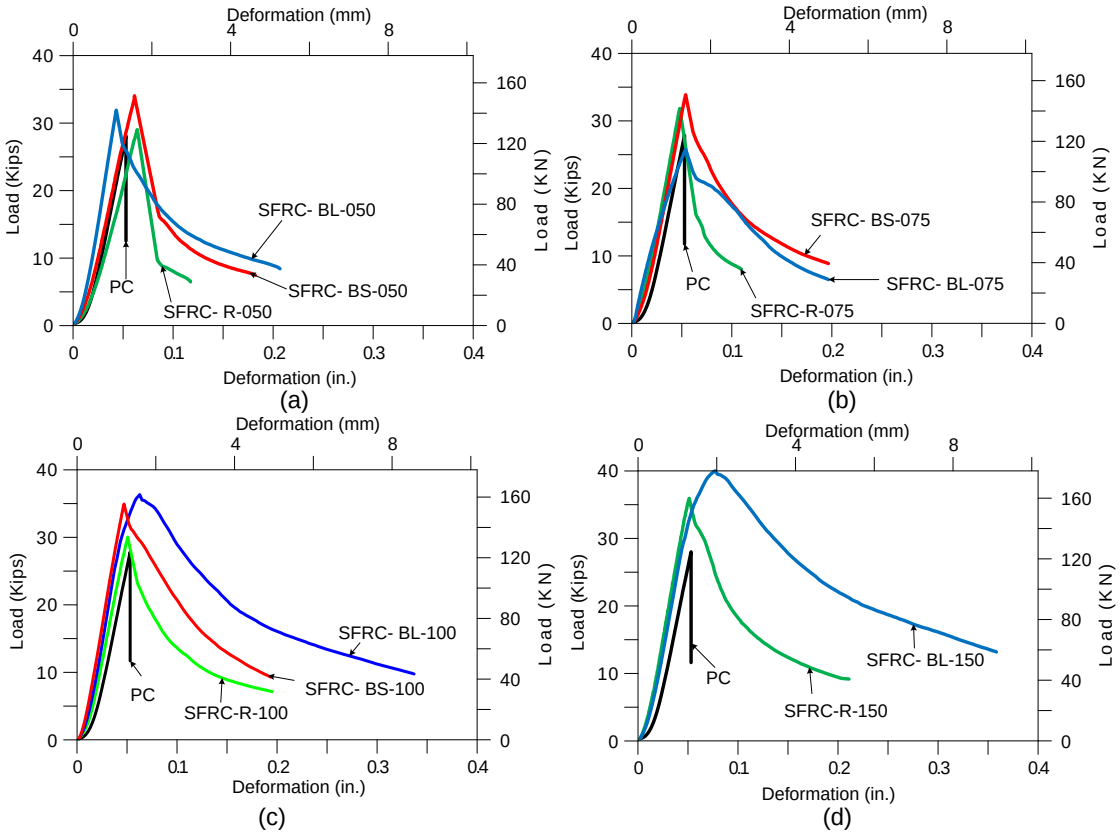

Figure 6.5 Comparisons of Average Curves for PC specimens and SFRC Specimens with Volume of Fraction in First Phase (a) 0.50%, (b) 0.75%, (c) 1.0% and (d) 1.50%

6.3 Second Phase Experimental Results

6.3.1 General

Similar to the first phase of the experiment, double punch tests were performed when the compressive strength reached 4 ksi. Based on results of the first phase (low peak strength, COV), number of specimens were reduced to four in the second phase of the experiment. One set of specimens were prepared at same time and also tested after 42 hours at same time, so that all specimens would have compressive strength more than 4 ksi for the reason discussed earlier.

6.3.2 Equivalent Tensile Strength

As in case of the first phase, the various properties including tensile strength are presented in Table 6.6. Figure 6.6 shows the comparison of equivalent tensile strength by the bar chart. SFRC specimens had shown higher peak equivalent tensile strength as compared to PC. It is seen clearly from the Table 6.6 that most of SFRCs showed higher equivalent tensile strength except SFRC R-100. As the volume fraction of fiber increased the equivalent tensile strength increased as well. For SFRC BL-150 specimens, the ultimate strength increased up to 39.5% as compared to PC specimens. As in the first phase, the specimens with Type 3 fibers were compared with specimens with Type 1 and Type 2 fibers as shown in Table 6.7. In general, specimens with Type 3 fiber also showed better strength (up to 27%) as compared to short fibers of Type 1 and Type 2.

Table 6.5 Average Peak Load, Equivalent Tensile Strength in Second Phase of Experiment

Specimens	Compressive strength (ksi)	Peak load (kips)	Equivalent tensile strength (psi)	Comparison with PC	Coefficient of variation	Tested after hours
PC	4.24	26.97	408	-	12.67	42
SFRC R-075	6.77	27.91	422	+ 3.4%	9.01	
SFRC R-100	6.65	26.20	396	- 2.9%	10.47	
SFRC R-150	6.71	29.55	447	+ 9.6%	15.17	
SFRC R-200	6.65	32.42	491	+ 20.3%	4.94	
SFRC BS-075	5.60	28.08	425	+ 4.2%	4.18	
SFRC BS-100	5.10	28.29	428	+ 4.9%	8.53	
SFRC BS-150	5.10	34.66	524	+ 28.4	9.32	
SFRC BL-075	6.53	27.64	418	+ 2.5%	4.39	
SFRC BL-100	5.73	28.02	424	+ 3.9%	4.80	
SFRC BL-150	6.81	37.62	569	+ 39.5%	9.03	

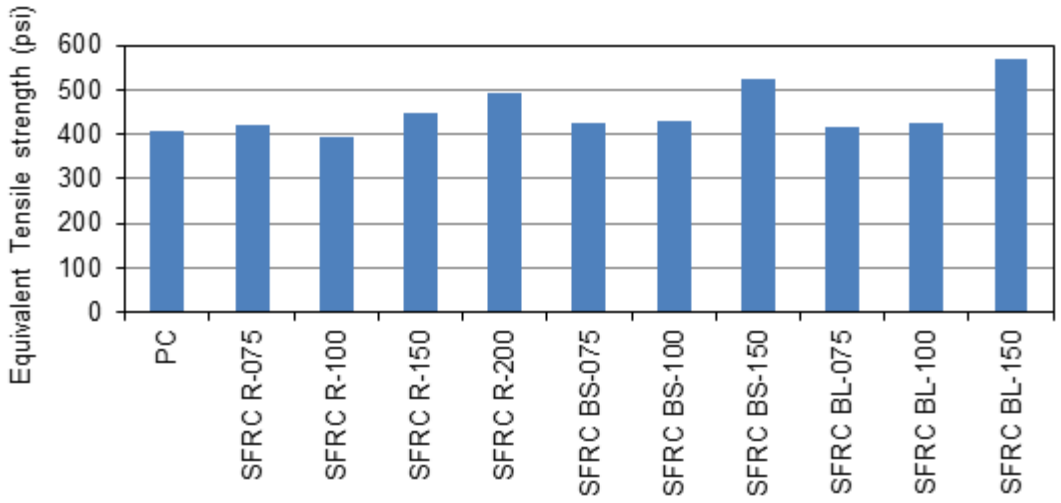

Figure 6.6 Comparison of Peak Equivalent Tensile Strength (Second Phase)

Table 6.6 Comparison of Peak Strength of Specimens with Type 3 Fiber with Specimens with Type 1 and Type 2 Fibers (Second Phase)

Volume fraction	Equivalent tensile strength of SFRC-BL (ksi)	Equivalent tensile strength of SFRC-R (ksi)	Difference with SFRC-R (ksi)	Equivalent tensile strength of SFRC-BS (ksi)	Difference with SFRC-BS (ksi)
0.75 %	418	422	-4 (0.95% ↓)	425	-3 (0.7% ↓)
1.00 %	424	396	28 (7.1% ↑)	428	-4 (0.9% ↓)
1.50 %	569	447	122 (27.3% ↑)	524	45 (8.6% ↑)

6.3.3 Residual Strength at 0.10 inches Deformation

Results of the second phase in the residual strength were similar to the results from the first phase. The SFRC-BL specimens showed higher residual strength compared to SFRC-R and SFRC-BS. Compared to SFRC-R the residual strength increased mo thn 100% for SFRC-BL. Table 6.8 and Figure 6.7 shows the comparison of residual strength of specimens with different types and different volumes fractions of fibers.

Table 6.7 Residual Strength at 0.10 inches Deformation (Second Phase)

Specimens	Corresponding load at diformation0.1 in. deformation (kips)	Coefficient of variation at 0.10 in. diformationdeformation
PC	-	-
SFRC R-075	7.5	7%
SFRC R-100	6.9	3%
SFRC R-150	13.9	13%
SFRC R-200	19.4	25%
SFRC BS-075	14.3	2%
SFRC BS-100	17.6	19%
SFRC BS-150	27.6	29%
SFRC BL-075	16.2	11%
SFRC BL-100	20.4	34%
SFRC BL-150	31.1	39%

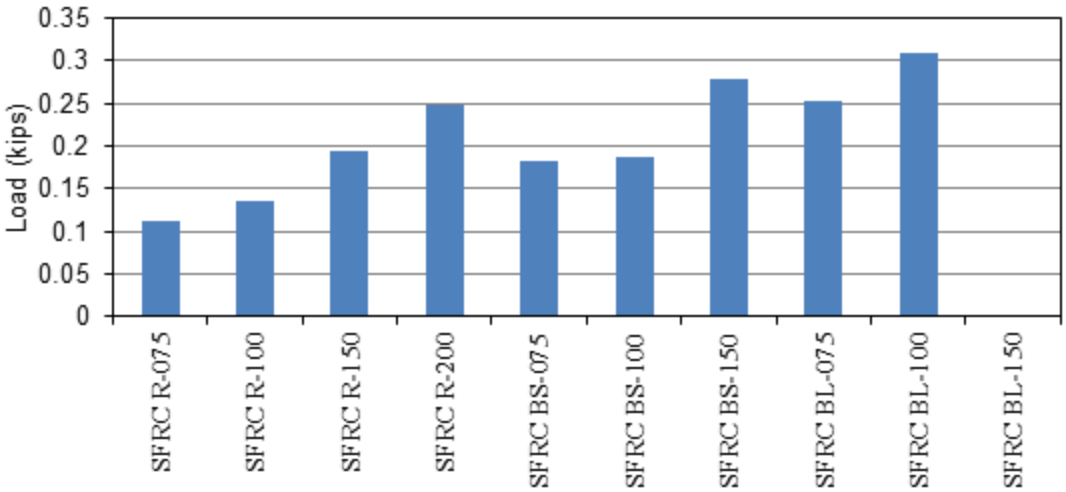

Figure 6.7 Comparison of Residual Strength at 0.10 inches Deflection (Second Phase)

Table 6.8 compares the residual strength of specimens with Type 3 with specimens of Type 1 and Type 2 as in case of the first phase. Results show that residual strengths of Type 3 specimens are as high as 166% compared to Type 1 and Type 3. Even though the peak load of SFRC-BL075 is slightly lower than SFRC-R-075 and SFRC-BS-075, its residual strength was quite high.

Table 6.8 Comparison of Residual Strength of Type 3 with Type 1 and Type 2 Fibers (Second Phase)

Volume fraction	Corresponding load at diformation 0.1 in. for SFRC-BL (kips)	Corresponding load at diformation 0.1 in. for SFRC-R (kips)	Difference with SFRC-R (kips)	Corresponding load at diformation 0.1 in. for SFRC-BS (kips)	Difference with SFRC-BS (kips)
0.75 %	16.9	6.3	10.5 (166% ↑)	14.4	2.4 (16.7% ↑)
1.00 %	16.7	8.2	8.7 (103% ↑)	18.1	-1.4 (7.6% ↓)
1.50 %	29.8	14.5	15.5 (106% ↑)	28.4	1.4 (5.0% ↑)

6.3.4 Coefficients of Variation

Tables 6.6 and 6.8 show the comparison of the coefficients of variation for peak strength and residual strength between different types of specimens. Even though the number of specimens was just four, much less as compared to the first phase, the coefficients of variation for peak strength for most of specimens were less than 10% except for PC (12.7%) and R-100 (15.2%). Similarly, coefficients of variation for residual strength for specimens were of the same order as those in the first phase. The COVs for some specimens were slightly higher.

6.3.5 Load versus Deformation Curves

Comparison of the equivalent tensile strength of PC with one type of fiber with different volume fractions of fibers is shown in Figure 6.8. Figure 6.9 shows load versus deformation curves with different types of fibers with the same volume fraction of fibers. These figures indicated that the initial stiffness (slope of curves before first crack load or peak load) were very close and consistent for all specimens (including PC). This is because the mix design for all specimens was same (except volume fractions of steel fibers), and effect of fibers occurred only after the first cracking. However, post crack slopes were very different with change in volume of fractions of steel fibers and types of fibers. Long fibers with higher volume fractions typically gave greater toughness).

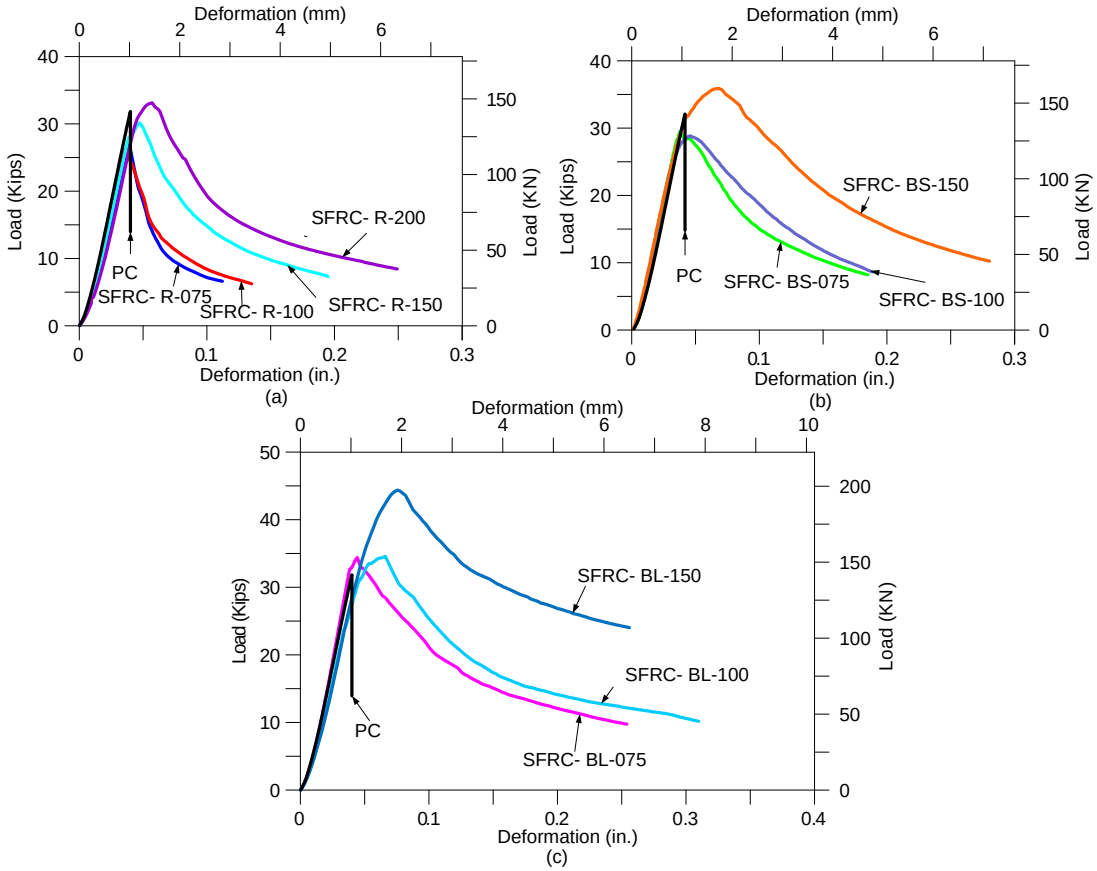

Figure 6.8 Comparisons of Average Curves for PC and SFRC Specimens with Different Types of Fibers (a) SFRC-R (b) SFRC-BS and (c) SFRC-BL from Second Phase

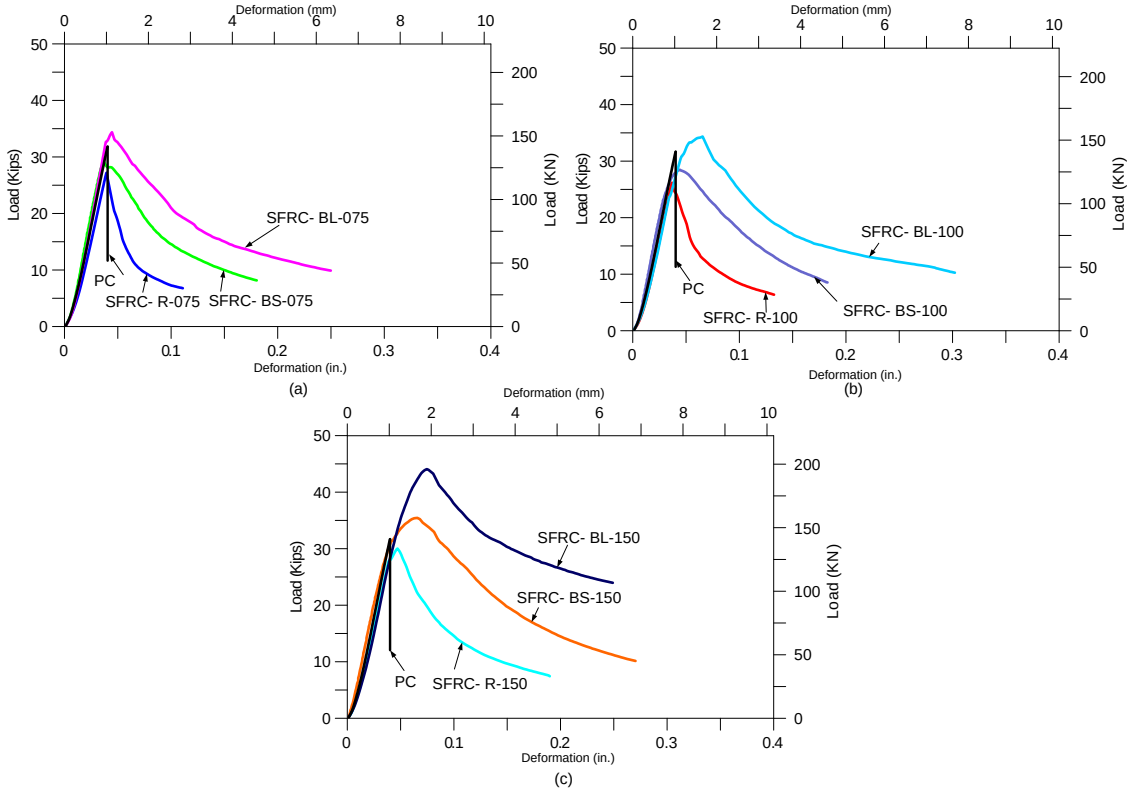

Figure 6.9 Comparisons of Average Curves for PC Specimens and SFRC Specimens with Volume of Fraction in Second Phase (a) 0.75%, (b) 1.0% and (c) 1.50%

6.3.6 Crack Pattern

Figure 6.10 shows the typical photographs from DPT for plain and SFRC specimens with 0.5% and 1.0% volume of fractions of steel fibers. It can be seen from the figure that when peak load was reached, PC specimen broke into four pieces whereasSFRC specimens had several radial cracks and the integrity was maintained by the fiber bridging. The test was continued until the load was approximatley one fourth of the peak load. Cracks generally developed from top and inner part of the specimens and propagated to the bottom along the depth.

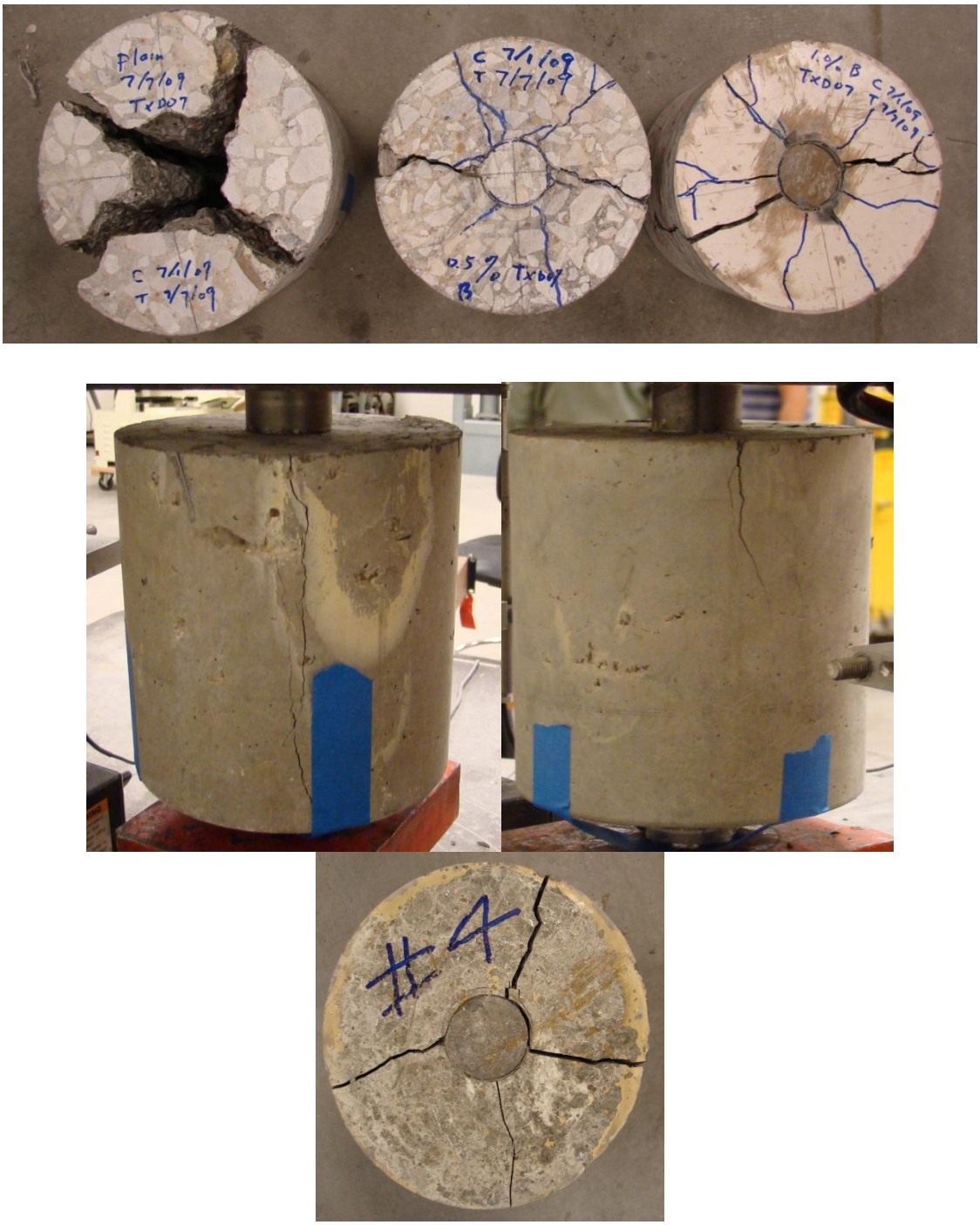

Figure 6.10 Typical Tested Photos Showing Radial Cracks

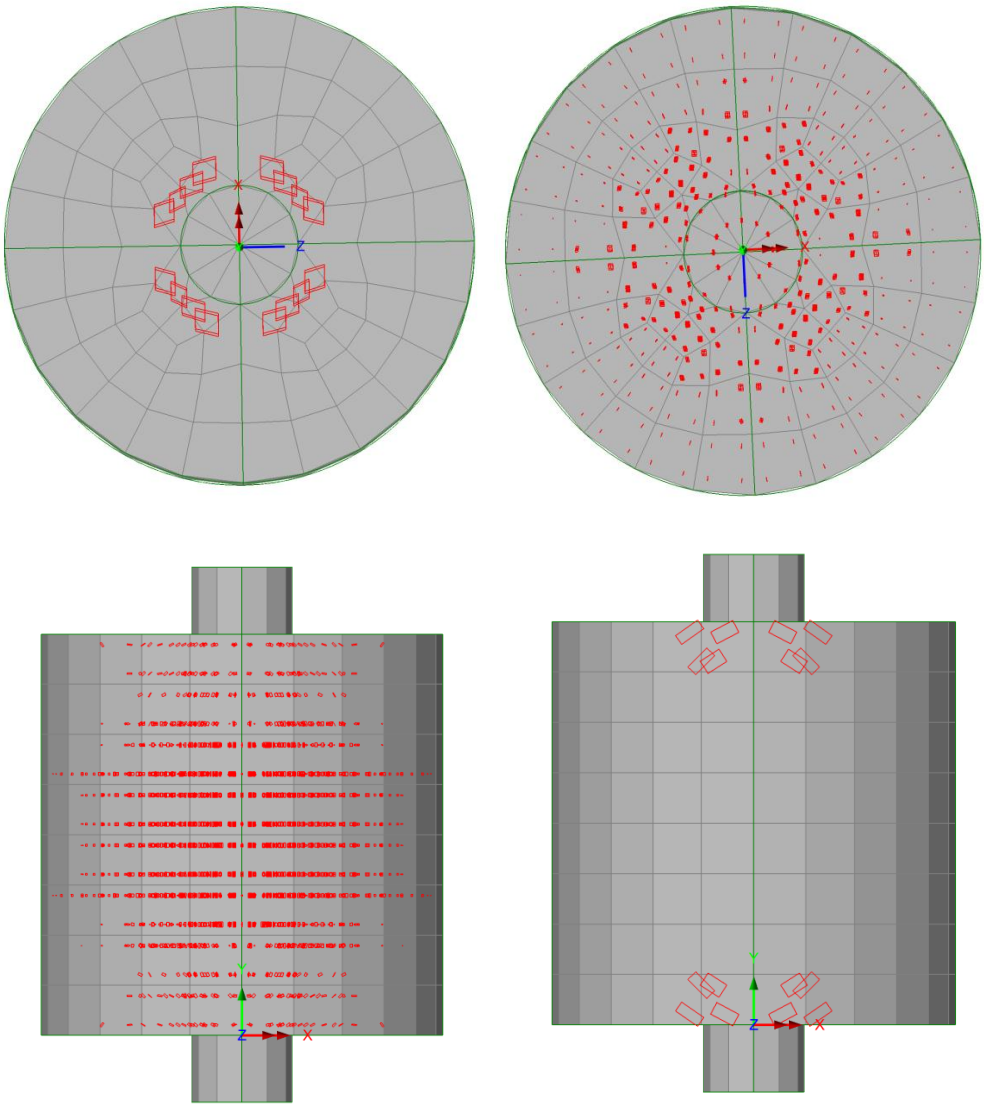

Figure 6.11 Crack Pattern Shown in Finite Element Analysis

6.4 Third Phase Experimental Results

6.4.1 General

As in the first and the second phases of the experiments, double punch tests were performed in this phase when the compressive strength was greater than 4 ksi. In the third phase of the experimental program, same sets of specimens were casted on one day and tested the next day, approximately within 24 hours after casting.

6.4.2 Equivalent Tensile Strength

As shown in Table 6.10 and Figure 6.12, in third phase nearly all of SFRC specimens showed higher equivalent tensile strength than that of PC specimens except…….. It was observed that increasing fiber contents normally increased the ultimate equivalent tensile strength of SFRC. Specimens with Type 2 fibers showed no or little increase in maximum tensile strength compared to PC, which was not expected. It could be inferred that the strength is one of factors too difficult control especially at the early age of concrete. Nevertheless, SFRC, in general, showed better performance in equivalent ultimate tensile strength as compared to PC. In addition, increase of fiber contents led to increase of the strengths. The test results agreed with the results from the first and the second phase experimental programs. Similar to the previous two phases, the longer fiber generally showed better performance.

Table 6.9 Average Peak Load, Equivalent Tensile Strength in Third Phase of Study

Specimen Type	Compressive strength (ksi)	Peak Load (kips)	Equivalent tensile strength (psi)	Increased strength compared to PC	Coefficient of Variation (COV)	Time of test after casting (hrs)
PC	4.7	27.1	410		5.20 %	24
SFRC-R-075	5.1	32.7	495	20.73 %	4.40 %	
SFRC -R-100	4.7	31.4	476	16.10 %	2.03 %	
SFRC -R-150	6.5	31.4	476	16.10 %	6.84 %	
SFRC -R-200	5.8	33.0	499	21.71 %	2.94 %	
SFRC -BS-050	5.3	30.1	456	11.22 %	4.17 %	
SFRC -BS-075	4.5	27.2	412	0.49 %	6.97 %	
SFRC -BS-100	4.9	30.2	457	11.46 %	4.38 %	
SFRC -BS-150	4.1	26.9	407	-0.73 %	2.40 %	
SFRC -BL-050	4.9	27.9	422	2.93 %	4.16 %	
SFRC- BL-075	5.2	30.3	458	11.71 %	4.87 %	
SFRC -BL-100	6.1	33.1	501	22.20 %	6.71 %	
SFRC -BL-150	6.0	41.7	631	53.90 %	10.64 %	

In the case of SFRC BL-150 specimens, the ultimate strength was 53.9% more than that of the PC ones. As done in the first phase and second phase, ultimate equivalent tensile strengths for Type 1 and Type 2 fibers were compared to Type 3 fiber shown in Table 6.10. The Type 3 fibers have larger diameter, thus, the higher stiffness and mechanical bonding strength due to higher plastic modulus of the hooks. This in turn led to higher ultimate strength of the composite. However, as mentioned earlier, the greater aspect ratio of long fibers as well as larger size and amount of coarse aggregate limited fiber amount to 1.5%.

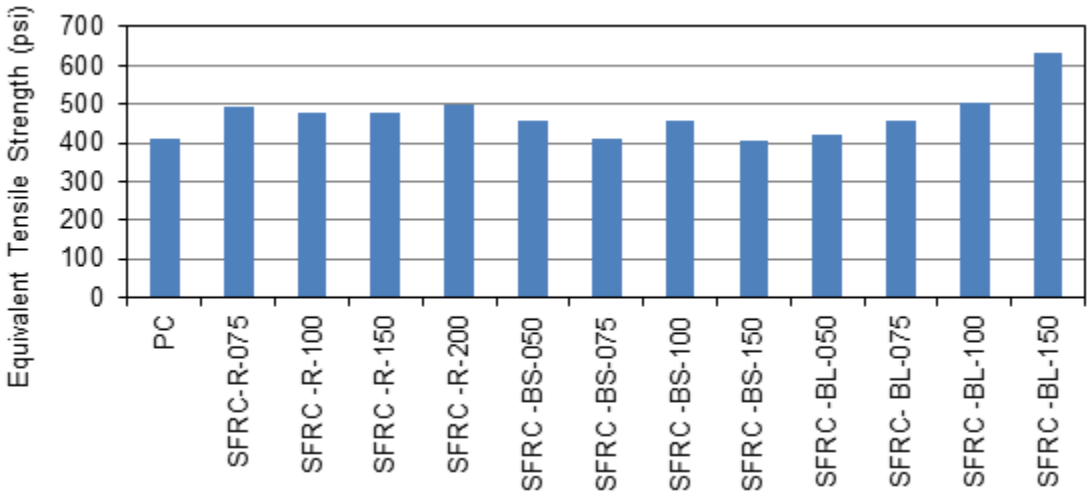

Figure 6.12 Comparisons of Peak Equivalent Tensile Strengths (Third Phase)

Table 6.10 Comparison of Peak Strength of Specimens with Type 3 and of Specimens with Type 1 and Type 2 Fibers (Third Phase)

Volume fraction	Equivalent tensile strength of SFRC-BL (ksi)	Equivalent tensile strength of SFRC-R (ksi)	Difference with SFRC-R (ksi)	Equivalent tensile strength of SFRC-BS (ksi)	Difference with SFRC-BS (ksi)
0.50 %	422	-	-	455	-33 (7.8% ↓)
0.75 %	458	495	-37 (8.1% ↓)	412	46 (10.0% ↑)
1.00 %	501	475	26 (5.2% ↑)	457	44 (8.8% ↑)
1.50 %	631	475	156 (24.7% ↑)	407	224 (35.5% ↑)

As observed in Figure or TableXX, specimens with Type 3 fibers in general showed better performance in terms of residual strengths. Comparison of residual strengths between specimens with Type 3 fiber and specimens with Type 1 and Type 2 fibers is presented in Table 6.11.

6.4.3 Residual Strength at 0.10 inches Deformation

As expected, the residual strengths only appeared in SFRCspecimens. Table 6.13 shows that the residual strengths for all specimens with different steel fiber are order of 6 to 38 kips at 0.10 inches deformation. The third phase experiment residual strength results were also similar to those of the first and second phase experimental programs. Specimens with Type 3 fiber showed higher residual strength compared to specimens with Type 2 fibers and Type 1 fibers. Figure 6.13 (bar chart) clearly shows that long fiber with larger volume of fraction of fiber shows higher residual strength.

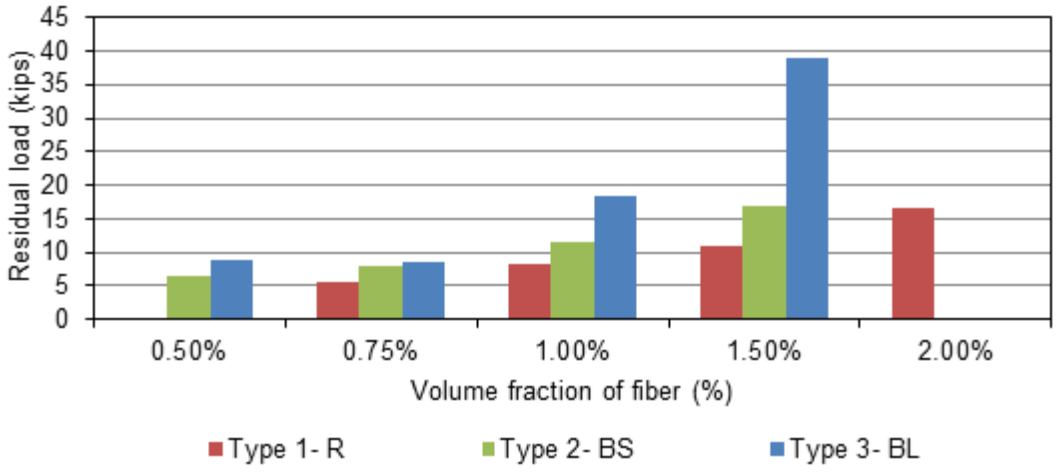

Figure 6.13 Comparison of Residual Strength at 0.10 inches Deformation (Third Phase)

Table 6.11 Comparisons of Residual Strength at 0.10 inches Deformation (Third Phase)

Specimen Type	Residual Strength at 0.1 in. Deformation		
	Coefficient Of Variation (COV)	Ultimate load (kips)	Equivalent tensile strength (psi)
SFRC-R-075	6.83	5.6	85
SFRC -R-100	19.49	8.3	126
SFRC -R-150	7.30	10.9	165
SFRC -R-200	17.10	16.6	251
SFRC -BS-050	10.76	6.6	100
SFRC -BS-075	22.77	7.9	120
SFRC -BS-100	3.03	11.5	174
SFRC -BS-150	17.17	17.0	257
SFRC -BL-050	24.48	9.0	136
SFRC- BL-075	33.86	8.6	130
SFRC -BL-100	15.11	18.5	280
SFRC -BL-150	30.24	38.8	587

Table 6.12 Comparison of Residual Strength between specimens with Type 3 and specimens with Type 1 and Type 2 Fibers

Volume fraction	Corresponding load at diformation 0.1 in. for SFRC-BL (kips)	Corresponding load at diformation 0.1 in. for SFRC-R (kips)	Difference with SFRC-R (kips)	Corresponding load at diformation 0.1 in. for SFRC-BS (kips)	Difference with SFRC-BS (kips)
0.50 %	9.0	-	-	6.6	2.4 (26.7% ↑)
0.75 %	8.6	5.6	3.0 (34.9% ↑)	7.9	0.7 (8.1% ↑)
1.00 %	18.5	10.2	11.6 (62.7% ↑)	11.5	7.0 (37.8% ↑)
1.50 %	38.8	10.9	27.9 (28.1% ↑)	17.0	21.8 (56.2% ↑)

6.4.4 Coefficienst of Variation

Tables 6.9 and 6.11 present the coefficients of variations for both peak and residual strength for the results in third phase of experiment. The average coefficient of variations is order of 5% which is less than those obtained from first phase and second phase studies. The result also proved that the double punch test showed the lowest value of COV among other test methods such as ASTM C1609 anddirect tensile test.. Even though the number of tested specimens was reduced to four, it was shown that double punch test provides reliable test results with relatively less numbers of specimens. COVs of residual strengths were varying And most of these were less 20% except for a few specimens.

6.4.5 Load versus Deformation Behavior

Comparison of the equivalent tensile strength of PC with specimens with same type of fiber but different volume fractions is shown in Figure 6.14. Figure 6.15 shows load versus deformation curves for specimens with different types of fiber but same volume fraction. These figures indicate that the initial stiffnesses (slope of curves before first crack load or peak load) are very close for all specimens (including PC); however, post crack slopes are very different with change in volume fractions of steel fibers and types of fibers. Longer fibers with higher volume fractions typically showed greater toughness).

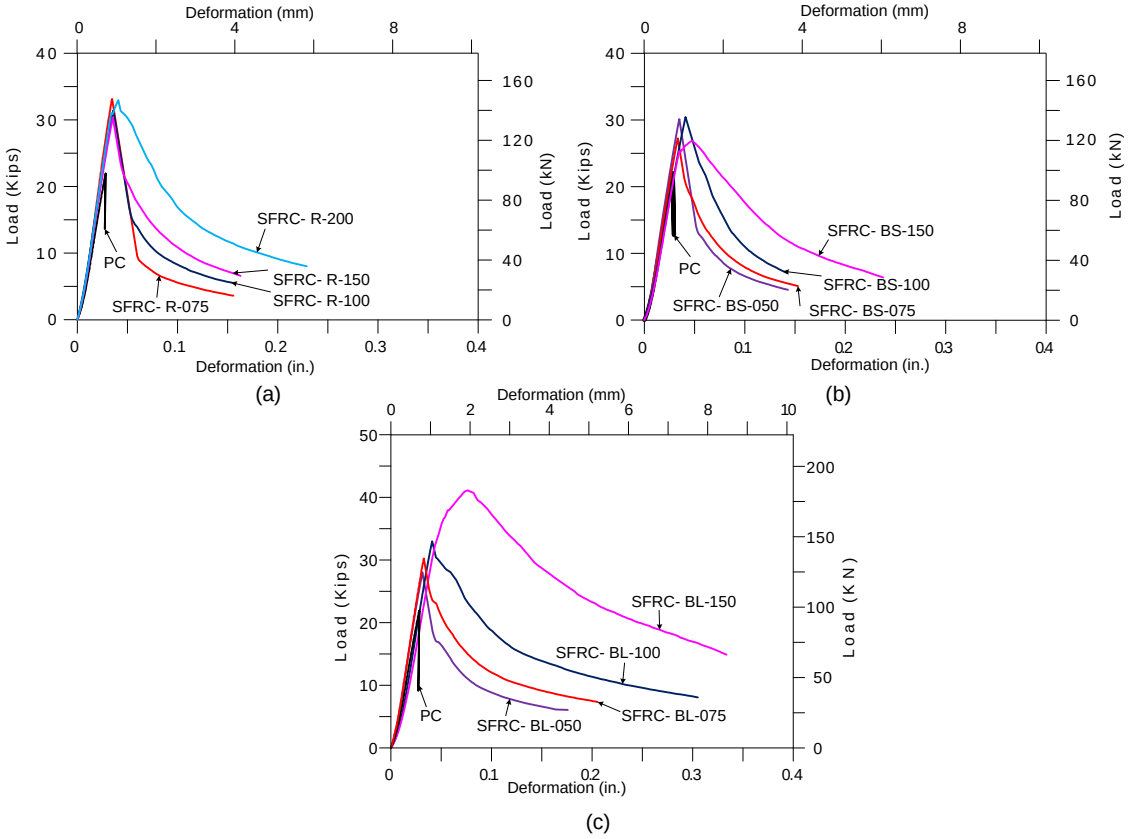

Figure 6.14 Comparison PC and SFRC Specimens with Different Types of Fibers (a) SFRC-R (b) SFRC-BS and (c) SFRC-BL

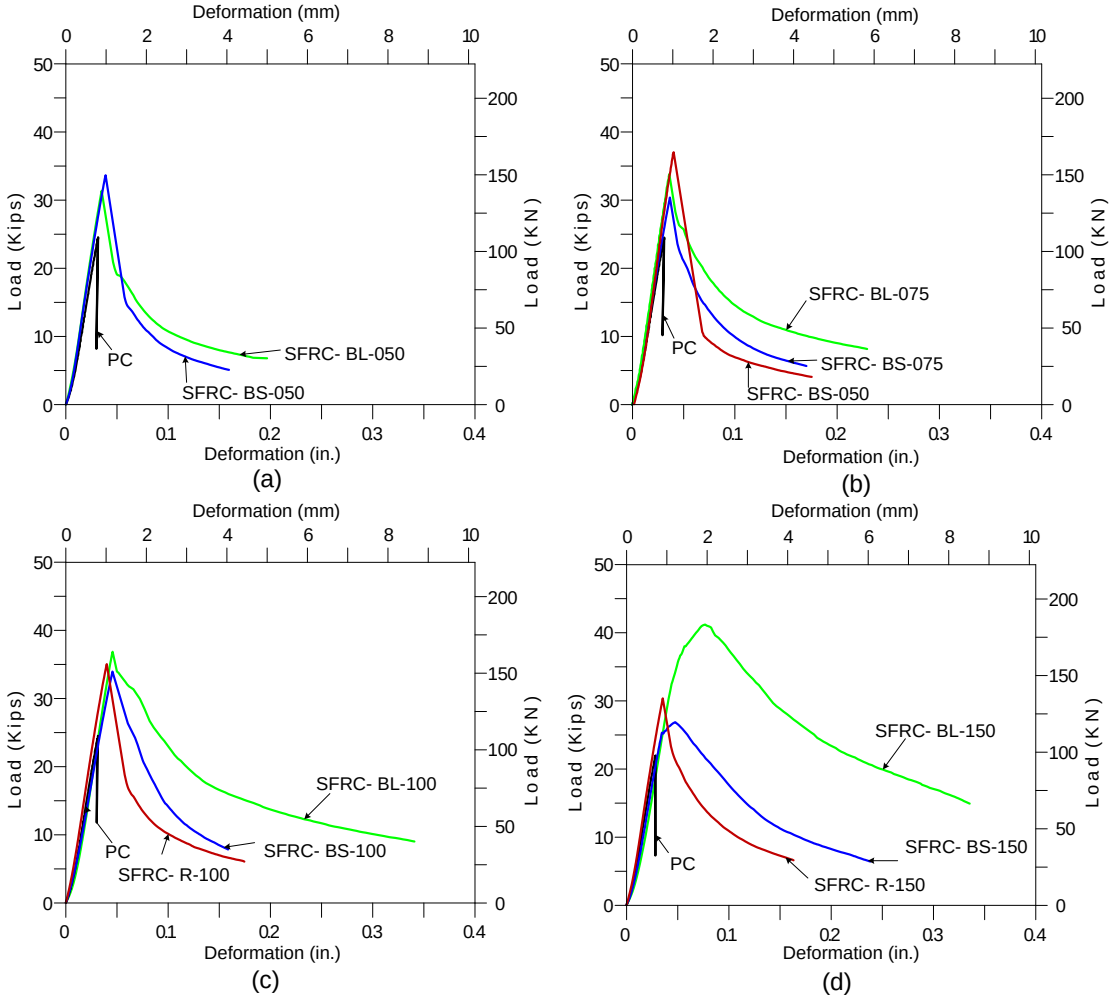

Figure 6.15 Comparisons between PC Specimens and SFRC Specimens with Different Volume of Fraction in Third Phase (a) 0.50%, (b) 0.75%, (c) 1.0%, and (d) 1.50%

Figures 6.16 (a) and (b) show the comparison of load versus deformation curves between the first phase and the third phase. It is seen that there were high variations in pre-peak response as well as residual strengths in the first phase. In contrast, those variations were significantly reduced in the third phase. This was primarily due to the improvement in testing technique, as discussed in Chapter Four, that the load was

applied up to 2 kips and then unloaded to 0.5 kips before starting the test, on order to somewhat "shakedown" the test setup. The improvement made the double punch test as more reliable test method.

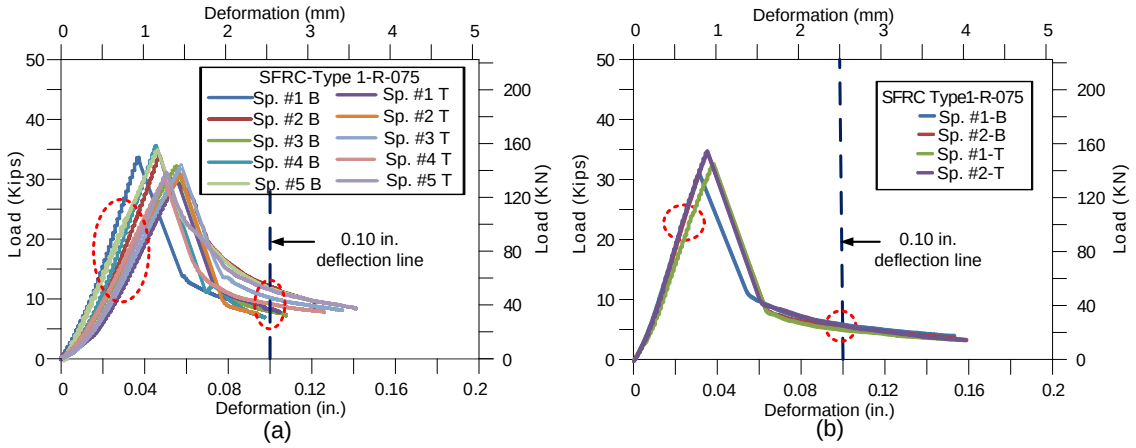

Figure 6.16 Comparison of Load versus Deflection Curves between (a) First Phase with SFRC-R-075 (Type 1 Fiber 0.75%) and (b) Third Phase with SFRC-R-075 (Type 1 Fiber 0.75%)

6.5 Fourth Phase Experimental Results

6.5.1 General

In previous phases of study it had been seen that some of the specimens showed uncontrolled results. Some SFRC with higher volume content showed lower ultimate strength. Some of them also showed high COV especially for residual strengths. It was mainly due to the difficulty in controlling the early age of strength of concrete . In this phase of experimental investigation all tests were carried out when concrete achieved its longer term compressive strength. All specimens were tested after 28 days. In general the specimens were tested at age of 55- 58 days.

6.5.2 Equivalent Tensile Strength

As shown in Table 6.14, almost all SFRC specimens showed higher equivalent tensile strength than that of PC specimens. Except SFRC BS-050 and SFRC H-050, they showed slightly lower peak strength as compared to PC. It was seen that increasing fiber contents normally increased the ultimate equivalent tensile strength. Nevertheless, SFRC, in general, showed better performance in equivalent ultimate tensile strength compared to PC. In the case of SFRC BL-150 specimens, the ultimate tensile strength was 39.4% more than that of the PC ones.

As in the previous phases, ultimate equivalent tensile strengths of Type 1 and Type 2 fibers specimens were compared to Type 3 fiber specimens as shown in Table 6.14. The comparison was also made for specimens with Type 4 (Helix) fibers The test results agreed with the results from the previous phases of the experimental program as the specimens with Type 3 fiber showed better performance in this phase of experiment. Type 3 fibers have larger diameter, thus, the higher stiffness and bonding strength. This, in turn, leads to higher mechanical anchorage inducing increase ultimate strength; however, as mentioned earlier, the greater aspect ratio of this type fibers as well as larger size and amount of coarse aggregate limited use of volume of fraction of fiber amount to 1.5%.

Table 6.13 Average Peak Load, Equivalent Tensile Strength in the Fourth Phase

S.N.	Specimen Type	Peak Load	Equivalent Tensile strength	Coefficient of Variation	Compressive strength	Tested Time
		kips	psi	%	ksi	Days
1	PC	38.63	585	5.15	7.12	55-58
2	SFRC -BL-050	38.74	586	4.25	6.47	
3	SFRC- BL-075	43.53	659	6.64	7.38	
4	SFRC -BL-100	44.09	667	3.2	7.68	
5	SFRC -BL-150	53.84	815	5.04	8.18	
6	SFRC -BS-050	37.72	571	4.69	6.9	
7	SFRC -BS-075	38.96	590	3.2	7.61	
8	SFRC -BS-100	40.85	618	2.91	7.82	
9	SFRC -BS-150	47.09	713	3.58	7.99	
10	SFRC-R-075	40.85	618	3.68	7.5	
11	SFRC -R-100	42.67	646	5.26	7.87	
12	SFRC -R-150	43.56	659	2.53	7.97	
13	SFRC -R-200	48.03	727	5.22	8.24	
14	SFRC -H-075	36.51	552	4.58	6.29	
15	SFRC -H-150	39.75	601	5.45	7.07	
16	SFRC -H-200	43.22	654	6.09	7.45	

.

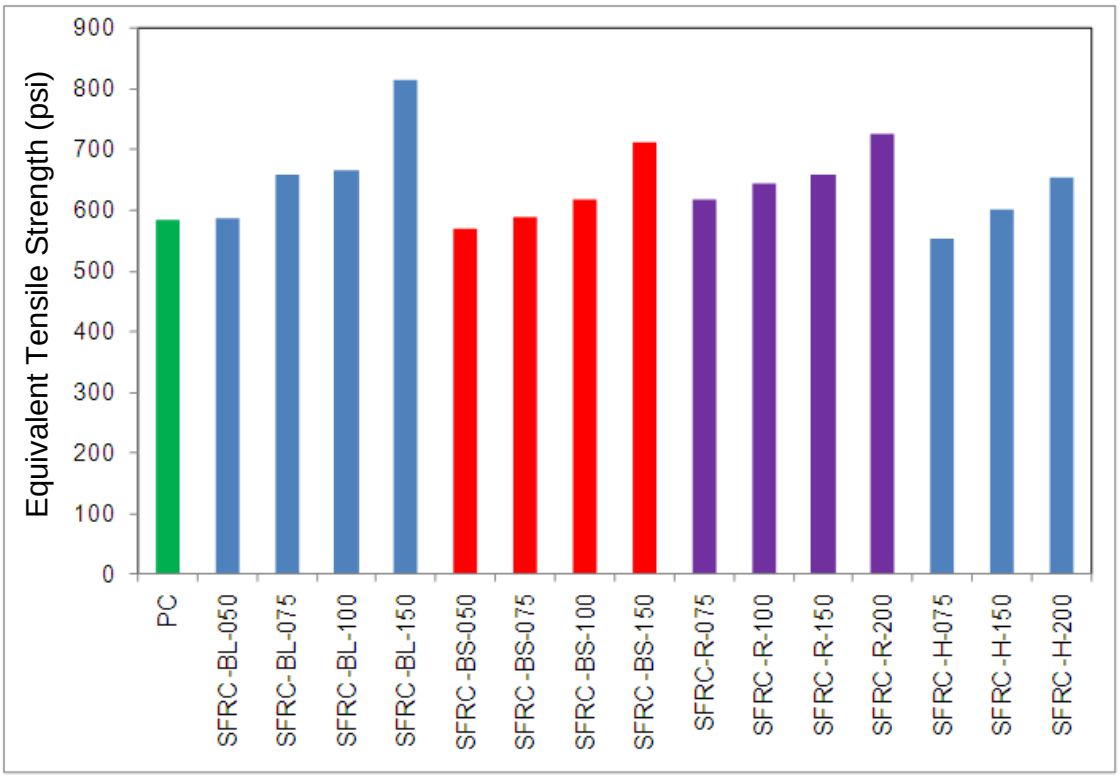

Figure 6.17 Comparisons of Peak Equivalent Tensile Strengths (Fourth Phase)

Table 6.14 Comparison of Peak Strength of SFRC Specimens of Type 3 Fiber and Specimens with Type 1, Type 2 and Type 4 (Helix) Fibers (Fourth Phase)

Volume fraction	Equivalent tensile strength SFRC-BL	Equivalent tensile strength SFRC-R	Compared to SFRC-R	Equivalent tensile strength SFRC-BS	Compared to SFRC-BS	Equivalent tensile strength SFRC-H	Compared to SFRC-H
	(psi)	(psi)	(psi)	(psi)	(psi)	(psi)	(psi)
0.50%	586	-	-	571	15 (2.5% ↑)	-	-
0.75 %	659	618	41 (6.3% ↑)	590	69 (10.5% ↑)	552	106 (16.1% ↑)
1.00%	667	646	21 (3.2% ↑)	618	49 (7.3% ↑)	-	-
1.50%	815	659	156 (19.1% ↑)	713	102 (12.5% ↑)	601	213 (26.1% ↑)

6.5.3 Residual Strength at 0.10 inches Deflection

The residual strengths were appeared in SFRC as expected. The residual strengths for all specimens with different steel fiber are of order 6.9 to 41.6 kips at 0.10 inches of deflections after peak load. For comparison purposes, residual strengths at average deflection of 0.1 inches are shown in Table 6.15 and Figure 6.17

Table 6.15 Comparisons of Residual Strength at 0.10 inches Deflection (Fourth Phase)

Specimen type	Residual strength at 0.1 in. deflection		
	Coefficient of variation (COV)	Load (kips)	Equivalent tensile strength (psi)
SFRC -BL-050	16.79	17.35	263
SFRC- BL-075	21.83	18.79	284
SFRC -BL-100	11.07	20.45	309
SFRC -BL-150	8.99	41.64	630
SFRC -BS-050	13.24	7.65	116
SFRC -BS-075	14.36	12.29	186
SFRC -BS-100	14.36	14.16	214
SFRC -BS-150	7.75	21.85	331
SFRC-R-075	17.27	6.88	104
SFRC -R-100	21.35	7.41	112
SFRC -R-150	11.68	14.92	226
SFRC -R-200	12.74	22.74	344
SFRC -H-075	10.29	11.26	170
SFRC -H-150	16.09	23.4	354
SFRC -H-200	10.37	32.78	496

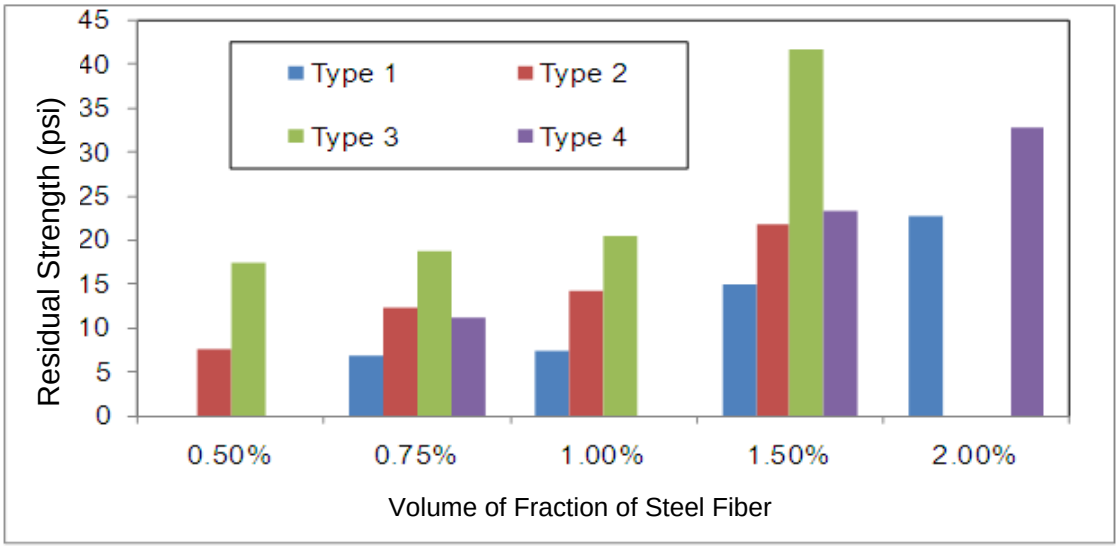

Figure 6.18 Comparison of Residual Strength at 0.10 inches Deflection (Fourth Phase)

As indicated in Table 6.17,SFRC-BL specimens showed higher residual strengths compared to that of SFRC-BS and SFRC-R specimens. SFRC-BL specimen also showed higher residual strength compared to SFRC-H (with Type 4 fiber) for all volume fractions of fibers.

Table 6.16 Comparison of Residual Strength of Specimens with Type 3 and Specimens with Type 1, Type 2, and Type 4 Fibers (Fourth Phase)

Volume fraction	Equivalent tensile strength SFRC-BL	Equivalent tensile strength SFRC-R	Compared to SFRC-R	Equivalent tensile strength to SFRC-BS	Compared to SFRC-BS	Equivalent tensile strength SFRC-H	Compared to SFRC-H
	(psi)	(psi)	(psi)	(psi)	(psi)	(psi)	(psi)
0.50%	263	-	-	116	147 (44.1% ↑)	-	-
0.75 %	284	104	180 (26.6% ↑)	186	98 (34.5% ↑)	170	114 (40.1% ↑)
1.00%	309	112	197 (63.8% ↑)	214	95 (30.7% ↑)		-
1.50%	630	226	404 (64.1% ↑)	331	299 (40.7% ↑)	496	134 (21.1% ↑)

6.5.4 Coefficients of Variation

The average coefficient of variations is of order 4.5% which is lower than in previous phases and very much smaller compared to ASTM C1609 tests. The average COVs for residual strength were also lower as compared to previous phases. It can be justified that double punch test provides reliable test results with relatively less numbers of specimens.

6.5.5 Load versus Deformation response, Toughness and Stiffness

Comparison of the equivalent tensile strength of PC with one Type of fiber with different volume fractions of fiber is shown in Figure 6.19. Figure 6.19 shows load versus deflection curves with different Types of fiber with same volume fraction of fiber. Similar to the previous phase, the figures indicate that which initial stiffness (slope of curves before first crack load or peak load are very close for all specimens (including PC). However, post crack slopes are very different with change in volume of fractions if steel fiber and types of fibers. Long fibers with higher volume fraction have more area under curves (more toughness). These have been analyzed and discussed more in later paragraphs of this chapter.

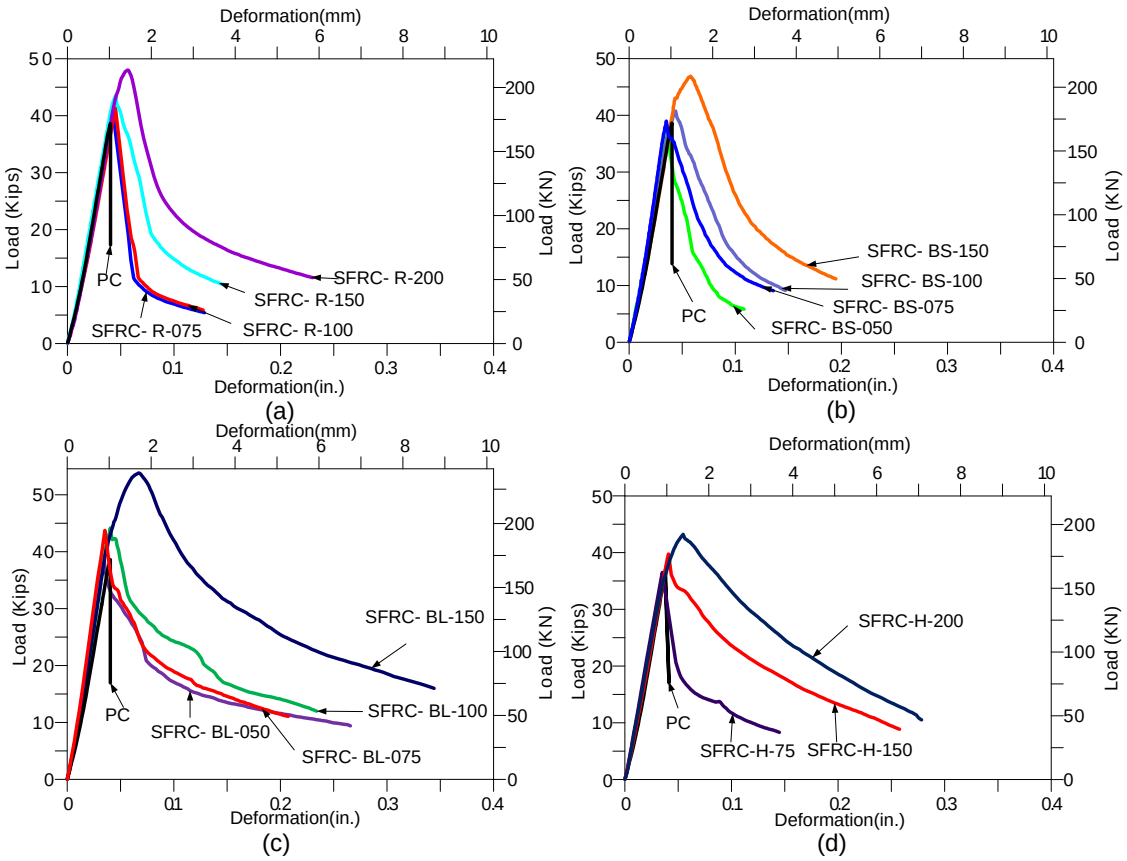

Figure 6.19 Comparisons of PC and SFRC Specimens with Different Types of Fibers (a) SFRC-R, (b) SFRC-BS, (c) SFRC-BL and (d) SFRC-H

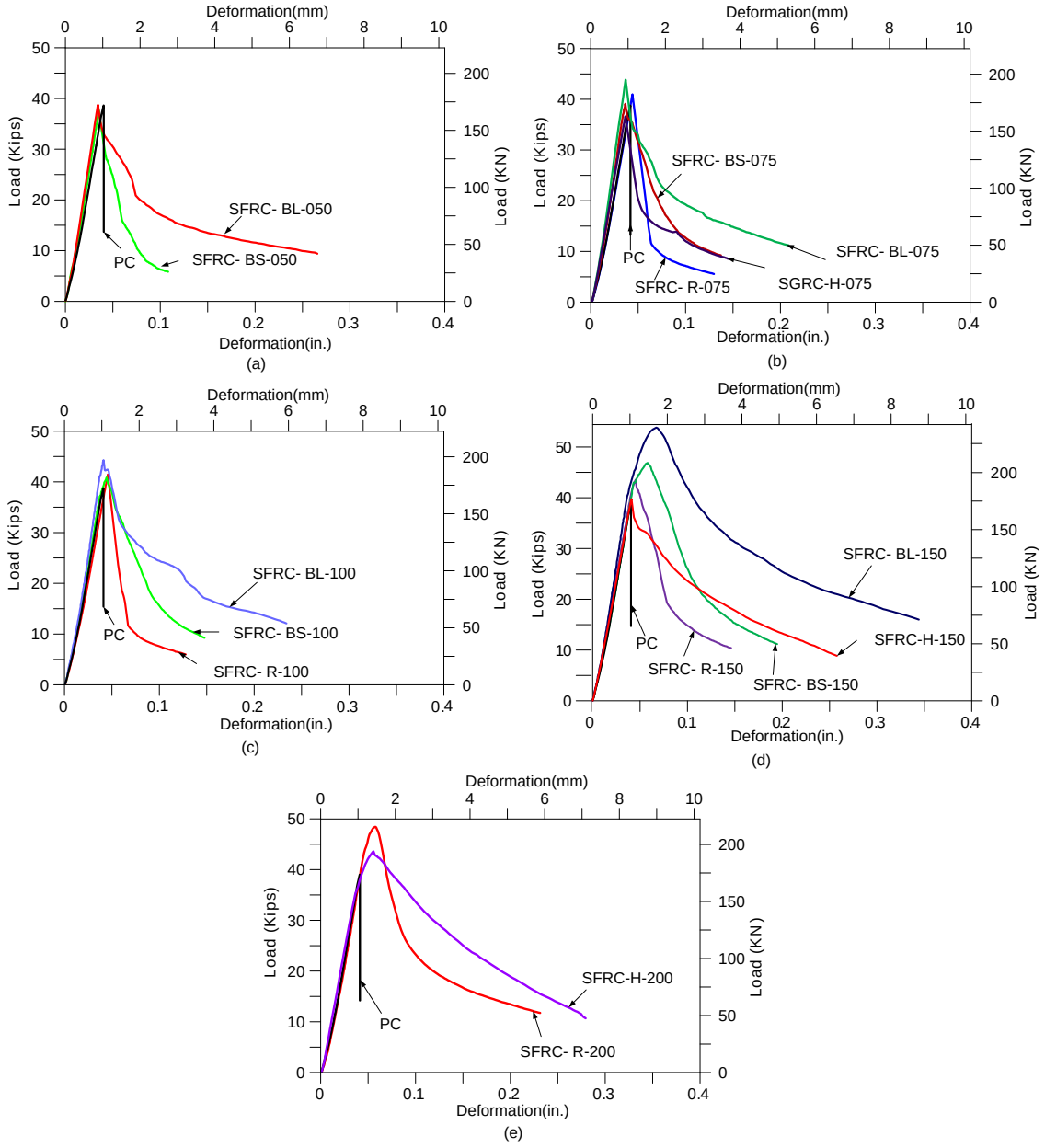

Figure 6.20 Comparisons of PC Specimen and SFRC Specimens with Different Volume of Fraction (a) 0.50%, (b) 0.75 %, (c) 1.0%, (d) 1.5% and (e) 2.0%

Table 6.18 shows the results for toughness from fourth phase of experiment. Specimens with Type 3 fiber (long fiber) have shown higher values of toughness about 3845.8 lb-in. Coefficients of variation for toughness were found in range of 10% for

most of specimens. The specimens with higher volume of fraction (R-200, H-200, and BL-150) have shown slight strain hardening and post crack stiffness. More studies were carried out in next phase regarding this matter.

Table 6.17 Average Toughness at 0.10 Inches Deflection (Fourth Phase)

S.N.	Specimen type	Average toughness at 0.10 in. deflection	Coefficient of variation
		lb-in	%
1	PC	752*	17.99
3	SFRC -BL-050	2246.5	9.92
4	SFRC- BL-075	2343.0	22.7
5	SFRC -BL-100	2598.0	8.56
6	SFRC -BL-150	3845.8	8.35
7	SFRC -BS-050	1437.5	11.7
8	SFRC -BS-075	2081.0	2.38
9	SFRC -BS-100	2318.3	4.25
10	SFRC -BS-150	3047.0	2.46
11	SFRC-R-075	1330.5	14.03
12	SFRC -R-100	1500.3	9.77
13	SFRC -R-150	2819.8	3.62
14	SFRC -R-200	2246.8	9.92
15	SFRC -H-075	1652.0	11.95
16	SFRC -H-150	2823.3	10.43
17	SFRC -H-200	3115.3	5.16

*Note : Toughness value for PC specimen is at end of test (at deflection of 0.05 inches)

6.5.6 Crack Pattern

Figure 6.21 shows the typical photographs from DPT for plain and specimens with different types of fibers with different volume of fraction of steel fiber (0.50% to 2%). In general it was observed that the crack started either from top of bottom of the cylinders. It can be seen from the Figure 6.21 when peak load reached; PC specimen was broken into four pieces where as for SFRC specimens showed several radial cracks

until the test was stopped at one fourth of peak load. Many cracks were developed along the depth of specimens.

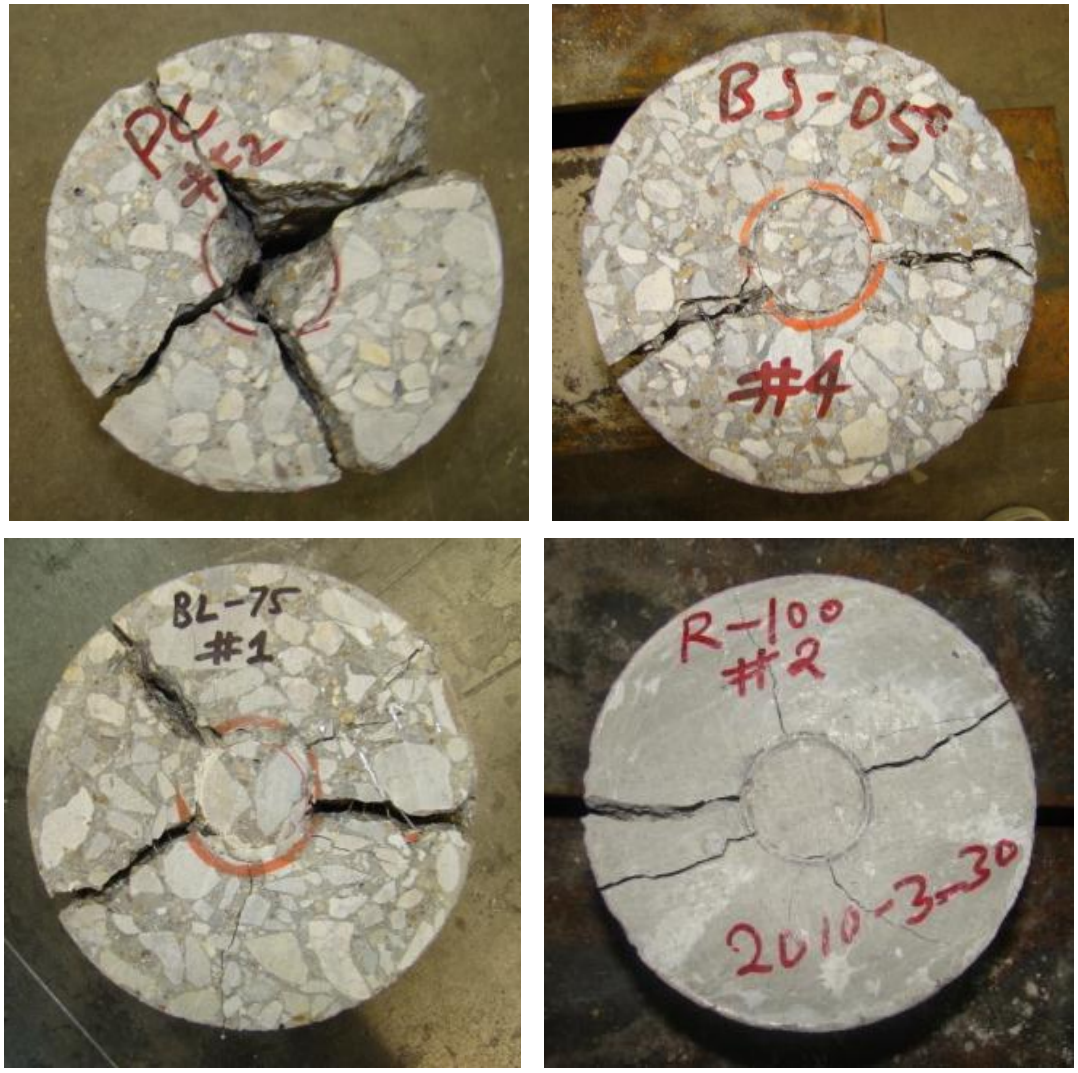

Figure 6.21 Typical Tested Specimens with Various Fiber Volume Fractions Showing Radial Cracks

6.6 Comparison of DPT with other Material Test Methods

The test results from DPT were compared with other material test methods such as third point bending test (ASTM C1609) and direct tensile test (Dog bone test.)

Comparison peak loads and coefficient of variation (COV) between three methods is presented in Table 6.19.

It can be seen from the Table 6.19 that for all three mixes used, the COVs at peak load for DPT are quite low order of 5-7% whereas for third point bending test and direct tensile test these values are more than 10% as high as 26% (ML-075 bending)

Table 6.18 Comparison of Peak Loads and COVs between DPT and Other Material Test Methods

Specimen	At peak load		Compressive strength
	Deflection	Load	
	in.	kips/COV	ksi
Tensile: ML 150	0.01	8.47	7.75
		12.83%	
Bending: ML150	0.014	15.41	
		12.97%	
DPT: ML150	0.05	41.59	
		4.58%	
Tensile:ML075	0.001	8.95	9.23
		14.30%	
Bending:ML075	0.004	10.97	
		26.18%	
DPT:ML075	0.04	38.98	
		6.85%	
Tensile: Hybrid	0.002	9.38	9.72
		23.98%	
Bending: Hybrid	0.018	16.98	
		11.36%	
DPT: Hybid	0.06	43.90	
		5.71%	

Next, Table 6.19 compares the results for residual strength and toughness with their COVs values at specified deflections for all three test methods. The second and the third columns of Table 6.19 present the average residual strengths, toughness and their COVs at a 0.12 inches deformation, which is deformation at which third point bending test was generally stopped.

Table 6.19 Comparison of Residual Strengths and Toughness with COVs between DPT and Other Material Test Methods

Specimen	At same deflection		At various selected deflection	
	Load/COV	Toughness/COV	Load/COV	Toughness/COV
	kips/%	(k-in)/%	kips/%	(k-in)/%
	At of 0.12 in. deflection		At of 0.04 in. deflection	
Tensile: ML 150	2.21	496.60	4.98	242.80
	23.43%	23.37%	17.75%	9.86%
Tensile: ML075	2.417	391.00	3.757	176.67
	68.9%	28.2%	39.5%	29.2%
Tensile: Hybrid	1.983	417.50	4.840	214.20
	64.49%	35.54%	38.80%	35.21%
	At of 0.12 in. deflection		At of 0.06 in. deflection	
Bending: ML150	3.82	1063.70	8.33	715.74
	23.57%	12.77%	15.68%	12.07%
Bending: ML075	3.483	741.40	6.284	490.80
	41.4%	45.5%	43.4%	43.1%
Bending: Hybrid	3.822	1174.96	9.719	801.00
	77.54%	25.63%	31.24%	17.25%
	At of 0.12 in. deflection		At of 0.10 in. deflection	
DPT: ML150	21.50	3045.20	24.25	2629.20
	6.89%	4.54%	6.84%	5.23%
DPT: ML075	10.69	2042.40	12.52	1814.40
	22.1%	15.9%	25.8%	15.0%
DPT: Hybid1	26.26	3337.80	30.90	2750.80
	14.11%	8.74%	11.73%	7.42%

It can be seen from the Table 6.19 the values of COVs for both residual strength and toughness are higher in case bending test and direct tensile test. These values are as high as 65%. Whereas from DPT test, coefficient of variations (COVs) for residual strengths and toughness are quite low except mix (ML-075) 0.75% of volume of fraction. Even for ML-075 the COVs for residual strength and toughness from DPT are lower as compared to than the COVs of similar properties of bending test and direct tensile test.

Table 6.19 also shows that the residual strength and toughness at the different selected deflections such as 0.04 inches for direct tensile test, 0.06 inches for bending test and 0.10 inches for DPT test. These points of deflections are the points where the ratio of peak to residual load is generally more than 50%. As per ACI 316-11 at 0.06 (L/150), this residual load should be 75% of the peak load. As discussed in previous phases of study from various tests with FRC specimens with different mix with different types of fiber and volume fraction of fiber the residual strength at 0.10 inches of deflection is quite important parameter from DPT. Table 6.20 shows that COVs for residuals strength and toughness at these points (selected deflection points) are also lower in case of DPT test as compared to bending and tensile test.

Figure 6.22 shows the comparison of the individual and average load versus deformations curves from DPT test for three different mixes (ML-075, ML-150 and hybrid). For all specimens, the slopes of all curves up to peak loads are similar (not much variation), after peak loads the variation between curves are large. These

variations are more in case ML-075 compare to ML-150 and hybrid specimens. Figure 6.20 (d) shows that with increase in volume of fractions of steel fiber, shape of curves after peak (or first crack) slope (strain softening) increase. Hence, the toughness increases with increase in volume of fraction of steel fibers, which is quite reasonable.

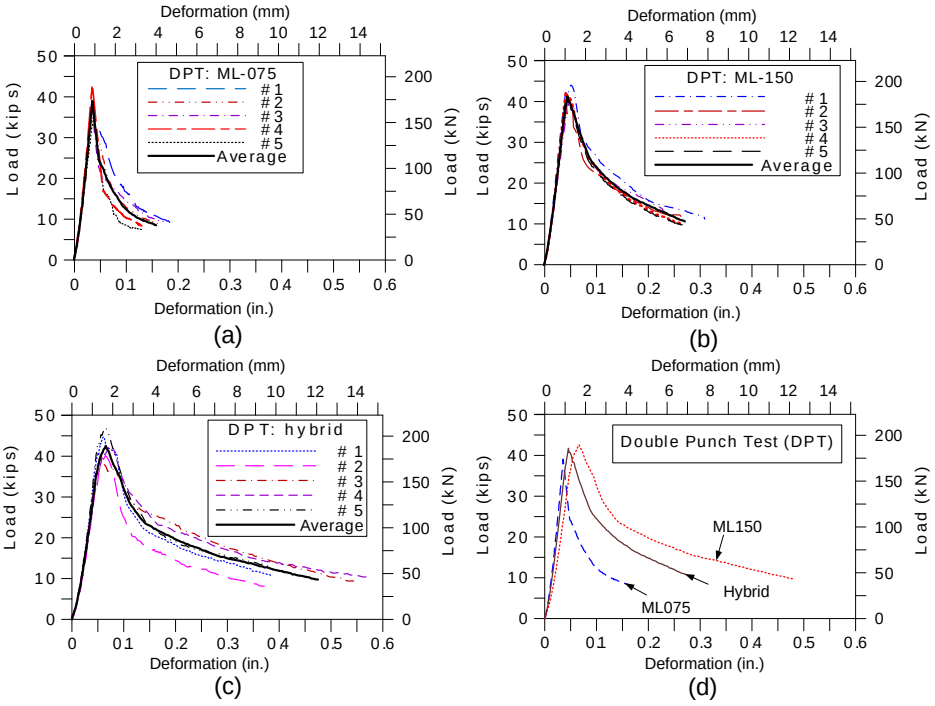

Figure 6.22 Load versus Deflection Curves from DPT Method

Figures 6.23 and 6.24 show the individual and average load deformation curves from third point bending test and direct tensile test. Result showed that the individual curves were greatly scattered from the average curves except for bending test with ML-150. Figure 2.23 (d) shows that residual load at 0.12 inches deflections for all type of specimens (in case bending test) are very close which could not be the case. That may be due to taking the average from very scattered data and not reflecting the true behavior. Figure 6.24 (d) shows that in case of direct tensile test, even though the peak

loads were quite close, the residual strength with higher volume content of steel fiber (hybrid) had shown lower than the specimen with lower volume of fiber content (ML-075). Hence this test is also not reflecting true properties of fiber mixed concrete.

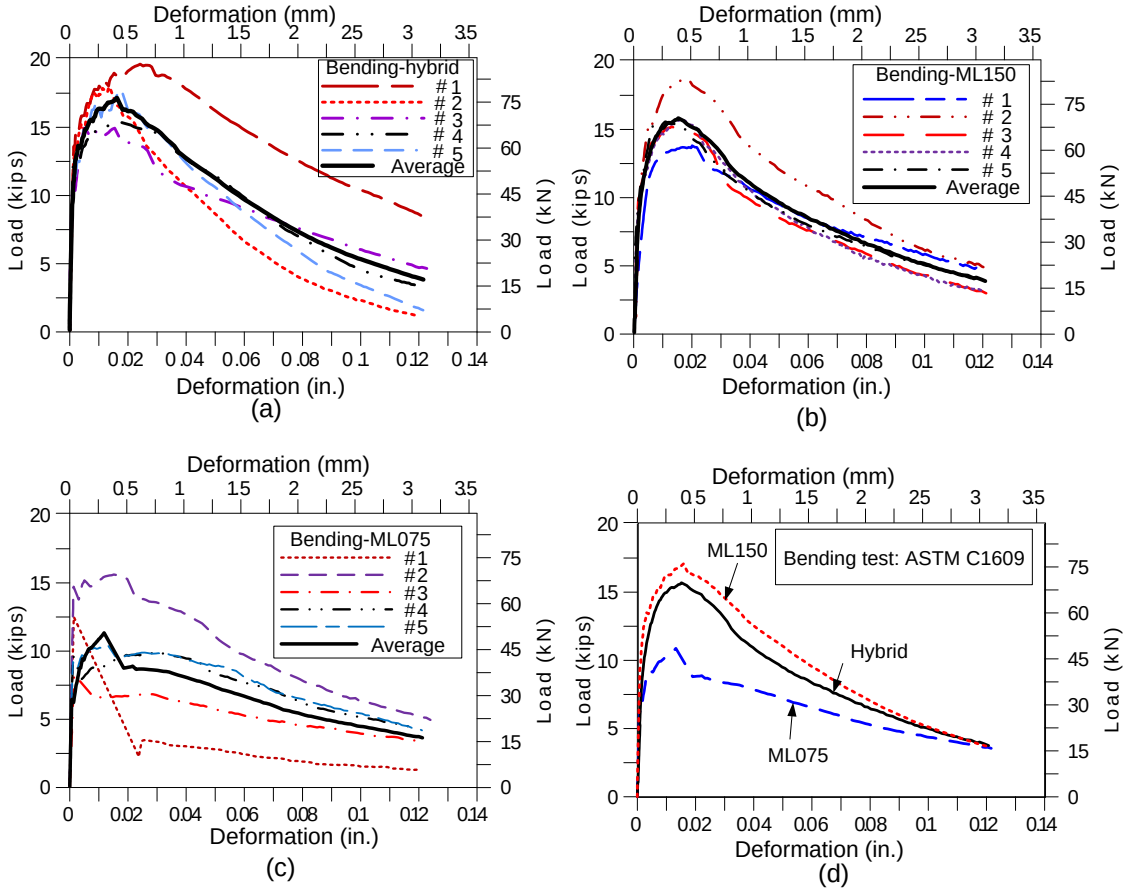

Figure 6.23 Load versus Deflection Curves from Third Point Bending Test (ASTM C1609)

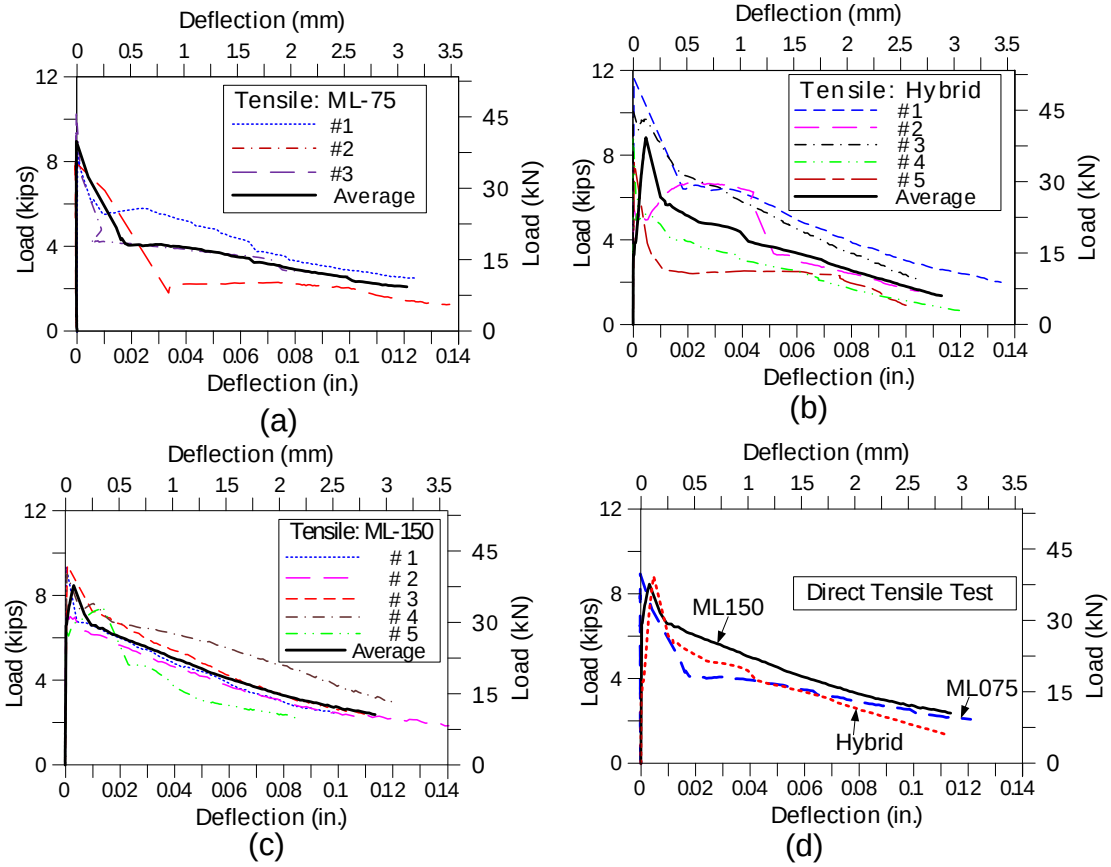

Figure 6.24 Load versus Deflection Curves from Direct Tensile Test (Dog Bone Shaped) Method

Table 6.20shows the comparison of residual loads at 0.06 inches and 0.12 inches of deflections with 90 % and 75 % of peak load from third point bending test. It can be seen from the table that criteria set by ACI 318-08 has not been satisfied any specimens. The corresponding the residual loads at these deflections are quite low compared to corresponding 90% and 75% of peak loads.

Table 6.20 Checking of Residual Strengths for Third Point Bending Test (ASTM C1609) as per ACI 318 -08

Specimen	Load at 0.06 in. (L/300) Deflection	Load at 0.12 in. (L/150) Deflection	90% of 1st peak load	75 % of 1st peak load	Check for ACI 318-08 Section 5.6.6.2	
	(kips)	(kips)	(kips)	(kips)		
ML-150						
ASTM#1	8.24	4.67	12.24	10.20	Not pass	Not pass
ASTM#2	10.60	4.82	16.77	13.97	Not pass	Not pass
ASTM#3	7.46	3.02	12.51	10.43	Not pass	Not pass
ASTM#4	7.54	2.95	14.06	11.72	Not pass	Not pass
ASTM#5	7.80	3.70	13.77	11.48	Not pass	Not pass
Mean	8.33	3.83	13.87	11.56	Not pass	Not pass
ML-075						
ASTM#1	7.49	4.28	10.08	8.40	Not pass	Not pass
ASTM#2	2.25	1.17	11.62	9.68	Not pass	Not pass
ASTM#3	9.29	4.96	13.41	11.18	Not pass	Not pass
ASTM#4	4.98	3.24	7.08	5.90	Not pass	Not pass
ASTM#5	7.30	4.11	8.30	6.92	Not pass	Not pass
Mean	8.57	3.55	10.10	8.41	Not pass	Not pass
Hybrid						
ASTM#1	14.68	8.40	16.90	14.09	Not pass	Not pass
ASTM#2	6.45	1.10	15.90	13.25	Not pass	Not pass
ASTM#3	6.70	3.39	15.81	13.18	Not pass	Not pass
ASTM#4	8.90	4.55	13.36	11.13	Not pass	Not pass
ASTM#5	8.90	3.20	13.67	11.39	Not pass	Not pass
Mean	9.13	4.13	15.13	12.61	Not pass	Not pass

Figure 6.25 shows the comparison of strength versus deformations curves from three type material test methods. Strengths are denoted as bending strength obtained for third point bending test, tensile strength obtained from direct tensile test and equivalent tensile strength obtained from double punch test. It can be seen from the figure that the bending strength is higher than direct tensile strength and equivalent tensile strength by

all three mixes; however, the direct tensile strength and equivalent tensile strength are quite close to each other.

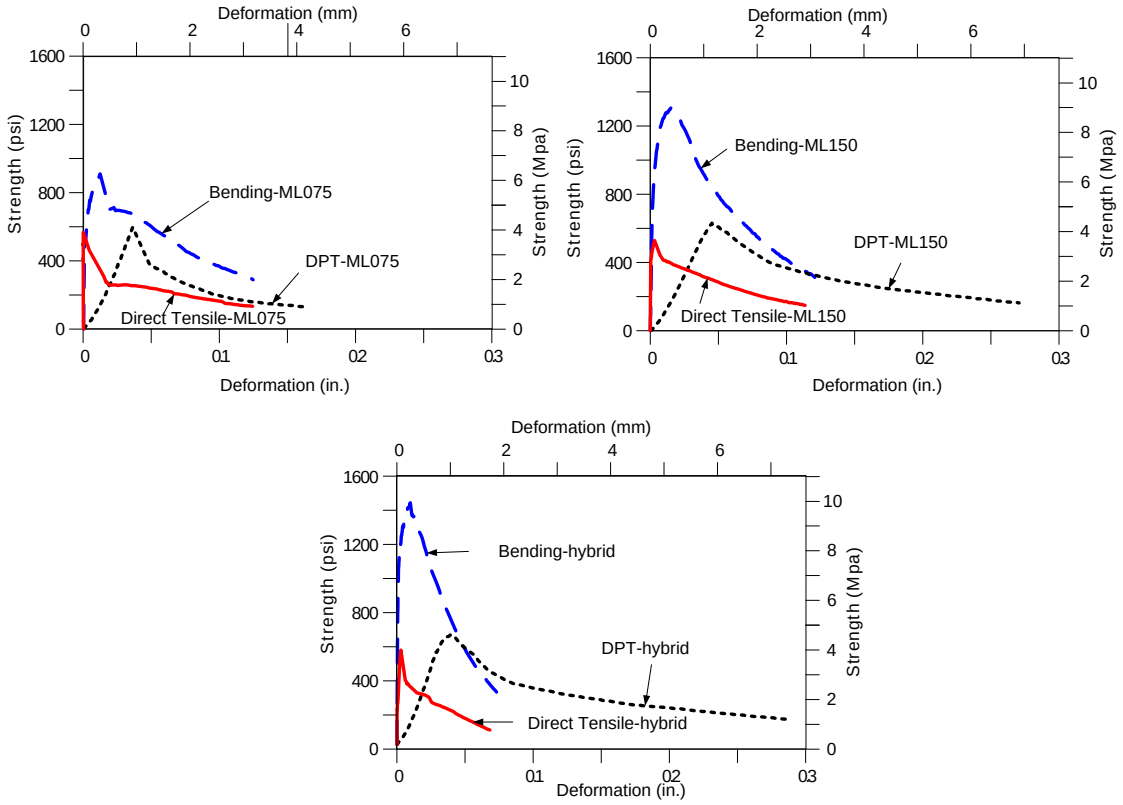

Figure 6.25 Comparisons of Strengths between Three Material Test Methods

Figure 6.26 shows the comparison of load versus deflection curves of bottom and top portion of cylinders from DPT. It can be seen that the load deflection curves for top portion are more scatter compared to load deflection curves for bottom portion. Coefficient of variations of peak strength, residual strength and toughness are 4.65%, 12.32% and 9.04% respectively for bottom portion whereas those values are 7.27%, 14.9% and 11.13% for top portion. One of the reasons behind this may be due settlement of more fibers in bottom portions of molds during time of mixing (while vibrating).

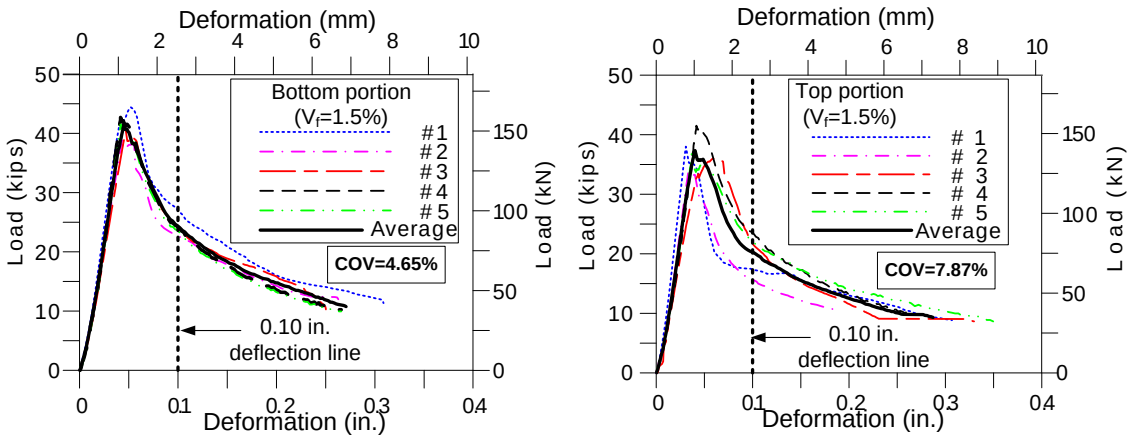

Figure 6.26 Comparison of Load versus Deflection Curves between Top and Bottom Portion Cylinders Used in DPT Methods

6.7 Results from Post Crack Investigation

As discussed earlier it has been shown from different phases of experimental study that DPT test method can show better performance in terms of peak and residual load as compared to other material test method such as third point bending test and direct tensile test. In order to evaluate the further post cracking performance some more DPT tests with carried out as discussed Chapter Four. The summary of the test results in terms of peak and residual strength with COV are presented on Table 6.22. Once again it can be seen from table that COV are order of 6% for peak strength and order of 10% for residual strength except for HYB4 and R-075. Similarly COV for toughness for all specimens were very low. However for the HYB1 specimens the peak occurred at 0.20 inches of deflection and first crack occurred at near about 0.10 inches deflection.

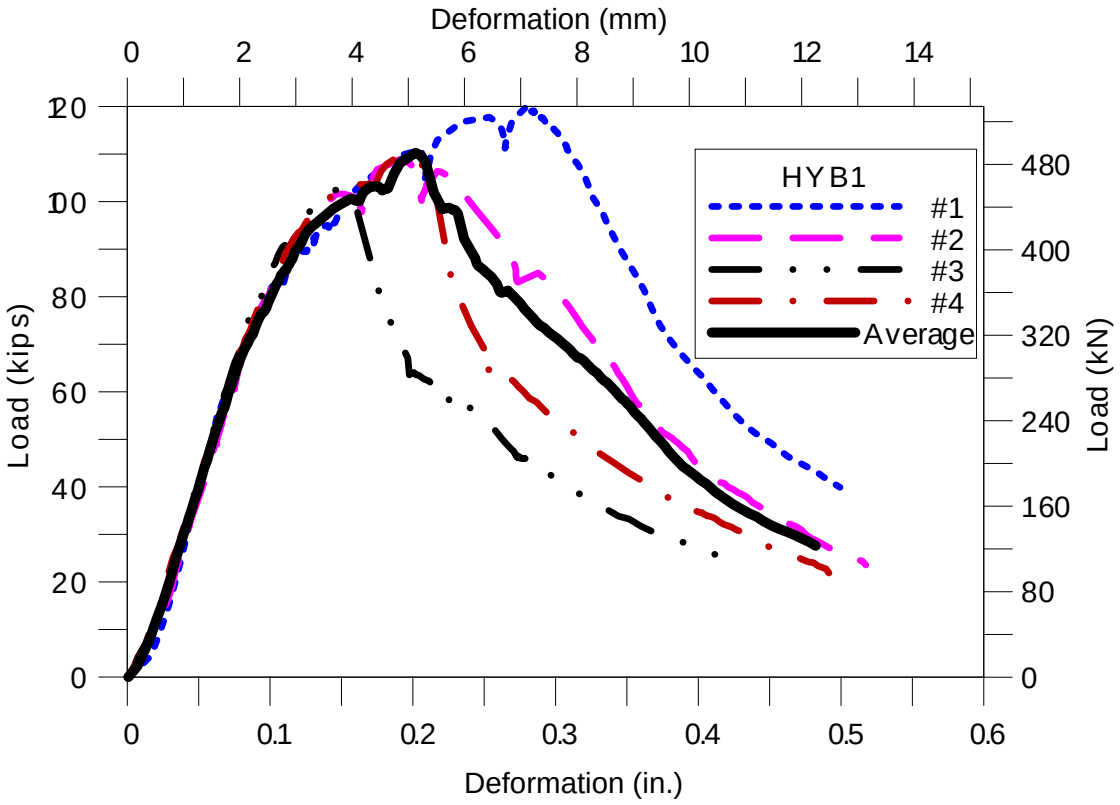

Figure 6.27 Load versus Deflection Curves from DPT with HYB1

Figure 6.27 shows the load versus deflection curves for cement mortar specimen (HYB1) with 3% of mixed steel fiber (Type 5: twisted and Type 6: micro maccaferri). It can be clearly shown that there is a strain hardening after first cracks. Larger numbers of small cracks were developed during test. This may the presence of large quantity of the short and tiny steel fibers. As the compressive strength as well as the peak strength were found very high (Table 6.21) as compared to other specimens, achievement of high performance FRC could be possible with use of the twisted and tiny steel fiber in large volume.

Table 6.21 Summary of the Results from Post Crack Evaluation Study of DPT

Specimen	Com. strength	AT peak load			At 0.10 in. deflection		
		Load	Deflection	Tensile strength	Load	Tensile strength	Toughness
		COV	COV	COV	COV	COV	COV
	(ksi)	(Kips)	(in.)	(psi)	(Kips)	(psi)	lb-in
HYB1	12.14	110.26	0.2	1668.4	84.76	1282.6	4110.25
		6.64%	28.10%	6.64%	4.98%	4.98%	3.23%
HYB2	7.375	46.44	0.08	702.8	42.31	640.2	2731.75
		5.48%	4.84%	5.48%	7.78%	7.78%	4.73%
HYB3	7.845	44.5	0.07	673.4	34.06	515.5	2395.5
		5.58%	9.04%	5.58%	8.87%	8.87%	10.16%
HYB4	6.03	38.24	0.08	578.6	26.57	402.1	2180.75
		4.77%	9.74%	4.77%	20.77%	20.77%	3.14%
ML-075	7.047	38	0.06	574.9	17.02	405.8	1821.75
		6.24%	2.64%	6.24%	10.94%	10.94%	3.99%
R-075	7.52	36.92	0.07	558.7	10.84	470.7	1594.08
		8.48%	9.27%	8.48%	15.02%	15.02%	7.27%

Figure 6.28 compares results between two hybrid mixes. First one (Hybrid) was the specimens having equal volume of fraction (0.75% Type 5 +0.75% Type 6) for both types of fiber and second one (HYB2) was specimens with more percentage of small twisted steel fibers (0.5% Type 5 +1% Type 6) (see Chapter Four). The both specimen has same mix ratios but different hybrid steel fibers compositions, later one showed higher peak and residual strength with less scatter curves. In terms of strain hardening both showed similar trends. However, HYB2 showed better strain softening and toughness (area under curve) as compared to Hybrid.

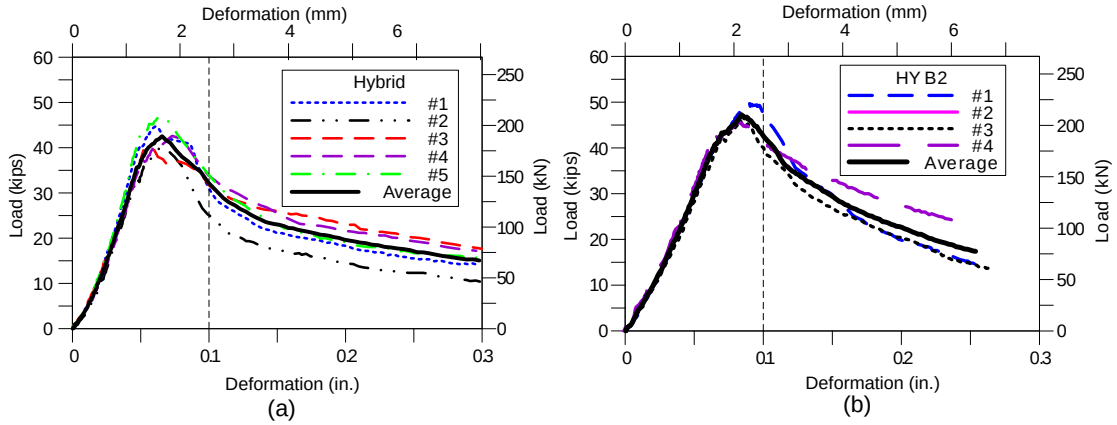

Figure 6.28 Comparison of Load versus Deflection Curves between Two SFRC Specimens (a) Hybrid (0.75% Type 5 Fiber + 0.75 Type 6 Fiber) (b) HYB2 (0.50% Type 5 Fiber +1% Type 6 Fiber)

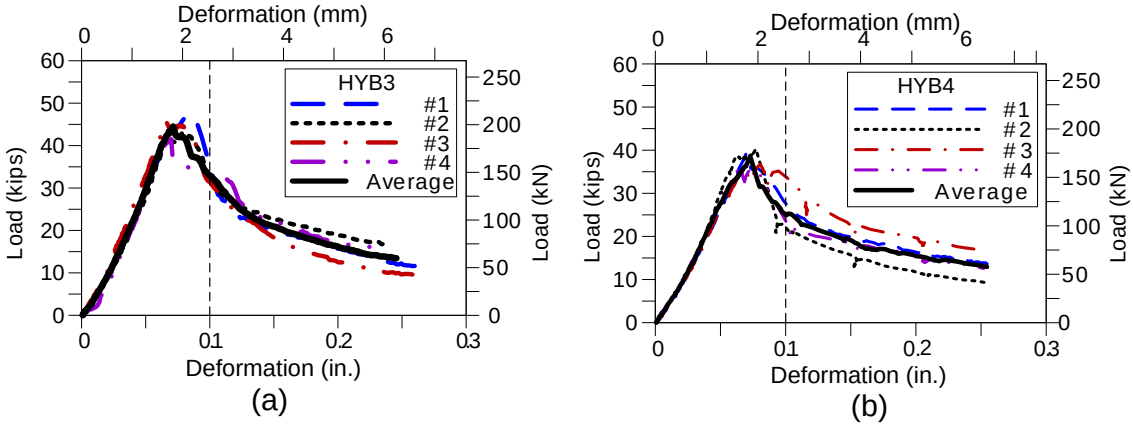

Figure 6.29 Comparison of Load versus Deflection Curves between Two Hybrid Specimens with Same Type of Steel Fibers and Same Volume of Fraction with Different Concrete Mix (a) HYB3 and (b) HYB4

Figure 6.29 compares the results from two specimens with same type and volume of fraction of steel fiber (mixed fiber, see Chapter Four for detail). First one was specimen with good mix (low water cement ratio and small aggregate size) with $f_c^{'} = 7.85 ksi$ concrete and second one was with relatively poor mix (high water cement ratio and large aggregate size) with $f_c^{'} = 6.03 ksi$ concrete. Figure 6.27 shows that HYB3 gave better performance in terms of peak and residual strength and their

variations. Load deflections curves were also less scatters in case of HYB3 as compared to HYB4.

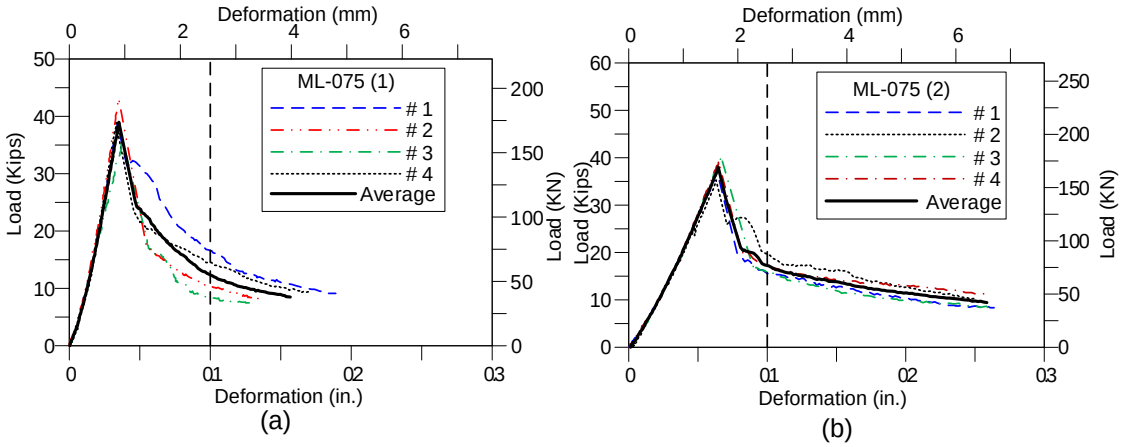

Figure 6.30 Comparison of Load versus Deflection Curves between Two Specimens with Same Concrete Mix with Different Methods of Preparation: (a) ML-075(1) and (b) +ML-075(2)

Figure 6.30 compares the results from two specimens with same type and volume of fraction of steel fiber and same mix of concrete (see chapter 4). First group of specimens were compacted with table vibrator. The second group of specimen was compacted only with tamping rod. It can be seen from the figure that ML-075(1) specimen showed larger stiffness but much scatters post cracking results. However, ML-075(2) had much less scatter post cracking results. But it has lower stiffness. The reason behind these may be due to less settlement of fibers in bottom part of the cylinder as the as compaction was less in ML-075(2) specimens as compare to ML-075(1).

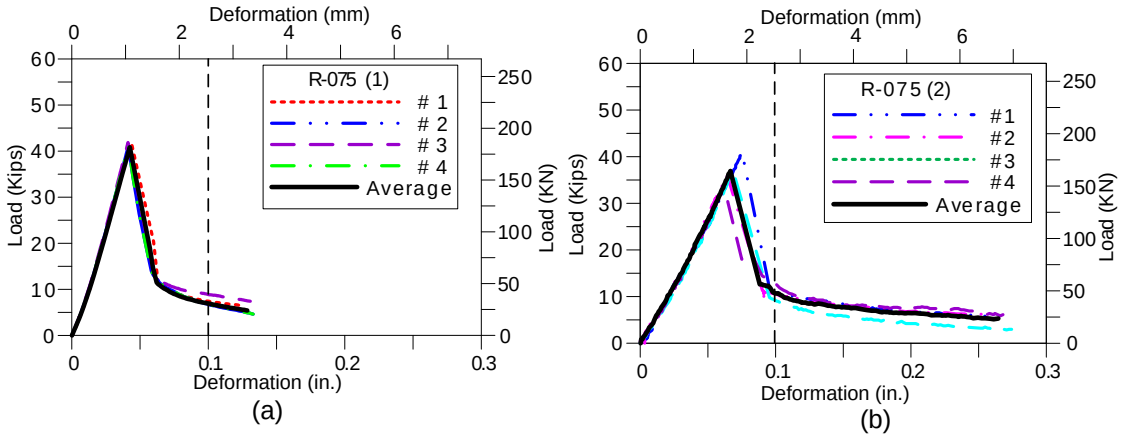

Figure 6.31 Comparison of Load versus deflection Curves between Two Specimens with Same Volume of Fraction of Steel Fiber Tested in Different Capacity of Testing Machine: (a) R-075(1) and (b) R-075(2)

Figure 6.31 compares the results from two set of specimen with Type 1 (Royal) steel fiber (R-075) with same volume of fraction of steel fibers with different testing machine. R-075(1) specimens was compacted with plate vibrator and tested in 60 kips compression machine while R-075(2) specimen was compacted with tamping rod and tested in 400 kips compression machine. It can be seen from the figure that R-075(1) has shown larger stiffness and peak strength as compared to R-075(2). However, latter one has slightly more residual strength.

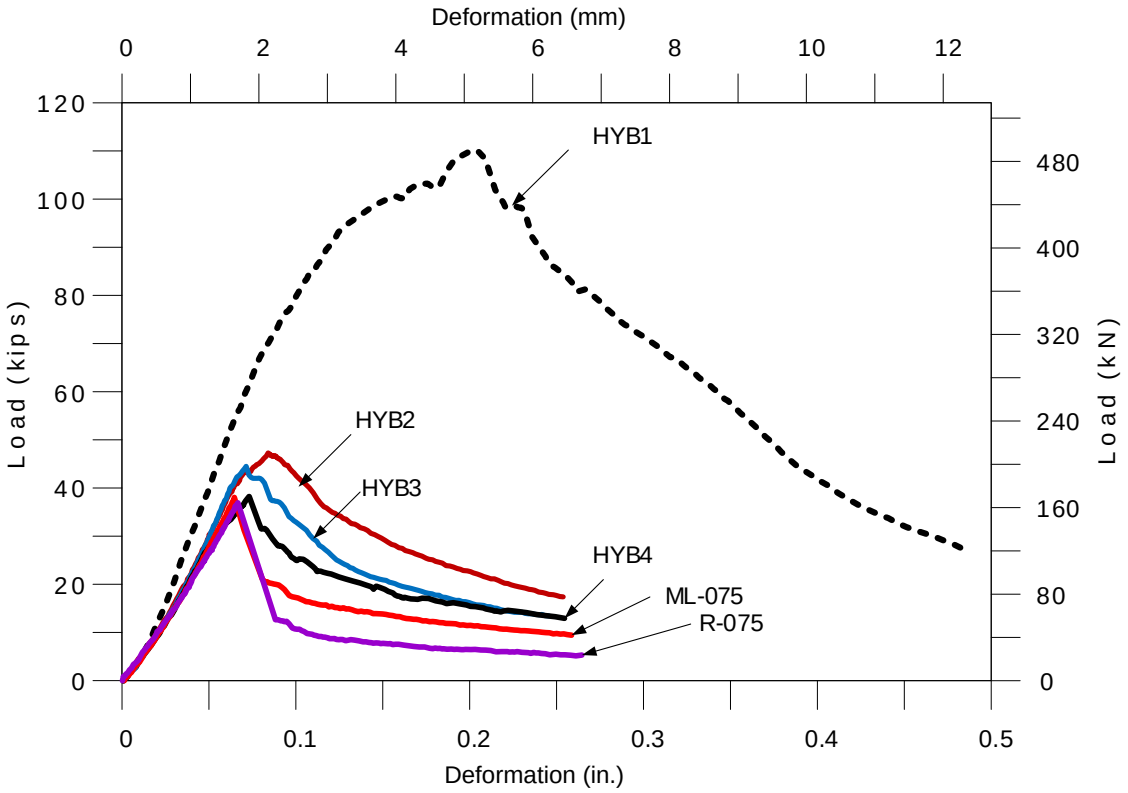

Figure 6.32 Comparison of Stiffness of Different Concrete Mixes with Different Types Fibers

Figure 6.30 shows that the pre peak (or pre crack) stiffness of the different types mixes. Mix with high compressive strength HYB1 (SFRC mortar mix) showed larger stiffness compared to mixes. Initial stiffness for other specimens with concrete mix are very close to each other compared to mortar mix. Some variation between each type of SFRC mixes were also found depending types of mixes.

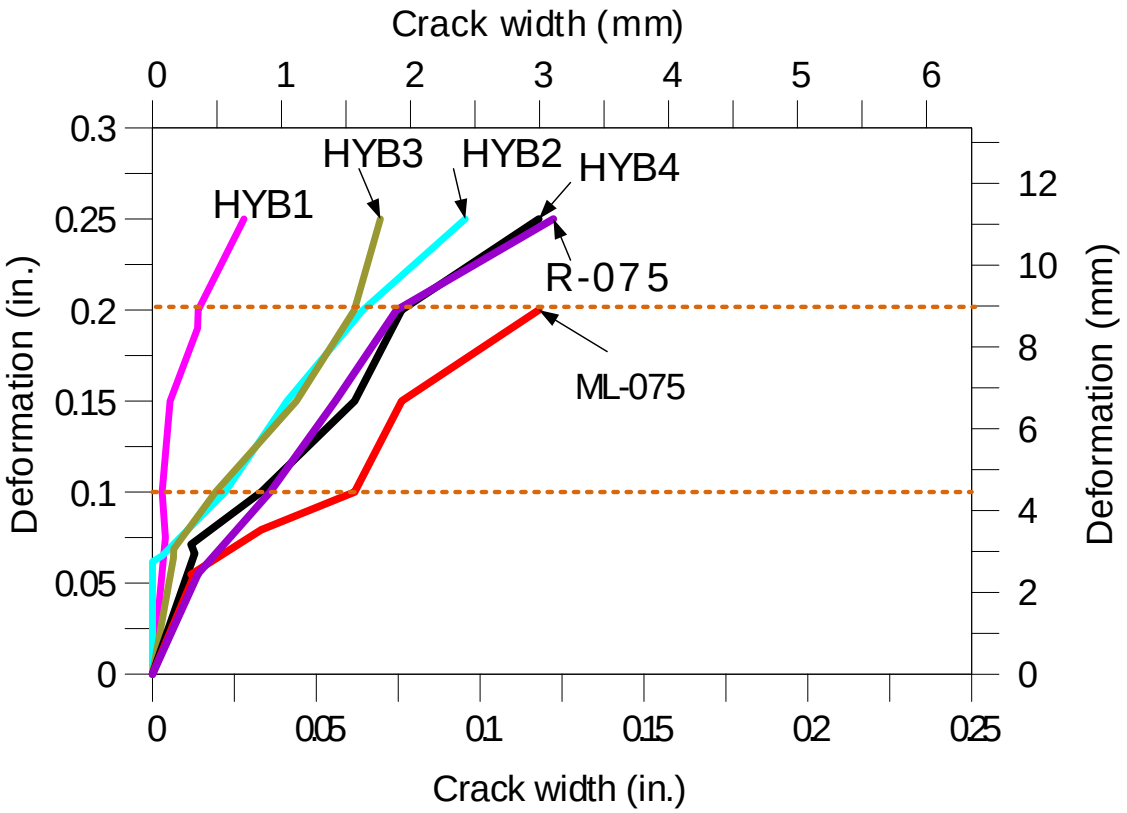

Figure 6.33 Comparison Average Total Crack Widths at Different Deflection for Different Specimens

Figure 6.33 shows the deflection versus average total crack width for different specimens. It can be seen that the HYB1 specimen having 3% volume fraction of steel fibers showed small crack width at all level of loading. HYB2, HYB3, HYB4 all having similar volume of fraction (1.5%) showed larger crack width compared to HYB1, but lower than the ML-075 and R-075 specimens which had low volume of fraction of steel fiber (0.75%). Among HYB2, HYB3 and HYB4, HYB2 showed slightly smaller crack width as it had slightly more volume of twisted fiber (1%) as compared to HYB3 and HYB4, which contained 0.75% of twisted fiber. Other specimen ML-075 and R-075 also showed larger crack width among all but are similar to each other. The results

shows that use small tiny steel fibers controlled in widening the crack width as this type of fiber can cover more space within the matrix and bridge the crack in more places.

As discussed in Chapter Four six more cylinders were tested by DPT method and results are shown Table 6.23. Since peak loads were occurred beyond 0.10 inches of deflection the residual load were compared at 0.20 inches of deflection in contrary of previous phases. For both the top and bottom portion of the cylinders were compared separately, it was noticed that the COVs for both peak are found around 3-6% and residual load are 9-12% which are quite reasonable as compared to previous phases results. This improvement may be due use of hand compaction instead of using plate vibrator. The use of viscous admixture (VMA) probably did not let the fiber settle down quickly.

Table 6.22 Summary of Results from More DPT

Specimen	AT peak load			At 0.20 in. deflection	
	Load	Deflection	Tensile strength	Load	Tensile strength
	(Kips)	in.	(psi)	(Kips)	(psi)
#1 Bottom	65.57	0.12	992.2	40.22	608.5
#3 Bottom	65.84	0.128	996.3	44.17	668.4
#4 Bottom	69.30	0.132	1048.6	48.48	733.6
Mean	66.90	0.126	1012.4	44.29	670.2
STDEV	2.08	0.007	31.5	4.13	62.6
COV	**3.11%**	**5.72%**	**3.11%**	**9.33%**	**9.33%**
#2 Top	64.08	0.120	969.6	25.87	391.5
#4 Top	62.99	0.116	953.1	29.74	450.0
#6 Top	59.37	0.106	898.4	23.49	355.5
Mean	62.14	0.114	940.4	26.37	399.0
STDEV	2.46	0.007	37.3	3.15	47.7
COV	**3.96%**	**6.33%**	**3.96%**	**11.96%**	**11.96%**

6.8 Discussions on Results from DPT Method

6.8.1 The First Three Phases of Experiment

The first three phases of study of DPT was concentrated on validation of DPT methods in terms of peak and residual strength. The tests were carried out with different volume of fraction from 0 to 2% and with three types of steel fiber. Use of simple 60 kips compression testing machine were successfully used for implementation of DPT method. Specimens with volume of fraction of fiber (V_f) less than 0.50% have not shown much effect in concrete. So FRC with V_f = 0.50% cannot be usable for tensile strength. For V_f more than 1.5% specially for long fiber (Type 3), there has been found potential problem in mixing. It should be noted that specimen size (6 × 6 inches

cylinder) may not be adequate to insure uniform distribution of fiber especially with long fibers (2.4 inches length). It could be the reason why the longer fiber did not always show the highest ultimate tensile strength. Additionally, the amount and the size of aggregate, which were also mentioned in previous study, possibly affected fiber distribution especially longer fiber.

It should be also noted that the results from these three phases of study were based on early strength (about 24 to 48 hours) of the specimens, and it is difficult to control strength in early age concrete.

The Fibers with double bend and hooked at end looked better than the fibers with single bend and hooked at ends as the SFRC specimens with Type 2 and Type 3 have shown larger peak and residual strength as compared to specimens with Type 1 steel fiber. In general, specimens with longer fiber (Type 3) have shown better performance compare to specimens with short fibers (Type1, and Type2). Similarly, increased in V_f of steel fibers have increased performance of SFRC as BL-150 (with Type 3 fiber), has shown higher peak load and residual load.

By comparing peak strength and residual strength at 0.1 inches of deflection, it can be suggested that in order to have equivalent performance, the amount of fibers should be used is approximately: (Royal: Short Bekaert: Long Bekaert) = (2.4: 1.55: 1.0).

There were lots of variations in post peak slope as well as elastic range slope in the first phase were 10 numbers of samples were used. In contrast, those variations were

significantly reduced in the third phase even with reduction of the sample to four. This may be due to the improvement in testing technique as discussed earlier; load was applied up to 2 kips and then unloaded to 0.5 kips such that preload was consistent with 1st and the second phase on the third phase as 500 lb. The improvement is able to make the double punch test be more reliable test method. PC specimen was usually broken into 3 or 4 pieces once cracked and reached to peak load; however, numbers of radial cracks were found developed in case of SFRC specimens. Cracks were generally developed top part (near loading point) and propagated to lower depth of the cylinder (specimens). Some large cracks with other smaller cracks were occurred.

6.8.2 The Fourth Phase of DPT

In the fourth phase of DPT, lots of improvement was found in case of residual strength. As the test was carried out after 28 days of having full compressive strength for all specimens, the coefficient of variation for both peak load and residual load were found lower comparing to previous phases (Table 6.24). COVs for residual strength at 0.10 inches of deflection were found less than 15%, which is still lower than other tests (discussed later). Besides small strain hardening for some specimens and good strain softening were seen in this phase. BL-150 and H-200 (with 2% new type of steel fiber, helix) showed some strain hardening.

Table 6.23 Comparison of Average Coefficients of Variations among Four Phases of study

Type of Specimen	At Peak Load				At Residual Load (0.10 in. Deflection)			
	Phase 1	Phase 2	Phase 3	Phase 4	Phase 1	Phase 2	Phase 3	Phase 4
PC	5.20%	12.7%	5.20%	5.15%	-	-	-	-
SFRC R-Type 1	5.72%	9.90%	4.05%	4.17%	11.63%	11.93%	13.66%	15.76%
SFRC BS-Type 2	5.17%	7.34%	4.48%	3.73%	14.76%	19.83%	16.86%	14.93%
SFRC BL-Type 3	8.34%	6.17%	4.54%	4.54%	20.00%	21.40%	25.92%	14.36%
SFRCHX-Type 4	-	-	-	5.37%	-	-	-	12.25%

6.8.3 Comparison with other Material Test Methods

Double punch test method (DPT) was compared with the third point bending test (ASTM C1609) and the direct tensile test (dog bone test). The test results have clearly shown that peak strength obtained from DPT have very low coefficient of variation (COV) about 5% as compared to COVs for peak strength from bending and direct tensile test, which have COV more than 10% (Table 6.24). Though COVs for residual strength from DPT were more than 10%, these values still were much less (less than half) than COVs for residual strength and toughness, from bending and direct tensile test. COVs for toughness from DPT was less than 10%, which much less than bending test and direct tensile test methods.

Table 6.24 Comparison of Average Coefficients of Variations among Three Material Test Methods

Type of test	Peak load	Residual strength	
		Strength	Toughness
Direct tensile test (DOG bone test)	17.8%	32. 0%	24.8%
Bending test (ASTM C1609 test)	16.8%	32.0%	24.2%
Double punch test (DPT)	5.71%	14.8%	9.21%

Similarly, load deformation curves from bending test and direct tensile tests were found more scatters from the mean curve.

From bending test results (Table 6.25) clearly indicated that the criteria set by ACI 318-11 in order to use the steel fiber in concrete has not been satisfied for non of the specimens. The reason behind this may be due the scatter residual values obtained from the test.

Table 6.25 Checking of Average Residual Strengths for Third Point Bending Test (ASTM C1609) as per ACI 318 -11

Specimen	Load at 0.06 in. (L/300) Deflection	Load at 0.12 in. (L/150) Deflection	90% of 1st peak load	75 % of 1st peak load	Check for ACI 318-08 Section 5.6.6.2	
	(kips)	(kips)	(kips)	(kips)		
ML-150	8.33	3.77	13.87	11.56	Not pass	Not pass
ML-075	8.57	3.63	9.7254	8.1045	Not pass	Not pass
Hybrid	2.98	2.69	15.11	12.59	Not pass	Not pass

In direct tensile test in spite of provided reinforcement (wire mesh) in transition portion, it was difficult to locate the cracks within gauge length (Figure 6.34). Hence, data from all specimens could never have been utilized.

On top of theses, both bending test (ASTM C1609) and direct tensile test were carried with closed loop servo controlled machine. Hence, the time required to carry out test was always greater as compared to DPT, where 60 kips compression was used. Similarly, size and preparation of DPT specimens (two half of 6 ×12 inches cylinders) was quite easy as compared to other two methods.

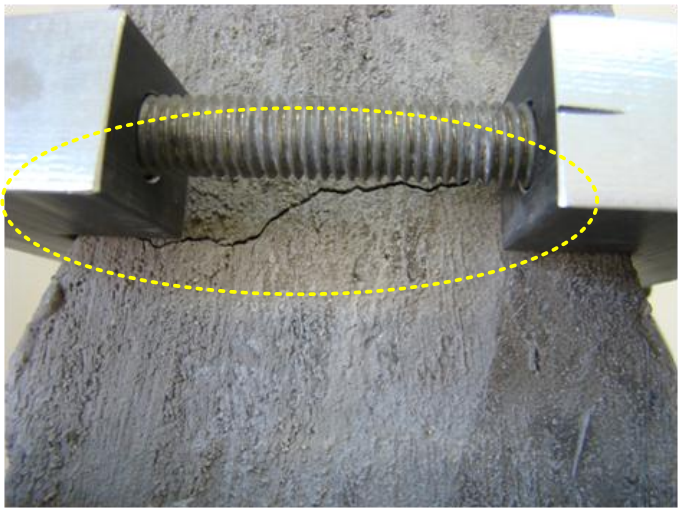

Figure 6.34 Example of Problem of Locating of Tensile Cracks in Direct Tensile Test (Dog Bone Test)

6.8.4 Post Crack Behavior

From the last phase of experimental studies as discussed earlier it can be concluded that DPT method can applicable to determine various post cracking parameters such as strain hardening, strain softening, and toughness. The concrete mixes with mixed fibers (hybrid) long fiber with twisted and micro fiber could considerably control the crack widening and could also increase the strength and ductility. The SFRC with larger volume of fiber twisted and micro fiber had shown high equivalent tensile strength and better strain hardening in order to achieve the high performance concrete. The various test results from the last phase of DPT program has also shown the capability of DPT test method to distinguish between good mix and poor mix by means of stiffness, effect of compaction during preparation specimens and effect of use of larger and small capacity of the compression machines.

CHAPTER 7

ANALYSIS OF EXPERIMENTAL RESULTS AND FE ANALYSIS

7.1 General

This Chapter deals with the further analysis of the results obtained from large scale prestressed beam test specially for SFRPC beam with larger longitudinal steel ratio (SFRPC#2-1) and comparison with results obtained from finite element analyses make some recommendation for the modification in the limit for reinforcement design for a partially prestressed flexure member with steel fibers.

7.2 Discussion on Results from Experimental Investigation

Figure 7.1 shows the load versus deflection curve, load versus strain at tensile steel and the load versus strain at compression fiber of concrete section of the SFRPC #2-1 specimen. It can be seen that yielding of the bar started (ε_t >0.002) around load of 240 kips, the corresponding strain in concrete at compression fiber was about 0.005, which more than the 0.003 (theoretical ultimate concrete strain at crushing). As per test results the strain value in concrete at compression zone reached to a value of 0.003 around load of 145 kips, the corresponding value of strain at tensile steel was only 0.001. This showed no bar was yielded at that time. The concrete at compression fiber was also not crushed. The crushing of concrete was occurred only after a load of 275 kips and corresponding strains at tensile steel at that load was more than 0.002, which means the bar yielded at started to take the load. However by this time the ultimate

compression strain at concrete already crossed the theoretical value of 0.003 (crushing concrete strain). This clearly indicated that crushing in concrete occurred with compressive strain more than 0.003. After peak load around load 320 kips the strain at tension steel reached to 0.0084. This increased ductility and failure occurred as tension-controlled section.

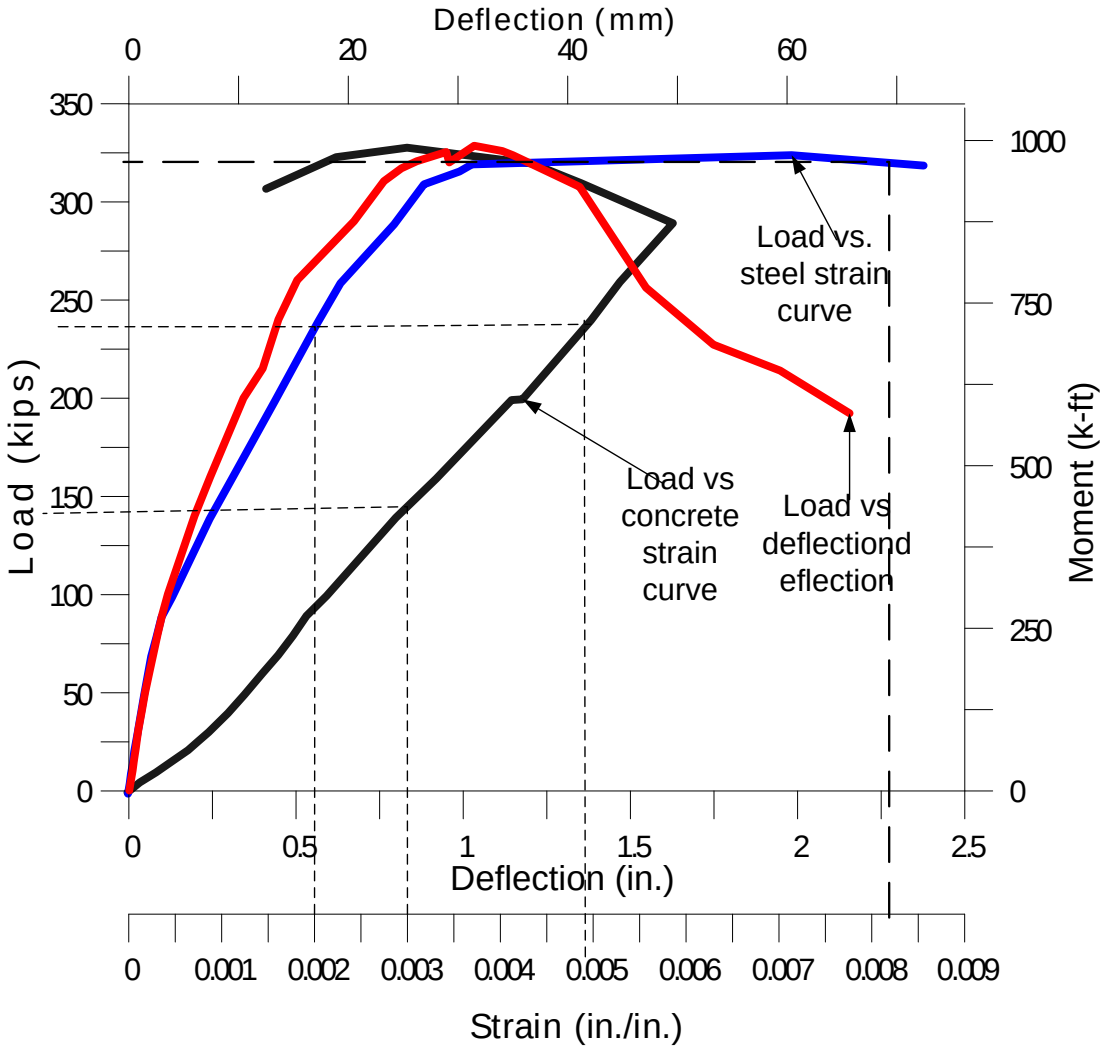

Figure 7.1 Load versus Deflection and Strsin Curves for SFRPC #2-1 Specimen

7.3 Nonlinear Finite Element Analyses for Large Scale Prestressed Beams

7.3.1 General

A nonlinear finite element (FE) analysis was carried out for the large scale beam with dimension and material properties similar to the tested large scale prestressed beam (SFRPC#2-1) and results are compared to tested results. The FE modeling and analysis was carried out using VecTor2, a two-dimensional nonlinear finite element analysis program for reinforced concrete structures developed at the University of Toronto. VecTor2 is based on the Modified Compression Field Theory (MCFT) by Vecchio and Collins [1986]), and the Disturbed Stress Field Model (DSFM) by Vecchio (2000). The use of VecTor2 for the numerical analysis of two-dimensional reinforced concrete membrane structures is facilitated by the pre-processor Form Works [Wong, 2002]. Augustus, the post-processor for VecTor2, (Bentz, 1996-2007), was used to observe the analysis results. VecTor2 is a user-friendly and capable of modeling two-dimensional reinforced concrete membrane structures under different type of loading condition such as monotonic, cyclic and reversed cyclic. VecTor2 is able to consider the post-cracking influences on concrete, such as compression softening, tension stiffening, and tension softening. Most of the finite element modeling tools available for nonlinear analysis of reinforced concrete structures require definition of the failure mechanism or are dependent on empirical values obtained through similar experimental tests. VecTor2 on contrary is able to perform the analysis by using only the sectional, material and loading system details of the specimens necessary to define the structure. Detail information

about the program can be found from "VecTor2 & FormWorks User's Manual" by Wong and Vecchio [2002].

7.3.2 Preparation of Model

In VecTor2 initial step of modeling are creating the geometry of the structure, selection of loading conditions and material behavior models. Then the regional properties, meshing options and restraint conditions of the structure are to be defined to simulate the actual loading system. Then element properties for concrete and reinforcement are individually assigned to the model. Both plain concrete and reinforced concrete with different types of reinforcement in are available. Similarly different types of reinforcing material options such as prestressing, conventional reinforcement are also available. There is also provision for discrete reinforcement like fibers. The simple and low-powered elements are available in VecTor2 which have linear displacement functions leading to fewer suspicious and mostly accurate behavior results. The analysis in VecTor2 can be performed with iterative secant stiffness procedure for the nonlinear analysis of the reinforced concrete structure under designated loading and restraint conditions. The results can either be obtained from the ASCII result files or simply by using the post-processor, Augustus.

7.3.3 Concrete Model

A four node rectangular element as shown in Figure has been used for concrete model in this study. This is a plane stress rectangle element (Figure 7.2) with uniform thickness in the out-of-plane direction. This element having eight degrees of freedom

allows translation at each node in x- and y-directions, and should be defined by a counter clockwise sequence.

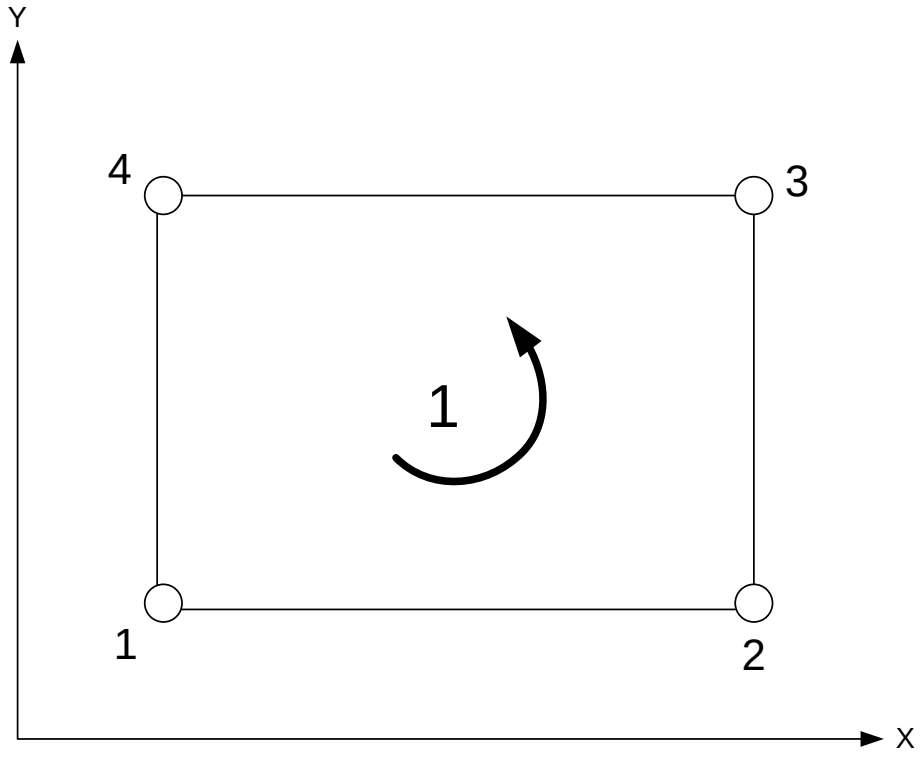

Figure 7.2 Rectangular Concrete Element [Wong and Vecchio, 2002]

For the pre-peak response for concrete was modeled using the default option. This is a simple compression curve model for concrete regions, and can be observed in Figure 7.2. The Hognestad Parabola can be used for concrete regions having a normal compressive strength $f_c' \leq$ 40 mpa (6 ksi) [Wong and Vecchio, 2002]. This model option can compute the principal compressive concrete stress before the compressive strain reaches the peak compressive strain value, ε_p.

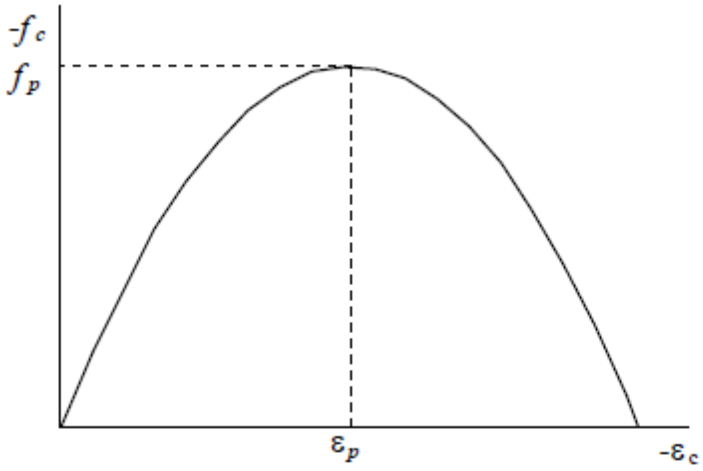

Figure 7.3 Hognestad Parabola for Concrete Pre-Peak Response [Wong and Vecchio, 2002]

The stress-strain relationship is symmetric about ε_p, diminishing to zero stress at zero strain and $2\varepsilon_p$. Note that the Hognestad parabola predefines the initial tangent stiffness, E_c, as follows:

$$E_c = \frac{2 f_p}{\varepsilon_p} \tag{7.1}$$

The concrete post-peak response can be modeled using the "Modified Park-Kent" option, as illustrated in Figure7.4 which is available in VeTor2. This is a modified "Park and Kent" model that accounts for the improved concrete compressive strength and ductility due to confinement. This option computes the principal compressive concrete stress after the compressive strain surpasses the peak compressive

strain value, ε_p. The descending linear branch after the peak strain is followed by a plateau at a value of 0.2 $f`_c$.

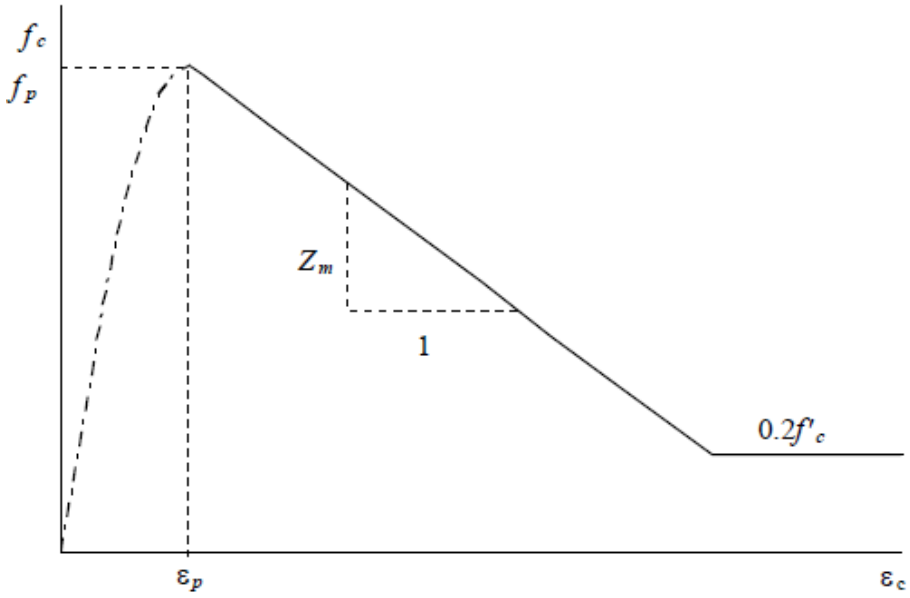

Figure 7.4 Modified Park-Kent for Concrete Post-Peak Response [Wong and Vecchio, 2002]

The Concrete compression softening models that are available in VecTor2 were developed from a series of panel and shell elements tested at the University of Toronto [Vecchio and Collins, 1992]. The effect of concrete cracking on the compression strength and stiffness are taken into account by either strength-and-strain softened or strength-only softened models. From the four different models available in VecTor2, the default model, "Vecchio 1992-A (e1/e2-Form)" was assigned to the concrete material properties. Briefly, this is a strength-and-strain softened model in which both uniaxial compressive strength and strain values are softened.

Other important phenomenon for finite element analyses, the concrete tension stiffening is the tensile resistance of cracked concrete arising from the bond with the reinforcement within the cracked regions. The coarseness of the element mesh has an important effect on simulating this behavior. The "Modified Bentz 2003" model, which is a rigorous adaptation of previous Bentz [2000] model, available in VecTor 2, was selected to represent this behavior. This model not only incorporates the bond actions to the tension stiffening behavior but also accounts for two-dimensional stress conditions and for the placement of each type of reinforcement.

Tension softening refers the post cracking tensile stresses in concrete. The tension softening response can be important to modeling in case of the stress redistribution. This is very much important in case fiber reinforce concrete as the stress redistribution occurs after cracking in the section. By including a descending post-cracking stress-strain branch for concrete, it can accurately determine the load-deformation response and ductility of the member.

The linear modeling where bas stress as shown in Figure 7.5 available in VecTor2 was used for this analysis. The tension softening base curve descends linearly from the cracking stress and strain to zero stress at the characteristic strain (i.e. the terminal strain is taken as the characteristic strain)

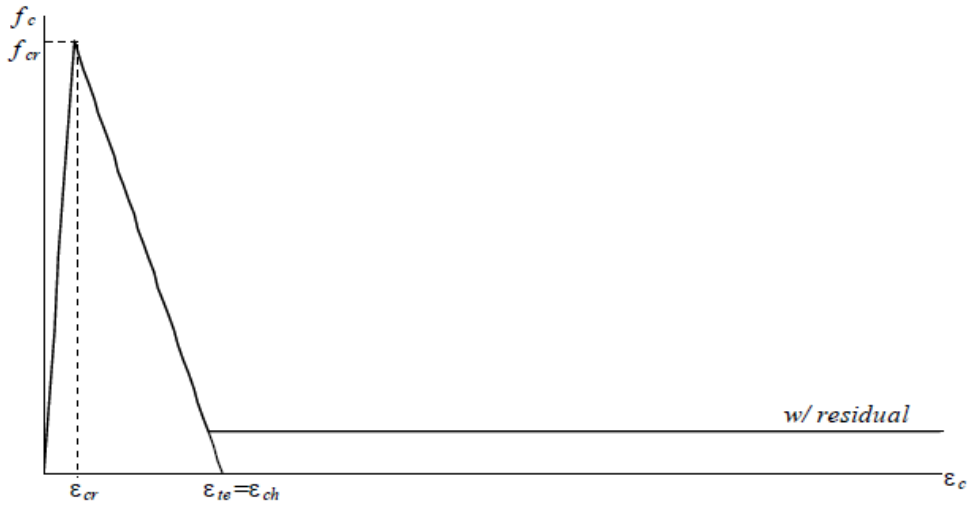

Figure 7.5 Linear Tension Softening Response with and without Residual [Wong and Vecchio, 2002]

To stimulate post-peak response generated by steel fiber reinforced concrete different models discussed in VecTor2 user manual was investigated. All modeling other parameters were taken same as plain concrete as discussed above. The tested parameters such as compressive strength, modulus of elasticity of concrete, stress and strains, were used for SFRC in place of default parameter for plain concrete.

7.3.4 Reinforcement Model

The reinforcement model consists of discrete bar elements. Reinforcement bars can be discretely represented with two-node truss elements which have nodal displacements in two directions and four degrees of freedom, as shown in Figure 7.6.

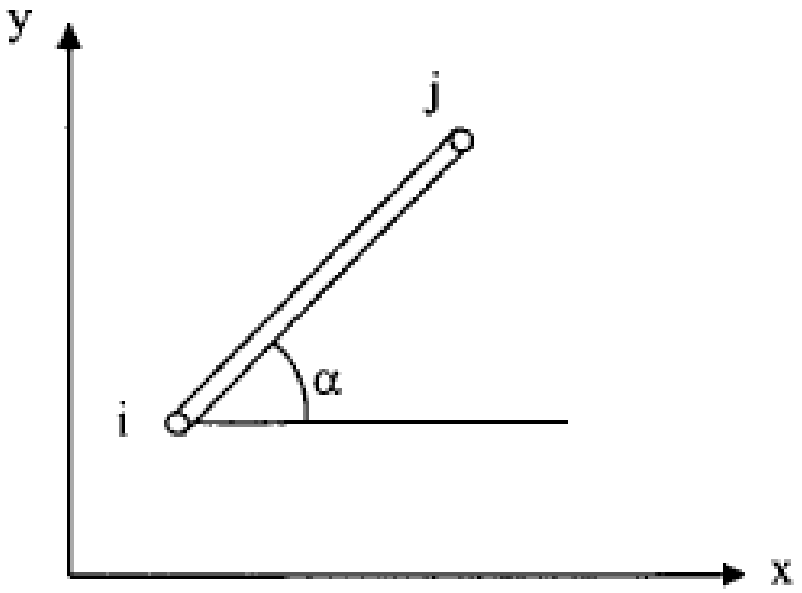

Figure 7.6 Truss Elements [Wong and Vecchio, 2002]

Two types of reinforcement models were used. These are ductile steel reinforcement model for longitudinal tensile reinforcement, compression reinforcement and web shear reinforcement and prestressing reinforcement model for prestressing strands.

For the ductile steel reinforcement model the stress-strain response is tri-linear, as shown in Figure 7.7. It consists of an initial linear-elastic response, a yield plateau, and a linear strain-hardening phase until rupture.

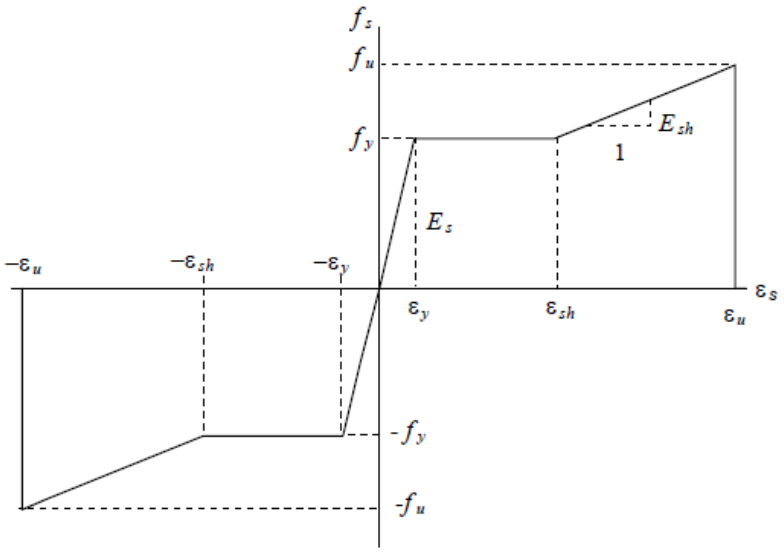

Figure 7.7 Ductile Steel Reinforcement Stress-Strain Responses [Wong and Vecchio, 2002]

The reinforcement stress, f_s, in tension and compression is determined as follows:

$$f_s = \begin{cases} E_s \varepsilon_s & for \ |\varepsilon_s| \le \varepsilon_y \\ f_y & for \ \varepsilon_y < |\varepsilon_s| \le \varepsilon_{sh} \\ f_y + E_{sh}(\varepsilon_s - \varepsilon_{sh}) & for \ \varepsilon_{sh} < |\varepsilon_s| \le \varepsilon_u \\ 0 & for \ \varepsilon_u < |\varepsilon_s| \end{cases} \qquad (7.2)$$

$$\varepsilon_u = \varepsilon_{sh} + \frac{(f_u - f_y)}{E_{sh}}$$

where ε_s is the reinforcement strain, ε_y is the yield strain, ε_{sh} is the strain at the onset of strain hardening, ε_u is the ultimate strain, E_s is the elastic modulus, E_{sh} is the strain hardening modulus, f_y is the yield strength, and f_u is the ultimate strength.

Prestressing Steel model used for presstressing strand is appropriate for cold-worked steel reinforcement that does not exhibit a distinct yield plateau, but rather an initial linear-elastic branch, followed by a transition curve to a second hardening linear branch, as shown in Figure 7.8. In place of Ramsberg-Osgood formulation mentioned in VecTor2, Monggoto and Pinto equation [Namaan,2004] as shown below for reinforcement stress, f_s, in tension and compression was used.

$$f_{ps} = E_{ps}\varepsilon \left[Q + \frac{1-Q}{\left[1+\left(\frac{E_{ps}\varepsilon}{Kf_{py}}\right)^N\right]^{1/N}} \right] \tag{7.3}$$

For stress relieved strands. Following parameter can be used [Namaan, 2004]

$f_{pu} = 270\ ksi$

$N = 5.05$

$K = 1.1155$

$Q = 0.01699$

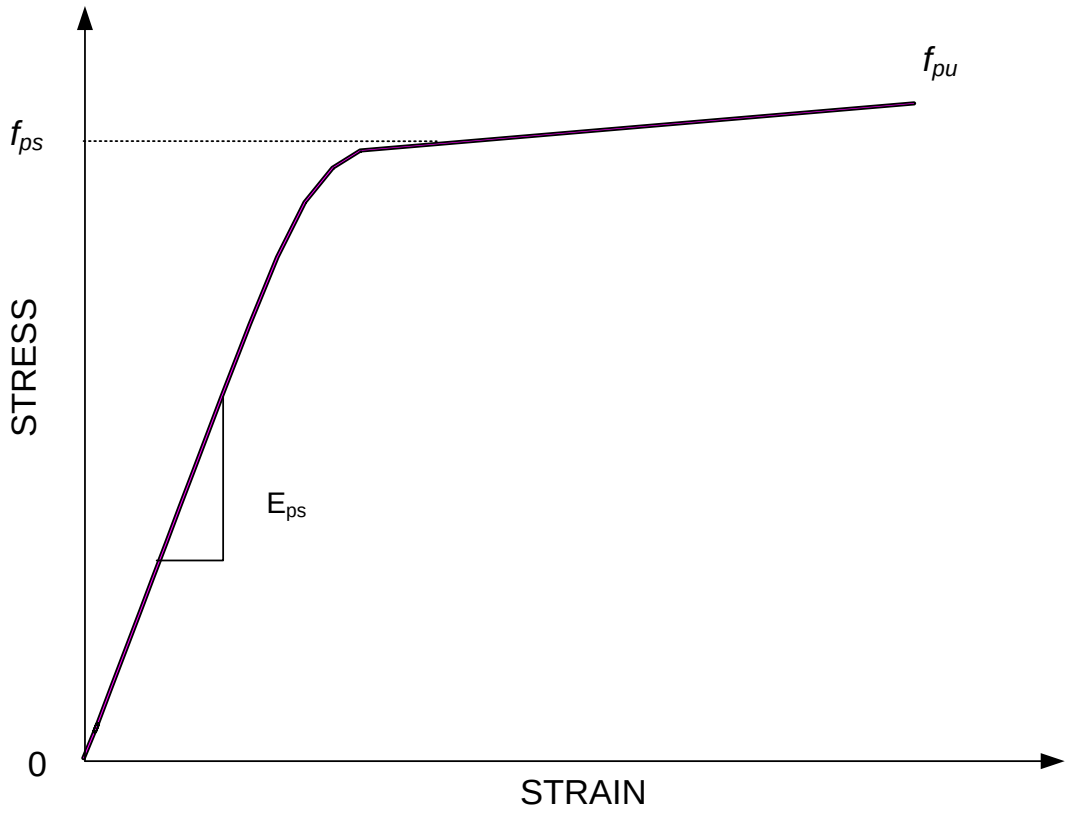

Figure 7.8 Prestressing Steel Reinforcement Stress-Strain Response [Naaman, 2004]

For hysteresis response the model described in the default option the "Seckin w/ Bauschinger Effect", as shown in Figure 7.9, was used. This is a formulation proposed by Seckin (1981) for the hysteretic response of reinforcement which includes the Bauschinger effect in which reinforcement shows premature yielding upon load reversal afterafter plastic prestraining due to the local stress changes. As shown in Figure 7.9,

the monotonic stress-strain curve is followed by a linear unloading curve.

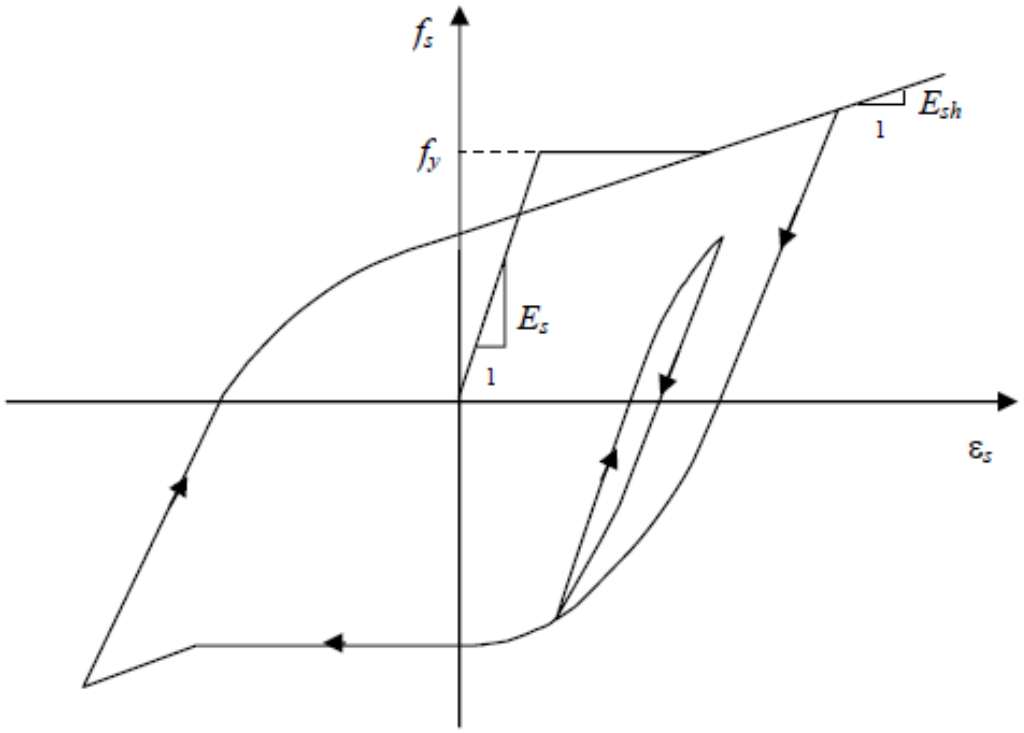

Figure 7.9 Seckin Model for Hysteretic Response of Reinforcement [Wong and Vecchio, 2002]

7.3.4 Running Analyses and Results

The total model prepared in VecTor2 is as shown Figure 7.10. The FE analysis was done by displacement control, the unit displacement. Various parametric analyses were carried out with model having longitudinal reinforcement ratio (2.11%) and less shear reinforcement, which is exactly same as the SFRPC#2-1 specimen (but with no fiber). The analyses were carried out varying ultimate compression strain in concrete (ε_c) from 0.003 to 0.006. The models are named as PC (ε_{cu}=0.003), PC (ε_{cu}=0.004) , PC (ε_{cu}=0.005), PC (ε_{cu}=0.0055) and PC (ε_{cu}=0.006).

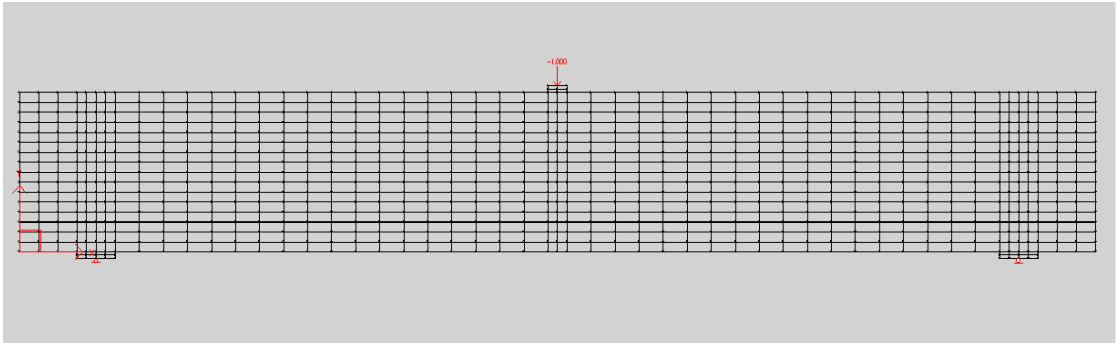

Figure 7.10 A 2D Simply Supported Beam Model Prepared in VecTor2.

All results were obtained by using the post-processor, Augustus. Figure 7.11 shows that with increase in value of ε_{cu} the peak load did not increase much but ductility increased considerably. PC (ε_{cu}=0.003) model showed lowest peak load and ductility. where as PC (ε_{cu}=0.005) shows the largest peak load. As ε_{cu} increases the load deflection curves are found more close to SFRPC#2-1.

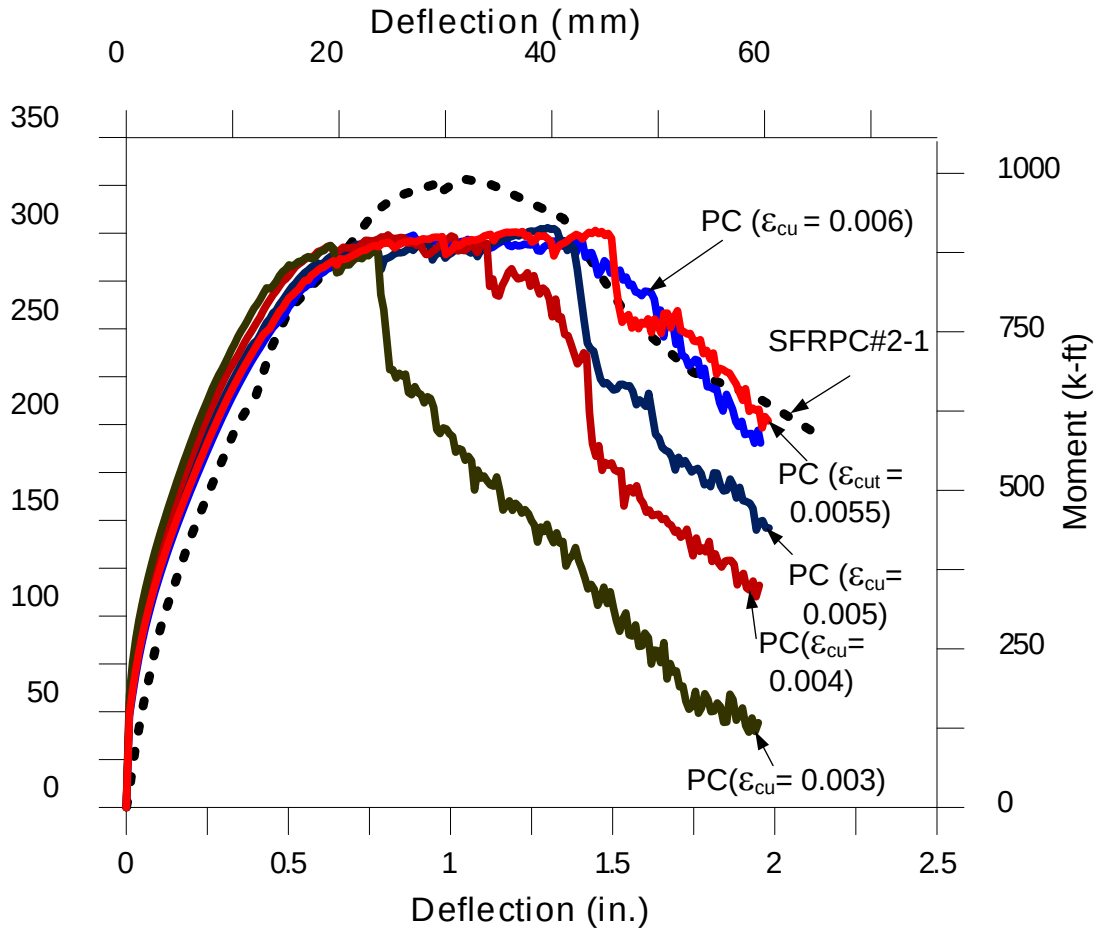

Figure 7.11 Comparisons of Load versus Deflection Curves for Different Values of Ultimate Value Crushing Strain in Concrete (ε_c)

Table 7.1 shows the comparison of various results from the FE analyses and experimental results for SRPC#2-1 specimen. The peak load from the experiment for SFRPC#2-1 specimen was 329 kips which occurred at deflection of 1.1 inches. The peak loads for PC (ε_{cu}=0.003) and PC (ε_{cu}=0.004) model occurred less at deflection 0.63 inches and 0.74 inches 1. Peak load for PC (ε_{cu}=0.005) was occurred at 1.28 inches of deflection. The toughness or total energy absorption (area under the curve) at 1.95 inches deflection were also compared between different FE model with SFRPC#2-1 as

shown in Table 7.2. It was found that with increase values of ε_{cu} the toughness of the PC models were found closer SFRPC#2-1.

Table 7.1 Comparison of results from FE analyses and experiment

Description	Peak load (kips)	Deflection (δ) (in.)	Load at δ= 1.95 in.	Total energy absorption at δ= 1.95 in.
SFRPC#2-1: Experiment	329	1.1	214	486
PC (ε_{cu}=0.003)	294	0.63	44.3	333
PC (ε_{cu}=0.004)	296	0.74	112	437
PC (ε_{cu}=0.005)	302	1.28	149	460
PC (ε_{cu}=0.0055)	301	1.22	208	493
PC (ε_{cu}=0.006)	298	0.86	197	486

From comparison of load versus deflection curve (Figure 7.12), the stiffness of PC (ε_{cu}=0.005) is slightly larger than SFRPC#2-1 specimen. Total energy absorption at deflection 1.95 inches for PC (ε_{cu}=0.005) and SFRPC#2-1 are 460 kip-in and 486 kip-in respectively. The flexural strength obtained from the analysis for PC (ε_{cu}=0.005) model is slightly less than the flexural strength of the SFRPC#2-1 but larger than nominal flexural strength determined as per ACI 318-11. This indicated that ductility behavior of PC (ε_{cu}=0.005) FE model and SFRPC#2-1 PC is quite close. As discussed earlier the average measured value of ultimate strain concrete at compression zone in SFRPC #2-1 is about 0.005. So it can be concluded that the ductility achieved in case SFRPC#2-1 beam from test was due to increase in compressive strain in the concrete.

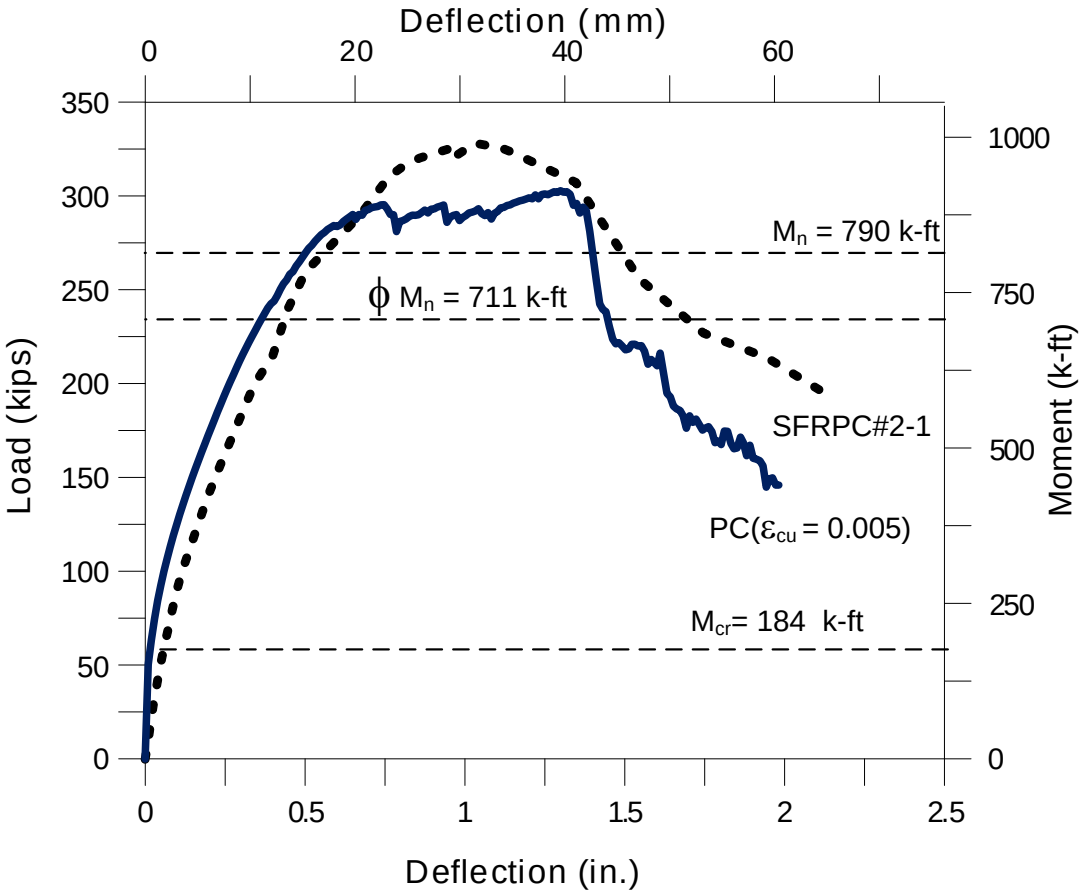

Figure 7.12 Comparisons of Load versus Deflection Curve

Figure 7.13 shows the comparison of crack patterns from the the FE anaysis and obtained from the test. The crack patterns from FE analysis and experiment looks similar in large.

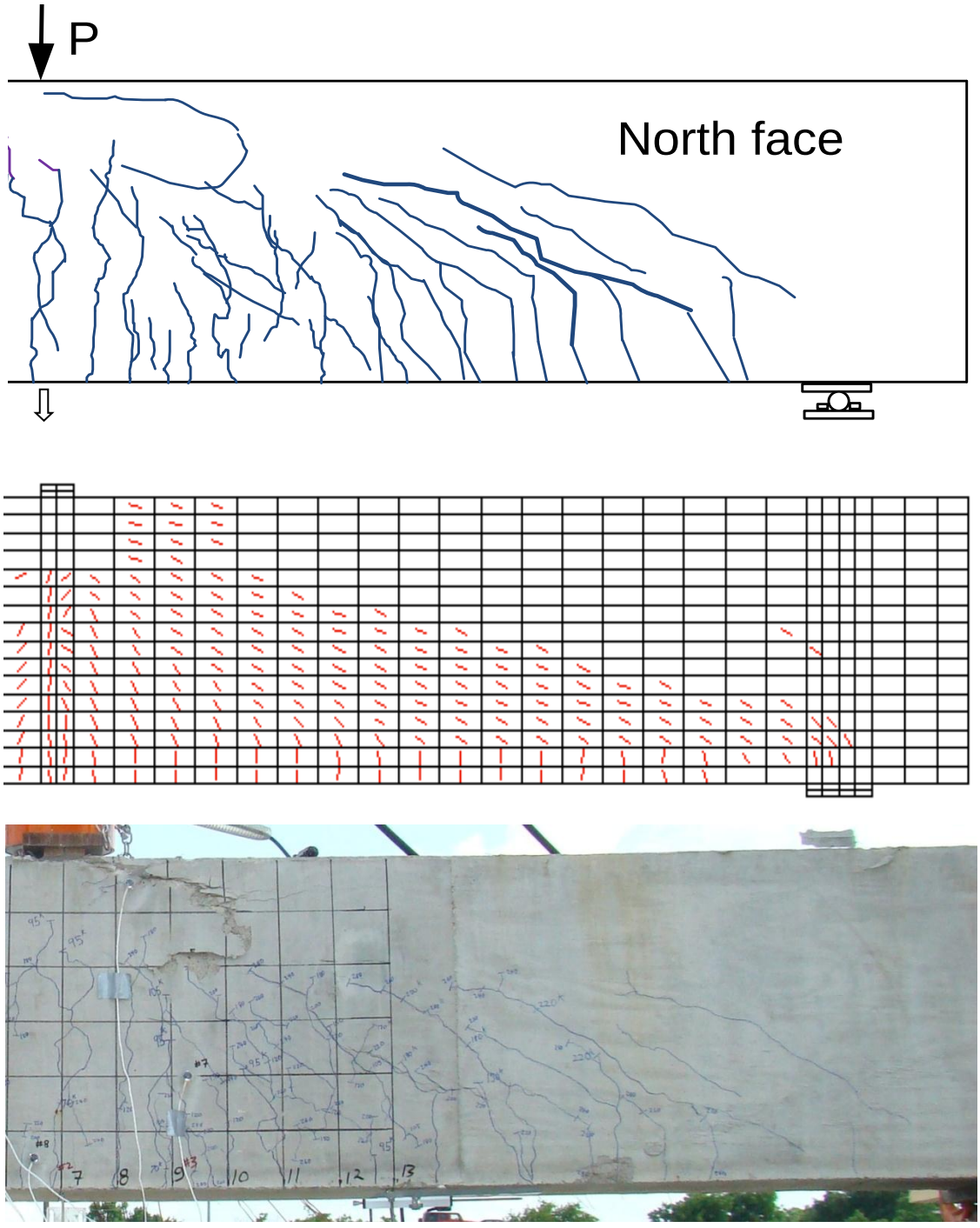

Figure 7.13 Comparison of Crack Patterns at Peak Load

7.4 Proposed Limits for Reinforcement Design in SFRPC Flexural Members

Based on the current experimental results and analysis the new limit for reinforcement design for SFRPC flexural member has been proposed. As discussed in Chapter Two according to ACI 318-11 a section of a flexure member (both prestressed and non prestressed) is designated as a tension controlled member when the net tensile strain in extreme steel (ε_t) is equal to or more than 0.005 and as a compression controlled when the value of ε_t is equal to or less than 0.002. Corresponding neutral axis depth to distance of extreme steel from compression fiber (c/d_t) ratio will be 0.375 (for tension controlled member) and 0.60 (for compression controlled member). ASSHTO 2010 has also used design limit similar to ACI (Figure7.15).

These criteria for limit of reinforcement were based on ultimate crushing strain on concrete of compression fiber as 0.003. As discussed in Chapter Two, the use of this value of strain in concrete of compression fiber in SFRC member is conservative. Some researchers had suggested using more than this limit depending upon volume of fraction of fiber used (Chapter Two, Table 2.3).

The experimental results from large scale test as discussed in earlier for prestressed concrete beams (both with fiber and without fiber) showed that the values of ultimate strain in concrete of compression fiber were found more than 0.003. As shown in Table 7.2 for PC specimens the mean value of ultimate compressive strain in concrete is 0.0040 whereas for SFRPC specimens this value is 0.0066.

Table 7.2 Ultimate Strains in Concrete at Compression Fiber

Specimen	Average	Mid section
PC#1-1	0.0022	0.0031
PC#2-1	0.0046	0.0037
PC#2-2	0.0051	0.0043
Mean	0.0040	0.0037
SFRPC#1-1	0.0036	0.0048
SFRPC#2-1	0.0051	0.00585
SFRPC#2-2	0.0112	0.0088
Mean	0.0066	0.0065

From the compressive stress – strain curve (Chapter 5, Figure 5.55) of obtained from test of (6 × 12 inches concrete cylinder which were prepared along with large scale beams, the maximum value of ultimate compressive strain in the concrete is about 0.005. From the FE analysis as discussed above the load vesus delction curves with PC-005 model (with $\varepsilon_{cu} = 0.005$) is close to load deflection curve for SFRPC#2-1). Hence for the proposed limit for reinforcement of flexure member the value of ultimate compressive strain in concrete has been adopted as 0.005.

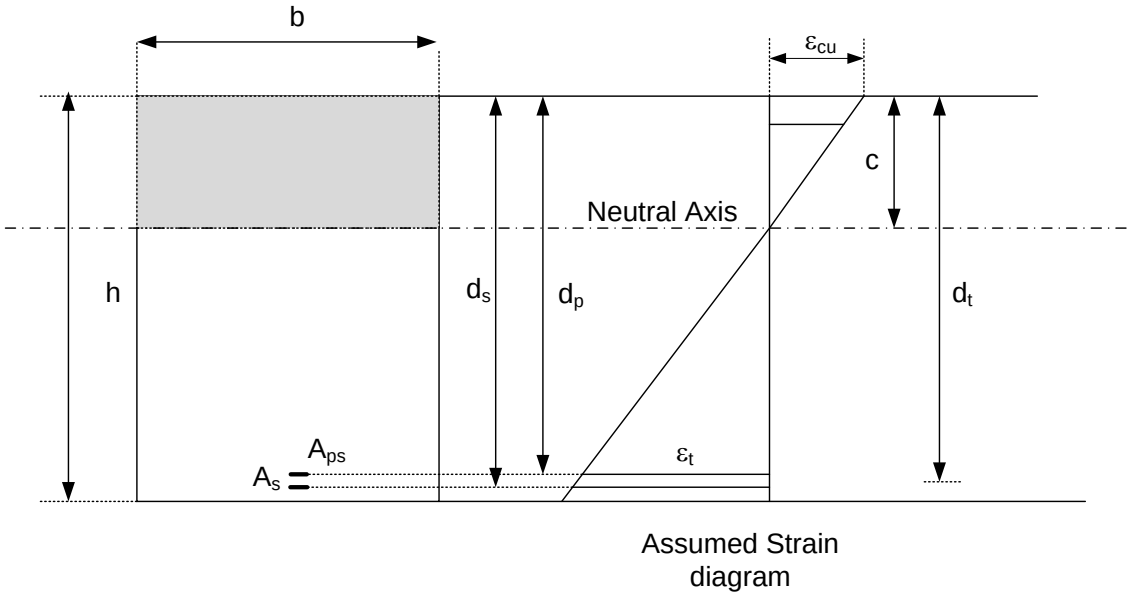

Figure 7.14 Assumed Strain Diagram for Flexural Member [ACI 318-11]

As shown in Figure 7.14 from the similar triangles of strain diagram the depth of neutral axis to distance of extreme tension reinforcement bar ratio is given by

$$\frac{c}{d_t} = \frac{\varepsilon_{cu}}{\varepsilon_{cu} + \varepsilon_t} \tag{7.4}$$

Where

ε_{cu} = *ultimate compressive strain in concrete*

ε_t = *net strain in extreme tensile steel*

c = the depth of the neutral axis at the ultimate load

d_t =*distance extreme steel from compression zone*

In Equation 7.4 the when value of ε_{cu} = 0.005 and ε_t = 0.005 for a tension controlled section the ratio c/d_t comes out to be 0.50 and ε_t = 0.002 for compression controlled the ratio c/d_t comes out to be 0.70. Accordingly the limit of c/d_t ratio has

been proposed for partially prestressed concrete beam with steel fiber (with volume of fraction of steel fiber of 0.75%). The proposed limit is compared with similar ratio given in ACI 318-11 and AASHTO [2010] as shown in Figure 7.15.

Similarly the strength reduction factor (ϕ) has to be also modified with corresponding values of c/d_t ratios in order to determine the nominal strength of the flexure member. The upper and lower limit of the value ϕ -factors are taken as 0.90 and 0.65 for tension controlled and compression controlled section which are exactly same as the ϕ factor given in ACI 318-11. The corresponding equations for ϕ factor for the transition zone are modified as shown in Figure 7.16 as per proposed limit of c/d_t.

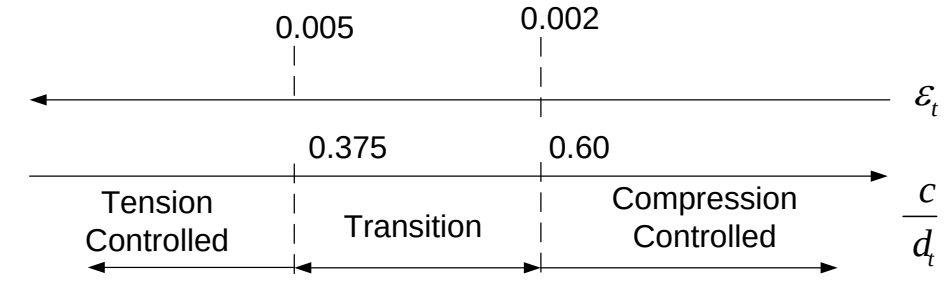

(a) ACI 318-11 and ASSHTO (2010)

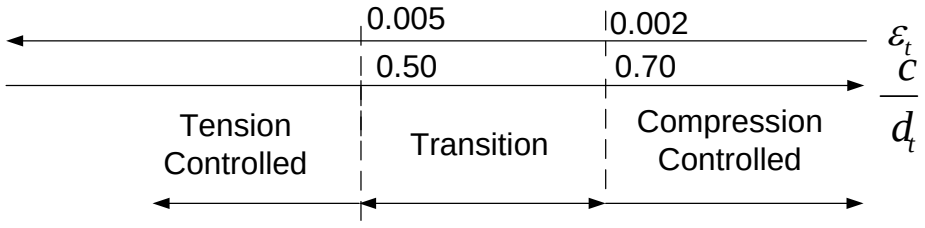

(b) Proposed Limit

Figure 7.15 Comparison of for Limits for Reinforcement in Flexural Members with 0.75% Steel Fiber

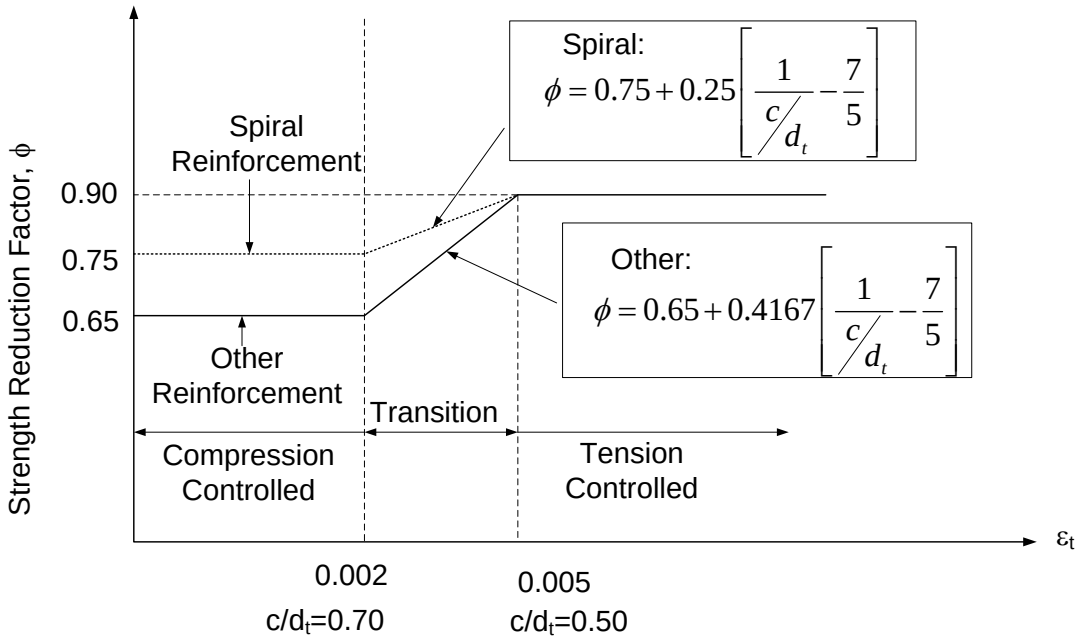

Figure 7.16 Strength Reduction Factors as per Proposed Limit

The experimental results of steel strains in tension reinforcement as discussed in earlier indicated that the average strain values for SFPRC#2-1 (with high longitudinal steel area) was 0.0066 (Table 7.2) which is larger than 0.005 and corresponding c/d_t ratio as 0.42 which satisfied the c/d_t ratio of 0.50 for tension controlled member as proposed limit (Figure 5.15). Table 7.3 shows the some examples of calculation of c/d_t ratio with different longitudinal ratio. It can be seen with use of higher value ε_{cu} (0.005) more efficient use of cross section is possible. With use of proposed limit a section with high longitudinal steel area (steel ratio of 2.7%) can be still considered as tension controlled, whereas as per ACI limit the section is no more tension controlled as it lies in transition zone.

Table 7.3 Comparison of c/d_t Ratios and ε_t with Varying Tensile Steel Ratio of Proposed Limit with Limit Given in ACI318-11

Beam Section : 24 × 16 inches, concrete with $f'_c = 6$ *ksi*, non prestressing steel with $f_y = 60$ ksi and prestressing steel with $f_{pu} = 270$ *ksi*					
Tensile steel ratio $\rho_{t\,(\%)}$	2.0	2.38	2.7	3.32	4.11
c/d_t ratio	0.4	0.444	0.488	0.594	0.705
With Proposed limit value of ε_t with $\varepsilon_{cu} = 0.005$	0.0075	0.0063	0.0052	0.0034	0.0025
Failure mode	Tension-Controlled	Tension-Controlled	Tension-Controlled	Transition-Zone	Compression-Controlled
As per ACI value of ε_t with $\varepsilon_{cu} = 0.003$	0.004	0.0035	0.0029	0.0023	0.0019
Failure mode	Transition Zone	Transition Zone	Transition Zone	Transition Zone	Compression Controlled

CHAPTER 8

SUMMARY AND CONCLUSIONS

8.1 General

This chapter summarizes the experimental works carried out during course of the dissertation work. Experimental investigations and results with large-scale prestressed concrete beams with and without steel fibers and evaluation of double punch test (DPT) as a simple and reliable alternative tensile test method are presented. The conclusions drawn from the the experimental results and some recommendations for further works are also presented at end of this chapter.

8.2 Large-Scale Prestressed Concrete Beams

8.2.1 Summary for Experimental Investigations

In the first phase of experimental program, the behavior of two beam specimens (one plain concrete, PC#1-1, and the other one with 0.75% volume fraction of steel fibers, SFRPC#1-1) of 168 × 24 × 16 inches (length × height × width) were investigated. Steel fibers used in the first phase were of hooked shape at ends with an aspect ratio of 80 (L/d = 80, l = 2.36 inches, d = 0.03 inches) and a tensile strength of 152 ksi. Both beams had the same geometry. A total of five 0.5 inches diameter prestressing strands (ASTM A416, Grade 270, stress relieved) were used in each beam. Initial prestressing of 189 ksi was applied to each strand, which in turn provided an

average initial prestress of 380 psi in the beams. Two No. 4 mild steel reinforcing bars at compression zone for holding stirrups and two No. 3 mild steel reinforcing bars in tension side of the beams for ease of installation of strain gauges were also provided. The strains measures from the tension mild steel bars are equivalent to the net tensile strain, ε_t, (excluding the effective prestress strain) as defined in ACI 318-11. The concrete had an average compressive strength of 5.62 ksi with a maximum aggregate size of 3/4 inches. In this phase only Type 1 cement was used. No Fly ash was added. Slightly less amount of web shear reinforcement than required as per ACI 318-11 was purposely provided for the PC#1-1 specimen to investigate whether the ultimate failure of the specimen would be induced by shear or flexural. Only two stirrups (conventional shear reinforcement) were provided along the clear span for SFRPC#1-1 specimen for fabrication purposes. Five extra stirrups were provided for both specimens near supports to avoid premature cracking when releasing the strands.

In the second phase experimental program, four more beam specimens of same sizes as in case of first phase, were tested for further investigation of flexural behavior of SFPRC beams. Two PC specimens were prepared for comparison purposes. Cement and coarse aggregates used in second phase were also the same as in the first phase. However the mix proportion was slightly different from that used in the first phase. In the second phase, fly ash was also used along with cement and steel fiber used was also different from that used in the first phase for SFRPC specimens. Two SFRPC specimens were prepared with 0.75% volume fraction of steel fibers: the first one SFRPC#2-1 with longitudinal reinforcement ratio of 2.11% and less web shear

reinforcement, and the second one SFRPC#2-2 with a longitudinal reinforcement ratio of 0.29%. For SFRPC#2-1, with steel ratio of 2.11%, c/d_t = 0.41 > 0.375 as per ACI 318-11, the section is no more tension-controlled and lies in transition zone. The main purpose of this specimen is to study the behavior of SFRPC beam with high longitudinal tensile steel ratio (as discussed in Chapters Two and Three, a test of simply supported beam can be used to represent the part near the interior support of an inverted continuous beam). First PC specimen PC#2-1 and both SFRPC specimens of the second phase were prepared using concrete mix with average compressive strength of 5.27 ksi. However the second PC specimen (PC#2-2) had compressive strength 6.96 ksi as it was cast using a different concrete mix at different condition. PC#2-1 was tested with single point loading at center of the beam over a 6-inch wide steel plate whereas PC#2-2, SFRPC#2-1, and SFRPC#2-2 were tested with single point loading at center of the beam over a 3-inch steel wide plate (same as that used by Mattock in 1964 and discussed in Chapter Two Literature Review) to reduce the possible confining area due to the applied loading. For both PC specimens, web shear reinforcements were provided as per ACI 318-11 requirements. No. 3 bars were used for shear reinforcement in a hooped form, at spacing of 8 to 12 inches depending on the location of the section. Based on previous shear tests results of SFRPC beams with the same dimensions and material properties [Cho and et al., 2009], SFRC can have ultimate shear strength of approximately $5.6\sqrt{f_c'}$ (psi), so the area of shear reinforcement provided for SFRPC#2-1 was much less as compared to area required based on current ACI code for regular concrete beams. Since the beam was designed with higher longitudinal tensile steel

reinforcement ratio, in order to avoid the beam fail in shear, more conventional shear reinforcement had to be provided if no fiber was used. For such beam without fibers the required spacing of No. 4 bar (in hooped form) as per ACI provisions would be 3 inches at near mid span and 5 inches near support. However, the spacing of conventional shear reinforcement provided in the whole span of SFRPC#2-1 beam was only 8 inches from center to center, which was slightly larger than the required spacing of 6 inches if assuming that SFRC has shear strength of $v_c = 5.6\sqrt{f_c'}$. Although shear demand for SFRPC#2-2 is smaller due to low steel ratio in the section, for similar PC beam (PC#2-1) the spacing of stirrup required was 8 inches (mid span) to 12 inches (near support),. However for SFRPC#2-2, only one stirrup (No. 3 bar) was provided at middle of beam span for fabrication purpose considering the shear strength of SFRC as , $v_c = 5.6\sqrt{f_c'}$.

For both phases of experimental programs internal concrete and steel strain gauges as well as concrete surface strain gauges were installed in the specimens. All specimens were tested with monotonic loading with necessary instrumentations.

8.2.2 Summary of the Experimental Results

The flexural strength for PC#1-1 and SFRPC#1-1 from first phase of experiment was 392 k-ft and 427 k-ft. The slightly higher ultimate strength of SFRPC#1-1 specimen might be attributed to the contribution of steel fibers in the tension zone of the beam, as assumed by other researchers such as Swamy and Al-Ta'an (1982) However, by examining the crack widths at the tension zone at failure and comparing with the stress versus elongation response from the direct tensile tests for the SFRC materials, it was concluded that the tensile stresses at the tension zone can be very small and cannot

be significant when computing the nominal flexural bending strength. The contribution from SFRC, however, could be used if fiber volume fraction is much greater. As stated earlier, PC#1-1 specimen was purposely under-designed so that the stirrup spacing of 14 inches was slightly larger than the required. The ultimate failure of PC#1-1, after significant flexural deformation, was induced by a shear crack. On the other hand, even without required web shear reinforcement, Specimen SFRPC#1-1 was failed by a gradual crushing of the concrete in the compression zone and fracture of the tension reinforcement after flexural crack became excessively wide. The corresponding shear stress demand for SFRPC#1-1 was 2.9 $\sqrt{f_c'}$ at ultimate, which is about 40% lower than the shear strength as mentioned earlier. The maximum compressive strains at concrete for PC#1-1 and SFRPC#1-1 specimens were found as 0.003 and 0.005, respectively.

In the second phase of the study, the failure modes of PC specimens (PC#2-1 and PC#2-2) were flexural failure after crushing of concrete, as sufficient shear reinforcements were provided for both specimens. The SFRPC#2-2 exhibited very large ductility compared to other specimens having large deformation of 3.8 inches before failure. It should be noted that the failure mode for all specimens were induced by crushing of concrete under the loading point. Even for SFRPC#2-1 (with high tensile steel ratio), failure mode was similar to PC#2-1 and PC#2-2 which were tension-controlled. Specimen SFRPC#2-1 not only had more longitudinal steel ratio, but also had less shear reinforcement, as mentioned previously. This indicated that steel fibers not only can be used for replacing conventional minimum shear reinforcement but also

for the reduction of shear reinforcement for a section with high longitudinal ratio. That is, the steel fibers and conventional shear reinforcement has a synergistic effect. The results showed that use of steel fiber could change the member with large steel area to tension-controlled member and make the construction easier as smaller section could be used with more longitudinal reinforcement and less shear reinforcement. For SFRPC#2-2 beam, the flexure shear crack propagated toward loading point, and eventually stopped under the loading point due to high-compression induced confinement effect. Nominal shear stresses for all SFRPC specimens were found larger than PC specimens. The ductility index and energy ratios for SFRPC specimen (SFRPC#2-2) was found larger as compared to PC specimens (PC#2-1 and PC#2-2).

The average net tensile strain of tension steel of the PC#2-1 and PC#2-1 were from 0.0050 and 0.0053 and those for SFRPC#2-1 and SFRPC#2-2 beams were 0.0066 and 0.0083. For SFRPC#2-1 the maximum strain in steel reached 0.0086, which is greater than 0.005 (lower limit for tension-controlled section as per ACI 318-11), indicating that the section is a tension-controlled section even with larger amount of steel area. This can be attributed to the addition of steel fibers, which provided better confinement thus increasing the ultimate strains of concrete. The results show that the section has greater amount of ductility, as value of ε_t of the steel is greater than 0.0075, even with small amount of compression reinforcing bars. This allows moment redistribution in a continuous beam as per current ACI code.

Test results also indicated that with application of load through 3-inch wide steel plate in place of 6-inch one, the concrete area having the biaxial stresses

(thus a higher confinement effect) in compression zone of the beam section, could be reduced. The depth of compression block was reduced by from 3.5 inches to 2.9 inches for SFRPC specimens (SFRPC#1-1 and SFRPC#2-2) and the corresponding flexural strength was also found reduced from 427 k-ft to 406 k-ft.

The average value of maximum compressive strains in concrete near the extreme compression fiber at failure was 0.004 for PC specimens and those for SFRPC beams was 0.0066. For all beams the maximum strain in concrete was found more than the one assumed in ACI 318-11 (0.003). The flexural strength obtained from the test for PC specimens PC#2-1 and PC#2-2 are 389 k-ft and 412 k-ft, respectively; whereas for Specimens SFRPC#2-1 and SFRPC#2-2, these values are 935 k-ft and 402 k-ft, respectively. However, the increase in ultimate strength due to the use of steel fiber was found marginal.

The measured crack widths during the testing indicated that up to peak load, the crack widths of SFRPC specimens are smaller as compared to the PC specimens. This indicates that the presence of steel fibers could arrest the cracks and control their widening.

With preliminary study on the comparison of labor/time required for preparation reinforcement cage (placing stirrups), it can be justified that the increased initial materials cost due to steel fibers is able to be more than offset by lesser labor hours and costs as well as enhanced constructability. This advantage can be even more significant when congested stirrups need to be used as per design.

8.2.3 Proposed Limits for Reinforcement Design in SFRPC Flexural Members

Based on the current experimental results and analysis a new limit for reinforcement design for SFRPC flexural member with at least 0.75% volume fraction of steel fibers has been proposed. The proposed modification for flexural design of SFRC beams is to use an ultimate concrete strain equal to 0.005. Based on this strain value the limits c/d_t ratios for tension-controlled section and compression-controlled member become 0.50 and 0.70,. Similarly the strength reduction factors have also been slightly modified with corresponding values of c/d_t ratios. The upper and lower limits of the strength reduction factors were taken as 0.90 and 0.65 for tension-controlled and compression-controlled sections (same in ACI 318-11). respectively. The corresponding equations for the transition zone were modified with corresponding c/d_t ratios.

8.3 Double Punch Test (DPT)

8.3.1 Summary of Experiments

In order to overcome limitations with existing material test methods the double punch test (DPT) was extensively evaluated for its potential as an alternative standard material test method to evaluate the tensile properties of steel fiber reinforced concrete. The simple test setup with two LVDTs, load cell, and loading steel punches (1.5 × 1 inches), were used to investigate material properties of plain and various steel fiber reinforced concrete mixtures. Specimens for DPT were prepared by just cutting 6 ×12 inches cylinders in half. Compressive force was applied through 60-kip Baldwin hydraulic or 400 kips compression testing machine with loading rate of 100 lb/sec

(0.002 inches/sec) up to the first crack and then 300 lb/sec (0.006 inches/sec) at post-crack stage. A steel plate was placed between bottom punch and load cell, and load was monitored by the load cell.

The experimental investigations were carried out in different phases. Different types of steel fibers were used with different volume fractions from 0.5% (67 lb per cubic yard) to 2.0% (268 lb per cubic yard). Plain concrete was also tested for comparison purposes. In the first phase of experiment, specimens with plain concrete and three different types of fibers with volume of fractions from 0.5 to 2% were tested. Each set had 10 numbers of specimens. Total number of specimens was 126. The tests were performed when the compressive strength were about 4 ksi so that allowable stress in concrete for typical prestressed members would have been achieved. This allowable stress corresponds to the initial stress at time of transfer of prestress (before prestress losses), which is 0.60 $f_{ci}^{'}$ and $f_{ci}^{'}$ is generally taken as $0.80f_{c}^{'}$. For the second and third phases, different sets of specimens were selected based on the first phase test results and each set of concrete was mixed on the same day. The set of specimens prepared on the same day were also tested on the same day in order to have the same strength. In the fourth phase the specimens were tested after 28 days with four types of fiber (one new type of steel fiber, the Helix fiber was added in this phase) and volume contents as in the previous phases. All specimens were tested at 55-58 days. In the later three phases (second phase to fourth phase) of studies, each set had just four specimens because of small variability in testing results that was observed from the first phase. In fifth phase, DPT method was compared to other material test methods such as the third point

bending test (ASTM C1609) and direct tensile test. The SFRC speciemns for DPT, ASTM beams and tensile specimens (dog-bone shaped)with three types of mixures with two types of steel fiber were prepared and tested. At last, experiment with DPT with mixed steel fibers (hybrid) were carried out to study the post-cracking behavior such as strain hardening, crack width and toughness.

8.3.2 Summary of Experimental Results

In the first three phases of experimental works, peak and residual loads and the average load versus deflection curves for specimens of different types of steel fibers with different volume of fraction were compared with those of plain concrete. Specimens with higher volume fraction of steel fibers showed higher tensile strength and slight hardening behavior after first cracking. Furthermore, steel fibers with double hooks at end of the fibers and longer length had given higher peak and residual strength for the DPT specimens. The strength ratio for Type1 (Royal with single hook at end), Type 2 (Baekert short, double hooks at end and Type 3 (Baekert long, double hooks at end) was found as 1.94: 1.44: 1.0. It is seen that DPT can clearly distinguish the performance of FRC mixtures with various amount of fibers in early age of concrete. Comparing COVs for peak and residual loads, the small numbers of sample specimens have been able to distinguish the properties of FRC. From the fourth phase of study DPT has shown its capacity to show the properties of FRC after 28 days compressive strength, such as peak and residual strengths, toughness at 0.10 inches deflection and strain hardening properties.

The fifth phase of experimental results have clearly shown that peak strength obtained from DPT have very low coefficient of variation (COV), approximately 5% as opposite to COVs for peak strengths from bending and direct tensile tests, which have COVs of 17% and 18% respectively. Though COVs for residual strength and toughness from DPT were also found more than 10% in some cases, these values were still very much lower than COVs for residual strength and toughness, from bending and direct tensile tests.

Comparison of load versus deflection curves from third point bending test (ASTM C1609) and direct tensile test with double punch test (DPT) showed a large deviation of mean curves with other curves in the cases of other material methods as compared to DPT method. The results indicated that the coefficient of variations (COV) for toughness is of lower 9%for SFRC specimens tested by DPT, whereas the variation was as high as 24-26 % for ASTM beams and direct tensile test. High variations were also observed at the post-cracking branches of the ASTM C1609 curves, as compared to those in the DPT curves

From the last phase of experimental program it has been seen that the concrete mixtures with mixed fibers (hybrid) including steel twisted fiber and steel micro fibers could considerably control the crack widening and could also increase the strength and ductility. Specimens with larger volume of twisted and micro fibers had shown high equivalent tensile strengths and strain hardening behavior. The various test results from this phase of DPT program has shown the sensitivity of DPT in using good mix and

poor mixes, compaction methods during preparation specimens and using compression machines with larger and small capacities.

From FE analyses it has been found that from DPT test method stresses were developed in both vertical direction and horizontal direction. From analysis it can be seen that a biaxial stress condition occurs in DPT specimens. However, except very close to loading point (near the steel punches) the tensile stresses elsewhere were found very much uniform both vertical (along the depth) and horizontal (along radial direction). The compressive stress decayed rapidly outward and toward mid-depth from top of the specimens. The tensile stresses obtained from analysis and equivalent tensile strengths calculated from empirical equation suggested by Chen (1970) were found very close.

While both the bending test (ASTM C1609) and direct tensile test have to be carried by a closed-loop servo-controlled machine, only a typically compression machine is needed for conducting DPT. In addition, preparation of DPT specimens (two half of 6 × 12 inches cylinders) is relatively easy as compared to the other two methods.

8.4 Conclusions

8.4.1 Large-Scale Prestressed Concrete Beams

- SFRPC beams (0.75% V_f) showed ductile flexural failure even without conventional shear reinforcement, which potentially saves labor and material costs, as well as time required for construction.
- With the addition of steel fibers, the shear reinforcement required in the section with higher amount of longitudinal reinforcement can be significantly reduced without having premature shear failure. Hence the beams with larger tensile steel reinforcement ratio can still be tension-controlled and show ductile failure, which leads to a smaller and more efficient section. This is particularly advantageous for long span beams (for example PC girders for a bridge) where the self-weight is the dominating load.
- The observed large net tensile strain in steel (ε_t) indicated that the test SFRPC beams are ductile enough to allow moment redistribution in continuous beams.
- In general SFRPC specimens exhibited higher ductility index and energy ratio as compared to PC a specimens.
- SFRPC beams showed smaller crack widths at first cracking, peak load, and residual load (0.75% peak load) as compared to the PC specimens.

- AE sensor results also showed that slightly more events happened are at first crack load, and peak load in case of SFRPC as compared to PC. which indicates more cracks developed in case SFRPC beams., The experimental results showed that the there was only marginal increase in ultimate strength with the use of 0.75% V_f of steel fibers but the significant increase in shear strength was verified with this amount of fibers.
- The flexural strength of SFRPC beams were found close to nominal strength of the corresponding PC beams.
- Based on test results an ultimate compressive strain of SFRC of 0.005 is recommended when at least 0.75% volume fraction is used. The corresponding new limit of c/d_t ratios are 0.50 for tension-controlled and 0.70 for compression-controlled section, for reinforcement design of flexure members. Similarly the modified expression for the strength reduction factor (ϕ) is also derived.

8.4.2 Double Punch Test

- DPT method can be used to distinguish the peak strength, residual strength, toughness, and stiffness, of different SFRC mixtures.
- DPT method showed much less scatter results as compared to the third point bending beam test (ASTM C1609) and direct tensile test.
- DPT does not need a closed-loop, servo-controlled machine, a simple small-capacity compression machine is sufficient.

- It is easy to prepare the specimens by just cutting in half the 6 × 12 inches cylinder
- Less number of samples is required for DPT. It was shown four specimens or two conventional 6 × 12 inches cylinders are generally sufficient.
- DPT results are not dependent to single crack but multi cracks developed during hence can predict actual properties of FRC material.
- As load versus deformation curves showed that individual curves are not very much scattered from the mean curve, mean curves can be used to compare between different FRC mixes.
- Finite element analysis indicates that tensile stresses was uniform throughout the height of the specimen and the maximum value is quite closed to the equivalent tensile strength determined by the equation suggested by Chen (1990) for DPT method.
- Tensile strengths from direct tensile test and DPT are close and within 15% difference.

8.5 Recommendation for Future Study

8.5.1 Large-Scale Prestressed Beams

- More large-scale prestressed beams with different geometries and volume of fraction fibers need to be studied.
- Multi-span beams results need to be compared with simple span beam to verify moment redistribution.

- Doubly reinforced beams and sections with very large amount of longitudinal reinforcement (with compression-controlled) and less transverse reinforcement and with steel fibers are to be studied to see the effect in ductility and type of failure.

8.5.2 Double Punch Test (DPT)

- Comparison of DPT with other material test such as split cylinder test and round panel tests are to be carried out in large extent (with different types of steel fibers and different volume of fractions of steel fibers).
- More comparison of DPT with type and capacity of the compression machine including servo-controlled machine to see the effect of testing machine.
- Comparison of FRC specimens with small sized fibers in different volume of fractions (from 0.75% to 5%) through DPT method can be carried out.
- Mores studies on various mixtures and type of fibers.

APPENDIX A

DESIGN OF BEAMS

Flexural Design of PC Beams with ACI methods: PC#1-1, PC#2-1

Sectional properties:

Overall Length (L) = 168 in.

Effective Length (L_e) = 144 in.

Overall Depth, h = 24 in, width, b= 16 in.

Clear cover c_t =3 in.

Effective depth for reinforcing steel d_s= 21in.

Effective depth for presstessing steel d_p=21 in.

Compression steel depth d_c = 3 in.

Area of section, A_c = 384 in^2

Moment of Inertia, I =18432 in^4

Sectional modulus, Z_b=Z_t= 1536 in^3

Eccentricity of prrestressing steel strand e =9 in.

Number of strand used = 5 no, Area of prestressing steel, A_{ps} = 0.765 in^2

Area of tension bar A_s = 0.22 in^2 Area compression bar, A_{sc} =0.40 in^2

Mechanical properties

Compressive stress in concrete, f'_c = 6000 psi

Modulus of elasticity in concrete, E_c = 4415 ksi

Yield stress in steel, f_y = 60 ksi

Modulus of elasticity for reinforcing steel, E_s =29000 ksi

Modulus of elasticity prestressing steel, E_{ps}=28500 ksi

Stress in strands, ultimate, f_{pu} =270 ks;, Initial f_{pi} = 189 ksi; f_{pe} = effective 148.5 ksi

Density of concrete = 150 pcf

Flexure Design (Ultimate strength method as discussed in chapter two)

$$\beta_1 = 0.85 - 0.05\left(\frac{f'_c - 4000}{1000}\right) = 0.75$$

$$\rho_p = \frac{A_{ps}}{bd_p} = 0.00228$$

$$\omega_s = \frac{A_s f_y}{bdf'_c} = 0.007,\ \ \omega_{ps}\frac{A_{ps} f_{ps}}{bdf'_c} = 0.0064,\ \ \omega' = \frac{A_{sc} f_y}{bdf'_c} = 0.012$$

$$\rho_p \frac{f_{pu}}{f'_c} + \frac{d_s}{d_p}(\omega_s - \omega') = 0.097 < 0.17,\quad So\ \ used, 0.17, d' \le 0.15 d_p$$

$$\gamma_p = 0.4\ for\ f_{py} \ge 0.85 f_{pu}$$

$$f_{ps} = f_{pu}1 - \frac{\gamma_p}{\beta_1}\left\{\rho_p \frac{f_{pu}}{f'_c} + \frac{d_s}{d_p}\left(\omega_s - \omega'\right)\right\} = 245.5 ksi$$

$$a = \frac{A_{ps}\ f_{ps} + A_s\ f_y - A_{sc}\ f_y}{0.85 f'_c\ f_{ps} b} = 2.17\, in.; c = \frac{a}{\beta_1} = 2.89\, in.$$

$$M_n = A_{ps}\ f_{ps}\left(d_p - \frac{a}{2}\right) + A_s\ f_y\left(d_s - \frac{a}{2}\right) - A_{sc}\ f'_y\left(d' - \frac{a}{2}\right) = 3944.0\ \ k.in$$

$$\frac{c}{d_t} = 0.138 < 0.375\ \ Ok$$

$$\varepsilon_s = \frac{\left(d - c\right)}{c}\varepsilon_c = 0.0188 > 0.00207,\ tension\ \ control$$

$$\varepsilon'_s = \frac{\left(c - d'\right)}{c}\varepsilon_c = -0.0002 < 0.00207, f'_s = \epsilon'_s E_s = -3.25 ksi$$

Assume new c = 3.24 in

$$New, f'_s = E_s \frac{\left(c - d'\right)}{c}\varepsilon_c = 6.5 ksi$$

$$New, \omega' = \frac{A_{sc} f'_s}{bdf'_c} = 0.0013$$

$$New, f_{ps} = f_{pu}1 - \frac{\gamma_p}{\beta_1}\left\{\rho_p \frac{f_{pu}}{f'_c} + \frac{d_s}{d_p}\left(\omega_s - \omega'\right)\right\} = 245.5 ksi$$

Check that,

$$A_{ps} f_{ps} + A_s f_y - A_{sc} f'_s - 0.85.c.f'_c.b = 0$$

$a = \beta_1 c = 2.43 in.$

$$New, M_n = A_{ps}\ f_{ps}\left(d_p - \frac{a}{2}\right) + A_s\ f_y\left(d_s - \frac{a}{2}\right) - A_{sc}\ f'_y\left(d' - \frac{a}{2}\right) = 3959.2\,k.in$$

$$de = \frac{A_{ps}.f_{ps}.d_p + A_s.f_y.d_s}{A_{ps}.f_{ps} + A_s.f_y} = 20.9\ in.$$

$$\frac{c}{d_e} = 0.15 < 0.375 Ok$$

$$Ultimate\ moment, M_u = \phi M_n = \ 329.9\,k.ft$$

$$> 1.2M_{cr} = 216.84\,k.ft\ Minimum\ ratio\ requirement\ is\ satisfied$$

$$Dead\ load\ moment,\ M_d = \frac{w_d l^2}{8} = 7\,k.ft$$

$$f_r = -0.75.\left(f'_c\right) - = -580.95\,psi$$

$$M_{cr} = A_{ps} f_{pe}\left(e_o + \frac{Z_b}{A_c}\right) - f_r Z_b = 184\,k.ft$$

Factor for plate (as discussed in Chapter two)

$$\beta = 1 - \frac{(w + 2kd)}{2L} = 1 - \frac{(6 + 2 \times 3.24)}{2 \times 12 \times 12} = 0.96$$ *where kd=c and w=3 in.*

$$Expected\ failure\ load\ \ P = \frac{4\left(M_u - M_d\right)}{\beta L} = 113 kips$$

Cracking Load,

$$P_{cr} = \frac{4M_{cr}}{\beta L} = 66.9\,kips$$

Shear design:

- *Shear force due to self-weight*

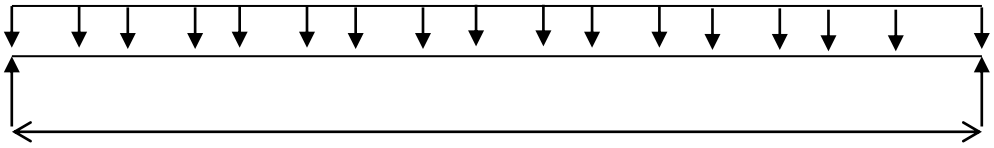

12 ft.

Self-weight of beam, $w_G = 0.4\frac{k}{ft}$

Moment and shear force as any section *x* due to gravity load are

$$M_g(x) = \frac{w_d.x.(l-x)}{2} = 0.20x(12-x)$$

(A.1)

$$V_g(x) = wd(\frac{l}{2} - x) = 0.40(6-x)$$

(A.2)

Eccentricities are same for whole length since there is no draping.

$e_0 = 9$ in.

Prestressing force is given by

$$F = f_{pe} \times A_{ps} = 148.5 \times 0.765 = 113.6 \; kips$$

- *Shear Strength Provided by Concrete*

Flexural-Shear Cracking Resistance and flexure shear stress are determined as:

$$v_{ci} = 0.6\lambda\sqrt{f`_c} + \frac{V_G}{b_w d_p} + \left(\frac{\Delta V_u \times \Delta M_{cr}}{\Delta M_u}\right)\frac{1}{b_w d_p} \geq 1.7\lambda\sqrt{f`_c}$$

$$V_{ci} = 0.6\lambda\sqrt{f`_c} b_w d_p + V_G + \left(\frac{\Delta V_u \times \Delta M_{cr}}{\Delta M_u}\right) \geq 1.7\lambda\sqrt{f`_c} b_w d_p$$

(A.3)

Where,

$\lambda = 1 \; for \; normal - weight \; concrete$

$v_{ci} = flexure - shear \; stress \; resistance, psi$

$V_{ci} = flexure - shear \; force \; resistance, lb$

$d_p = d_p \; or \; 0.80h \; whichever \; is \; larger \; at \; section \; considered$

$V_G = shear \; force \; due \; to \; self$

$- weight \; of \; member \; at \; section \; considered$

ΔV_u

$= factored \; shear \; force \; due \; to \; superimposed \; dead \; load \; plus \; live \; load$

$at \; section \; considered \; under \; same \; loading \; as \; \Delta M_u$

$\Delta M_u = factored\ bending\ moment\ due\ to\ superimosed\ dead\ load\ plus\ live\ load$

$at\ section\ considered$

$\Delta M_{cr} = Moment\ in\ excess\ of\ self$

$- weight\ moment, causing\ flexural\ cracking$

$in\ the\ precompressed\ tensil\ fiber\ at\ section\ considered\ (equal\ M_{cr} -$

$M_G)$ and calculated as following equation

$$\Delta M_{cr} = Z_b[6\sqrt{f_c'} + \frac{F}{A_c}(1+\frac{e_0 A_c}{Z_b})] - M_G$$

(A.4)

For x = 1.75 ft (first critical point)

$$=1536\left[6\sqrt{6000} + \frac{113.6\times10^3}{384}\left(1+\frac{9\times384}{1536}\right)\right] - 0.40\frac{x(12-x)}{2}\times12000$$

$$\Delta M_{cr} = 179\,k.ft$$

$$\sigma_g = \frac{F}{A} = \frac{113.6\times10^3}{384} = 296\,psi$$

$$\sin\alpha \cong \tan\alpha = 0$$

$$V_p = F\sin\alpha = 113.6\times0 = 0\,kips$$

$0.8h = 19.2\,in.$

$d_p' = e_0 + y_t = 9 + 12 = 21\,in.$

$$d_p = (19.2, d_p')_{\max} = 21 in.$$

$\lambda = 1$

$$v_{ci} = 0.6\lambda\sqrt{f_c'} + \frac{V_G + \left(\frac{\Delta V_u}{\Delta M_u}\right) \times \Delta M_{cr}}{b_w d_p}$$

(A.5)

For x = 1.75 ft (first critical point)

$$v_{ci} = 0.6 \cdot 1 \cdot \sqrt{6000} + \frac{0.4\left(\frac{L}{2} - x\right) \times 10^3 + \left(\frac{\Delta V_u}{\Delta M_u}\right) \times \Delta M_{cr}}{16 \times d_p} \geq 1.7\sqrt{f_c'} = 132.5\ psi$$

$$v_{ci} = 355.8\ psi$$

$$v_{cw} = 3.5\sqrt{f_c'} + 0.3\sigma_g + \frac{V_P}{b_w d_p}$$

$V_{cw} = 359.9\ psi$

$\sigma_g = compressive\ stress\ in\ the\ concrete\ at\ the\ centroid\ of\ the$

$cross\ section\ or\ at\ the\ junction\ of\ web\ and\ flange\ if\ the\ centroid\ is\ in\ the$

$flange, due\ to\ effective\ prestress$

$V_p = vertical\ componet\ of\ prestressing\ force\ at\ section\ considered,$

$= F \sin\alpha$

$v_c = (v_{ci}, v_{cw})_{\min}$

For x = 1.75 ft (first critical point)

$v_c = (355.9, 359.9)_{\min} = 355.9\ psi$

$$V_u(x) = 1.2 \times w_G \left(\frac{L}{2} - x\right) + \Delta V_u(x) = 1.2 \times 0.40 \left(\frac{L}{2} - x\right) + P/2 \text{ kips}$$

(A.6)

For x = 1.75 ft (first critical point) for P =113 kips

$V_u(x) = 58.2\ kips$

$$\frac{v_u}{\phi} = \frac{V_u}{\phi b_w d_p} = \frac{V_u \times 10^3}{0.75 \times 16 \times d_p} = 231.0\ psi > \frac{v_c}{2} = 178\ psi$$

$$v_s - v_n - v_c = 231.0 - 355.9 = -125.1\ psi \quad \begin{matrix} < 4\sqrt{f_c'} = 309.8\ psi \\ < 8\sqrt{f_c'} = 619.7\ psi \end{matrix} \quad OK$$

Use No. 3 stirrups $A_v = 0.22\ in^2,\ f_y = 60\ ksi$

$$\textit{Spacing required, } s_v = \frac{f_y A_v \times 1000}{0.75 \times b_v \sqrt{f_c^{'}}} = 14.2\,in. \begin{cases} \le 0.75h = 18\,in. \\ \le 24\,in. \\ \ge 3\,in. \end{cases}$$

Provide Spacing s_v = 14.0 in.

Area minimum required

$$(A_v)_{\min} = \frac{A_{ps} f_{pu} s}{80 f_y d_p} \sqrt{\frac{d_p}{b_w}} = 0.033 in^2 < 0.22\ in^2 \quad OK$$

$$(A_v)_{\min} = \frac{50 b_w s_v}{f_y} = 0.19 in^2 < 0.22 in^2 \quad OK$$

Detailed of shear design at various section of PC beams PC#1-1 and PC #2-1 are presented in Table A.1 and A.2

Table A.1 Detail Shear Design at Various Section of PC#1-1 Beam

X, (ft)	1.75	3	4	6
$V_d(x), kips$	1.7	1.2	0.8	0.0
$M_d(x), k.ft$	3.6	5.4	6.4	7.2
ΔV_u (kips)	56.5	56.5	56.5	56.5
ΔM_u (k.ft)	98.9	169.5	226.0	339.0
ΔM_{cr} (k.ft)	179.0	177.2	176.2	175.4
$v_{ci} \geq 1.7\lambda\sqrt{f_c'}\ (psi)$	355.9	225.8	179.9	133.5
$v_{cw}\ (psi)$	359.9	359.9	359.9	359.9
$v_c\ (psi)$	355.9	225.8	179.9	133.5
V_u (kips)	58.2	57.7	57.3	56.5
$v_n = \frac{v_u}{\phi}\ (psi)$	231.0	229.0	227.4	224.2
$\frac{v_c}{2}\ (psi)$	178.0	112.9	90.0	66.7
$v_s = \frac{v_u}{\phi} - v_c \begin{cases} < 4\sqrt{f_c'} \\ < 8\sqrt{f_c'} \end{cases}\ (psi)$	-125.0	3.2	47.5	90.7
$s = \min\left(\frac{A_v f_y}{v_s b}, \frac{f_y A_v}{0.75 \times b\sqrt{f_c'}}\right)\ (in.)$	14.2	14.2	14.2	9.1
Spacing as per A_{min} (in.)	14.2	14.2	14.2	14.2
S_{max} = min(0.75h,24) (in.)	18	18	18	18
Required s (in.)	14.2	14.2	14.2	9.1
Provided s (in.)	14	14	14	14
$(A_v)_{min} = \frac{50 b_w s_v}{f_y}\ (in^2)$	0.19	0.19	0.19	0.19
$(A_v)_{min} = \frac{A_{ps} f_{pu} s}{80 f_y d_p}\sqrt{\frac{d_p}{b_w}}\ (in^2)$	0.033	0.03	0.03	0.03

Table A.2 Detail Shear Design at Various Section of PC#2-1 Beam

X, (ft)	1.75	3	4	6
$V_d(x), kips$	1.7	1.2	0.8	0.0
$M_d(x), k.ft$	3.6	5.4	6.4	7.2
ΔV_u (kips)	56.5	56.5	56.5	56.5
ΔM_u (k.ft)	98.9	169.5	226.0	339.0
ΔM_{cr} (k.ft)	179.0	177.2	176.2	175.4
$v_{ci} \geq 1.7\lambda\sqrt{f_c'}\ (psi)$	355.9	225.8	179.9	133.5
$v_{cw}(psi)$	359.9	359.9	359.9	359.9
$v_c\ (psi)$	355.9	225.8	179.9	133.5
V_u (kips)	58.2	57.7	57.3	56.5
$v_n = \frac{v_u}{\phi}\ (psi)$	231.0	229.0	227.4	224.2
$\frac{v_c}{2}\ (psi)$	178.0	112.9	90.0	66.7
$v_s = \frac{v_u}{\phi} - v_c \begin{cases} < 4\sqrt{f_c'} \\ < 8\sqrt{f_c'} \end{cases}\ (psi)$	-125.0	3.2	47.5	90.7
$s = \min\left(\frac{A_v f_y}{v_s b}, \frac{f_y A_v}{0.75 \times b\sqrt{f_c'}}\right)\ (in.)$	14.2	14.2	14.2	9.1
Spacing as per A_{min} (in.)	14.2	14.2	14.2	14.2
S_{max} = min(0.75h,24) (in.)	18	18	18	18
Required s (in.)	14.2	14.2	14.2	9.1
Provided s (in.)	12	12	8	8
$(A_v)_{min} = \frac{50 b_w s_v}{f_y}\ (in^2)$	0.16	0.16	0.16	0.16
$(A_v)_{min} = \frac{A_{ps} f_{pu} s}{80 f_y d_p}\sqrt{\frac{d_p}{b_w}}\ (in^2)$	0.0282	0.0282	0.0188	0.0188

PC#2-2

Sectional properties

All sectional properties are same as in case of PC#1-1

Mechanical properties

Compressive stress in concrete, f'_c = 7000 psi

Other mechanical properties are same as in case of PC#1-1

Flexure Design (Ultimate strength method as discussed in chapter two with initial stresses)

$$\beta_1 = 0.85 - 0.05\left(\frac{f'_c - 4000}{1000}\right) = 0.70$$

$$\rho_p = \frac{A_{ps}}{bd_p} = 0.000228$$

$$\omega_s = \frac{A_s f_y}{bdf'_c} = 0.007,\ \omega_{ps}\frac{A_{ps} f_{ps}}{bdf'_c} = 0.0060,\ \omega' = \frac{A_{sc} f_y}{bdf'_c} = 0.01$$

$$\rho_p \frac{f_{pu}}{f'_c} + \frac{d_s}{d_p}(\omega_s - \omega') = 0.083 < 0.17,\quad So\ \ used, 0.17, d' \le 0.15 d_p$$

$$\gamma_p = 0.4\ for\ f_{py} \ge 0.85 f_{pu}$$

$$f_{ps} = f_{pu}1 - \frac{\gamma_p}{\beta_1}\left\{\rho_p \frac{f_{pu}}{f'_c} + \frac{d_s}{d_p}\left(\omega_s - \omega'\right)\right\} = 243.8 ksi$$

$$a = \frac{A_{ps}\, f_{ps} + A_s\, f_y - A_{sc}\, f_y}{0.85 f'_c\, f_{ps} b} = 1.84\, in.; c = \frac{a}{\beta_1} = 2.64\, in.$$

$$M_n = A_{ps}\, f_{ps}\left(d_p - \frac{a}{2}\right) + A_s\, f_y\left(d_s - \frac{a}{2}\right) - A_{sc}\, f'_y\left(d' - \frac{a}{2}\right) = 3946.1 k.in$$

$$\frac{c}{d_t} = 0.128 < 0.375\ \ Ok$$

$$\varepsilon_s = \frac{(d-c)}{c}\varepsilon_c = 0.029 > 0.00207,\ \ tension\ control$$

Therefore value f_s is taken as f_y.

$$\varepsilon'_s = \frac{\left(c - d'\right)}{c}\varepsilon_c = -0.0004 < 0.00207,\ f'_s = \epsilon'_s\, E_s = -12\, ksi$$

Assume new c = 3.0 in

$$New,\ f'_s = E_s \frac{\left(c - d'\right)}{c}\varepsilon_c = 0\, ksi$$

$$New, \omega' = \frac{A_{sc} f'_s}{b d f'_c} = 0$$

$$New,\ f_{ps} = f_{pu} 1 - \frac{\gamma_p}{\beta_1}\left\{\rho_p \frac{f_{pu}}{f'_c} + \frac{d_s}{d_p}\left(\omega_s - \omega'\right)\right\} = 243.8\, ksi$$

Check that,

$$A_{ps} f_{ps} + A_s f_y - A_{sc} f'_s - 0.85.c.f'_c.b = 0$$

$$a = \beta_1 c = 2.1\ \ in.$$

$$New, M_n = A_{ps}\, f_{ps}\left(d_p - \frac{a}{2}\right) + A_s\, f_y\left(d_s - \frac{a}{2}\right) - A_{sc}\, f'_y\left(d' - \frac{a}{2}\right) = 3970.5\, k.in$$

$$\frac{c}{d_e} = 0.14 < 0.375\, Ok$$

$$Ultimate\ moment, M_u = \phi M_n = \ 330.9\ k.ft$$

$$> 1.2M_{cr} = 216.84 k.ft\ Minimum\ ratio\ is\ satisfied$$

$$Dead\ load\ moment,\ M_d = \frac{w_d l^2}{8} = 7\, k.ft$$

$$f_r = -0.75.\left(f'_c\right) - = -580.95\, psi$$

$$M_{cr} = A_{ps} f_{pe}\left(e_o + \frac{Z_b}{A_c}\right) - f_r Z_b = 189.9 k.ft$$

Factor for plate (as discussed in Chapter two)

$$\beta = 1 - \frac{(w + 2kd)}{2L} = 1 - \frac{(3 + 2\times 3.0}{2\times 12\times 12} = 0.97\ \ where\ \ kd=c\ \ and\ w=3\ in.$$

$$Expected\ failure\ load\ \ P = \frac{4\left(M_u - M_d\right)}{\beta L} = 112.6\, kips$$

$$Cracking\ Load,\ \ P_{cr} = \frac{4M_{cr}}{\beta L} = 65.3\, kips$$

Shear Design: For shear design test compressive strength and tested ultimate load was considered.

$$\Delta M_{cr} = Z_b[6\sqrt{f_c^{'}} + \frac{F}{A_c}(1+\frac{e_0 A_c}{Z_b})] - M_G$$

$$= 1536\left[6\sqrt{7000} + \frac{113.6\times10^3}{384}\left(1+\frac{9\times384}{1536}\right)\right] - 0.40\frac{x(12-x)}{2}\times12000$$

For x = 1.75 ft (first critical point)

$$\Delta M_{cr} = 183.7\ k.ft$$

$$\sigma_g = \frac{F}{A} = \frac{113.6\times10^3}{384} = 296\,psi$$

$$\sin\alpha \cong \tan\alpha = 0$$

$$V_P = F\sin\alpha = 113.6\times0 = 0\,kips$$

$$d_p' = e_0 + y_t = 9+12 = 21\ in.$$

$$d_p = (0.8h, d_p^{'})_{\max} = (19.2, 21)_{\max} = 21in.$$

$$\lambda = 1$$

$$v_{ci} = 0.6\lambda\sqrt{f_c^{'}} + \frac{V_G + \left(\frac{\Delta V_u}{\Delta M_u}\right) \times \Delta M_{cr}}{b_w d_p}$$

$$= 0.6 \cdot 1 \cdot \sqrt{7000} + \frac{0.4\left(\frac{L}{2} - x\right) \times 10^3 + \left(\frac{\Delta V_u}{\Delta M_u}\right) \times \Delta M_{cr}}{16 \times d_p} \geq 1.7\sqrt{f_c^{'}} = 193.1\, psi$$

For x = 1.75 f.t (first critical point)

$$v_{ci} = 367.7\ psi$$

$$v_{cw} = 3.5\sqrt{f_c^{'}} + 0.3\sigma_g + \frac{V_P}{b_w d_p} = 381.6\ psi$$

$$v_c = (v_{ci}, v_{cw})_{\min}$$

$$v_c = (367.2, 381.6)_{\min} = 367.2\ psi$$

$$V_u(x) = 1.2 \times w_G\left(\frac{L}{2} - x\right) + \Delta V_u(x) = 1.2 \times 0.40\left(\frac{L}{2} - x\right) + P/2 \text{ kips}$$

For x = 1.75 ft (first critical point) for P=112.6 kips

$$V_u(x) = 58.0\ kips$$

$$\frac{v_u}{\phi} = \frac{V_u}{\phi b_w d_p} = \frac{V_u \times 10^3}{0.75 \times 16 \times d_p} = 230.2\ psi > \frac{v_c}{2} = 183.9\ psi$$

$$v_s - v_n - v_c = 230.2 - 367.2 = -137.2\ psi$$

$$\begin{cases} < 4\sqrt{f_c^{'}} = 334.7\ \ psi \\ < 8\sqrt{f_c^{'}} = 669.3\ psi \end{cases} \quad OK$$

Use No. 3 stirrups $A_v = 0.22\ in^2,\ f_y = 60\ ksi$

$$\text{Spacing required, } s_v = \frac{f_y A_v \times 1000}{0.75 \times b_v \sqrt{f_c^{'}}} = 13.1 in. \begin{cases} \le 0.75h = 18 in. \\ \le 24 in. \\ \ge 3 in. \end{cases}$$

Provided, s_v *=12 in.*

Area minimum required

$$(A_v)_{\min} = \frac{A_{ps} f_{pu} s}{80 f_y d_p} \sqrt{\frac{d_p}{b_w}} = 0.033 in^2 < 0.22\ in^2 \quad OK$$

$$(A_v)_{\min} = \frac{50 b_w s_v}{f_y} = 0.16 in^2 < 0.22 in^2 \quad OK$$

Shear design in other sections of beams for PC#2-2 at other section is presented in Table A.3.

Table A.3 Details of Shear Design for PC#2-2 Beam at Various Sections

X, (ft)	1.75	3	4	6
$V_d(x), kips$	1.7	1.2	0.8	0.0
$M_d(x), k.ft$	3.6	5.4	6.4	7.2
ΔV_u (kips)	56.3	56.3	56.3	56.3
ΔM_u (k.ft)	98.5	168.9	225.2	337.8
ΔM_{cr} (k.ft)	183.7	181.9	180.9	180.1
$v_{ci} \geq 1.7\lambda\sqrt{f_c'}\ (psi)$	367.7	234.2	187.2	139.5
$V_{cw}(psi)$	381.6	381.6	381.6	381.6
$V_c\ (psi)$	367.7	234.2	187.2	142.2
V_u (kips)	58.0	57.5	57.1	56.3
$v_n = \frac{v_u}{\phi}\ (psi)$	230.2	228.2	226.6	223.4
$\frac{v_c}{2}\ (psi)$	183.9	117.1	93.6	71.1
$v_s = \frac{v_u}{\phi} - v_c \begin{cases} < 4\sqrt{f_c'} \\ < 8\sqrt{f_c'} \end{cases}\ (psi)$	-137.6	-6.1	39.4	81.2
$s = \min\left(\frac{A_v f_y}{v_s b}, \frac{f_y A_v}{0.75 \times b\sqrt{f_c'}}\right)\ (in.)$	13.1	13.1	13.1	10.2
Spacing as per A_{min} (in.)	13.1	13.1	13.1	13.1
S_{max} = min(0.75h,24) (in.)	18	18	18	18
Required s (in.)	13.1	13.1	13.1	10.2
Provided s (in.)	12	12	8	8
$(A_v)_{min} = \frac{50 b_w s_v}{f_y}\ (in^2)$	0.16	0.16	0.11	0.11
$(A_v)_{min} = \frac{A_{ps} f_{pu} s}{80 f_y d_p}\sqrt{\frac{d_p}{b_w}}\ (in^2)$	0.03	0.03	0.02	0.02

A.3 Flexural Design of SFRPC Specimen: SFRPC # 1-1 (Based on Hanengar and et al)

Sectional and mechanical properties are same as in case of PC#1-1

Orientation factor for three dimensional random orientations, $\eta_o = 0.41$

Bond efficiency factor $\eta_b = 1.2$

Fiber length,l_f = 2.37 in. fiber diameter d_f = 0.029 in, matrix shear modulus, G_m = 4350 ksi, [Benture and Mindness, 2007], fiber cross sectional area A_f = 0.00066 in^2, radius of the fiber, r_f = 0.0145 in

Mean centroid spacing

$$S = 25\sqrt{\frac{d_f}{\rho l_f}} = 0.125 in$$

$$\beta = \sqrt{\frac{2\pi G_m}{E_f A_f ln\left(S / r_f\right)}} = 25.48$$

Length correction factor

$$\eta_L = 1 - \frac{\tan h\left(\beta l_f / 2\right)}{\left(\beta l_f / 2\right)} = 0.97 \qquad \tau = 363.6\ psi \quad [Swamy\ and\ et\ al, 1981]$$

$$\sigma_{cu} = \eta_o \eta_L \eta_b 2\tau \frac{l_f}{d_f} V_f = 218.2\ psi$$

$$f_r = 0.75.\left(f'_c\right) = 581\ psi$$

ϵ_u = 0.003, $\varepsilon_o = \frac{f_r}{E_c} = 0.0001$

Assume d_n =3.34 in

Tensile force due to steel fiber, $F_{ft} = \sigma_{cu} b\left(D - d_n\right) = 72.1 kips$

Tensile force due to tensile reinforcement $F_{st} = A_s f_f = 13 kips$

Tensile force due to prestress, $F_{ps} = A_{ps} f_{ps} = 188 kips$

Compression forced due to concrete $F_c = \frac{0.85 f_{cu}}{\epsilon_u}\left(\epsilon_u - \frac{\epsilon_0}{3}\right) b d_n = 273 kips$

Compression force due to compression reinforcement

$$F_{sc} = \frac{d_n - d'}{d_n} \epsilon_u E_s A'_s = 0.40 ksi$$

For ACI, $k_2 = 0.425 d_n = 1.42 in$

$$M_u = F_c\left(d_n - k_2\right) + F_{sc}\left(d_n - d'\right) + F_{st}\left(d_{st} - d_n\right) + F_{st}\left(\frac{D - d_n}{2}\right) + F_{ps}\left(d_{ps} - d_n\right)$$

$$= 4818.7 k.in = 401.6 k.ft$$

$$> 1.2 M_{cr} = 216.84 k.ft \; Minimum\ ratio\ is\ satisfied$$

Check for reinforcement steel reaches to yield stress or not

$$f_s = \frac{d - d_n}{d} \varepsilon_u E_c = 460 ksi > 60 ksi \; tension\ bar\ yeilds$$

$$f'_s = \frac{d_n - d'}{d_n} \varepsilon_c E_s = 8.86 ksi < 60 \; ksi \; compression\ bar\ do\ not\ yeild$$

Plate factor

$$\beta = 1 - \frac{(w + 2kd)}{2L} = 1 - \frac{(3 + 2 \times 3.34)}{2 \times 12 \times 12} = 0.956 \; where \;\; k\,d = d_n \; and \; w = 3 \; in.$$

$$P_u = \frac{4 M_u}{\beta L} = 140.02 kips$$

Shear design in other sections of beams for SFRPC#1-1 with assumed tested properties of concrete and test ultimate load in Table A.4

Table A.4 Details of Shear design at different section of *SFRPC#1-1* beams

X, (ft)	1.75	3	4	6
$V_d(x), kips$	1.7	1.2	0.8	0.0
$M_d(x), k.ft$	3.6	5.4	6.4	7.2
ΔV_u (kips)	69.5	69.5	69.5	69.5
ΔM_u (k.ft)	121.6	208.5	278.0	417.0
ΔM_{cr} (k.ft)	179.0	177.2	176.2	175.4
$v_{ci} = 5.6\sqrt{f_c^{'}}^{*} \geq 1.7\lambda\sqrt{f'_c}\,(psi)$	433.8	433.8	433.8	433.8
$v_{cw}(psi)$	359.9	359.9	359.9	359.9
$v_c(psi)$	359.9	359.9	359.9	359.9
V_u (kips)	71.2	70.7	70.3	69.5
$v_n = \frac{v_u}{\phi}\,(psi)$	282.5	280.6	279.0	275.8
$\frac{v_c}{2}\,(psi)$	180.0	180.0	180.0	180.0
$v_s = \frac{v_u}{\phi} - v_c \begin{cases} < 4\sqrt{f_c^{'}} \\ < 8\sqrt{f_c^{'}} \end{cases}\,(psi)$	-77.4	-79.4	-80.9	-84.1
$s = \min\left(\frac{A_v f_y}{v_s b}, \frac{f_y A_v}{0.75 \times b\sqrt{f_c^{'}}}\right)(in.)$	14.2	14.2	14.2	14.2
Spacing as per A_{min} (in.)	14.2	14.2	14.2	14.2
S_{max} = min(0.75h,24) (in.)	18	18	18	18
Required s (in.)	14.2	14.2	14.2	14.2
Provided s (in.)	48	48	48	48
$(A_v)_{min} = \frac{50 b_w s_v}{f_y}(in^2)$	0.64	0.64	0.64	0.64
$(A_v)_{min} = \frac{A_{ps} f_{pu} s}{80 f_y d_p}\sqrt{\frac{d_p}{b_w}}\,(in^2)$	0.11	0.11	0.11	0.11

*Note Shear strength for SFRC is calculated based previous study [Cho and et al, 2009]

SFRPC2-1

Sectional and mechanical properties are same as in case of PC#1-1

Orientation factor for three dimensional random orientations, $n_o = 0.41$

Bond efficiency factor $\eta_b = 1.2$

Fiber length, l_f *= 2.0* in. fiber diameter d_f *= 0.031* in, matrix shear modulus,

G_m *= 4350 ksi,*

[Benture and Mindness, 2007], fiber cross sectional area A_f *= 0.00070 in*^{2},

radius of the fiber,

r_f *= 0.015 in*

Mean centroid spacing $S = 25\sqrt{\left(\frac{d_f}{\rho l_f}\right)} = 0.138 in$

$$\beta = \sqrt{\frac{2\pi G_m}{E_f A_f ln\left(S / r_f\right)}} = 24.49$$

Length correction factor $\eta_L = 1 - \frac{\tan h\left(\beta l_f / 2\right)}{\left(\beta l_f / 2\right)} = 0.96$

τ *= 363.6 psi [Swamy and et al 1981]*

$$\sigma_{cu} = \eta_o \eta_L \eta_b 2\tau \frac{l_f}{d_f} V_f = 171.7 psi$$

$$f_r = 0.75.\left(f'_c\right) = 581 psi$$

$\epsilon_u = 0.003,\ \varepsilon_o = \frac{f_r}{E_c} = 0.0001$

Assume d_n =7.16 inches

Tensile force due to steel fiber, $F_{ft} = \sigma_{cu} b(D - d_n) = 46.3 kips$

Tensile force due to tensile reinforcement $F_{st} = A_s f_f = 379 kips$

Tensile force due to prestress, $F_{ps} = A_{ps} f_{ps} = 176 kips$

Compression forced due to concrete $F_c = \frac{0.85 f_{cu}}{\epsilon_u}\left(\epsilon_u - \frac{\epsilon_0}{3}\right) b d_n = 584 \ kips$

Compression force due to compression reinforcement

$$F_{sc} = \frac{d_n - d'}{d_n} \epsilon_u E_s A'_s = 17.4 ksi$$

For ACI, $k_2 = 0.85 d_n / 2 = 3.04 in$

$$M_u = F_c(d_n - k_2) + F_{sc}(d_n - d') + F_{st}(d_{st} - d_n) + F_{st}\left(\frac{D - d_n}{2}\right) + F_{ps}(d_{ps} - d_n)$$
$$= 10545 k.in = 879 k.ft$$

Check for reinforcement steel reaches to yield stress or not

$$f_s = \frac{d - d_n}{d} \varepsilon_u E_c = 166 ksi > 60 ksi \ tension \ bar \ yeilds$$
$$f'_s = \frac{d_n - d'}{d_n} \varepsilon_c E_s = 50.85 ksi < 60 \ ksi \ compression \ bar \ do \ not \ yeild$$
$$\beta = 1 - \frac{(w + 2kd)}{2L} = 1 - \frac{(3 + 2 \times 7.16)}{2 \times 12 \times 12} = 0.94 \ \ where \ k \ d = d_n \ and \ w = 3 \ in.$$

$$P_u = \frac{4M_u}{\beta L} = 311.7 kips$$

Shear design at different sections of SFRPC#2-1 beams with tested compressive strength and tested ultimate load is presented in Table A.5.

Table A.5 Details of Shear design at different section of SFRPC#2-1 beam.

X, (ft)	1.75	3	4	6
$V_d(x), kips$	1.7	1.2	0.8	0.0
$M_d(x), k.ft$	3.6	5.4	6.4	7.2
ΔV_u (kips)	155.9	155.9	155.9	155.9
ΔM_u (k.ft)	272.7	467.6	623.4	935.1
ΔM_{cr} (k.ft)	179.0	177.2	176.2	175.4
$v_{ci} = 5.6\sqrt{f_c^{'*}} \geq 1.7\lambda\sqrt{f'_c}\ (psi)$	433.8	433.8	433.8	433.8
$v_{cw}\ (psi)$	359.9	359.9	359.9	359.9
$v_c\ (psi)$	359.9	359.9	359.9	359.9
V_u (kips)	157.6	157.1	156.7	155.9
$v_n = \frac{v_u}{\phi}\ (psi)$	625.2	623.2	621.6	618.5
$\frac{v_c}{2}\ (psi)$	180.0	180.0	180.0	180.0
$v_s = \frac{v_u}{\phi} - v_c \begin{cases} < 4\sqrt{f_c^{'}} \\ < 8\sqrt{f_c^{'}} \end{cases}\ (psi)$	265.3	263.3	261.7	258.5
$s = \min\left(\frac{A_v f_y}{v_s b}, \frac{f_y A_v}{0.75 \times b\sqrt{f_c^{'}}}\right)\ (in.)$	5.7	5.7	5.7	5.8
Spacing as per A_{min} (in.)	25.8	25.8	25.8	25.8
S_{max} = min(0.75h,24) (in.)	18	18	18	18
Required s (in.)	5.7	5.7	5.7	5.8
Provided s (in.)	8	8	8	8
$(A_v)_{min} = \frac{50 b_w s_v}{f_y}(in^2)$	0.107	0.107	0.11	0.11
$(A_v)_{min} = \frac{A_{ps} f_{pu} s}{80 f_y d_p}\sqrt{\frac{d_p}{b_w}}\ (in^2)$	0.02	0.02	0.02	0.02

*Note Shear strength for SFRC is calculated based previous study [Cho and et al, 2009]

SFRPC#2-2

Sectional and mechanical properties are same as in case of PC#1-1

Orientation factor for three dimensional random orientations, $n_o = 0.41$

Bond efficiency factor $\eta_b = 1.2$

Fiber length, l_f *= 2.0 in.* fiber diameter d_f *= 0.031 in.*, matrix shear modulus,

G_m *= 4350 ksi*,

[Benture and Mindness, 2007], fiber cross sectional area A_f *= 0.00070 in*^{2},

radius of the fiber,

r_f *= 0.015 in*

Mean centroid spacing $S = 25\sqrt{\left(\frac{d_f}{\rho l_f}\right)} = 0.138 in$

$$\beta = \sqrt{\frac{2\pi G_m}{E_f A_f ln\left(S / r_f\right)}} = 24.49$$

Length correction factor $\eta_L = 1 - \frac{\tan h\left(\beta l_f / 2\right)}{\left(\beta l_f / 2\right)} = 0.96$

τ *= 363.6 psi [Swamy and et al 1981]*

$$\sigma_{cu} = \eta_o \eta_L \eta_b 2\tau \frac{l_f}{d_f} V_f = 171.7 psi$$

$$f_r = 0.75.\left(f'_c\right) = 581 psi$$

$\epsilon_u = 0.003,\ \varepsilon_o = \frac{f_r}{E_c} = 0.0001$

Assume $d_n = 3.21\ in$

Tensile force due to steel fiber, $F_{ft} = \sigma_{cu} b\left(D - d_n\right) = 57.1 kips$

Tensile force due to tensile reinforcement $F_{st} = A_s f_f = 13 kips$

Tensile force due to prestress, $F_{ps} = A_{ps} f_{ps} = 188 kips$

Compression forced due to concrete $F_c = \frac{0.85 f_{cu}}{\epsilon_u}\left(\epsilon_u - \frac{\epsilon_0}{3}\right) b d_n = 258\ kips$

Compression force due to compression reinforcement

$F_{sc} = \frac{d_n - d'}{d_n} \epsilon_u E_s A'_s = 0.10 ksi$

For ACI, $k_2 = \frac{0.85 d_n}{2} = 1.58\ in.$

$$M_u = F_c\left(d_n - k_2\right) + F_{sc}\left(d_n - d'\right) + F_{st}\left(d_{st} - d_n\right) + F_{st}\left(\frac{D - d_n}{2}\right) + F_{ps}\left(d_{ps} - d_n\right)$$

$= 4590.3 k.in = 131.8 k.ft$

$> 1.2 M_{cr} = 216.84 k.ft$ *Minimum ratio is satisfied*

Check for reinforcement steel reaches to yield stress or not

$f_s = \frac{d - d_n}{d} \varepsilon_u E_c = 482.4 ksi > 60 ksi$ *tension bar yeilds*

$f'_s = \frac{d_n - d'}{d_n} \varepsilon_c E_s = 5.66 ksi < 60$ *ksi compression bar do not yeild*

$\beta = 1 - \frac{(w + 2kd)}{2L} = 1 - \frac{(3 + 2 \times 3.21)}{2 \times 12 \times 12} = 0.967$ *where k d =d_n and w =3 in.*

$$P_u = \frac{4M_u}{\beta L} = 131.8\,kips$$

Shear design at different sections of SFRPC#2-2 beams with tested compressive strength and tested ultimate load is presented in Table A.6.

Table A.6 Details of Shear design at different section of SFRPC#2-2 beam

X, (ft)	1.75	3	4	6
$V_d(x), kips$	1.7	1.2	0.8	0.0
$M_d(x), k.ft$	3.6	5.4	6.4	7.2
ΔV_u (kips)	65.9	65.9	65.9	65.9
ΔM_u (k.ft)	115.3	197.7	263.6	395.4
ΔM_{cr} (k.ft)	179.0	177.2	176.2	175.4
$v_{ci} = 5.6\sqrt{f_c^{'}}^{*} \geq 1.7\lambda\sqrt{f'_c}\,(psi)$	433.8	433.8	433.8	433.8
$v_{cw}(psi)$	359.9	359.9	359.9	359.9
$v_c(psi)$	359.9	359.9	359.9	359.9
V_u (kips)	67.6	67.1	66.7	65.9
$v_n = \frac{v_u}{\phi}\,(psi)$	268.3	266.3	264.7	261.5
$v_s = \frac{v_u}{\phi} - v_c \begin{cases} < 4\sqrt{f_c^{'}} \\ < 8\sqrt{f_c^{'}} \end{cases}\,(psi)$	-91.7	-93.6	-95.2	-98.4
$s = \min\left(\frac{A_v f_y}{v_s b}, \frac{f_y A_v}{0.75 \times b\sqrt{f_c^{'}}}\right)(in.)$	14.2	14.2	14.2	14.2
Spacing as per A_{min} (in.)	14.2	14.2	14.2	14.2
S_{max} = min(0.75h,24) (in.)	18	18	18	18
Required s (in.)	14.2	14.2	14.2	14.2
Provided s (in.)	72	72	72	72
$(A_v)_{min} = \frac{50 b_w s_v}{f_y}(in^2)$	0.96	0.96	0.96	0.96
$(A_v)_{min} = \frac{A_{ps} f_{pu} s}{80 f_y d_p}\sqrt{\frac{d_p}{b_w}}\,(in^2)$	0.17	0.17	0.17	0.17

*Note Shear strength for SFRC is calculated based previous study [Cho and et al, 2009]

Calculation of Plastic Rotation Ductility Index and Moments:

Theoretical values of plastic rotations were calculated based on text book by Naaman, 2004. The value plastic hinge length L_p is taken as $\frac{d_e}{2}$. The average value of plastic rotation is calculated as follows:

$$\theta_p = \left(\frac{1.07 - 1.34\beta_1 \frac{c}{d_e}}{7.22\beta_1 \frac{c}{d_e} - 35} \right) \frac{2L_p}{d_e} \quad \text{(A.7)}$$

And ductility index is calculated as follows:

$$\mu_\phi = \frac{1}{1..275\beta_1 \frac{c}{d_e} - 0.075} \quad \text{(A.8)}$$

For PC#1-1, from Section A.1, $c = 3.25$ inches, $d_e = 20.9$ *inches*, $\beta_1 = 0.75$ from equation of (A.7), value $\theta_p = 0.019$ radian and from equation (A.8) ductility index $\mu_\phi =$ 13.57. The detail calculation for other beams is shown in Table A.7.

Table A.7 Details of calculation of plastic ratio and ductility index for all beams.

Specimens	c (in.)	d_e (in.)	β_1	Ductility ratio (μ_ϕ)	Plastic rotation (θ_p)
PC#1-1	3.25	20.9	0.75	13.57	0.019
SFRPC#1-1	3.25	20.9	0.75	13.57	0.019
PC#2-1	3	20.9	0.7	18.83	0.025
PC#2-2	3.34	20.3	0.75	12.15	0.017
SFRPC#2-1	7.16	20.9	0.75	3.96	0.005
SFRPC#2-2	3.21	20.9	0.75	13.91	0.019

The plastic rotations were calculated based on experimental parameters such as loads and deflections at different stage of loading [Mattock, 2008)

Elastic deflection is calculated by

$$\delta_e = \frac{PL^3}{24E_cI} \quad \text{(A.9)}$$

Where, P = Applied load

L = Effective length of beam = 144 in.

E_c = Modulus elasticity of concrete

I = Moment of Inertia= 18432 in^4

Plastic deflection is given by

$$\delta_p = \delta_t - \delta_e \quad \text{(A.10)}$$

Where,

δ_t is total deflection from the test.

Then Plastic rotation is determined by

$$\theta_p = \tan^{-1}\left(\frac{\delta_p}{z}\right) \quad \text{(A.11)}$$

Where z = L/2 = 72 inches

For PC #1-1, Detail calculation of plastic at yield load is given.

P= 100 kips, from equation A.9, δ_e = 0.078 inches and δ_p = 0.142 inches

And plastic rotation θ_p = 0.002 radian

The calculation of plastic rotation for other beams and in other stages of loads is shown is given in Table A.8

Table A.8 Calculation of plastic rotation with tested parameters.

Beams	Load (kips)	Total deflection (inches)	Compressive strength (psi)	E_c (ksi)	Elastic Deflection (inches)	Plastic Deflection (inches)	Plastic Rotation (Radians)
At Yield							
PC#1-1	100	0.22	5763	4327.1	0.078	0.142	0.0020
SFRPC#1-1	100	0.199	5470	4215.7	0.080	0.119	0.0017
PC#2-1	100	0.184	5405	4190.6	0.081	0.103	0.0014
PC#2-2	105	0.23	6963	4756.3	0.075	0.155	0.0022
SFRPC#2- 1	200	0.342	5127	4081.4	0.165	0.177	0.0025
SFRPC# 2-2	100	0.256	5130	4082.6	0.083	0.173	0.0024
At Maximum Load							
PC#1-1	134	1.84	5763	4327.1	0.105	1.735	0.0241
SFRPC#1-1	146	1.77	5470	4215.7	0.117	1.653	0.0230
PC#2-1	133	1.65	5405	4190.6	0.107	1.543	0.0214
PC#2-2	139	1.25	6963	4756.3	0.099	1.151	0.0160
SFRPC#2- 1	329	1.03	5127	4081.4	0.272	0.758	0.0105
SFRPC# 2-2	137	2.87	5130	4082.6	0.113	2.757	0.0383
At Ultimate Deflection							
PC#1-1	130	2.26	5763	4327.1	0.101	2.159	0.0300
SFRPC#1-1	136	1.79	5470	4215.7	0.109	1.681	0.0233
PC#2-1	130	2.66	5405	4190.6	0.105	2.555	0.0355
PC#2-2	133	2.88	6963	4756.3	0.094	2.786	0.0387
SFRPC#2- 1	214	1.95	5127	4081.4	0.177	1.773	0.0246
SFRPC# 2-2	131	3.6	5130	4082.6	0.108	3.492	0.0485

A.7 Calculation of Yield Moment:

$$M_y = \left(A_s f_y + A_{ps} f_{ps}\right) d_e \left(1 - k\gamma\right)$$

(A.12)

$$\alpha = \frac{\int_0^{\varepsilon_c} f_c^{'}\left[\frac{2\varepsilon_c}{0.002} - \left(\frac{\varepsilon_c}{0.002}\right)^2\right]}{f_c^{'}\varepsilon_c} = 500\varepsilon_c\left(1 - \frac{\varepsilon_c}{0.006}\right)$$

(A.13)

$$f_c = f_c^{'}\left[\frac{2\varepsilon_c}{0.002} - \left(\frac{\varepsilon_c}{0.002}\right)^2\right]$$

(A.14)

$$\gamma = 1 - \gamma = 1 - \frac{\int_0^{\varepsilon_c} f_c^{'}\varepsilon_c\left[\frac{2\varepsilon_c}{0.002} - \left(\frac{\varepsilon_c}{0.002}\right)^2\right]}{\alpha f_c^{'}\varepsilon_c^2} = 1 - \frac{500\varepsilon_c}{\alpha}\left(\frac{2}{3} - \frac{\varepsilon_c}{0.008}\right)$$

(A.15)

$$T = A_s f_y + A_{ps} f_{ps}$$

(A.16)

$$C = A_{sc} f_s^{'} + \alpha f_c^{'} bkd$$

(A.17)

$$k = \frac{\varepsilon_c}{\varepsilon_c + \varepsilon_s}$$

(A.18)

$$\varepsilon_s = \frac{f_{py}}{E_{ps}}$$

(A.19)

Assumed ε_c find k, $\propto$ and γ

Then Calculate *C* and *T* Check *C* = *T*

Check value of f_s *and* $f_s^{'}$ for yielding

For *PC #1-1* Beam

Assuming all steel bars yield, $f_s = f_s^{'} = f_y = 60\,ksi$ and

$f_{ps} = f_{py} = 0.85 f_{pu} = 229.5\,ksi$

Assume $\varepsilon_c = 0.00155$ $\quad \varepsilon_s = \dfrac{f_{py}}{E_{ps}} = 0.008$ $\quad k = \dfrac{\varepsilon_c}{\varepsilon_c + \varepsilon_s} = 0.161$

From Equation A.14 and A.15 value of α and γ are determined.

$\alpha = 0.574$

$\gamma = 0.362$

$T = A_s f_y + A_{ps} f_{py} = 188.8\,kips$

$C = A_{sc} f_s^{'} + \alpha f_c^{'} bkd = 188.8\,kips$

Check for stress for compression and tensile steel.

$$f_s^{'} = \left(\frac{kd - d^{'}}{kd} \right) \varepsilon_c E_s = 5.12\,ksi < 60\,ksi,\ compression\,bar\,does\,not\,yield$$

$$f_s = \left(\frac{d - kd}{kd} \right) \varepsilon_c E_s = 233.5\,ksi > 60\,ksi,\ tension\ bar\ yields$$

$$f_{ps} = \left(\frac{d - kd}{kd} \right) \varepsilon_c E_{ps} = 230.2\,ksi > 229.5\,ksi,\ prestressed\ strand\ yields$$

Moment at yield is calculated from equation A.12,

$M_y = \left(A_s f_y + A_{ps} f_{ps} \right) d_e \left(1 - k\gamma \right) = 311 k.ft$

The yield moment for all beams with ultimate load as calculated above (sections A.1 to A.5) and moment due to tested peak and yield loads are shown in Table A.9.

Table A.9 Comparison of Tested and Calculated Values

Beams	M_d	Test					Calculated		$\frac{M_y(\text{Test})}{M_y(\text{Calculated})}$	$\frac{M_u(\text{Test})}{M_u(\text{Calculated})}$
		β	P_y	$M_y = M_d + \frac{\beta P_y L}{4}$	P_u	$M_u = M_d + \frac{\beta P_u L}{4}$	M_y	M_u		
	k-ft		kips	k-ft	kips	k-ft	k-ft	k-ft		
PC # 1-1	7.2	0.96	100	294.64	134	392.37	311.0	329.9	0.947	1.189
SFRPC # 1-1	7.2	0.96	100	294.64	146	426.86	306.0	401.6	0.963	1.063
PC # 2-1	7.2	0.96	100	294.64	133	389.49	311.0	329.9	0.947	1.181
PC # 2-2	7.2	0.97	105	313.00	139	412.02	316.0	330.9	0.990	1.245
SFRPC # 2-1	7.2	0.94	200	571.20	329	934.98	703.2	879.0	0.812	1.064
SFRPC # 2-2	7.2	0.97	100	298.43	137	406.19	306.0	382.5	0.975	1.062

REFERENCES

ACI Committee 318, Building Code Requirements for Structural Concrete (ACI 318-11) and Commentary), an ACI Standard, American Concrete Institute, Detroit, 2008

ACI Committee 544, State of the Art Report on Fiber Reinforced Concrete, Report 544-1R-96 (Reapproved 2002), ACI Committee 544, Fiber Reinforced Concrete, 2002

ACI Committee 544, Design Consideration for Steel Fiber Reinforced Concrete, Report ACI 544R-88, American Concrete Institute, Farmington Hill, MI, 1998

ACI-ASCE Committee 326, "Shear and Diagonal Tension," ACI Journal Proceedings, Vol. 59, No. 3, March, 1962

ASTM C172-10 "Standard Practice for Sampling Freshly Mixed Concrete," ASTM International, West Conshohocken, PA

ASTM C617-11 "Standard Practice for Capping Cylindrical Concrete Specimens," ASTM International, West Conshohocken, PA

ASTM C1550-08, "Standard Test method for Flexural Toughness of Fiber Reinforced Concrete (Using Centrally Loaded Round Panel)," ASTM International, West Conshohocken, PA, 2008,

ASTM C39 / C39M-11 "Standard Test Method for Compressive Strength of Cylindrical Concrete Specimens," ASTM International, West Conshohocken, PA

ASTM C496/C496M-11 "Standard Test Method for Spitting Tensile Strength of Cylindrical Concrete Specimens," ASTM International, West Conshohocken, PA

ASTM C1609/C1609M-10, “Standard Test method for Flexural Performance of Fiber-Reinforced Concrete (Using Beam with Third-Point Loading),” ASTM International, West Conshohocken, PA, 2010, 9 pp

Aveston, J., Mercer, R. A., and Sillwood, J. M. "Fibre Reinforced Cements – Scientific Foundation for Specifications," *Proceedings of National Physical Laboratory Conference,* UK, 93-103

Batson, G., Jenkins, E., and Spatney, R. (1972), "Steel Fibers as Shear Reinforcement in Beams," *ACI journal Proceedings,* 69(10), pp. 640-644

Bentur, A, and Mindness, S. “Fiber Reinforced Cementitious Composites,” 2nd edition published 2007 by Taylor and Francis 2 Park Square, Milton Park, Abingdon, Oxon, OX 14 4RN

Bernard, E. S., “Behaviour of Round Steel Fibre Reinforced Concrete Panels under Point Loads,” Materials and Structures, 33, 2000, pp.181-188

Bernard, E. S. and Pircher, M., “Influence of Geometry on Performance of Round Determinate Panels Made with Fiber Reinforced Concrete,” Engineering Report No. CE10, School of Civil Engineering and Environment, UWS Nepean, Kingswood NSW, Australia, January, 2000

Bernard, E. S., “The Influence of Strain Rate on Performance of Fiber-Reinforced Concrete Loaded in Flexure,” Cement, Concrete, and Aggregates, CCAGDP, American Society for testing and Materials, Vol. 23, No. 1, June 2001, pp. 11-18

Bernard, E. S. and Pircher, M., “The Influence of Thickness on Performance of Fiber-Reinforced Concrete in a Round Determinate Panel Test,” Cement, Concrete, and

Aggregates, CCAGDP, American Society for testing and Materials, Vol. 23, No. 1, June 2001, pp. 27-33.

Bernard, E. S., "Correlations in the Behaviour of Fiber Reinforced Shotcrete Beam and Panel Specimens," Materials and Structures, 35, 2002, pp.156-164

Bortolotti, L., "Double Punch Test for Tensile and Compressive Strength in Concrete," IACI *Materials Journal*, Vol, 85-M4, Jan.- Feb., 1988 pp. 26-32

Chao, S.-H., Cho, J.-S., Karki, N., and Yazadani, N., "FRC Performance Comparison: Direct Tensile Test, Beam-Type Bending Test, and Round Panel Test," *ACI Special Publication 2011*, pp. 395-405

Carmo, Ricardo N.F do and Lopes, Sergio M.R. "Available Plastic Rotation in Continuous High Strength Concrete Beams," NRC press web site Canada Oct. 2008 Can. J. Civ 35: pp. 1152-1162

Chen, W. F., "Double Punch Test for Tensile Strength of Concrete," *ACI Materials Journal*, 1970, pp. 993–995

Chen, W. F., "Limit Analysis and Soil Plasticity," Elsevier Scientific Publishing Company, Amsterdam, Oxford, New York, 1975, Chapter 11, pp. 501-541.

Chen, W. F., M. ASCE and Yuan R. L., "Tensile strength of concrete: Double-Punch Test," *Journal of Structural Division, Proceeding of American Society of Engineers*, Vol. 106, No ST8, August, 1980 pp.1673-1693

Cho, J.-S., Lundy, J. M., and Chao, S.-H., 2009, “Shear Strength of Steel Fiber Reinforced Prestressed Concrete Beams,” ASCE Structures Congress ’09, April 30-May 2, 2009, Austin, Texas

Cox, H. L. (1952) "The Elasticity and Strength of Paper and Other Fibrous Materials," *British Journal of Applied Physics (Bristol),* 3, pp. 72-79.

Demeke, Ayele and Tegos, I.A. “Steel Fiber Reinforced Concrete in Biaxial Stress Tension – Compression Condition,” *ACI Structural Journal* Sept.-Oct. 1994, pp. 579-584

Dinh, H. H. “Shear Behavior of Steel Fiber Reinforced Concrete Beams without Stirrup reinforcement,” A PhD Thesis, 2009 University of Michigan

Elices, M, and Planas, J., “Measurement of Tensile Strength of Concrete at very Low Temperature,” *ACI Journal may-June* 1982 pp 195-200

Fanella, D. A., and Naaman, A. E. (1985), "Stress-Strain Properties of Fiber Reinforced Mortar in Compression," *ACI Journal Proceedings,* 82(4), pp. 475-483

Foster, Stephen J., “The Application of Steel Fibers as Concrete Reinforcement in Australia from Material to Structure,” *Material and Structure* Vol. 42 2009, pp.1209-1220

Hasegawa, T., Shioya, T., and Okada,T., “Size Effect on Splitting Tensile Strength of Concrete,” Proceeding, 7th JCI Conference, Japan Concrete Institute, Tokyo, 1985, pp. 309-312

Han, S.-M., Kong, J.-S., Kim, S.-W., Kang, S.-T., and Park, H.-G., (2004), "Shear and Flexural Behavior of I-Shaped RC Beams Made of Steel Fiber Reinforced Cementious,"

Hannant, D. J. (1978), *fiber Cements and fiber Concretes*, John Wiley and Sons Ltd

Hognestad, E., Hanson, N. W., and McHenry, D. (1955), "Concrete Stress Distribution in Ultimate Strength Design," *ACI Journal Proceedings*, 52(12), pp. 455-480

Henager, C. H., and Doherty, T.J., ”Analysis of Reinforced Fiborous Concrete Beams,” Proceedings, ASCE V. 102, ST1, Jan 1976, pp. 177-188

Khaloo, A. R., and Kim, N. (1996), "Mechanical Properties of Normal to High-Strength Steel Fiber-Reinforced Concrete," *Cement, Concrete and Aggregates*, 18(2), pp. 92-97.

Khaloo, A. R., and Kim, N. (1997), "Influence of Concrete and Fiber Characteristics on Behavior of Steel Fiber Reinforced Concrete under Direct Shear," *ACI Materials Journal*, 94(6), pp. 592-601

Kim, S.-W., Kang, S.-T., Koh, K.-T., Kim, D.-G., and Han, S.-M., (2004), "Shear and Flexural Behavior of Rectangular Beams Made of Steel Fiber Reinforced Cementitious Composite,"

Kronenberg, J. (2006). "Sliding Arch Construction Method Used on the Gotthard Base Tunnel," *Concrete Engineering International*, 10(1), pp. 19-20

Kwak, Y.-K., Eberhard, M.O.,Kim, W.-S. and Kim, J. “Shear Strength of Steel Fiber-Reinforced Concrete Beams without Stirrups,” *ACI Structural Journa*l, Technical Paper July-August 2002, pp 531-532

Lim, T. Y., Paramasivam, P., and Lee, S. L. (1987), "Analytical Model for Tensile Behavior of Steel-Fiber Concrete," *ACI Materials Journal*, 84(4), pp. 286-298.

Lim, T. Y., Paramasivam, P., and Lee, S. L. (1987), "Shear and Moment Capacity of Reinforced Steel-Fiber-Concrete Beams," *Magazine of Concrete Research,* 39(140), pp. 148-160

Lok, T. S., and Xiao, J. R. (1999), "Flexural Strength Assessment of Steel Fiber Reinforced Concrete," *ASCE Journal of Materials in Civil Engineering,* 11(3), pp. 188-196

Marti, P., "Size Effect in Double-Punch Test on Concrete Cylinders," *ACI Materials Journal*, Vol. 86 No. 6, Nov.-Dec. 1989, pp. 597-601

Mass, G. R. (1997). "SFRC Lining for an Embankment Dam," *Concrete International,* 19(6), pp. 24-27.

Mattock, A. H., "Rotational Capacity of Hinge Regions in Reinforced Concrete Beams," *Proceeding of the International Symposium on Fracture Mechanics of Reinforced Concrete*, Miami, ACI SP-12, 1964, pp. 143-181

Mindess, S., Young, J. F., and Darwin, D., Concrete, 2nd Edition, Prentice Hall, Upper Saddle River, NJ, 2003, 644 pp

Molins, C., Aguado, A. and Saludes, S., "Double Punch Test to Control the Energy Dissipation in Tension of FRC (Barcelona Test)," *Material and Structures*, May, 2008

Naaman, A. E., and Najm, H. (1991), "Bond-Slip Mechanisms of Steel Fibers in Concrete," *ACI Materials Journal,* 88(2), pp. 135-145.

Naaman, A. E., and Reinhardt, H. W (1995) "Characterization of High Performance Fiber Reinforced Cement Composites," Proceedings of the Second International

Workshop ' High Performance Fiber Reinforced Cement Composites', Ann Arbor, USA, 528

Naaman, A. E., "Fiber Reinforced Concrete," *Concrete International*, Vol. 7, No. 3, March, pp. 21-25

Naaman, A. E., Prestressed Concrete Analysis and Design—Fundamentals, Second Edition, Techno Press 3000, 2004, 1072

Naaman, A. E. and Reinhardt and Fritz, C. "Reinforced Concrete Beams with SIFCON matrix," *ACI Structural Journal*, Jan.-Feb., 1992

Naaman, A.E., "High Performance Fiber Reinforced Concrete," Chapter 3 (pp 91-153) for book edited by C., Shi and Y.L., M. titled " High Performance Construction Materials, Science and Applications," *World Scientific*, June 2008 Engineering material and Technological Needs Vol. 448 pp

Parameswaran, V. S., and Raja Gopalan, K. S. "Strength of Concrete Beams with Aligned and Random Steel Fiber Micro Reinforcement," *Rilem Symposium of Fiber Reinforced Cement and Concrete*, pp. 95-103

Pros, A., Diez P. and Molins, C., "Model Validations of Numerical Simmulation of Double Punch Test," *ECCM 2010, IV European Conference on Computational Mechanics*, Paris, France May 16-21, 2010

Ramakrishnan, V., Brandshaug, T., Coyle, W. V., and Schrader, E. K. (1980)," Comparative Evaluation of Concrete Reinforced with Straight Steel Fibers and Fibers with Deformed Ends Glued Together into Bundles," *ACI Journal Proceedings*, 77(3), pp. 135-143.

Robinson, C, Colasanti, A., and Boyd, G. (1991), "Steel Fibers Reinforced Auto Assembly Plant Floor," *Concrete International*, 13(4), pp. 30-35

Rokugo, Keitetsu, Kand Testsushu and Yokota, Hiroshi, “Application and Recommendation of High Performance Fiber Reinforced Cement Composites with Multiple Fine Cracking (HPFRCC) in Japan,” *Material and Structure* Vol. 42 2009, pp. 1197-1208

Romualdi, J. P., and Batson, G. B. (1963), "Mechanics of Crack Arrest in Concrete," *ASCE Journal of the Engineering Mechanics,* 89(EM3), pp. 147-168.

Thomas, J., and Ramaswamy, A. (2007), "Mechanical Properties of Steel Fiber reinforced Concrete," *ASCE Journal of Materials in Civil Engineering,* 19(5), pp. 385-392

Serna, P., Arango, S., Riberio, T. and Nunez, A.M., “Structural Cast in Place SFRC: Technology Control Criteria and Recent Applications in Spain,” *Material and Structure* Vol. 42 2009, pp. 1233-1246

Shah, S., and Rangan, B. V. (1971) "Fiber Reinforced Concrete Properties," *ACI Journal Proceedings,* 68(2), pp. 126-35

Shivkumar, A. and Santhanam, M. “Mechanical Properties of High Strength Concrete Reinforced With Metallic and Non-Metallic Fiber.” *Concrete and Composite,* Vol. 29 Issues 8, September 2007, pp 603-608

Soroushian, P., and Bayasi, Z. (1991), "Fiber Type Effects on the Performance of Steel Fiber Reinforced Concrete," *ACI Materials Journal,* 88(2), pp. 129-134

Swamy, R. N. and Al-Ta’an, S. A., “Deformation and Ultimate strength in Flexure of Reinforced Concrete Beams Made with Steel Fiber Concrete,” *ACI Journa*l, Sept.-Oct., 1981

Swamy, R. N., and Mangat, P. S. (1974), "Theory for the Flexural Strength of Steel Fiber Reinforced Concrete," *Cement and Concrete Research,* 4(2), pp. 313-325.

Thomas, J., and Ramaswamy, A. (2007), "Mechanical Properties of Steel Fiber reinforced Concrete," *ASCE Journal of Materials in Civil Engineering,* 19(5), pp. 385-392,

Wafa, F. F., and Ashour, S. A. (1992) "Mechanical Properties of High-strength Fiber Reinforced Concrete," *ACI Materials Journal,* 89(5), pp. 449-455

Wight, J. K. and MacGregor, J. G., Reinforced Concrete: Mechanics and Design, 5th Edition, Prentice Hall, 1126 pp., 2008

Williamson, G. R., and Knab, L. I. "Full Scale Fiber Concrete Beam Tests," *Rilem Symposium 'Fiber Reinforced Cement Concrete*

Wright, P. J. F. (1955). "Comments on Indirect Tensile Test on Concrete Cylinders," *Magazine of Concrete Research,* 7(20), 87-96

BIOGRAPHICAL INFORMATION

Mr. Netra Bahadur Karki is from Nepal, land of Mt. Everest. After having high school education from his home town school, in 1982 he joined the University of Roorkee in India and completed his undergraduate degree in Bachelors in Civil Engineering in 1986. After completing his bachelor's degree, he joined the Department of Irrigation, Ministry of Water Resources, and Government of Nepal. He continued to work there for more than 20 years. In the mean time, he completed Master's of Science in Structural Engineering from Tribhuvan University of Nepal in 1998. After pursuing Master's degree, he also worked part time as structural engineer in a private company for about 7 years. He joined the Graduate School at the University of Texas at Arlington in Fall 2007 as a Doctorate Student. Dr. Ali Abolmaali was his first advisor for initial period. And consequently he did his research under the supervision of Dr. Shih-Ho Chao. After graduation, he has plans to gain more experience of design and research in the United States and become a professional engineer.